Applications and Industry®

May 1960

Transactions Papers

Industry Division

60-61	Determining Pole Locations of Feedback Amplifiers...........Gamblin . . .	41
	Control Design for Minimum Probabilistic Error....Zaborszky, Diesel	
59-830	Continuous Linear Control Systems.............................. . . .	44
59-831	Sampled-Data Control Systems................................... . . .	54
60-29	Continuous Linear Control Systems Subject to Constraints........... . . .	63
59-1152	Homing Aircraft Flight Control Systems........................... . . .	66
60-36	Paralleled Mercury-Arc and Silicon Rectifiers................Hodgson . . .	70
60-39	Series Capacitors Applied to Power Rectifiers............Hibbard, Bliss . . .	75
60-12	Ground-Fault Current in Metal Conduit..Gienger, Davidson, Brendel . . .	84
60-38	Heating of Unequally Loaded Underground Duct....Chamlee, McCall . . .	90
60-105	Rapid Determination of Approximate Closed-Loop Poles..........Basu . . .	96
60-106	Selection of Electric Winder Drives for Paper Industry...........Fisher . . .	99

General Applications Division

60-48	Pennsylvania RR Class GG-1 Electric Locomotives.......Horine, Ogden . . .	107
60-25	Train Performance Calculated by Digital Computer.............Hogan . . .	114

Science and Electronics Division

59-111	Capacitance of Parallel Rectangular Cylinders..................Horgan . . .	119

Conference Papers Open for Discussion....................................See 3rd Cover

NUMBER 48

Published Bimonthly by

AMERICAN INSTITUTE OF ELECTRICAL ENGINEERS

Communication and Electronics—May 1960

Science and Electronics Division

60-73 Tubes or Transistors: A Realistic Assessment .... Moe . . . 81
60-77 The Empretron, a Mercury Pool Arc Tube .... Hernqvist, Norman . . . 85
60-33 Potentials in D-C Corona Fields .... Penney, Matick . . . 91
60-91 Unblocking of Self-Saturating Magnetic Amplifiers .... Bourne, Nitzan . . . 99
60-96 Recent Developments on Magnetic-Coupled Multivibrators .... Geyger . . . 106
60-103 Sparkover as Influenced by Surface Conditions .... Penney, Craig . . . 112
60-128 Automation of Computer Panel Wiring...Altman, DeCampo, Warburton . . . 118
60-66 Symmetrical Frequency Multiplier Circuits .... Dick . . . 125
60-57 Locking Range of an Oscillator for Different Nonlinearities .... Nag . . . 134
60-102 Current, Voltage in Negative Pulsed Corona .... Thomas, Williams . . . 136
60-76 Voltage Transients Due to Arc Extinction .... Steiner, Strecker . . . 139
60-31 Generalized Brillouin Flow .... Kent . . . 144

General Committees of TOD

60-17 Education for Expanding Horizons in Electric Power .... Brown . . . 149

Instrumentation Division

60-245 Time-Division Multiplexing Telemetering Equipment..Almon, Donelson . . . 155
60-64 A New Impulse Metering System .... Snyder, Booker . . . 159
60-113 Characteristics of a High-Speed Wide-Chart Recorder .... Garrigus . . . 163
60-112 A Power-Line Transient Recorder .... Hoshall . . . 170

Communication Division

60-260 Dial-Selected Television for Ticket Reservation Facilities .... Alinsky . . . 174
59-259 Military 4-Wire Field Telephone .... Faherty, Howell . . . 177
60-45 A Delay Distortion Simulation Set .... Dunbar . . . 183
60-59 Redstone Arsenal Closed-Circuit Educational TV .... Argo, Howell . . . 185
60-11 Omnidirectional Circular Antenna Array .... Neff, Tillman . . . 190

(See inside back cover)

Note to Librarians. The six bimonthly issues of "Applications and Industry," March 1960–January 1961, will also be available in a single volume (no. 79) entitled "AIEE Transactions—Part II. Applications and Industry," which includes all technical papers on that subject presented during 1960. Bibliographic references to Applications and Industry and to Part II of the Transactions are therefore equivalent.

Applications and Industry. Published bimonthly by the American Institute of Electrical Engineers, from 20th and Northampton Streets, Easton, Pa. AIEE Headquarters: 33 West 39th Street, New York 18, N. Y. Address changes must be received at AIEE Headquarters by the first of the month to be effective with the succeeding issue. Copies undelivered because of incorrect address cannot be replaced without charge. Editorial and Advertising offices: 33 West 39th Street, New York 18, N. Y. Nonmember subscription $8.00 per year (plus 75 cents extra for foreign postage payable in advance in New York exchange). Member subscriptions: one subscription at $5.00 per year to any one of three divisional publications: Communication and Electronics, Applications and Industry, or Power Apparatus and Systems: additional annual subscriptions $8.00 each. Single copies when available $1.50 each. Second-class mail privileges authorized at Easton, Pa. This publication is authorized to be mailed at the special rates of postage prescribed by Section 132.122.

Printed in United States of America

Number of copies of this issue 5,300

An Analytical Method of Determining Pole Locations of Certain Types of Feedback Amplifiers

RODGER L. GAMBLIN
ASSOCIATE MEMBER AIEE

ynopsis: The pole locations of feedback nplifiers of an arbitrarily large number of ages, but with only one or two character-tic time constants, can be solved analyti-illy. The resulting expression is then gen-ral for all of one class of amplifiers. A solu-on of the case of n stages of one time con-ant and m stages of another with $n/m \gg 1$ presented. The case with $m=1$ and with eal matched transmission lines in the loop also solved. Other cases presented are for $=0$ and $m=n$. The analysis is shown to e good for high- or low-frequency investiga-ons where the system bandwidth is broad nough to prevent high- and low-frequency esponse interference.

BASICALLY, three methods are presently used in predicting the response f feedback amplifiers when the number f stages becomes larger than three. hese are construction of a Nyquist iagram,[1,2] construction of a Bode Diaram,[2,3] or construction of a root-locus lot.[4] All three methods are extremely seful, but have the common disadvanage of being graphical in nature and deanding considerable experience in their se in order for them to be a meaningful ool.

As will be shown, when the open-loop ansfer function of a system is of a kind ith only one or two characteristic time onstants, an analytical approach exists hich yields an expression for pole locaons in terms of the amplifier characterstics. The solution is then applicable any of a class of feedback amplifiers hich have the same form of transfer unction.

aper 60-61, recommended by the AIEE Feedback ontrol Systems Committee and approved by the IEE Technical Operations Department for presntation at the AIEE Winter General Meeting, ew York, N. Y., January 31–February 5, 1960. anuscript submitted May 26, 1959; made availble for printing December 10, 1959.

ODGER L. GAMBLIN, formerly with Project Matterorn, Atomic Energy Commission, is now with nternational Business Machines Corporation, ndicott, N. Y.

he author expresses his appreciation to Ira B. ernstein of Project Matterhorn whose comments n various portions of the analysis proved inaluable; and to N. W. Mather, also of Matterorn, for his careful reading of the manuscript.

his work was supported by the Atomic Energy ommission at Project Matterhorn, Princeton, N. , under contract *AT(30-1)-1238*.

The following analysis depends upon the amendability of factorization of polynominals of the following form:

$$(s+a)^n(s+b)^m=K'\beta \tag{1}$$

where s is the Laplace transform variable and a, b, m, K', and β are constants dependent upon amplifier characteristics. Since only amplifiers which have the above form of characteristic equation (the terms in the denominator of the feedback amplifier transfer function) are solvable, the analytical approach, to be described later, is limited to amplifiers which have no internal feedback loops encompassing more than two stages. It is also limited to systems which have resistive voltage feedback with or without a distributed element in the loop, and to systems where methods of compensation do not lead to individual stage transfer functions containing a power of s greater than 1.

In spite of the restrictions, a large class of amplifiers, especially those used in audio and analog-computer work, can be approximated so as to be encompassed by the analysis. An analytical expression for the stabilizing influence of a low-pass stage within a multistage system is presented which is useful in approximating stability limitations easily and quickly.

Preliminary Considerations

When the small signal approximation is used in the analysis of the high-frequency transfer function of a single-stage amplifier, the complex gain, neglecting stray inductance, transit time, and other higher order effects, is usually:

Fig. 1. Circuit diagrams for high-frequency response of ordinary amplifier

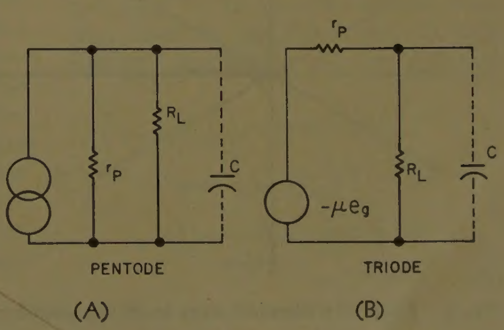

$$A=K/(s+B) \tag{2}$$

In the particular case shown in Fig. 1(B),

$$K=-\mu/r_pC;\ B=(r_p+R_L)/r_pR_LC$$

Neglecting any interactions between stages, the output of a series of cascaded amplifiers is the product of the gain of individual stages. When a voltage feedback loop is formed around the series of cascaded units, the resultant complex gain becomes:

$$A=\frac{K_1K_2K_3\ldots K_n}{(s+B_1)(s+B_2)(s+B_3)\ldots(s+B_n)-\beta K_1K_2\ldots K_n} \tag{3}$$

An amplifier which feeds directly into a matched lossless transmission line has a complex gain characteristic of the following form:

$$A=K\epsilon^{-\alpha s} \tag{4}$$

where α represents the time delay associated with the line and K is the amplifier gain. When a multistage amplifier has one or more stages connected through a series of matched transmission lines, the complex gain becomes:

$$A=\frac{(K_1K_2K_3\ldots)(\epsilon^{-(\alpha_1+\alpha_2+\alpha_3\ldots)s})}{(s+B_1)(s+B_2)(s+B_3)\ldots} \tag{5}$$

The gain, when the amplifier is fed back, becomes:

$$A=\frac{(K_1K_2K_3\ldots)}{(s+B_1)(s+B_2)\ldots\epsilon^{(\alpha_1+\alpha_2\ldots)s}-\beta(K_1K_2K_3\ldots)} \tag{6}$$

Exact Solution in Two Cases

When equation 1 has either m or n equal to zero or when $m=n$ an exact solution for the roots of the equation is possible. In the first instance, equation 1 can be written as:

$$(s+B)^n=K'\beta \tag{7}$$

with K' equal to $K_1K_2K_3\ldots K_n$. By application of De Moivre's Theorem, the solution can be found as:

$$s_r=K'^{1/n}\beta^{1/n}\epsilon^{i[(\theta+2k\pi)/n]}-B$$

$$k=0,\ 1,\ 2,\ 3,\ \ldots,\ (n-1)$$

$$s_r=\text{roots of 7} \tag{8}$$

Normally β will be chosen for negative feedback so that θ will equal π.

Substituting in the appropriate values of K', β, and B for pentode circuits, equation 8 becomes:

$$s_r=\frac{1}{C}\,(g_m'\beta^{1/n}\epsilon^{i[(\pi+2k\pi)n]}-(r_p+R_L)/(r_pR_L)) \quad (9)$$

and for triode circuits:

$$s_r=1/(r_pC)(\mu'\beta^{1/n}\epsilon^{i(\pi+2k\pi)/n}-(r_p+R_L)/R_L) \quad (10)$$

In both equations, it is to be noted that if the numerical value of B is identical in each stage, then by letting K' equal K_1K_2-$\ldots K_n$ an equivalent gain can be defined. Thus μ' is such an equivalent gain. A graph of the root structure of equation 10 is shown in Fig. 2.

When $n=m$ in equation 1 an exact solution can also be found, for in such a case the characteristic equation is of the form:

$$(s+B_1)^n(s+B_2)^n=K'\beta \quad (11)$$

A substitution of $(w-N)$ for s where $N=(B_1+B_2)/2$ and $D=(B_1-B_2)/2$ leaves

$$(w^2-D^2)^n=K'\beta \quad (12)$$

Applying De Moivre's Theorem twice:

$$w_r=(|K'^{1/n}\beta^{1/n}\epsilon^{i[(\pi+2k')/n]}+D^2|)^{1/2}\times \epsilon^{i\left((\arg(K'\beta)^{1/n}\epsilon^{i(\pi+2k'\pi)/n+D^2})/2+(2k''\pi)/2\right)}$$

$$k'=0,\,1,\,2,\,\ldots(n-1),\ k''=0,\,1 \quad (13)$$

The roots for an example of equation 13 are shown in Fig. 3. The case illustrated is for $B_1=2B_2$ and $B_1=1/r_pC_1$; and the graph is shown in units of $1/r_pC_1$. Advantage is taken of the fact that $R_L/(r_p+R_L)\cong 1$ for triodes. This latter restriction is unnecessary and has been taken only for convenience and, as can be seen later, can easily be included in analysis by redefining some constants.

Approximate Solutions

Perhaps the most important type of feedback amplifier is that with a number of wide band stages and one narrow band or low-frequency response stage. In such a case the complex gain under conditions of feedback has a characteristic equation of the form:

$$(s+B_1)^n(s+B_2)=\beta K' \quad (14)$$

If the equation is normalized by substituting $r_{p1}C_1=\rho r_{p2}C_2$ and $w=sr_{p1}C_1$, and for convenience, advantage is taken of the fact that $R_L/(R_L+r_p)\cong 1$ for triodes; if m' is defined to be an equivalent gain:

$$(w+1)^n\left(w+\frac{1}{\rho}\right)=\mu^{n+1}\beta/\rho \quad (15)$$

Letting $z=(u+1)$ and allowing for the fact that $1/\rho$ is small compared to unity:

$$z^n(z-1)=\mu^{n+1}\,\beta/\rho \quad (16)$$

As will be seen later it is not necessary that $1/\rho$ be small compared with unity to solve the equation. In cases where it is large or equal to unity, however, the above solution closely approaches either the n identical case with additional gain or the $n+1$ identical stage case. Letting

$$z^{n+1}=re^{i\theta}$$

then:

$$z=r^{1/(n+1)}\epsilon^{i[(\theta+2k\pi)/n+1]} \quad (17)$$

$$k=0,\,1,\,2,\,3,\,4,\,\ldots,\,n$$

Substituting equations 17 into equation 16, the result becomes:

$$r\epsilon^{i\theta}\left(1-\frac{1}{r^{1/(n+1)}}\,\epsilon^{-i\left(\frac{\theta}{n+1}+\frac{2\pi k}{n+1}\right)}\right)=\mu^{n+1}\,\beta/\rho \quad (18)$$

Unless $\mu^{n+1}\,\beta/\rho$ is either very large or very small, r is going to be close to unity. If r is close to unity, then $1/r^{1/(n+1)}$ will vary from 1 at worst as $(r-1)/n+1$. Later, an estimate of the error involved in letting $1/r^{1/(n+1)}\cong 1$ will be investigated. At the present time, however, let $1/r^{1/(n+1)}\rightarrow 1$.

$$r\epsilon^{i\theta}\left(1-\epsilon^{-i\left(\frac{\theta}{n+1}+\frac{2\pi k}{n+1}\right)}\right)=\mu^{n+1}\,\beta/\rho \quad (19)$$

The quantity in parenthesis represents a vector on the complex plane. Let the modulus of this vector equal a and the argument equal β', then:

$$r\epsilon^{i\theta}(a\epsilon^{i\beta'})=\mu^{n+1}\,\beta/\rho \quad (20)$$

From the form of equation 20 it can be seen that $ra=\mu^{n+1}\,\beta/\rho$ and $\theta+\beta=\pi$ where these latter quantities are, of course, real. The quantity in parentheses in equation 19 is an isosceles triangle whose apex angle is just $(\theta+2\pi k)/(n+1)$. Letting this apex angle equal α, from the geometry of the triangle:

$$\pi-2\beta=\alpha \quad (21)$$

A relation thus exists between α and θ and since α is in terms of θ alone, α can be determined in terms of n and k, and:

$$r\epsilon^{i\theta}(1-\epsilon^{i(4k+1)/(2n+1)})=-\mu^{n+1}\,\beta\rho \quad (22)$$

Remembering that $r\epsilon^{i\theta}=z^{n+1}$, the solution for z is:

$$z_r=\frac{\mu\beta^{1/(n+1)}}{\rho^{1/(n+1)}}\left(\epsilon^{-1\left(\frac{\pi(4k+1)}{2n+1}\right)}-1\right)^{-1/(n+1)} \quad (23)$$

By again noting that the quantity in parentheses is an isosceles triangle, roots of equation 19 can be determined by a somewhat simpler form of equation 23 since $a=2$ (cos $\theta/2$) and $\beta=\theta/2$, and since the roots occur in complex conjugate pairs:

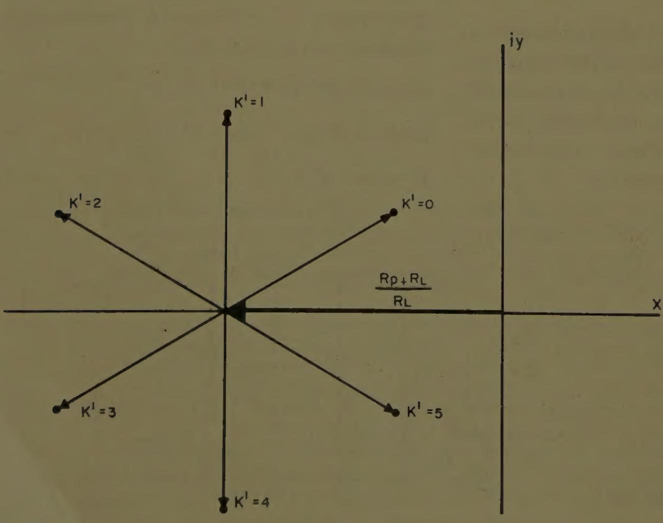

Fig. 2. Roots of n identical stage feedback amplifier in units of $1/R_pC$

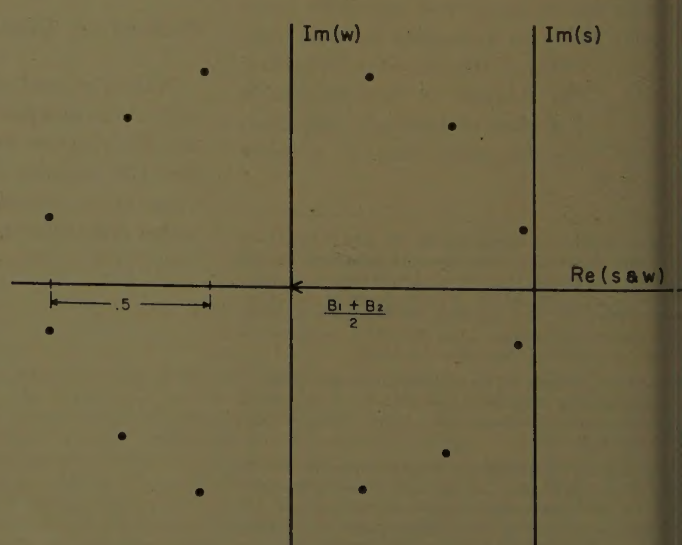

Fig. 3. Poles of amplifier with six stages of one band pass and six of another

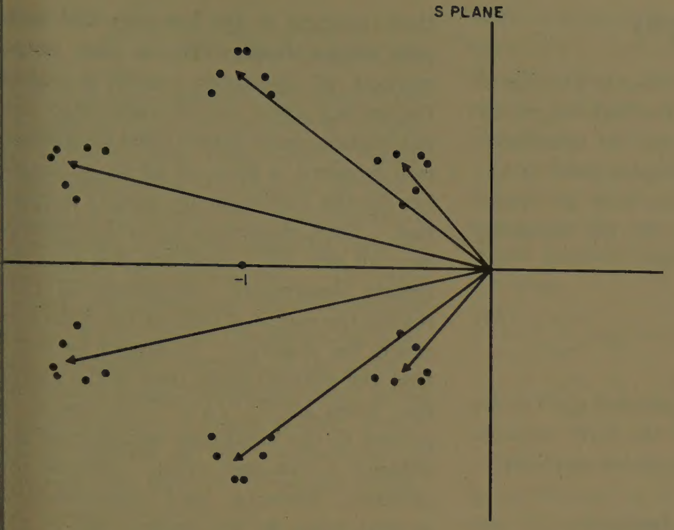

g. 4. Approximate poles of n-stage high-pass and 1-stage low-pass feedback amplifier in units of $1/R_pC$

$$=\frac{\mu\beta^{1/(n+1)}}{\rho^{1/(n+1)}}\left(\frac{1}{\left(2\cos\frac{\pi(4k+1)}{2n+1}\right)^{1/(n+1)}}\right)\epsilon^{\pm i\left(\frac{(4k+1)\pi}{(4n+2)(n+1)}+\frac{2\pi k'}{n+1}\right)} \qquad (24)$$

$$\frac{\ldots+1}{\ldots n+1}\leq\pi$$

$=0, 1, 2, 3, 4, 5, \ldots n$

$'=0, 1, 2, 3, 4, 5, \ldots n$

quation 24, by resubstituting in the quations for s and w, becomes:

$$=\frac{1}{r_{p1}C_1}\left(\frac{\mu'\beta^{1/(n+1)}}{\rho^{1/(n+1)}}\left(\frac{1}{\left(2\cos\frac{\pi(4k+1)}{2n+1}\right)^{1/(n+1)}}\right)\epsilon^{\pm i\left(\frac{(4k+1)\pi}{(4n+2)(n+1)}+\frac{2\pi k'}{n+1}\right)}-1\right) \qquad (25)$$

Equation 25 is the approximate solu-on for the roots of the characteristic quation of an n identical stage amplifier ith one additional relatively low pass age. It should be noted that the above olution gives $(n+1)^2$ roots instead of the equired $n+1$. The reason for this fact the nature of the approximation, and if is large enough, the cosine term in the mit approaches unity and the contribu-on of the k as opposed to the k' angles nds to zero. It should be noted that in he limit of large n, the cosine term pproaches unity for all k values and, urther, that this term cannot be zero he expression $\pi(rk+1)/(2n+1)$ cannot qual $\pi/2$ for positive integral k and n alues) except in the limit. For moder-ely large values of n (e.g., 4), the above olution gives a cluster of n roots located each of the $(n+1)$ values of k'. An lustration of the solution for $n=5$ is own in Fig. 4.

A check on the error involved in the $/r^{1/(n+1)}$ approximation can be made y examining equation 22 with more re. As is illustrated in Fig. 5 with a representative value of apex angle, the quantity in parentheses in equation 22 can be vectorially added to form a triangle. If the error due to the $1/r^{1/(n+1)}$ approximation is taken into account, the maximum error in a is $1-1/r^{1/(n+1)}$. Remembering that $ar=M$ where $M=\mu^{(n+1)}\beta/\rho$, the error in r can be determined by perturbing r and a simultaneously and keeping M constant and is:

$$E_r=\frac{r^2(1-1/r^{1/(n+1)})}{M} \qquad (26)$$

The error in θ can be found by noting that the error in β is approximately equal to $(1-1/r^{1/(n+1)}/a)$ and that $\beta+\theta=\pi$

$$E_\theta=\frac{r^2(1-1/r^{1/(n+1)})}{M} \qquad (27)$$

Using the value of r given by the solution of equation 22, an estimate in the error of the solution of that equation can be formed. It is to be noted that for very small M, $(\mu^{n+1}\beta/\rho<<1)$, the approximation is invalid; also it should be noted that for large n the approximation becomes better. Since M is a quantity related to feedback, the first condition is that for feedbacks that are low compared to possible feedbacks (without instability) the approximation does not hold.

The approximation $(1/\rho<<1)$ used in forming equation 16 is obviously not essential as a linear relation would still exist between α and β if a constant other than unity multiplied the exponential term of the quantity in parentheses in equation 18. The solution is tedious but in principle can still be solved.

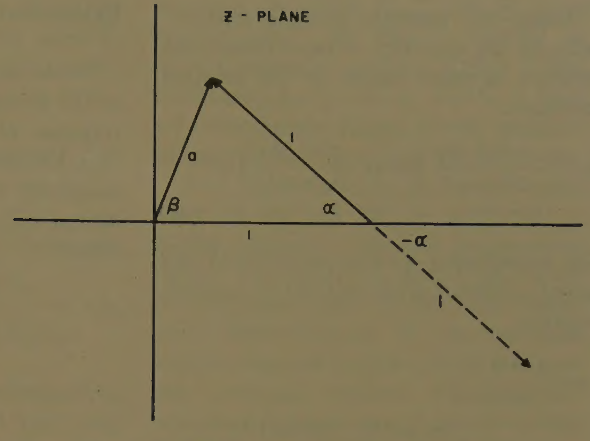

Fig. 5. Relation between α, β, and a

Case for $n/m>>1$

The method of solution in the analysis for $m=1$ can still be applied for $m=1$, 2, 3, or other values provided that n/m is much greater than 1. In the case of two low-pass stages, the square root of each side of the equation can be taken and the result is:

$$z^{n/2}(z-1)=\frac{\mu'^{(n+1)/2}\beta^{1/2}}{\rho}\,\epsilon^{i\pi/2},\ \epsilon^{i3\pi/2} \qquad (28)$$

and provided $n/2>>1$ the solution still holds.

Case with Ideal Matched Transmission Line in Loop

A final case of importance is when a transmission line appears in the amplifier feedback loop as shown in equation 7. The characteristic equation, using some of the above notational simplifications, is:

$$z^n(z-1)\epsilon^{(d\sqrt{LC'}/r_{p1}C_1)(z-1)}=\mu^{n+1}\beta/\rho \qquad (29)$$

where d is the total length of the transmission line in the loop in suitable units and $(LC)^{1/2}$ is the velocity constant of the line again in suitable units. Letting $re^{i\theta}=z^{n+1}$ and letting $d(LC)^{1/2}/r_{p1}C_1=\alpha$:

$$re^{i\theta}\left(1-\frac{1}{r^{1/(n+1)}}\right)\epsilon^{-i(\theta+2k\pi)/(n+1)}\times$$
$$\epsilon^{\alpha/r[1/(n+1)]\left[\cos\frac{\theta+2k\pi}{n+1}\right]}\times$$
$$\epsilon^{i(\alpha/r[1/(n+1)])[\sin(\theta+2k\pi)/(n+1)])}$$
$$=\mu^{(n+1)}\beta e^{\alpha/\rho} \qquad (30)$$

$k=0, 1, 2, \ldots, n$

Using the isosceles triangle relationship for the quantity in parentheses, the relation between angles in the solution becomes:

$$\theta-\frac{\pi}{2}-\frac{1}{2}\left(\frac{\theta+2k\pi}{n+1}\right)+\sin\alpha\left(\frac{\theta+2k\pi}{n+1}\right)=0 \tag{31}$$

By substituting $\gamma=(\theta+2k\pi)/(n+1)$ and using a perturbation method of approximation:

$$\gamma=\frac{\pi(4k+1)}{2n+1}-\frac{\sin\alpha\pi(4k+1)/(2n+1)}{(2n+1)/(2)+\alpha\cos\left[\alpha\pi(4k+1)/(2n+1)\right]} \tag{32}$$

The solution of equation 32 then becomes:

$$z=\frac{\mu(\beta\epsilon^{\alpha})^{1/(n+1)}}{\rho^{1/(n+1)}}\left(\frac{1}{\rho^{\alpha}\cos\gamma}\right)^{1/(n+1)}\times\left(\frac{1}{\epsilon^{i\beta}\epsilon^{i\alpha}\sin\gamma}\right)^{1/(n+1)} \tag{33}$$

Because of the approximation implicit in the perturbation solution of γ, it is not reasonable to assume that equation 33 will adequately represent the roots of the characteristic equation if α is not considerably less than $\rho r_{p1}C_1$.

Extensions of Analysis

These methods are directly applicable to the investigation of the high-frequency response of certain types of amplifiers. The low-frequency complex gain of capacitively coupled units may be represented by an equation of the following form:

$$A=\frac{\mu^{R}L^{C}}{\frac{1}{s}+C(R_L+r_p)} \tag{34}$$

By transforming s by means of $w=1/s$ the gain may be put into the form suitable for investigation by the above methods.

Certain Results of Analysis

Equation 25 relates to the location of the poles of the transfer function of an amplifier of n high-pass stages and one low-pass stage. If n is relatively large it can be seen from the equation that an approximate stability criterion becomes:

$$\frac{\mu\beta^{1/(n+1)}}{\rho^{1/(n+1)}}\leq 1 \tag{35}$$

or

$$\mu\beta^{1/(n+1)}\leq\rho^{1/(n+1)}$$

Since ρ is the ratio of the long-to-short-time constant in the low-pass and high-pass stages, respectively, a very simple method of specifying stability exists. Depending upon the characteristic output impedance or output noise discrimination required, a value of $\mu\beta$ for an amplifier (in the midfrequency range) is specified. Then, depending upon the required over-all gain after feedback, β is approximately determined. Equation 35 then relates the required ratio of the time constants for stability. It should be noted that the over-all band pass of the amplifier, when $\mu\beta^{1/(n+1)}/\rho^{1/(n+1)}$ is close to 1, is close to the band pass open looped and without a low-pass stage. Output impedance, linearity, and discrimination against noise in the output end of the amplifier is achieved at the expense of gain.

References

1. Regeneration Theory, H. Nyquist. *Bell System Technical Journal,* New York, N. Y., vol. II, Jan. 1932.

2. Network Analysis and Feedback Amplifier Design (book), H. W. Bode. D. Van Nostrand Company, Inc., Princeton, N. J., 1945.

3. Principles of Servomechanisms (book), Gordon S. Brown, Donald P. Campbell. John Wiley & Sons, Inc., New York, N. Y., 1948, pp. 166–292.

4. Control-System Dynamics (book), W. R. Evans. McGraw-Hill Book Company, Inc., New York, N. Y., 1954.

Design of Continuous Linear Control Systems for Minimum Probabilistic Error

J. ZABORSZKY
MEMBER AIEE

J. W. DIESEL
ASSOCIATE MEMBER AIEE

A PREVIOUS PAPER[1] has proposed the "probabilistic error" as measure of performance and basis of design for control systems. The probabilistic error or "end-sigma error" was defined as the average value of the suitably penalized error occurring at such times when the output of the system is actually utilized. This measure of performance was mathematically formulated[1] and, for squared-error penalizing and invariant linear systems, was evaluated in a general way in the s or the t domain. An integral equation was also obtained[1] which defines the optimum time invariant linear system in the sense that it has the smallest probabilistic error.

Starting with the results obtained, the present paper evolves a complete design process leading to the weighting function and to the value of the probabilistic error of the optimum system. This process is presented as a complete sequence of definitions and equations which can be easily followed "cookbook fashion" by the programer of the digital computer; in fact, such programs have already been established.

It is significant that this process is worked out here for a case which is far from trivial. It is quite general, covering a broad class of important and involved practical situations.

Paper 59-830, recommended by the AIEE Feedback Control Systems Committee and approved by the AIEE Technical Operations Department for presentation at the AIEE Summer and Pacific General Meeting and Air Transportation Conference, Seattle, Wash., June 21–26, 1959. Manuscript submitted March 23, 1959; made available for printing May 12, 1959.

J. Zaborszky is with Washington University, St. Louis, Mo., and consultant to McDonnell Aircraft Corporation; J. W. Diesel is with the McDonnell Aircraft Corporation, St. Louis, Mo.

The authors thank R. C. Cowles for his help in computations and algebra connected with the material for this paper.

Solving for Optimum System

The probabilistic square error has been defined[1] generally as

$$s=\int_0^T \overline{{}^{l}p(t)({}^{l}i(t)-{}^{l}c(t))^2}\,dt \tag{1A}$$

and for time invariant linear systems this definition was reduced[1] to:

$$s=\psi_{ii}(0,0)-2\int_0^T dt_1 k(t_1)\psi_{ir}(0,-t_1)+\int_0^T dt_3 k(t_3)\int_0^T dt_1 k(t_1)\psi_{rr}(t_3,t_3-t_1) \tag{1B}$$

where

$$\psi_{rr}(t_1,\tau)=\psi''(t_1,\tau)=\int_0^T dt_2\,\overline{{}^{l}p(t_2+t_1)\,{}^{l}r(t_2)\,{}^{l}r(t_2+\tau)} \tag{2}$$

$$\psi_{ir}(t_1,\tau)=\psi'(t_1,\tau)=\int_0^T dt_2\,\overline{{}^{l}p(t_2+t_1)\,{}^{l}i(t_2)\,{}^{l}r(t_2+\tau)} \tag{3}$$

$$i(t_1,\tau)=(t_1,\tau)$$
$$=\int_0^T dt_2 \overline{{}^l p(t_2+t_1)^l i(t_2)^l i(t_2+\tau)} \quad (4)$$

here ${}^l r(t)$ is the number l member of the nsemble of inputs to the control system, (t) is the corresponding desired output hich need not be identical to the input, nd ${}^l p(t)$ is the probability distribution of mes when the output resulting from input of type ${}^l r(t)$ is utilized.[1] The solid ne indicates averaging over the ensemble dexed by l;[1] $k(t)$ is the weighting function, or impulse response of the system; is the end sigma, the form of letter sigma sed at the end of Greek words; and T an be infinite in these equations: it epresents the duration of output utilization so that $p(t)=0$ if $t>T$.

The impulse response of the optimum ystem usually contains a Dirac delta nnction at $t=0$:

$$(t)=A\delta(t)+k_c(t) \quad (5)$$

hysically this delta function represents a arallel branch in the closed-loop transfer nnction which is a simple gain A; $k_c(t)$ is e continuous part of the impulse esponse.

To establish the optimum system it is und advantageous to expand ${}^l p(t)$, (t), ${}^l i(t)$ and $k(t)$ as follows:

$$(t)=\sum_a {}^l p_a\phi_a{}^I(t) \quad (6)$$

$$(t)=\sum_a {}^l r_a\phi_a{}^{II}(t) \quad (7)$$

$$t)=\sum_a {}^l i_a\phi_a{}^{III}(t) \quad (8)$$

$$(t)=\sum_a k_a\phi_a{}^{IV}(t) \quad (9)$$

here $\phi_a{}^I(t)$, $\phi_a{}^{II}(t)$, $\phi_a{}^{III}(t)$, and $\phi_a{}^{IV}(t)$ re four sets of functions which may be ifferent or may coincide with each other nd which are defined over the interval $<t<T$. These functions must be sectionally continuous and bounded on the nterval but otherwise can be arbitrary. he sets may consist of a finite or infinite umber of members. For instance, equations 6 through 9 may represent Taylor xpansions:

$$(t)=\sum_{a=0}^{L} {}^l r_a t^a \quad (10)$$

hen:

$$^{II}(t)=t^a \quad (11)$$

r the selection of an orthogonal or orthormal set on the interval $0<t<T$ can be ade for any of the $\phi(t)$ sets since this ads to a ready determination of the efficients. As an example:

$$_a=\int_0^T {}^l p(t)\phi_a{}^I(t)dt \quad (12)$$

With orthogonal base functions, of course equations 6 through 9 represent general Fourier series. It will be assumed for the rest of this paper that the $\phi_a{}^{IV}(t)$ in equation 9 form an orthogonal set.

It is shown in Appendix I that with the expansions of equations 5 through 8 the expression for the end-sigma error of a given system (equation 1[B]) assumes the form:

$$\varsigma=2A\left(\sum_m k_m f_m{}''-f'\right)+A^2f''+f-2\sum_m k_m f_m{}'+\sum_m\sum_n k_m k_n f_{mn}{}'' \quad (13)$$

It is also shown in Appendix I that the k_n coefficients of the continuous part of the optimum impulse response can be obtained by inverting a set of linear equations. In matrix form:

$$k_n]=[f_{mn}]^{-1}f_m] \quad (14)$$

while the strength of the delta function part of the optimum impulse response is defined by the equation:

$$A=\frac{1}{f''}\left[f'-\sum_n k_n f_n{}''\right] \quad (15)$$

and the end-sigma error of the optimum system can be obtained as

$$\varsigma=f-Af'-\sum_m k_m f_m{}' \quad (16)$$

where the elements of the matrix are defined as:

$$f_{mn}=f_{mn}{}''-\frac{f_m{}''f_n{}''}{f''} \quad (17)$$

$$f_m=f_m{}'-f_m{}''\frac{f'}{f''} \quad (18)$$

$$f=\sum_a\sum_b\sum_c \Psi_{abc}F_{abc} \quad (19)$$

$$f'=\sum_a\sum_b\sum_c \Psi_{abc}{}'F_{abc} \quad (20)$$

$$f''=\sum_a\sum_b\sum_c \Psi_{abc}{}''F_{abc} \quad (21)$$

$$f_m{}'=\sum_a\sum_b\sum_c \Psi_{abc}{}'F_{abcm} \quad (22)$$

$$f_m{}''=\sum_a\sum_b\sum_c \Psi_{abc}{}''F_{abcm} \quad (23)$$

$$f_{mn}{}''=\sum_a\sum_b\sum_c \Psi_{abc}{}''F_{abcmn} \quad (24)$$

The factors on the right of equations 19 through 24 are defined in Appendix I. The most significant thing about these definitions is that F_{abc}, F_{abcmn}, and F_{abcm} are determined solely by the selection of the specific sets of functions $\phi_a{}^I(\theta)$, $\phi_a{}^{II}(\theta)$, $\phi_a{}^{III}(\theta)$, and $\phi_a{}^{IV}(\theta)$. On the other hand, factors $\Psi_{abc}{}'$ and $\Psi_{abc}{}''$ are determined solely by the coefficients p_a, r_a, and i_a. Consequently it is possible to select some specific sets of orthogonal functions for which F_{abcmn} and F_{abcm} are precalculated. All that is needed to solve a particular problem is then to find coefficients p_a, r_a, and i_a, which, at least for deterministic inputs, simply amounts to carrying out three Fourier expansions.

Next, these data can be fed into equations 13 through 25, or preferably a digital computer program representing them. The result is k_n and A, or, respectively by equations 5, 9, and 16, a Fourier series representation of the optimum impulse response function, $k(t)$; and ς for this optimum system. Function $k(t)$ represents a linear time invariant system realizable in the sense that it produces no effect before the cause, because equation 9 describes such a system. But the solution of $k(t)$ is not necessarily a rational function or lumped constant realizable. This means that for realization, $k(t)$ now must be approximated by a physical system. For this purpose, standard time or frequency-domain techniques can be used. Once a rational function approximation is obtained, its end-sigma error can be evaluated by the general s-plane equations of reference 1 or by the general t-domain equation 13, where now, of course, k_n for the approximate lumped-constant system is used. A comparison with the end-sigma value of the optimum system permits an evaluation of the quality of approximation. It should be noted that equation 13 applies to any system. Equation 16 applies only to the optimum system.

Specific Orthogonal Sets for Solution

Precalculated definitions for $\Psi_{abc}{}''$, $\Psi_{abc}{}'$, Ψ_{abc}, F_{abc}, F_{abcm}, and F_{abcmn} are given for three sets of orthogonal functions in Tables I and II (see also Table III). The first set are trigonometric functions:

$$\phi_x(t)=C_x(t)=\cos\pi x\frac{t}{T} \qquad 0<t<1, x=0,1,2\ldots L \quad (25)$$

These functions form an orthogonal set on $0<t<T$, which is complete if $L=\infty$. The assumption is that time scale is normalized to make $T=1$.

The second set used in Tables I and II is derived from Legendre polynomials and is frequently a logical choice since inputs of control systems tend to be available in the form of polynomials in t.

$$\phi_x(t)=\mathcal{P}_x(t)=\sum_{y=0}^{x} M_{xy}\left(\frac{t}{T}\right)^y \qquad 0<t<1, x=0,1,2\ldots L \quad (26)$$

Table I(A). Ensembles of Deterministic Inputs

Definitions or Computation Steps	Trigonometric orthogonal set $C_x(t) = \cos\frac{x\pi t}{T}$, $0 \le x \le L$, $0 \le t \le T$; time normalized so that $T = 1$.	Legendre orthogonal set $\mathcal{P}_x(t) = \sum_{y=0}^{x} M_{xy}\left(\frac{t}{T}\right)^y$, $0 \le x \le L$, $0 \le t \le T$, M_{xy} in Table IV; time normalized so that $T = 1$.	Exponential polynomial orthogonal set $\mathcal{E}_x(t) = \sum_{y=1}^{x} N_{xy} e^{-\rho y t}$, $1 \le x \le L$, $0 \le t \le \infty$, N_{xy} in Table V; time normalized so that $\rho = 1$.
1.	${}^{i}r(t)$ Deterministic input number i in ensemble, ${}^{i}r(t) = 0$, $t < 0$		
2.	${}^{i}i(t)$ Desired output number i in ensemble, ${}^{i}i(t) = 0$, $t < 0$		
3.	${}^{i}p(t)$ Probability distribution of output utilization time for input number i, ${}^{i}p(t) = 0$, $t < 0$, $t > T$		
4.	${}^{i}Q$ Probability of input number i in ensemble		
5.	${}^{i}r_o = \int_0^1 {}^{i}r(t)\,dt$ ${}^{i}r_a = 2\int_0^1 {}^{i}r(t)\cos a\pi t\,dt$, $1 \le a \le L$	${}^{i}r_o = \int_0^1 {}^{i}r(t)\,dt$ ${}^{i}r_a = (2a+1)\int_0^1 {}^{i}r(t)\,\mathcal{P}_a(t)\,dt$	${}^{i}r_o = \lim_{T\to\infty} \frac{1}{T}\int_0^T {}^{i}r(t)\,dt$ ${}^{i}r_a = 2a\int_0^\infty [{}^{i}r(t) - {}^{i}r_o]\,\mathcal{E}_a(t)\,dt$, $1 \le a \le L$
6.	${}^{i}i_o = \int_0^1 {}^{i}i(t)\,dt$ ${}^{i}i_a = 2\int_0^1 {}^{i}i(t)\cos a\pi t\,dt$, $1 \le a \le L$	${}^{i}i_o = \int_0^1 {}^{i}i(t)\,dt$ ${}^{i}i_a = (2a+1)\int_0^1 {}^{i}i(t)\,\mathcal{P}_a(t)\,dt$	${}^{i}i_o = \lim_{T\to\infty} \frac{1}{T}\int_0^T {}^{i}i(t)\,dt$ ${}^{i}i_a = 2a\int_0^\infty [{}^{i}i(t) - {}^{i}i_o]\,\mathcal{E}_a(t)\,dt$, $1 \le a \le L$
7.	${}^{i}p_o = \int_0^1 {}^{i}p(t)\,dt$ ${}^{i}p_a = 2\int_0^1 {}^{i}p(t)\cos a\pi t\,dt$, $1 \le a \le L$	${}^{i}p_o = \int_0^1 {}^{i}p(t)\,dt$ ${}^{i}p_a = (2a+1)\int_0^1 {}^{i}p(t)\,\mathcal{P}_a(t)\,dt$	${}^{i}p_a = 2a\int_0^\infty {}^{i}p(t)\,\mathcal{E}_a(t)\,dt$, $1 \le a \le L$
8.	${}^{i}R_o = {}^{i}r_o$ ${}^{i}R_\alpha = \frac{1}{2}\,{}^{i}r_a$, $\begin{cases} a = \alpha, & 1 \le \alpha \le L \\ a = -\alpha, & -L \le \alpha \le -1 \end{cases}$	${}^{i}R_\alpha = \sum_{a=\alpha}^{L} M_{a\alpha}\,{}^{i}r_a$, $0 \le \alpha \le L$	${}^{i}R_o = {}^{i}r_o$ ${}^{i}R_\alpha = \sum_{a=\alpha}^{L} N_{a\alpha}\,{}^{i}r_a$, $1 \le \alpha \le L$
9.	${}^{i}I_o = {}^{i}i_o$ ${}^{i}I_\alpha = \frac{1}{2}\,{}^{i}i_a$, $\begin{cases} a = \alpha, & 1 \le \alpha \le L \\ a = -\alpha, & -L \le \alpha \le -1 \end{cases}$	${}^{i}I_\alpha = \sum_{a=\alpha}^{L} M_{a\alpha}\,{}^{i}i_a$, $0 \le \alpha \le L$	${}^{i}I_o = {}^{i}i_o$ ${}^{i}I_\alpha = \sum_{a=\alpha}^{L} N_{a\alpha}\,{}^{i}i_a$, $1 \le \alpha \le L$
10.	${}^{i}P_o = {}^{i}p_o$ ${}^{i}P_\alpha = \frac{1}{2}\,{}^{i}p_a$, $\begin{cases} a = \alpha, & 1 \le \alpha \le L \\ a = -\alpha, & -L \le \alpha \le -1 \end{cases}$	${}^{i}P_\alpha = \sum_{a=\alpha}^{L} M_{a\alpha}\,{}^{i}p_a$, $0 \le \alpha \le L$	${}^{i}P_\alpha = \sum_{a=\alpha}^{L} N_{a\alpha}\,{}^{i}p_a$, $1 \le \alpha \le L$
11.	$\overline{\overline{\Psi}}''_{\alpha\beta\gamma} = \sum {}^{i}Q\,{}^{i}P_\alpha\,{}^{i}R_\beta\,{}^{i}R_\gamma$		
12.	$\overline{\overline{\Psi}}'_{\alpha\beta\gamma} = \sum {}^{i}Q\,{}^{i}P_\alpha\,{}^{i}R_\beta\,{}^{i}I_\gamma$		
13.	$\overline{\overline{\Psi}}_{\alpha\beta\gamma} = \sum {}^{i}Q\,{}^{i}P_\alpha\,{}^{i}I_\beta\,{}^{i}I_\gamma$		

Note: Throughout these tables the position of the subscript defines its nature, the symbol appearing in this position defines the value of the subscript. For instance $R\beta$ in line 11, Table I(A), denotes $R\alpha$ from line 8, Table I(A), with $\alpha = \beta$, or $M_{a\alpha}$ in line 8, Table I(A), denotes the number in row a and column α of Table IV.

Table I(B). Slices of Stationary Random Signal and Noise Input with Random Time-Varying Gain

	Trigonometric orthogonal set, T finite.	Legendre orthogonal set, T finite.	Exponential orthogonal set, T infinite.
1.	${}^{ij}s(t) = {}^{i}g(t)\,{}^{j}s(t)$, signal input; a product of ${}^{i}g(t)$, the number i member of a set of time-varying gain functions, and ${}^{j}s(t)$, the number j member of an ergodic ensemble of signals. i and j ensembles statistically independent. Functions of j ensembles have zero mean. ${}^{i}g(t) = 0$, $t < 0$, $t > T$. ${}^{j}s(t)$ to be specified only through power spectral densities in line 6.		
2.	${}^{ij}n(t) = {}^{i}h(t)\,{}^{j}n(t)$, noise input; a product of ${}^{i}h(t)$, the number i member of a set of time-varying gain functions, and ${}^{j}n(t)$, the number j member of an ergodic ensemble of noise functions. ${}^{i}h(t) = 0$, $t < 0$, $t > T$. See line 6.		
3.	${}^{ij}i(t) = {}^{ij}s(t)$, desired output		
4.	${}^{i}p(t)$, probability distribution of output utilization time, member i in ensemble of ${}^{i}g$, ${}^{i}h$, ${}^{i}p$.		
5.	${}^{i}Q$, probability of member number i in ensemble of ${}^{i}g$, ${}^{i}h$, ${}^{i}p$.		
6.	$\Phi_{ss}(s) = B^{I}\dfrac{\prod_{\xi}(s-w_{\xi}^{I})}{\prod_{\lambda}(s-q_{\lambda}^{I})}$, $1 \le \lambda \le H^{I}$; $\Phi_{nn}(s) = B^{II}\dfrac{\prod_{\xi}(s-w_{\xi}^{II})}{\prod_{\lambda}(s-q_{\lambda}^{II})}$, $1 \le \lambda \le H^{II}$; $\Phi_{sn}(s) = B^{III}\dfrac{\prod_{\xi}(s-w_{\xi}^{III})}{\prod_{\lambda}(s-q_{\lambda}^{III})}$, $1 \le \lambda \le H^{III}$; $\Phi_{ns}(s) = B^{IV}\dfrac{\prod_{\xi}(s-w_{\xi}^{IV})}{\prod_{\lambda}(s-q_{\lambda}^{IV})}$, $1 \le \lambda \le H^{IV}$; power spectral densities and cross-spectral densities of ergodic ensembles ${}^{j}s(t)$, ${}^{j}n(t)$. In general, $q_{\lambda}^{(u)} = q_{\lambda}^{I}$ if $u = I$.		
7.	K_{λ}^{I} = Residue at q_{λ}^{I} of $\Phi_{ss}(s)$, K_{λ}^{II} = Residue at q_{λ}^{II} of $\Phi_{nn}(s)$, K_{λ}^{III} = Residue at q_{λ}^{III} of $\Phi_{sn}(s)$, K_{λ}^{IV} = Residue at q_{λ}^{IV} of $\Phi_{ns}(s)$, $K_{\lambda}^{(u)} = K_{\lambda}^{I}$ if $u = I$.		
8.	${}^{i}g_{x} = \dfrac{1}{x!}\cdot\dfrac{d^{x}}{dt^{x}}\,{}^{i}g(t)\Big\vert_{t=0}$, $0 \le x \le X$; ${}^{i}h_{x} = \dfrac{1}{x!}\cdot\dfrac{d^{x}}{dt^{x}}\,{}^{i}h(t)\Big\vert_{t=0}$, $0 \le x \le X$.		
9.	$\Delta_1 = \begin{cases} 1, & \mathrm{Re}\{q_{\lambda}^{(u)}\} > 0 \\ 0, & \mathrm{Re}\{q_{\lambda}^{(u)}\} < 0 \end{cases}$; $\Delta_2 = \begin{cases} 0, & \mathrm{Re}\{q_{\lambda}^{(u)}\} > 0 \\ 1, & \mathrm{Re}\{q_{\lambda}^{(u)}\} < 0 \end{cases}$; $\Delta_3 = \begin{cases} 1, & \xi+\eta = 0 \\ 0, & \xi+\eta \neq 0 \end{cases}$; $\Delta_4 = \begin{cases} 0, & \xi+\eta = 0 \\ 1, & \xi+\eta \neq 0 \end{cases}$		
10.	$\overset{(u)}{V}(\xi,\eta,x,y) = \sum_{\lambda=1}^{H^{(u)}} K_{\lambda}^{(u)}\Bigg\{\left[\dfrac{y!(-1)^{\xi}e^{-q_{\lambda}^{(u)}}\Delta_1}{(j\pi\eta - q_{\lambda}^{(u)})^{y+1}} + \Delta_2\sum_{k=0}^{y}\dfrac{y!(-1)^{\xi+\eta}}{(y-k)!(j\pi\eta - q_{\lambda}^{(u)})^{k+1}}\right] \cdot\left[\dfrac{-x!(-1)^{\xi}e^{q_{\lambda}^{(u)}}}{(j\pi\xi + q_{\lambda}^{(u)})^{x+1}} + \sum_{\ell=0}^{x}\dfrac{x!}{(x-\ell)!(j\pi\xi + q_{\lambda}^{(u)})^{\ell+1}}\right] + \sum_{k=0}^{y}\dfrac{y!}{(y-k)!(j\pi\eta - q_{\lambda}^{(u)})^{k+1}} \cdot\left[\dfrac{\Delta_3}{x+y-k+1} + \Delta_4\left(\dfrac{(x+y-k)!}{(j\pi[\xi+\eta])^{x+y-k+1}} - \sum_{\ell=0}^{x+y-k}\dfrac{(x+y-k)!(-1)^{\xi+\eta}}{(x+y-k-\ell)!(j\pi[\xi+\eta])^{\ell+1}}\right)\right]\Bigg\}$	$\overset{(u)}{V}(\xi,\eta,x,y) = \sum_{\lambda=1}^{H^{(u)}} K_{\lambda}^{(u)}\Bigg\{\left[\dfrac{(y+\eta)!e^{-q_{\lambda}^{(u)}}\Delta_1}{(-q_{\lambda}^{(u)})^{y+\eta+1}} + \Delta_2\sum_{k=0}^{y+\eta}\dfrac{(y+\eta)!}{(y+\eta-k)!(-q_{\lambda}^{(u)})^{k+1}}\right] \cdot\left[\dfrac{-(x+\xi)!e^{q_{\lambda}^{(u)}}}{(q_{\lambda}^{(u)})^{x+\xi+1}} + \sum_{\ell=0}^{x+\xi}\dfrac{(x+\xi)!}{(x+\xi-\ell)!(q_{\lambda}^{(u)})^{\ell+1}}\right] + \sum_{k=0}^{y+\eta}\dfrac{(y+\eta)!}{(y+\eta-k)!(-q_{\lambda}^{(u)})^{k+1}} \cdot\left[\dfrac{1}{x+\xi+y+\eta-k+1}\right]\Bigg\}$	$\overset{(u)}{V}(\xi,\eta,x,y) = \sum_{\lambda=1}^{H^{(u)}} K_{\lambda}^{(u)}\Bigg\{\left[\dfrac{y!\,\Delta_1}{(\eta - q_{\lambda}^{(u)})^{y+1}}\right] \cdot\left[\dfrac{-x!}{(\xi + q_{\lambda}^{(u)})^{x+1}}\right] + \sum_{k=0}^{y}\dfrac{y!}{(y-k)!(\eta - q_{\lambda}^{(u)})^{k+1}} \cdot\left[\dfrac{(x+y-k)!}{(\xi+\eta)^{x+y-k+1}}\right]\Bigg\}$
11.	$\overset{(u)}{J}(\beta,\gamma,x,y) = \dfrac{1}{4}\left[\overset{(u)}{V}(\beta,\gamma,x,y) + \overset{(u)}{V}(-\beta,\gamma,x,y) + \overset{(u)}{V}(\beta,-\gamma,x,y) + \overset{(u)}{V}(-\beta,-\gamma,x,y)\right]$	$\overset{(u)}{J}(\beta,\gamma,x,y) = \sum_{\xi=0}^{L}\sum_{\eta=0}^{L}\left[\sum_{b=0}^{L}\dfrac{M_{b\beta}M_{b\xi}}{(2b+1)^{-1}}\right]\cdot\left[\sum_{c=0}^{L}\dfrac{M_{c\gamma}M_{c\eta}}{(2c+1)^{-1}}\right]\overset{(u)}{V}(\xi,\eta,x,y)$	$\overset{(u)}{J}(\beta,\gamma,x,y) = \sum_{\xi=1}^{L}\sum_{\eta=1}^{L}\left[\sum_{b=1}^{L}\dfrac{N_{b\beta}N_{b\xi}}{(2b)^{-1}}\right]\cdot\left[\sum_{c=1}^{L}\dfrac{N_{c\gamma}N_{c\eta}}{(2c)^{-1}}\right]\overset{(u)}{V}(\xi,\eta,x,y)$
12.	$\overline{\overline{\overline{\Psi}}}''_{\alpha\beta\gamma} = \sum_{i}{}^{i}Q\left\{\sum_{x=0}^{X}\sum_{y=0}^{X}{}^{i}P_{\alpha}\left[{}^{i}g_{x}\,{}^{i}g_{y}J^{I}(\beta,\gamma,x,y) + {}^{i}h_{x}\,{}^{i}h_{y}J^{II}(\beta,\gamma,x,y) + {}^{i}g_{x}\,{}^{i}h_{y}J^{III}(\beta,\gamma,x,y) + {}^{i}h_{x}\,{}^{i}g_{y}J^{IV}(\beta,\gamma,x,y)\right]\right\}$		
13.	$\overline{\overline{\overline{\Psi}}}'_{\alpha\beta\gamma} = \sum_{i}{}^{i}Q\left\{\sum_{x=0}^{X}\sum_{y=0}^{X}{}^{i}P_{\alpha}\left[{}^{i}g_{x}\,{}^{i}g_{y}J^{I}(\beta,\gamma,x,y) + {}^{i}h_{x}\,{}^{i}g_{y}J^{IV}(\beta,\gamma,x,y)\right]\right\}$		
14.	$\overline{\overline{\overline{\Psi}}}_{\alpha\beta\gamma} = \sum_{i}{}^{i}Q\left\{\sum_{x=0}^{X}\sum_{y=0}^{X}{}^{i}P_{\alpha}\left[{}^{i}g_{x}\,{}^{i}g_{y}J^{I}(\beta,\gamma,x,y)\right]\right\}$		

Table II. Optimum System

	Trigonometric orthogonal set, T finite	Legendre orthogonal set, T finite	Exponential orthogonal set, T infinite
1.	$\Psi''_{\alpha\beta\gamma}=\overline{\Psi}''_{\alpha\beta\gamma}+\overline{\overline{\Psi}}''_{\alpha\beta\gamma}$, $\Psi'_{\alpha\beta\gamma}=\overline{\Psi}'_{\alpha\beta\gamma}+\overline{\overline{\Psi}}'_{\alpha\beta\gamma}$, $\Psi_{\alpha\beta\gamma}=\overline{\Psi}_{\alpha\beta\gamma}+\overline{\overline{\Psi}}_{\alpha\beta\gamma}$, (See lines 11-13, Table I.A, and lines 12-14, Table I.B).		
2.	$F_{\alpha\beta\gamma mn}$ (See Table III)	$F_{\alpha\beta\gamma mn}=\sum_{\mu=0}^{m}\sum_{\nu=0}^{n}M_{m\mu}M_{n\nu}\sum_{b=0}^{\beta}\sum_{c=0}^{\gamma}\left[\frac{1}{\mu+c+1}+\frac{1}{\nu+c+1}\right]\cdot\left[\frac{\binom{\beta}{b}\binom{\gamma}{c}(-1)^{b+c}}{(\mu+\nu+b+c+2)(\mu+\nu+\alpha+\beta+\gamma+3)}\right]$	$F_{\alpha\beta\gamma mn}=\sum_{\mu=1}^{m}\sum_{\nu=1}^{n}N_{m\mu}N_{n\nu}\left[\frac{1}{\mu+\alpha+\gamma}+\frac{1}{\nu+\alpha+\gamma}\right]\left[\frac{1}{(\mu+\nu+\alpha)(\alpha+\beta+\gamma)}\right]$
3.	$F_{\alpha\beta\gamma m}$ (See Table III)	$F_{\alpha\beta\gamma m}=\sum_{\mu=0}^{m}M_{m\mu}\sum_{b=0}^{\beta}\left[\frac{\binom{\beta}{b}(-1)^{b}}{(\mu+b+1)(\mu+\alpha+\beta+\gamma+2)}\right]$	$F_{\alpha\beta\gamma m}=\sum_{\mu=1}^{m}\frac{N_{m\mu}}{(\alpha+\mu+\gamma)(\alpha+\beta+\gamma)}$
4.	$F_{\alpha\beta\gamma}=\begin{cases}1, & (\alpha+\beta+\gamma)=0\\ 0, & (\alpha+\beta+\gamma)\neq 0\end{cases}$	$F_{\alpha\beta\gamma}=\frac{1}{(\alpha+\beta+\gamma+1)}$	$F_{\alpha\beta\gamma}=\frac{1}{(\alpha+\beta+\gamma)}$
5.	$f=\sum_{\alpha=-L}^{L}\sum_{\beta=-L}^{L}\sum_{\gamma=-L}^{L}\Psi_{\alpha\beta\gamma}F_{\alpha\beta\gamma}$	$f=\sum_{\alpha=1}^{L}\sum_{\beta=0}^{L}\sum_{\gamma=0}^{L}\Psi_{\alpha\beta\gamma}F_{\alpha\beta\gamma}$	$f=\sum_{\alpha=0}^{L}\sum_{\beta=0}^{L}\sum_{\gamma=0}^{L}\Psi_{\alpha\beta\gamma}F_{\alpha\beta\gamma}$
6.	$f'=\sum_{\alpha=-L}^{L}\sum_{\beta=-L}^{L}\sum_{\gamma=-L}^{L}\Psi'_{\alpha\beta\gamma}F_{\alpha\beta\gamma}$	$f'=\sum_{\alpha=1}^{L}\sum_{\beta=0}^{L}\sum_{\gamma=0}^{L}\Psi'_{\alpha\beta\gamma}F_{\alpha\beta\gamma}$	$f'=\sum_{\alpha=0}^{L}\sum_{\beta=0}^{L}\sum_{\gamma=0}^{L}\Psi'_{\alpha\beta\gamma}F_{\alpha\beta\gamma}$
7.	$f''=\sum_{\alpha=-L}^{L}\sum_{\beta=-L}^{L}\sum_{\gamma=-L}^{L}\Psi''_{\alpha\beta\gamma}F_{\alpha\beta\gamma}$	$f''=\sum_{\alpha=1}^{L}\sum_{\beta=0}^{L}\sum_{\gamma=0}^{L}\Psi''_{\alpha\beta\gamma}F_{\alpha\beta\gamma}$	$f''=\sum_{\alpha=0}^{L}\sum_{\beta=0}^{L}\sum_{\gamma=0}^{L}\Psi''_{\alpha\beta\gamma}F_{\alpha\beta\gamma}$
8.	$f'_m=\sum_{\alpha=-L}^{L}\sum_{\beta=-L}^{L}\sum_{\gamma=-L}^{L}\Psi'_{\alpha\beta\gamma}F_{\alpha\beta\gamma m}$	$f'_m=\sum_{\alpha=1}^{L}\sum_{\beta=0}^{L}\sum_{\gamma=0}^{L}\Psi'_{\alpha\beta\gamma}F_{\alpha\beta\gamma m}$	$f'_m=\sum_{\alpha=0}^{L}\sum_{\beta=0}^{L}\sum_{\gamma=0}^{L}\Psi'_{\alpha\beta\gamma}F_{\alpha\beta\gamma m}$
9.	$f''_m=\sum_{\alpha=-L}^{L}\sum_{\beta=-L}^{L}\sum_{\gamma=-L}^{L}\Psi''_{\alpha\beta\gamma}F_{\alpha\beta\gamma m}$	$f''_m=\sum_{\alpha=1}^{L}\sum_{\beta=0}^{L}\sum_{\gamma=0}^{L}\Psi''_{\alpha\beta\gamma}F_{\alpha\beta\gamma m}$	$f''_m=\sum_{\alpha=0}^{L}\sum_{\beta=0}^{L}\sum_{\gamma=0}^{L}\Psi''_{\alpha\beta\gamma}F_{\alpha\beta\gamma m}$
10.	$f''_{mn}=\sum_{\alpha=-L}^{L}\sum_{\beta=-L}^{L}\sum_{\gamma=-L}^{L}\Psi''_{\alpha\beta\gamma}F_{\alpha\beta\gamma mn}$	$f''_{mn}=\sum_{\alpha=1}^{L}\sum_{\beta=0}^{L}\sum_{\gamma=0}^{L}\Psi''_{\alpha\beta\gamma}F_{\alpha\beta\gamma mn}$	$f''_{mn}=\sum_{\alpha=0}^{L}\sum_{\beta=0}^{L}\sum_{\gamma=0}^{L}\Psi''_{\alpha\beta\gamma}F_{\alpha\beta\gamma mn}$
11.	$f_m=f'_m-f''_m\frac{f'}{f''}$		
12.	$f_{mn}=f''_{mn}-\frac{f''_m\cdot f''_n}{f''}$		
13.	$\left.k_n\right]=\left[f_{mn}\right]^{-1}\left.f_m\right]$, $0\leq m\leq M$, $0\leq n\leq M$		$\left.k_n\right]=\left[f_{mn}\right]^{-1}\left.f_m\right]$, $1\leq m\leq M$, $1\leq n\leq M$
14.	$A=\frac{1}{f}\left[f'-\sum_{n=0}^{M}k_n f''_n\right]$		$A=\frac{1}{f}\left[f'-\sum_{n=1}^{M}k_n f''_n\right]$
15.	$k(t)=A\delta(t)+\sum_{n=0}^{M}k_n\cos n\pi t$	$k(t)=A\delta(t)+\sum_{n=0}^{M}k_n\mathcal{P}(t)$	$k(t)=A\delta(t)+\sum_{n=1}^{M}k_n\mathcal{E}(t)$
16.	$\zeta=f-Af'-\sum_{m=0}^{M}k_m f'_m$		$\zeta=f-Af'-\sum_{m=1}^{M}k_m f'_m$

Table III

$$= \begin{cases} 1, & x=0 \\ 0, & x\neq 0 \end{cases}$$

$$(x)=(1-\delta x)\frac{(-1)^x-1}{j\pi x}+\delta x(-1)^x$$

$$(x)=(1-\delta x)\left\{-\frac{(-1)^x-1}{(j\pi x)^2}+\frac{(-1)^x}{j\pi x}\right\}+\delta x\frac{(-1)^x}{2}$$

$$(x)=(1-\delta x)\left\{2\frac{(-1)^x-1}{(j\pi x)^3}-2\frac{(-1)^x}{(j\pi x)^2}+\frac{(-1)^x}{j\pi x}\right\}+\delta x\frac{(-1)^x}{3}$$

$$u,\ w)=\frac{1-\delta u}{j\pi u}\{(-1)^uE_1(w)-E_1(u+w)\}+\delta u\{(-1)^uE_1(u)-E_2(u+w)\}$$

$$\begin{aligned} u,\ v,\ w)=\frac{1-\delta u}{j\pi u}\Bigg\{(-1)^u&\left[\frac{1-\delta v}{j\pi v}((-1)^vE_1(w)-E_1(v+w))+\delta v((-1)^vE_1(w)-E_2(v+w))\right]-\\ &\left[\frac{1-\delta u+v}{j\pi(u+v)}((-1)^{u+v}E_1(w)-E_1(u+v+w))+\delta u+v((-1)^{u+v}E_1(w)-E_2(u+v+w))\right]\Bigg\}+\\ \delta u\Bigg\{(-1)^u&\left[\frac{1-\delta v}{j\pi v}((-1)^vE_1(w)-E_1(v+w))+\delta v((-1)^vE_1(w)-E_2(v+w))\right]-\\ &\left[\frac{1-\delta u+v}{(j\pi(u+v))^2}((-1)^{u+v}E_1(w)-E_1(u+v+w))+\frac{\delta u+v}{2}((-1)^{u+v}E_1(w)-E_3(u+v+w))+\right.\\ &\left.\frac{1-\delta u+v}{j\pi(u+v)}((-1)^{u+v}E_1(w)-E_2(u+v+w))\right]\Bigg\}\end{aligned}$$

$$\begin{aligned} u,\ v,\ w)=\frac{1-\delta u}{j\pi u}\Bigg\{(-1)^u&\left[\frac{1-\delta v}{j\pi v}(E_1(v+w)-E_1(w))+\delta vE_2(v+w)\right]-\\ &\left[\frac{1-\delta v}{j\pi v}(E_1(u+v+w)-E_1(u+w))+\delta vE_2(u+v+w)\right]\Bigg\}+\\ \delta u\Bigg\{(-1)^u&\left[\frac{1-\delta v}{j\pi v}(E_1(v+w)-E_1(w))+\delta vE_2(v+w)\right]-\\ &\left[\frac{1-\delta v}{j\pi v}(E_2(u+v+w)-E_2(u+w))+\delta vE_3(u+v+w)\right]\Bigg\}\end{aligned}$$

$$=-(\alpha+\beta+\gamma)\qquad g_{1y}=(-1)^yn+\beta\qquad h_{1z}=(-1)^zm+\gamma$$
$$g_{2y}=(-1)^yn+\gamma\qquad h_{2z}=(-1)^zm+\beta$$

$$\beta\gamma mn=\frac{1}{4}\sum_{z=1}^{2}\sum_{y=1}^{2}C(f_1,\ g_{1y},\ h_{1z})+D(f_1,\ g_{2y},\ h_{2z})$$

$$\beta\gamma m=\frac{1}{2}\sum_{z=1}^{2}B(f_1,\ h_{2z})$$

here the M_{xy} coefficients are defined in able IV. These functions form an thogonal set on $0<t<T$, which is comete if $L=\infty$. The assumption is that e time scale is normalized to make $=1$.

When T is infinite an exponential polyomial[2] set is useful:

$$(t)=\mathcal{E}_x(t)=\sum_{y=1}^{x}N_{xy}\epsilon^{-yt}$$
$$0<t<T, x=1,2\ldots L \quad (27)$$

here the N_{xy} coefficients are defined in able V. These functions form a complete orthogonal set on $0<t<\infty$. Time should be normalized for best fit on the functions to be expanded.

Sometimes it is convenient to work with some linear combination of the functions of these orthogonal sets even though these are not orthogonal. For instance, if the input ${}^ir(t)$ is given as a polynomial in t then powers of t could be suitable base functions. On the other hand, an orthogonal set like Legendre polynomials will be needed to deal with random inputs, so a joint use of both of these sets of base functions is somewhat desirable. Such combined use is incorporated in Tables I and II:

$${}^ip(t)=\sum_a {}^ip_a\phi_a(t)=\sum_\alpha {}^iP_\alpha\varphi_\alpha(t) \quad (28)$$

$${}^ir(t)=\sum_a {}^ir_a\phi_a(t)=\sum_\alpha {}^iR_\alpha\varphi_\alpha(t) \quad (29)$$

$${}^ii(t)=\sum_a {}^ii_a\phi_a(t)=\sum_\alpha {}^iI_\alpha\varphi_\alpha(t) \quad (30)$$

$$k(t)=\sum_a k_a\phi_a(t)=\sum_\alpha K_\alpha\varphi_\alpha(t) \quad (31)$$

It has been assumed that the φ sets are linear combinations of the orthogonal ϕ sets or vice versa. As an example:

$$\phi_a(t)=\sum_{\alpha=0}^{a}M_{a\alpha}\varphi_\alpha(t) \quad (32)$$

Again, as an example:

$${}^iP_\alpha=\sum_{a=\alpha}^{L}M_{a\alpha}{}^ip_a \quad (33)$$

These relations are utilized in Tables I and II, where in addition to a ϕ set of modified Legendre polynomials a φ set of simple powers of t are also utilized. Similarly, in addition to orthogonal exponential polynomials as a ϕ set, powers of ϵ^{-t} are also used as a φ set. Inputs can be expanded on either set and fed into Table I depending on what is more convenient.

A General Input Environment Selected for Detailed Study

A complete step-by-step list of definitions and steps of computation is given in Tables I and II for a general class of input environments which include many practically important special cases.

The input environment considered consists of noise and signal; the desired output is assumed to derive from only the signal input in a prescribed way:

$${}^{ij}r(t)={}^ir(t)+{}^ig(t)^js(t)+{}^ih(t)^jn(t) \quad (34)$$

$${}^{ij}i(t)={}^ii(t)+{}^ig(t)^js(t) \quad (35)$$

Table IV. M_{xy} Coefficients for the Legendre Polynomials

y = 0	1	2	3	4	5	6	7	8	9	10
1	0	0	0	0	0	0	0	0	0	0
−1	2	0	0	0	0	0	0	0	0	0
1	−6	6	0	0	0	0	0	0	0	0
−1	12	−30	20	0	0	0	0	0	0	0
1	−20	90	−140	70	0	0	0	0	0	0
−1	30	−210	560	−630	252	0	0	0	0	0
1	−42	420	−1,680	3,150	−2,772	924	0	0	0	0
−1	56	−756	4,200	−11,550	16,632	−12,012	3,432	0	0	0
1	−72	1,260	−9,240	34,650	−72,072	84,084	−51,480	12,870	0	0
−1	90	−1,980	18,480	−90,090	252,252	−420,420	411,840	−218,790	48,620	0
1	−110	2,970	−34,320	210,210	−756,756	1,681,680	−2,333,760	1,969,110	−923,780	184,756

Table V. N_{xy} Coefficients for the Exponential Polynomials

x	y = 0	1	2	3	4	5	6	7	8	9	10
0	0	0	0	0	0	0	0	0	0	0	0
1	0	1	0	0	0	0	0	0	0	0	0
2	0	−2	3	0	0	0	0	0	0	0	0
3	0	3	−12	10	0	0	0	0	0	0	0
4	0	−4	30	−60	35	0	0	0	0	0	0
5	0	5	−60	210	−280	126	0	0	0	0	0
6	0	−6	105	−560	1,260	−1,260	462	0	0	0	0
7	0	7	−168	1,260	−4,200	6,930	−5,544	1,716	0	0	0
8	0	−8	252	−2,520	11,550	−27,720	36,036	−24,024	6,435	0	0
9	0	9	−360	4,620	−27,720	90,090	−168,168	180,180	−102,960	24,310	0
10	0	−10	495	−7,920	60,060	−252,252	630,630	−960,960	875,160	−437,580	92,378

Definitions of the symbols follow.

1. *Noise.* The noise ${}^ih(t)\,{}^jn(t)$ is derived by passing a stationary random function ${}^jn(t)$ through a continuous deterministic time-varying gain ${}^ih(t)$ (which is zero outside $0<t<T$, where T can be infinite). The ${}^jn(t)$ function is the number j member of a stationary random ensemble with zero average and a rational power spectral density $\Phi_{nn}(s)$. The stationary random process ${}^jn(t)$ may be correlated with the corresponding part, ${}^js(t)$, of the signal through rational cross-power spectral densities $\Phi_{sn}(s)$ and $\Phi_{ns}(s)$. The ergodic theorem applies to ensemble j, so that $\Phi_{nn}(s)$, $\Phi_{sn}(s)$, $\Phi_{ns}(s)$ are independent of j. The gain ${}^ih(t)$ is a member of an ensemble of functions, indexed by i, to which the ergodic principle does not apply.

2. *Signal.* The signal consists of two additive parts of which both or just one may be present:

   a. A deterministic set of functions ${}^ir(t)$ which are indexed by i and which are members of the i ensemble of functions. The ergodic principle does not apply to this ensemble.

   b. A set of functions ${}^ig(t)\,{}^js(t)$ which is derived by passing a stationary random function ${}^js(t)$ through a continuous deterministic time-varying gain ${}^ig(t)$ (which is zero outside $0<t<T$, where T can be infinite). The ${}^js(t)$ function is the number j member of a stationary random ensemble with zero average and a rational-power spectral density $\Phi_{ss}(s)$. The stationary random process ${}^js(t)$ may be correlated with the corresponding part of the noise, ${}^jn(t)$, through rational cross-power spectral densities $\Phi_{sn}(\omega)$ and $\Phi_{ns}(s)$. The ergodic theorem applies to ensemble j so that $\Phi_{ss}(s)$, $\Phi_{sn}(s)$, and $\Phi_{ns}(s)$ are independent of j. The gain ${}^ig(t)$ is the number i member of an ensemble, indexed by i, to which the ergodic principle does not apply.

3. *The Desired Output.* It is assumed that the desired output is based only on the signal and not the noise.

   a. The part of the desired output, ${}^ii(t)$, which is based on item 2(a) of the signal input, can be derived in any selected manner from the corresponding ${}^ir(t)$ and is the corresponding member of the same ensemble.

   b. The part of the desired output which is based on item 2(b) of the signal input, is assumed to be always identical to ${}^ig(t)\,{}^js(t)$.

4. *Correlations.* As is apparent from the foregoing there are two sets of ensembles of functions permitted in this general case.

   a. An ensemble of functions ${}^ih(t)$, ${}^ig(t)$, ${}^ir(t)$, ${}^ii(t)$, and ${}^ip(t)$, the last one being the probability distribution of utilization times. This ensemble is indexed by i and to every value of i belongs one definite specific case of all five functions; or in other words, this ensemble could be visualized as an ensemble of a matrix of these five functions. The probability of occurrence of the number i member within the ensemble is ${}^iQ$.

   It should be noted that since ${}^ip(t)$ is a probability distribution it actually represents a third ensemble, an ensemble of utilization times, which is correlated to the i ensemble in the special way defined in this paragraph; that is, to every function of the i ensemble belongs a specific ${}^ip(t)$ probability distribution of the utilization times. The five functions within the matrix of the i ensemble may be correlated with each other but they are all statistically independent from any members of the j ensemble. Averaging over the i ensemble is shown in brief by a dashed line over the symbols.

   b. A stochastic and ergodic ensemble consisting of two functions, ${}^jn(t)$ and ${}^js(t)$, slices of which are sources of, respectively, the noise, $({}^ih(t)\,{}^jn(t))$, and item 2(b) of $({}^ig(t)\,{}^js(t))$ of the signal. This can also be viewed as an ensemble of matrices of two functions. To each index j of the ensemble belongs one specific matrix of two functions, which may be correlated to each other. This ensemble can be described by the rational-power spectral densities and cross-power spectral densities $\Phi_{ss}(s)$, $\Phi_{nn}(s)$, $\Phi_{sn}(s)$, and $\Phi_{ns}(s)$ which, in view of the ergodic theorem, need not carry the index j. Functions of the j ensemble have zero first moments. The j ensemble is statistically uncorrelated with the i ensemble. Averaging over the j ensemble is indicated by a dotted overline. Averaging over both ensembles is shown by a solid line over the symbols.

The environment described here can be recognized as a general one; it is far from being trivial nor does it include only simple cases. Instead, it permits a high degree of complexity and it includes as special cases most practical input environments for which the design of time invariant linear control systems would be required. In fact, the environment assumed here even includes some time-varying systems, an important subclass which can be described by a time-varying gain.

The solution for the assumed environment is carried out in Appendix II on the basis of the relations of Appendix I.

To help in giving physical contents to the foregoing rather mathematical definitions, the case of fire control or homing will be briefly considered here. There would be signals deriving from intelligent maneuvers (in attack or avoidance) of the target which would form deterministic ensemble ${}^ir(t)$. There would be random signals, ${}^js(t)$, resulting from gust-induced and other random target maneuvers. There also would be random noise input, ${}^jn(t)$, from radar and other sources. All of these inputs will be subject to essentially time-varying gains ${}^ig(t)$, ${}^ih(t)$ resulting from the varying range which will be correlated to or depend substantially on the intelligent target maneuvers, ${}^ir(t)$, but only to a lesser degree on the other inputs. The probability distribution ${}^ip(t)$ of time between lock-on or transition to homing and explosion will depend principally on intelligent target maneuvers; ${}^ir(t)$. The desired output should be the target position or its prediction. Unfortunately it still would require the equivalent length of a full paper to describe the details beyond this sketch of the foregoing applications.[5] Anyone familiar with fire control or homing problems will recognize a number of open questions left by this sketch. However, it was the purpose here merely to tie the foregoing definitions to a physical situation rather than to show how to apply these to the fire control or homing problem. These applications furthermore represent just one of many physical

nditions which fall within the selected eneral environment.

omplete Computation Program for the Selected General Input Environment

The definitions and the corresponding ep-by-step computation program is prenented in Tables I and II. These tables ere set up visualizing programing for a ajor digital computer, and, in fact, they ave already served as a basis for such ograming. The tables are self-conained; all necessary information is within e tables. As soon as the specific input nd desired output conditions are estabshed for a system, these can be fed as put data, represented by lines 1–4 of able I(A) and lines 1–6 of Table I(B), to Table I. From here on they are rocessed through the operations given in etail in Tables I and II leading to the esult of the computation: a plot or nuical table of the optimum impulse reonse $k(t)$ (line 15, Table II), the value A f the impulse part of the response (line 4, Table II), and the value of the probailistic square error (line 16, Table II). or facilitating programing each quantity r function is defined or computed in ese tables before it is entered into any ormula in the tables, in other words a ue step-by-step process is given.

One hint for efficient programing hould be incorporated here. The bulk f the computation is represented by $_{\alpha\beta\gamma mn}$ and $F_{\alpha\beta\gamma m}$ in Table II. For the igonometric case with ten Fourier coficients ($M=L=10$) this could take 1 or hours running time on a present-day aximum-speed digital computer. Howver, this need be merely a once-in-afetime operation. The $F_{\alpha\beta\gamma mn}$ and $_{\alpha\beta\gamma m}$ are dependent only on the specific rthogonal sets and the practical number f those will not much exceed the three onsidered here in Tables I and II. Conequently $F_{\alpha\beta\gamma mn}$ and $F_{\alpha\beta\gamma m}$ can be stored ermanently on magnetic tape. The me used up with $F_{\alpha\beta\gamma mn}$ and $F_{\alpha\beta\gamma m}$ durg the solution of an individual problem then merely the sequential (without earch) reading time of the tape. Simarly $\Psi_{\alpha\beta\gamma}''$, etc., which depend on the ata of the specific problem and which are uch smaller in number than $F_{\alpha\beta\gamma mn}$ can e computed and put in the quick access emory before starting to read the tape of $_{\alpha\beta\gamma mn}$. The fact that many of the $_{\alpha\beta\gamma mn}$ are zero permits further savings time. Such steps reduce the computer nning time for the solution of even the ost involved individual problem to the der of minutes.

Complete programing for the trigonometric orthogonal set (the most complete) in Tables I and II requires about 50–100 man-hours. This too is a once-in-a-lifetime need. After the program is set up, merely the Fourier or Taylor coefficients and pole and zero locations, describing the specific input-output environment, need to be introduced into the program for an individual solution. This means that, given the general program, only a few minutes are needed to adapt it to the individual case.

One more remark is needed in connection with the tables. In these it has been assumed that the power spectral density of the noise $\Phi_{nn}(s)$ is a rational fraction. This excludes white noise in the strict sense although it can always be represented completely adequately in the rational form of $\Phi_{nn}(s)=N_0/(s^2-(q_1^{II})^2)$ if q_1^{II} is selected large enough. It should be emphasized that the equations are adaptable to white noise in the usual sense, but this was omitted in the tables for the sake of brevity.

Illustrative Example

Statement of Problem

What is desired is a system to produce the minimum probabilistic square error in the following environment.

1. Probability distribution function is independent of the input and it is defined by:

$$^{1}p(t)=\frac{1}{2}[u(t)-u(t-2)] \tag{36}$$

meaning uniform probability of utilization of the output between $t=0$ and $t=2$, zero probability of utilization outside these limits.

2. The input signal consists of two components:

a. A deterministic input:

$$^{1}r(t)=u(t)[1+t] \tag{37}$$

b. A stationary random signal with a power spectral density of:

$$\Phi_{ss}(s)=\frac{84.4}{(2.25-s^2)(4-s^2)} \tag{38}$$

which acts upon the system without modification, $0<t<2$, that is, through a gain of:

$$^{1}g(t)=u(t)-u(t-2) \tag{39}$$

3. Input noise consists of a stationary random function with a power spectral density of:

$$\Phi_{nn}(s)=\frac{168.8}{(9-s^2)(16-s^2)} \tag{40}$$

which enters the system without modification, $0<t<2$, that is, through a gain of:

$$^{1}h(t)={}^{1}g(t)=u(t)-u(t-2) \tag{41}$$

4. Correlations are absent between the two random inputs ($\Phi_{ns}(s)=\Phi_{sn}(s)=0$) and between the random and deterministic inputs. The i ensemble has only one single set of functions $^{1}p(t)$, $^{1}r(t)$, $^{1}g(t)$, and $^{1}h(t)$ which have probability unity:

$$^{1}Q=1 \qquad {}^{i}Q=0 \text{ if } i\neq 1 \tag{42}$$

5. Desired output is identical at all times to the sum of the deterministic and the random parts of the signal input excluding noise.

Selection of Orthogonal Sets

The first step toward solution is the decision on the use of one specific orthogonal set. Since $p(t)=0$ for $t>2$ it appears to be desirable to select an orthogonal set over the finite interval $0<t<1$, that is, either trigonometric or Legendre functions if Tables I and II are to be used. Should $r(t)$ be a higher-order polynomial, it might be advantageous to use Legendre polynomials. Since, however, $r(t)$ is only first order, trigonometric functions will be used because they tend to give better fits.

Normalization of Time Scale

Since the trigonometric set, as used in Tables I and II, is defined on the interval $0<t<1$, the time scale will be changed in the above specifications so that $T=2$ on the old scale will now coincide with $T=1$ on the new. This modifies the specifications to:

$$^{1}p(t)=[u(t)-u(t-1)] \tag{36A}$$

$$^{1}r(t)=u(t)[1+2t] \tag{37A}$$

$$\Phi_{ss}(s)=\frac{672}{(9-s^2)(16-s^2)} \tag{38A}$$

$$\Phi_{nn}(s)=\frac{1{,}344}{(36-s^2)(64-s^2)} \tag{39A}$$

$$^{1}g(t)={}^{1}h(t)=[u(t)-u(t-1)] \tag{40A}$$

Input Data to Table I Now Prepared

First, decision is made on the length of the Fourier series representations to be used. Selected is:

$$L=12 \qquad M=20 \tag{43}$$

Now it is necessary to determine from the above specifications of the problem the quantities going into lines *1* through *7* of Table I(A) and lines *1* through *8*, Table I(B). Lines *1* through *4* of Table I(A) and lines *1* through *6* of Table I(B) refer to data to be directly taken from the specifications of the problem, whereas

lines 5 through 7 of Table I(A) and lines 7 and 8 of Table I(B) represent preliminary computations to be performed for the individual problem from its specifications before starting the machine computation.

Quantities, Table I(A)

Line 1:

${}^1r(t) = u(t)[1+2t]$

from equation 37(A).

Line 2:

${}^1i(t) = {}^1r(t) = u(t)[1+2t]$

from statement of problem.

Line 3:

${}^1p(t) = [u(t) - u(t-1)]$

from equation 36(A).

Line 4:

$${}^iQ = \begin{cases} 1, & i=1 \\ 0, & i \neq 1 \end{cases}$$

from equation 42.

Lines 5 and 6, by Fourier expansion of the functions given in lines 1 and 2:

$i_0 = r_0 = 2.000000$
$i_1 = r_1 = 0.810569$
$i_2 = r_2 = 0.000000$
$i_3 = r_3 = 0.090063$
$i_4 = r_4 = 0.000000$
$i_5 = r_5 = 0.032423$
$i_6 = r_6 = 0.000000$
$i_7 = r_7 = -0.016542$
$i_8 = r_8 = 0.000000$
$i_9 = r_9 = -0.010007$
$i_{10} = r_{10} = 0.000000$
$i_{11} = r_{11} = 0.006699$
$i_{12} = r_{12} = 0.000000$

Line 7, by Fourier expansion of the function given in line 3:

$p_0 = 1.000000$
$p_i = 0.000000$ if $1 \leqslant i \leqslant 12$

Quantities, Table I(B)

Line 1:

${}^1g(t) = u(t) - u(t-1)$

from equation 40(A).

${}^js(t)$, specified in line 6 through Φ_{ss}

Line 2:

${}^1h(t) = u(t) - u(t-1)$

from equation 40(A).

${}^jn(t)$, specified in line 6 through Φ_{nn}

Line 3:

${}^{1j}i(t) = {}^1g(t){}^js(t)$

from Table I(B).

Line 4:

${}^1p(t) = [u(t) - u(t-1)]$

from equation 36(A).

Line 5:

$${}^1Q = \begin{cases} 1, & i=1 \\ 0, & i \neq 1 \end{cases}$$

from equation 42.

Line 6:

$$\Phi_{ss} = \frac{672}{(9-s^2)(16-s^2)}$$

from equation 38(A).

$$\Phi_{nn} = \frac{1,344}{(36-s^2)(64-s^2)}$$

from equation 39(A).

$\Phi_{sn} = \Phi_{ns}(s) = 0$

no w_ξ^I or w_ξ^{II} present

$q_1^I = -3 \quad q_2^I = +3 \quad B^I = 672 \quad H^I = 4$

$q_3^I = -4 \quad q_4^I = +4$

$q_1^{II} = -6 \quad q_2^{II} = +6 \quad B^{II} = 1,344 \quad H^{II} = 4$

$q_3^{II} = -8 \quad q_4^{II} = +8$

Line 7:

$K_1^{II} = 16 \quad K_2^I = -16$

$K_3^I = -12 \quad K_4^I = +12$

$K_1^{II} = +4 \quad K_2^{II} = -4$

$K_3^{II} = -3 \quad K_4^{II} = +3$

Line 8:

${}^1g_0 = 1 \quad {}^1g_x = 0 \quad x \neq 0$

from equation 40(A).

${}^1h_0 = 1 \quad {}^1h_x = 0 \quad x \neq 0$

Results of Example

At this point the IBM (International Business Machines Corporation) *709* takes over and in short order the results appear:

Minimum end-sigma error: $s = 0.8567$
Impulse part of the response: $A = 0.9571$

Fourier coefficients of the continuous part, $k_c(t)$, of the impulse response for the optimum system:

$k_0 = +0.01908$
$k_1 = -0.19435$
$k_2 = -0.32922$
$k_3 = -0.38183$
$k_4 = -0.37539$
$k_5 = -0.34687$
$k_6 = -0.30923$
$k_7 = -0.27329$
$k_8 = -0.23716$
$k_9 = -0.20527$
$k_{10} = -0.18201$
$k_{11} = -0.15777$
$k_{12} = -0.13243$
$k_{13} = -0.05770$
$k_{14} = -0.02594$
$k_{15} = -0.01758$
$k_{16} = -0.01404$
$k_{17} = -0.09945$
$k_{18} = -0.08963$
$k_{19} = -0.06394$
$k_{20} = -0.06098$

The Fourier coefficients including those belonging to the impulse A are graphically shown in Fig. 1. While this spectrum cannot, strictly speaking, be described as a frequency response, still it is of a similar nature. In this sense Fig. 1 represents a partial band suppression filtering effect.

The continuous part of the impulse response of the optimum system as a function of time, $k_c(t)$, is shown in Fig. 2. This curve can be approximated quite well by three exponentials as also shown in Fig. 2 by curve $\tilde{k}_c(t)$. Considering that the waviness of $k_c(t)$ is actually a Fourier ripple, the approximation is seen to be quite good.

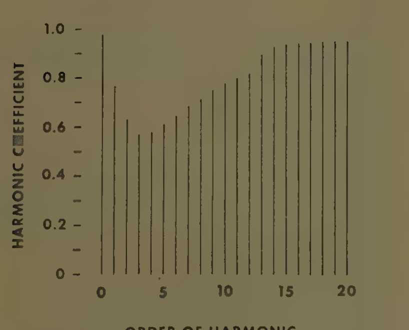

Fig. 1. Fourier coefficient of optimum impulse response

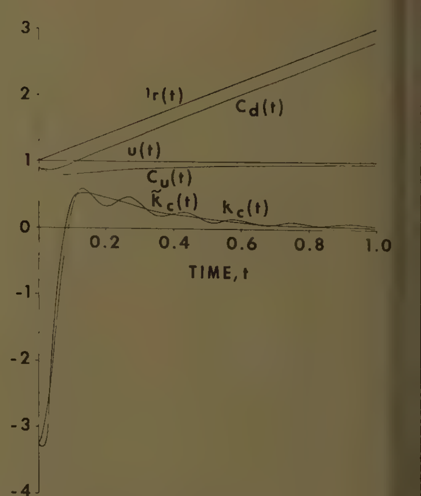

Fig. 2. Optimum impulse response, $k_c(t)$, its approximation, $\tilde{k}_c(t)$, response $c_u(t)$ to unit step function $u(t)$ and response $c_d(t)$ to deterministic input ${}^1r(t)$

The equation of curve $\tilde{k}_c(t)$ is:

$$k_c(t)=1.08\epsilon^{-4.24t}-35.33\epsilon^{-45.9t}+31.00\epsilon^{-55.1t} \quad (44)$$

So that the approximate optimum transfer function including the impulse:

$$K(s)=\frac{1.08}{s+4.24}-\frac{35.33}{s+45.9}+\frac{31.00}{s+55.1}+0.9571 \quad (45)$$

$$=1.005\frac{8.883\times 10^{-5}s^3+9.047\times 10^{-3}s^2-1.845\times 10^{-2}s+1}{9.325\times 10^{-5}s^3+9.814\times 10^{-3}s^2+2.282\times 10^{-2}s+1}$$

From $k_c(t)$ and A the response to a unit step $u(t)$ is easily obtained by numerical integration and it is shown as curve $c_u(t)$ in Fig. 2. Similarly the response $c_d(t)$ to the deterministic part of the input of the example, ${}^1r(t)$, is obtained by numerical convolution with $k_c(t)$ and is also plotted in Fig. 2.

In reviewing these last two response curves it should be borne in mind that what is designed here is not a system that gives optimum response to a step input or even the deterministic input ${}^1r(t)$ by itself. Rather, this is a system which gives optimum response on the average to the deterministic input ${}^1r(t)$ and the random signal input $s(t)$ in the presence of noise $n(t)$. Also the noise conditions of this example are very severe since the noise power nearly equals the total signal power with the noise bandwidth not too significantly different from the signal bandwidth. Yet the accomplished optimum filtering is quite effective, about an order of magnitude reduction in mean square error, from 8.0 without filtering to $s=0.86$ with filtering.

Conclusions

A complete design process is introduced to obtain the impulse response function of the continuous time invariant linear system which has the smallest average square error for such times when its output is used. To solve problems of a complexity common in control-engineering practice it is necessary to utilize major digital computers, and the paper presents all the necessary equations in an organized form for the programing of the computers. An example is given illustrating the use of the equations and the programs prepared from the equations. This example is carried to the determination of an approximate optimum Laplace transfer function. In a companion paper[3] a corresponding design process is introduced for sampled systems.

Appendix I

Substituting equations 2 through 9 into equation 16 there results equation 13 with the following definitions:

$$f=\psi_{ii}(0,0)=\psi(0,0) \quad (46)$$

$$f'=\psi'(0,0) \quad (47)$$

$$f''=\psi''(0,0) \quad (48)$$

$$f_m'=\int_0^T dt_1\phi_m(t_1)\psi'(t_1,t_1) \quad (49)$$

$$f_m''=\int_0^T dt_1\phi_m(t_1)\psi''(t_1,t_1) \quad (50)$$

$$f_{mn}''=\int_0^T dt_1\phi_m(t_1)\int_0^T dt_2\phi_n(t_2)\times \psi''(t_1,t_1-t_2) \quad (51)$$

Defining:

$$\Psi_{abc}=\overline{p_a i_b i_c} \quad (52)$$

$$\Psi_{abd}'=\overline{p_a r_b i_c} \quad (53)$$

$$\Psi_{abc}''=\overline{p_a r_b r_c} \quad (54)$$

and

$$F_{abcm}=\int_0^T dt_3\phi_m(\tau_3)\int_{t_3}^T \phi_a(t_1)\times \phi_b(t_1-t_3)\phi_c(t_1)dt_1 \quad (55)$$

$$F_{abcmn}=\int_0^T dt_3\phi_m(t_3)\int_0^T dt_2\phi_n(t_2)\times \int_{t_3}^T dt_1\phi_a(t_1)\phi_b(t_1-t_3)\phi_c(t_1-t_2) \quad \text{if } t_2\leqq t_3 \quad (56A)$$

$$F_{abcmn}=\int_0^T dt_3\phi_m(t_3)\int_0^T dt_2\phi_n(t_2)\times \int_{t_2}^T dt_1\phi_a(t_1)\phi_b(t_1-t_2)\phi_c(t_1-t_3) \quad \text{if } t_2\geqq t_3 \quad (56B)$$

Using the definitions of equations 52 through 56(B) and 2 through 8, equations 46 through 51 are transformed into equations 19 through 24.

It is now assumed that ${}^\circ A$ is the strength of impulse and

$${}^\circ k_c(t)=\sum_n {}^\circ k_n\phi_n(t)$$

is the continuous part in the impulse response of the system which is optimum in the sense of having the smallest end sigma error among all invariant linear systems:

$${}^\circ k(t)={}^\circ A\delta(t)+k_c(t)$$
$$={}^\circ A\delta(t)+\sum_n {}^\circ k_n\phi_n(t) \quad (57)$$

Further, ${}^\epsilon A$ is an arbitrary constant and ${}^\epsilon k_c(t)=\Sigma{}^\epsilon k_n\phi_n(t)$ are arbitrary functions on $0<t<T$, for which ${}^\epsilon k_c(0)={}^\epsilon k_c(T)=0$. Then, any invariant linear impulse response of the form of equation 5 can be expressed for $0<t<T$ as:

$$k(t)={}^\circ A\delta(t)+\sum_n {}^\circ k_n\phi_n(t)+\epsilon_1{}^\epsilon A\delta(t)+\epsilon_2\sum {}^\epsilon k_n\phi_n(t) \quad (58)$$

with ϵ_1 and ϵ_2 arbitrary parameters.

Substituting equation 58 into equation 13, a necessary condition of equation 57 representing the optimum system is recognized as:

$$\left.\frac{\partial s}{\partial \epsilon_1}\right|_{\substack{\epsilon_1=0\\ \epsilon_2=0}}=0 \qquad \left.\frac{\partial s}{\partial \epsilon_2}\right|_{\substack{\epsilon_1=0\\ \epsilon_2=0}}=0 \quad (59)$$

From simultaneous solution of these last equations considering that ${}^\epsilon A$ and ${}^\epsilon k_n$ are arbitrary, there results equations 14 through 18.

Appendix II

With the definitions and notations of Table I as explained under "A General Input Environment Selected for Detailed Study" the input and desired output can be written respectively:

$${}^{ij}r(t)={}^i r(t)+{}^i g(t){}^j s(t)+{}^i h(t){}^j n(t) \quad (60)$$

$${}^{ij}i(t)={}^i i(t)+{}^i g(t){}^j s(t) \quad (61)$$

and by Taylor expansion:

$${}^i g(t)=\sum_x {}^i g_x t^x \quad (62)$$

$${}^i h(t)=\sum_x {}^i h_x t^x \quad (63)$$

The base functions $\phi_a{}^{I}(\theta)$, $\phi_a{}^{II}(\theta)$, $\phi_a{}^{III}(\theta)$, and $\phi_a{}^{IV}(\theta)$ in equations 6–9 will now be assumed to form complete orthonormal sets on $0<t<T$. Then, in the manner of equation 12, the coefficients of equations 6 through 9 can be expressed as:

$${}^{ij}p_a={}^i p_a \quad (64)$$

$${}^{ij}r_b={}^i r_b+\sum_x {}^i g_x{}^j s_{xb}+\sum_x {}^i h_x{}^j n_{xb} \quad (65)$$

$${}^{ij}i_b={}^i i_b+\sum_x {}^i g_x{}^j s_{xb} \quad (66)$$

where, in general:

$${}^i u_\zeta=\int_0^T {}^i u(\theta)\phi_\zeta(\theta)d\theta \quad (67)$$

$${}^j v_{x\zeta}=\int_0^T {}^j v(\theta)\theta^x\phi_\zeta(\theta)d\theta \quad (68)$$

Index l of equation 12 has been replaced by ij since the general ensemble l includes both the i and j ensembles of the present problem. Now, if the probability of function i within the i ensemble is ${}^iQ$ and the probability of the function j within the j ensemble is ${}^jQ$, then, substituting equations 64–66 into equation 54 and replacing, respectively, subscript b by c and x by y where it is necessary to keep the indexes of two terms in a product separate:

$$\Psi_{abc}''=\overline{p_a r_b r_c}+\sum_x\sum_y \overline{(p_a g_x g_y)}\,\overline{(s_{xb}s_{yc})}+\sum_x\sum_y \overline{(p_a g_x h_y)}\,\overline{(s_{xb}n_{yc})}+\sum_x\sum_y \overline{(p_a h_x g_y)}\,\overline{(n_{xb}s_{yc})}+\sum_x\sum_y \overline{(p_a h_x h_y)}\,\overline{(n_{xb}n_{yc})} \quad (69)$$

where assumptions made under "A General Input Environment Selected for Detailed Study" regarding statistical correlation or statistical independence of the various components have been considered, as well as the

fact that functions of the j ensemble have zero averages and where the dashed line denotes averaging over the i ensemble and the dotted line denotes averaging over the j ensemble, so that, for example:

$$\overline{({}^ip_a{}^ig_x{}^ig_y)}=\sum_i {}^iQ^i p_a{}^ig_x{}^ig_y \tag{70}$$

$$\overset{\cdots\cdots}{(s_{xb}s_{yc})}=\sum_j {}^jQ^j s_{x\beta}{}^js_{y\gamma} \tag{71}$$

Similarly, from equations 52 and 53:

$$\Psi_{abc}'=\overline{p_a r_b i_c}+\sum_x\sum_y \overline{(p_a g_x g_y)}\overset{\cdots\cdots}{(s_{xb}s_{yc})}+\sum_x\sum_y \overline{(p_a h_x g_y)}\overset{\cdots\cdots}{(n_{xb}s_{yc})} \tag{72}$$

$$\Psi_{abc}=\overline{p_a i_b i_c}+\sum_x\sum_y \overline{(p_a g_x g_y)}\overset{\cdots\cdots}{(s_{xb}s_{yc})} \tag{73}$$

Up to this point no use was made of the assumption that the j set is stationary and the ergodic principle applies to it. Consequently, it is necessary now to further explore the terms of the type of equation 71, that is, the last factors in the right-hand side of equations 69, 72 and 73. From equation 68 and 71:

$$\overset{\cdots\cdots}{(s_{xb}s_{yc})}=\sum_j {}^jQ\int_0^T t_1{}^x\, {}^js(t_1)\phi_b{}^I(t_1)dt_1\times\int_0^T t_2{}^y\, {}^js(t_2)\phi_c{}^I(t_2)dt_2 \tag{74}$$

Interchanging integrals and summations:

$$\overset{\cdots\cdots}{(s_{xb}s_{yc})}=\int_0^T dt_1\int_0^T dt_2 t_1{}^x t_1{}^y\phi_b{}^I(t_1)\times\phi_c{}^I(t_2)\sum {}^jQ^j s(t_1){}^js(t_2) \tag{75}$$

but

$$\phi_{ss}(t_2-t_1)=\sum_j {}^jQ^j s(t_1){}^js(t_2) \tag{76}$$

where $\phi_{ss}(t_2-t_1)$ is the autocorrelation function of the signal component ${}^js(t)$ which can be obtained from the power spectral density by inverse Fourier transformation:

$$\begin{aligned}\phi_{ss}(\tau)&=\frac{1}{2\pi j}\int_{-j\infty}^{j\infty}\Phi_{ss}(s)\epsilon^{s\tau}ds\\&=\sum_\eta \delta_\tau\, Res_{q_\eta I}[\Phi_{ss}(s)\epsilon^{s\tau}]\\&=\sum_\eta \delta_\tau\epsilon^{q_\eta{}^I\tau}\, Res_{q_\eta}{}^I[\Phi_{ss}(s)]\\&=\sum_\eta \delta_\tau K_\eta{}^I\epsilon^{q_\eta{}^I\tau}\end{aligned} \tag{77}$$

where the notations are explained in lines 6–10 of Table I(B), except:

$$\delta_\tau=\begin{cases}1 & \text{if } \tau>0,\ Re\ [q_\eta]<0\\-1 & \tau<0,\ Re\ [q_\eta]>0\\0 & \tau>0,\ Re\ [q_\eta]>0\\0 & \tau<0,\ Re\ [q_\eta]<0\end{cases} \tag{78}$$

Then:

$$\overset{\cdots\cdots}{(s_{xb}s_{yc})}=\sum_\eta K_\eta{}^I\int_0^T dt_1\int_0^T dt_2 t_1{}^x t_2{}^y\delta_{t_2-t_1}\times\epsilon^{q_\eta I(t_2-t_1)}\phi_b{}^{II}(t_1)\phi_c{}^{II}(t_2) \tag{79}$$

Equation 79 establishes the pattern for all the averages over the j ensemble contained in equations 69–75 whether they refer to the residues of a power spectral density or a cross-power spectral density.

References

1. Probabilistic Error as Measure of Control-System Performance, J. Zaborszky, J. W. Diesel. *AIEE Transactions*, pt. II (*Applications and Industry*), vol. 78, July 1959, pp. 163–68.

2. Random Processes in Automatic Control (book), J. H. Laning, Jr., R. H. Battin. McGraw-Hill Book Company, Inc., New York, N. Y., 1956, App. D.

3. Design of Sampled-Data Control Systems for Minimum Probabilistic Error, J. Zaborszky, J. W. Diesel. *AIEE Transactions*, see pp. 54–62 of this issue.

4. Optimum Design and Mass Distributions of Homing Missiles, R. C. Booton, Jr. Dynamic Analysis and Control Laboratory, Massachusetts Institute of Technology, Cambridge, Mass., 1950.

5. Investigation of Feasibility of Designing Homing Aircraft Flight Control Systems for Minimum Probabilistic Error, J. Zaborszky, John W. Diesel. *AIEE Transactions*, see pp. 66–70 of this issue.

Design of Sampled-Data Control Systems for Minimum Probabilistic Error

J. ZABORSZKY
MEMBER AIEE

J. W. DIESEL
ASSOCIATE MEMBER AIEE

THE "PROBABILISTIC ERROR" or "end-sigma error," meaning the average penalized error for such times when the output is actually being used, has been proposed as a measure of control system performance in an earlier publication.[1] A companion paper[2] presents a complete design process to find the time invariant continuous linear system which possesses the minimum probabilistic square error in a given environment of random and deterministic signals and random noise. A corresponding design process is presented in this paper for impulse-sampled systems. The result of this design is a linear digital filter to be used with a given plant in order to keep the probabilistic square error to a minimum. Working equations are presented, which were developed with digital computer programing and solutions in mind. Such solutions can be obtained for very general signal input and noise environments. However, the proposed method works best when the output is being utilized within a time interval including a nonexcessive number of samples.

In addition to the design process of a minimum end-sigma error filter, the paper also contains an s domain expression for evaluating the end sigma error of a given linear system. The latter can be used for any length of time within which the output is to be used.

Some General Aspects of the Method

Probabilistic square error has been defined:[1]

$$\text{s}=\int_0^T \widetilde{p(t)e^2(t)dt} \tag{1}$$

where $p(t)$ is the probability distribution of all times when the output is used, and $e(t)$ is the error of the control system. T can be infinity if the output may be used over all times. s is the end sigma.

In both the methods presented in this paper, error $e(t)$ is defined continuously, not just at the sampling instants, as the difference of the desired output $i(t)$, and the actual output $c(t)$. The actual output $c(t)$ is assumed to be produced by a type of system sketched in Fig. 1. Here $G(s)$ is a linear and fixed plant of known transfer function; $H(s)$ is a fixed linear and continuous filter; and $D^*(z)$ is a digital type filter, the target of optimization. The two impulse samplers are assumed to be synchronized with a sampling interval of T_s.

An s domain expression for end sigma has also been obtained[1] for a deterministic input

$$\text{s}=\lim_{t=0}\mathfrak{L}_2^{-1}[P(-s)((E(s)^{\circledast}E(s))] \tag{2}$$

where $\mathfrak{L}_2^{-1}$ means the two-sided inverse Laplace transform and the $^{\circledast}$ denotes complex convolution. $E(s)$ is the La-

Paper 59-831, recommended by the AIEE Feedback Control Systems Committee and approved by the AIEE Technical Operations Department for presentation at the AIEE Summer and Pacific General Meeting and Air Transportation Conference, Seattle, Wash., June 21–26, 1959. Manuscript submitted February 3, 1959; made available for printing May 13, 1959.

J. Zaborszky is with Washington University, St. Louis, Mo., and Consultant to the McDonnell Aircraft Corporation; J. W. Diesel is with the McDonnell Aircraft Corporation, St. Louis, Mo.

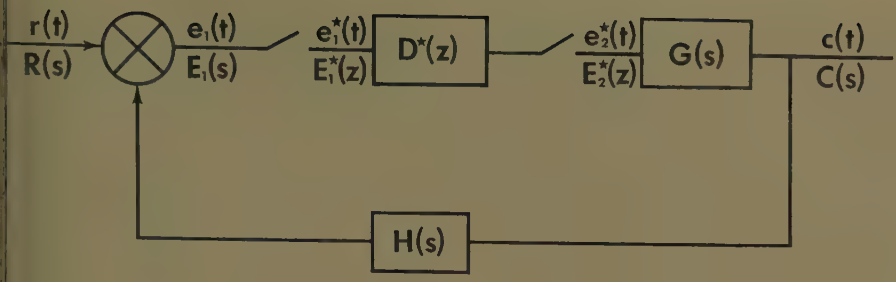

Fig. 1. Block diagram of system

ace transform of the error $e(t)$. $P(s)$ is
ne Laplace transform of $p(t)$.

-Domain Evaluation of End-Sigma Error

Equation 2 can be restated as

$$=-\sum \mathrm{Res}_{P(-s)}\,[P(-s)(E(s)^{\oplus}E(s))] \quad (3)$$

here $\Sigma\,\mathrm{Res}_{P(-s)}[\quad]$ means the sum of
ne residues of the expression in brackets
t all poles of $P(-s)$. Inherent in
quation 3 is the assumption that all
ngularities of $P(-s)$ are in the right
alf s plane to the right of some positive
bscissa of uniform convergence, a, and
l singularities of $E(s)^{\oplus}E(s)$ are to the
ft of the abscissa of uniform con-
ergence a. This assumption will tend
be automatically satisfied for all
ctual cases since $t=0$ is the time of
ctivation so that all errors and all times
f output utilization lie in positive time.
urther, $p(t)$ being a probability dis-
ibution: $\lim_{t=\infty} p(t)=0$ so that $P(s)$
as no singularities on the axis of imagin-
ries. Note that the foregoing restric-
ons admit all stable control systems
nd many unstable ones.

It is not necessary to assume that
$(-s)$ is a rational function, although
must be single valued and it must
pproach 0 when s is approaching
nfinity. Generally it will be convenient,
owever, to express $P(s)$ as a rational
unction, potentially by expanding $p(t)$
ver a set of orthogonal exponential
olynomials[3] which transform into
ational partial fractions. By the latter
rocess all unstable linear systems can
e also included along with the stable
ne if the exponential, powers of which
re forming the polynomials, is selected
be e^{bt} with $b>a$, where a is the abscissa
f uniform convergence for $E(s)$ in the
plane. So it will be assumed for the
est of this discussion that $P(-s)$ is a
ational fraction

$$(-s)=\frac{A(s)}{B(s)} \quad (4)$$

and further

$$B(q_i)=0,\quad A(q_i)\neq 0,\quad B'(q_i) = \left.\frac{dB(s)}{ds}\right|_{s=q_i}\neq 0,\quad i=1,2,3\ldots J \quad (5)$$

all q_i different, all poles of first order. Again the latter assumption is not necessary but convenient.

Now with reference to Fig. 1

$$C(s)=G(s)E_2{}^*(z)=G(s)K_1{}^*(z)R^*(z) \quad (6)$$

$$K_1{}^*(z)=\frac{D^*(z)}{1+D^*(z)GH^*(z)} \quad (7)$$

and the transform of the error is

$$E(s)=I(s)-C(s) \quad (8)$$

if $I(s)$ is the transform of the desired output. Further, the notation is introduced

$$X(s)=E(s)^{\oplus}E(s) \quad (9)$$

which in Appendix I is reduced to

$$\begin{aligned}X(s)=\sum \mathrm{Res}_z[&z^{-1}\,II^*(z,s)-\\ &K_1{}^*(z)R^*(z)GI^*(z,s)-\\ &K_1{}^*(\epsilon^{sT_s}z^{-1})R^*(\epsilon^{sT_s}z^{-1})IG^*(z,s)+\\ &K_1{}^*(z)K_1{}^*(\epsilon^{sT_s}z^{-1})R^*(z)R^*\times\\ &(\epsilon^{sT_s}z^{-1})GG^*(z,s)]\end{aligned} \quad (10)$$

where $\Sigma\,\mathrm{Res}_z$ is the sum of the residues in the z plane of the expression following Res_z at all singularities located within the circle around the origin of the z plane with a radius of e^{aT_s}. Here a is the abscissa of uniform convergence for $E(s)$ in the s plane and T_s is the sampling interval. Further, as an example

$$GI^*(z,s)=Z_v[G(v)I(s-v)] \quad (11)$$

where Z_v means the z transform of the expression in brackets with z being defined as $z=e^{vT}$. The variable s is to be treated as a parameter. The meaning of other notations in equations 6–11 is the conventional one of the extensive z-transform literature. Substituting into equation 3

$$s=-\sum_{i=1}^{J}\frac{A(q_i)}{B'(q_i)}X(q_i) \quad (12)$$

Note that $X(s)$ need be evaluated only at specific values of s.

The end-sigma error can be computed from equation 12 using definitions of equations 4–11 for any rational $G(s)$, $H(s)$, $D^*(z)$, $R(s)$, and $I(s)$ regardless of stability if $p(t)$ is expanded on orthogonal polynomial exponential functions.[3]

Illustrative Example

The following case, highly simplified for brevity, will be discussed.

A plant of transfer function

$$G(s)=\frac{1}{s+1} \quad (13)$$

is to be incorporated into a loop with a digital filter to yield zero error at all sampling instants after the first two.

The input is

$$r(t)=1+2t \quad (14)$$

The desired output is

$$i(t)=r(t) \quad (15)$$

The probability distribution of times of utilization of the output is

$$p(t)=(\epsilon^{-0.5t}-\epsilon^{-t}) \quad (16)$$

The sampling interval is

$$T_s=1/3 \quad (17)$$

Solution

First the necessary z transforms are found by conventional techniques

$$G^*(z)=GH^*(z)=\frac{1}{1-z^{-1}\epsilon^{-1/3}} \quad (18)$$

$$D^*(z)=\frac{(1-z^{-1}\epsilon^{-1/3})(2z^{-1}-z^{-2})}{(1-z^{-1})^2} \quad (19)$$

This latter can be found[4] from the condition of zero error at the sampling instants after 2/3 seconds. Then from equation 7

$$K_1{}^*(z)=(1-z^{-1}\epsilon^{-1/3})(2z^{-1}-z^{-2}) \quad (20)$$

Further

$$R^*(z)=\frac{1-0.3333z^{-1}}{(1-z^{-1})^2} \quad (21)$$

Now with equations 11, 13, 14, and 15 and the residue theorem

$$\begin{aligned}GI^*(z,s)&=Z_v\left\{\frac{1}{v+1}\left[\frac{1}{s-v}+\frac{2}{(s-v)^2}\right]\right\}\\ &=Z_q\left\{\frac{s-v+2}{(s-v)^2(v+1)}\right\}\\ &=\frac{1}{2\pi j}\int_{-j\infty}^{+j\infty}\frac{s-u+2}{(u-s)^2(u+1)}\,\frac{1}{1-z^{-1}\epsilon^{uT_s}}\,du\\ &=\frac{z^{-1}[s(3\epsilon^{-s/3}-\epsilon^{1/3})+(9\epsilon^{-s/3}-7\epsilon^{1/3})]+z^{-2}[s(3\epsilon^{(s+1)/3}-5)+(9\epsilon^{(s+1)/3}-11)]}{3\epsilon^{s/3}(\epsilon^{1/3}-z^{-1})(\epsilon^{-s/4}-z^{-1})^2(s+1)^2}\end{aligned} \quad (22)$$

Similarly,

$$II^*(z,s)=\left[\frac{1}{3s^3(1-z^{-1})^2(1-z^{-1}\epsilon^{S/3})^2}\right]\times$$
$$\{z^{-2}[s^2(3\epsilon^{2S/3}-8\epsilon^{S/3}-3)+s(12\epsilon^{2S/3}-16\epsilon^{S/3}-12)+(24\epsilon^{2S/3}-24)]+(z^{-1}+z^{-3}\epsilon^{S/3})[s^2(5-\epsilon^{S/3})+s(16-8\epsilon^{S/3})+(24-24\epsilon^{S/3})]\} \tag{23}$$

$$IG^*(z,s)=\left[\frac{1}{3(s+1)^2(1-z^{-1}\epsilon^{(s+1)/3})(1-z^{-1})^2}\right]\times$$
$$\{z^{-1}[s(5-3\epsilon^{(s+1)/3})+(11-9\epsilon^{(s+1)/3})]+z^{-2}[s(\epsilon^{(s+1)/3}-3)+(7\epsilon^{(s+1)/3}-9)]\} \tag{24}$$

$$GG^*(z,s)=\frac{z^{-1}(\epsilon^{-1/3}-\epsilon^{(S+1)/3})}{(s+2)(1-z^{-1}\epsilon^{-1/3})(1-z^{-1}\epsilon^{(S+1)/3})} \tag{25}$$

Now from equation 16[1]

$$P(-s)=\frac{A(s)}{B(s)}=\frac{0.5}{(s-0.5)(s-1)} \tag{26}$$

So

$$q_1=+0.5$$

$$q_2=+1 \tag{27}$$

and then with equation 12

$$\varepsilon=-\frac{A(0.5)}{B'(0.5)}X(0.5)-\frac{A(1)}{B'(1)}X(1) \tag{28}$$

Equation 26 defines $A(s)$ and $B(s)$. Further, by equation 10

$$X(0.5)=\sum \mathrm{Res}_z\left[\frac{1}{z^2(z-1)^2(z-\epsilon^{1/6})^2}\right] \tag{29}$$

$$[-0.09663z^6+0.7456z^5-2.2733z^4+3.4481z^3-2.6952z^2+1.0406z-0.1593]=4.550$$

$$X(1.0)=\sum \mathrm{Res}_z\left[\frac{1}{z^2(z-1)^2(z-\epsilon^{1/3})^2}\right]$$

$$[-0.07534z^6+0.6630z^5-2.2738z^4+3.7893z^3-3.1733z^2+1.2913z-0.2048]=1.136 \tag{30}$$

To calculate the residues in these sums the path of integration can be any circle with radius $\epsilon^{a/3}$ where $0<a<0.5$, so no residues are to be found for poles outside this circle.

Finally, from equations 28–30

$$\varepsilon=3.414 \tag{31}$$

This indicates that, although after the second sampling instant the error is zero at the sampling instants, end sigma is still quite large. The reason is that end sigma, the average square error for such times when the output is used, includes the error building up between sampling instants, and this is substantial for the simple system selected for the example. In fact, the error just preceding the nth sampling instant is easily shown to be $(1+2nT_s)(1-1/\sqrt[3]{\epsilon})=0.28(1+2nT_s)$; about 28% of the output and linearly increasing with time.

t-Domain Evaluation of End-Sigma Error and Finding Optimum System Under End-Sigma Criterion

Applying the general definition of the end-sigma error, as given in equation 1, to a sampled-data system of the type shown in Fig. 1, it reduces (Appendix II) to a form

$$\varepsilon=f-2\sum_m k_1(mT_s)f_m+\sum_m\sum_n k_1(mT_s)k_1(nT_s)f_{mn} \tag{32}$$

and for the optimum system the following condition equation results:

$$[f_{mn}]k_1(nT_s)]=f_m] \qquad \begin{matrix} n=0,1,2\ldots M \\ m=0,1,2\ldots M\end{matrix} \tag{33}$$

where

$$f=\Psi_{ii}(0,0)=\overbrace{\int_0^T {}^lp(t)^li^2(t)dt} \tag{34}$$

$$f_m=\Psi_{ig}'(0,m)=\sum_{\mu=0}^{M}\times \overbrace{{}^lr((\mu-m)T_s)\int_0^T {}^li(t)g(t-\mu T_s)^lp(t)dt} \tag{35}$$

$$f_{mn}=\Psi_{gg}''(m,m-n)=\sum_{\mu=0}^{M}\sum_{\nu=0}^{M}\times \overbrace{{}^lr((\mu-m)T_s)^lr((\nu-n)T_s)}\times \int_0^T\overbrace{g(t-\mu T_s)g(t-\nu T_s)^lp(t)dt} \tag{36}$$

Here ${}^lr(t)$ is the number l member of the ensemble of inputs to the control system, ${}^li(t)$ is the corresponding desired output which need not be identical to the input and, ${}^lp(t)$ is the probability distribution of times when the output resulting from an input of type ${}^lr(t)$ is used.[1] $g(t)$ is the inverse transform of $G(s)$, that is, the impulse response of the fixed continuous plant. The bracket indicates averaging over the ensemble indexed by l. $k_1(mT_s)$ is the inverse z transform of $K_1^*(z)$ in equation 7. In equation 32 $k_1(nT_s)$ means the sampled-impulse response for the general system; in equation 33 it refers to the same quantity for the optimum system. T_s is the sampling interval; m, n, μ, ν are numbers of individual sampling instants. $T=MT_s$ is the duration of output utilization, that is $p(t)=0$, $t>T$.

The optimum system is readily obtained by inverting matrix equation 33,

$$k_1(nT_s)]=[f_{mn}]^{-1}f_m] \tag{37}$$

and using this, equation 32 for the optimum system reduces to

$$\varepsilon=f-\sum_m k_1(mT_s)f_m \tag{38}$$

As in the case of continuous systems[2] it is found to be advantageous to employ expansions of ${}^lp(t)$ and ${}^li(t)$ like

$${}^lp(t)=\sum_\alpha^L {}^lp_\alpha\phi_\alpha{}^I(t) \tag{39}$$

$${}^li(t)=\sum_\delta^L {}^li_\delta\phi_\delta{}^{II}(t) \tag{40}$$

These can be either Taylor or Fourier series as explained in reference 2. With these assumptions the elements of the matrix take the form (Appendix IV).

$$f=\sum_\alpha^L\sum_\delta^L\sum_\epsilon^L \Psi_{\alpha\delta\epsilon}F_{\alpha\delta\epsilon} \tag{41}$$

$$f_m=\sum_{\mu=m}^M\sum_\alpha^L\sum^L \Psi_{\alpha(\mu-m)\delta}{}'F_{\alpha\delta\mu}{}' \tag{42}$$

$$f_{mn}=\sum_{\mu=m}^M\sum_{\nu=n}^M\sum_\alpha^L \Psi_{\alpha(\mu-m)(\nu-n)}{}''F_{\alpha\mu\nu}{}'' \tag{43}$$

Again there is an important similarity to the case of the continuous system. Of the two factors in equations 41–43 the last ($F_{\alpha\delta\epsilon}$, $F_{\alpha\delta\mu}{}'$, and $F_{\alpha\mu\nu}{}''$) depend on the specific selection of the base functions $\phi_\alpha{}^I(t)$ and $\phi_\delta{}^{II}(t)$ in equations 37 and 38 and on the $G(s)$ transfer function of the fixed part of the system, $G(s)$ in Fig. 1. These factors are independent, however, of the specific input environment. On the other hand, the first factors ($\Psi_{\alpha\delta\epsilon}$, $\Psi_{\alpha(\mu-m)\delta}{}'$, and $\Psi_{\alpha(\mu-m)(\nu-n)}{}''$) depend essentially on the specific input environment. Consequently, as in the continuous case, it is possible to precompute the F factors for a given system and use the Ψ factors to represent specific input conditions. Beyond this over-all similarity there actually are significant differences in the details. Notably the F factors depend only on the selected ϕ sets for the continuous system but they also depend on the fixed plant for the discrete one.

The final result of the design should be the transfer function or program $D^*(z)$ of the digital filter. From equation 7

$$D^*(z)=\frac{K_1^*(z)}{1-K_1^*(z)GH^*(z)} \tag{44}$$

Now $G(s)$ and $H(s)$ represent the fixed part of the system. Consequently $GH^*(z)$ would be known either as a rational fraction or as a series with all terms known.

$$GH^*(z)=gh(0)+gh(T_s)z^{-1}+gh(2T_s)z^{-2}+\ldots \tag{45}$$

n the other hand, in the series of $K_1^*(z)$

$$^*(z)=k_1(0)+k_1(T_s)z^{-1}+\ldots+ k_1(MT_s)z^{-M}+\ldots \quad (46)$$

ly the first $M+1$ terms are defined by uation 37. Consequently, only the st $M+1$ terms of $D^*(z)$ can be found om equation 44. True, the rest of the rms are inconsequential since it has en assumed that $p(t)=0$ if $t>MT_s$, at is the output is not used beyond MT_s. Let

$$^*(z)=d(0)+d(T_s)z^{-1}+\ldots+ d(MT_s)z^{-M}+\ldots \quad (47)$$

Then after substituting equations 45–47 to equation 44, multiplying through by e denominator of equation 44, and uating coefficients of like powers of z both sides

$$))(1-k_1(0)gh(0))=k_1(0) \quad (48)$$

$$d(0)(k_1(0)gh(T_s)+k_1(T_s)gh(0))+ d(T_s)(1-k_1(0)gh(0))=k_1(T_s) \quad (49)$$

$$d(0)(k_1(0)gh(2T_s)+k_1(T_s)gh(T_s)+ k_1(2T_s)gh(0)) \quad (50)$$

$$d(T_s)(k_1(0)gh(T_s)+k_1(T_s)gh(0))+ d(2T_s)(1-k_1(0)gh(0))=k_1(2T_s)$$

ne continuation is obvious, and so is e fact that the coefficients (up to the efficient of z^{-M}) in equation 47 can found one by one from the successive uation of 48–50.

There only remains finding a rational nction $D^*(z)$ which has an expansion e first M terms of which are now de- ned.

Let

$$^*(z)=\frac{d_0'+d_1'z^{-1}+d_2'z^{-2}+\ldots+d'_{M'}z^{-M'}}{1+d_1''z^{-1}+\ldots+d''_{M''}z^{-M''}} \quad (51)$$

$M=M'+M''$, and an M'' value is lected, then equations 47 and 51 termine all coefficients in equation 51, rough the $M+1$ simultaneous linear uations:

$$'=d(0) \quad (52)$$

$$'=d(T_s)+d(0)d_1'' \quad (53)$$

$$'=d(2T_s)+d(T_s)d_1''+d(0)d_2'' \text{ etc.} \quad (54)$$

ne $D^*(z)$ transfer function defined in is manner is realizable as a linear gital filter program[5] although it is of potentially higher order than is desir- ble.

In the latter case, approximations lower order can be substituted. The ality of such approximations can be served by finding their probabilistic ror from equations 12 or 32 and compar- g it with the probabilistic error of the timum system, equation 38.

A General Input Environment Selected for Detail Study

The same general input environment is selected here for finding the optimum sampled data system as was selected in the companion paper[2] for continuous systems. The advantage of this selection is that it is very broad so that it includes as special cases many practically important environmental conditions. The environment is described by the equations

$${}^{ij}r(t)={}^ir(t)+{}^i\mathfrak{g}(t)\,{}^js(t)+{}^i\mathfrak{h}(t)\,{}^jn(t) \quad (55)$$

$${}^{ij}i(t)={}^ii(t)+{}^i\mathfrak{g}(t)\,{}^js(t) \quad (56)$$

The input defined in equation 55 consists of a deterministic input ${}^ir(t)$, a slice of a random-signal input ${}^js(t)$ through a time varying gain ${}^i\mathfrak{g}(t)$, and a slice of random noise ${}^in(t)$ through another time varying gain ${}^i\mathfrak{h}(t)$. The part of the desired output, ${}^{ij}i(t)$, deriving from the random part of the input signal ${}^i\mathfrak{g}(t)\,{}^js(t)$ is assumed to be identical to this part of the input. However, the deterministic part of the desired output, ${}^ii(t)$, can derive in any arbitrary way from ${}^ir(t)$, the deterministic part of the input. The basic definitions of this assumed environment are summarized, lines 1–4, in Table I(A) and lines 1–6 in Table I(B). In the companion paper[2] the details of this input environment are discussed at length.

Complete Computation Program

The definitions and the corresponding step-by-step computation program are presented in Tables I and II. These tables were set up visualizing programing for a major digital computer, and in fact they have already served as a basis for such programing. The tables are self contained; all necessary information is within the tables. As soon as the transfer function of the fixed plant part of the system is obtained and the specific input and desired output conditions are established for a system, these can be fed as input data (represented by line 2 of Table II; lines 1–7 of Table I(A) and lines 1–7 of Table I(B)) into Tables I and II. From here on they are processed through the operation given in detail in Tables I and II leading to the results of the computation: a numerical table of the optimum impulsive response $k_1(mT_s)$ (line 12, Table II), and the value of the true mean square error (line 14, Table II). For facilitating programing each quantity or function is defined or computed in these tables before it is entered into any formula in the tables, in other words, a true step-by-step process is given. The structure of the tables very closely parallels those presented for continuous systems. This is not surprising since the same input environment was selected in both papers. Nevertheless, there are some important differences in the details most of which can be traced to two principal causes:

1. The system considered here is sampled. As a result, data of the samplers must be introduced (lines 5–7, Table I(A)). Values of some functions at individual sampling instants (e.g., $\mathfrak{h}(mT_s)$ or $\mathfrak{g}(mT_s)$) are used in the computation in addition to the Fourier or Taylor coefficients (e.g., r_β or $\mathfrak{g}_x$) of these same functions. The latter exclusively are used in Table I and II of reference 2.

2. In contrast to reference 2 the system considered here has two fixed plants, $G(s)$ and $H(s)$ (Fig. 1) within the loop. Consequently the data of this transfer function $G(s)\ H(s)$ must also be introduced into the computation (line 2, Table II). Furthermore coefficients $F_{\alpha\mu\nu}''$ and $F_{\alpha\delta\mu}'$ are in turn products of three factors (lines 6 and 7, Table II). The Φ factor (with appropriate subscripts) is a function of the selected orthogonal sets only and accordingly can be precalculated on the basis of its defining equations (lines 4 and 5, Table III). The other two factors G_κ or G_χ are Fourier coefficients of the impulsive response of the fixed plant.

Finally, Tables I and II of this paper give the computation process for only two sets of base functions, both defined on a finite interval $0<t<T$. This is because the assumption of finite duration of output utilization ($p(t)=0$, $t<T$) is inherent in the method developed to deal with sampled systems, while this restriction was absent in the continuous case. The two orthogonal sets (trigonometric and Legendre polynomial) are defined in the headings of Table I(A). More details about these are given in the companion paper.[2] In spite of these minor deviations of detail the entire structure and the method of using these tables parallels the case of continuous systems[2] so closely that the use of these tables is believed to be adequately illustrated by the extensive example given in reference 2. Accordingly, no additional example will be included here.

Conclusion

Two ways are explored in this paper to measure the performance of sampled data control systems by their probabilistic error.

The s-plane approach permits the evaluation of the probabilistic error for

Table I(A). Ensembles of Deterministic Inputs

Definitions or Computation Steps	Trigonometric orthogonal set $C_x(t) = \cos\frac{x\pi t}{T}$, $0 \le x \le L$, $0 \le t \le T$; time normalized so that $T = 1$.	Legendre orthogonal set $\mathcal{P}_x(t) = \sum_{y=0}^{x} M_{xy}\left(\frac{t}{T}\right)^y$, $0 \le x \le L$, $0 \le t \le T$; M_{xy} in Table IV of reference 2, time normalized so that $T = 1$.
1.	${}^ir(t)$ Deterministic input number i in ensemble, ${}^ir(t) = 0$, $t < 0$.	
2.	${}^ii(t)$ Desired output number i in ensemble, ${}^ii(t) = 0$, $t < 0$.	
3.	${}^ip(t)$ Probability distribution of output utilization time for input number i.	
4.	${}^iQ$ Probability of input number i in ensemble.	
5.	T_s Sampling interval.	
6.	$t = \mu T_s$, time at the number μ sampling instant. $t = \nu T_s$, time at the number ν sampling instant.	
7.	$T = MT_s$, duration of output utilization; ${}^ip(t) = 0$, $t > T$.	
8.	${}^ii_o = \int_0^1 {}^ii(t)\,dt$ ${}^ii_\delta = 2\int_0^1 {}^ii(t)\cos\delta\pi t\,dt$, $1 \le \delta \le L$	${}^ii_o = \int_0^1 {}^ii(t)\,dt$ ${}^ii_\delta = (2\delta+1)\int_0^1 {}^ii(t)\mathcal{P}_\delta(t)\,dt$
9.	${}^ip_o = \int_0^1 {}^ip(t)\,dt$ ${}^ip_\alpha = 2\int_0^1 {}^ip(t)\cos\alpha\pi t\,dt$, $1 \le \alpha \le L$	${}^ip_o = \int_0^1 {}^ip(t)\,dt$ ${}^ip_\alpha = (2\alpha+1)\int_0^1 {}^ip(t)\mathcal{P}_\alpha(t)\,dt$
10.	${}^iI_o = {}^ii_o$ ${}^iI_\delta = \frac{1}{2}{}^ii_d, \begin{cases} d = \delta, & 1 \le \delta \le L \\ d = -\delta, & -L \le \delta \le -1 \end{cases}$	${}^iI_\delta = \sum_{d=\delta}^{L} M_{d\delta}\,{}^ii_d$, $0 \le \delta \le L$
11.	${}^iP_o = {}^ip_o$ ${}^iP_\alpha = \frac{1}{2}{}^ip_a, \begin{cases} a = \alpha, & 1 \le \alpha \le L \\ a = -\alpha, & -L \le \alpha \le -1 \end{cases}$	${}^iP_\alpha = \sum_{a=\alpha}^{L} M_{a\alpha}\,{}^ip_a$, $0 \le \alpha \le L$
12.	$\overline{\overline{\Psi}}''_{\alpha\mu\nu} = \sum_i {}^iQ\,{}^iP_\alpha\,{}^ir(\mu T_s)\,{}^ir(\nu T_s)$	
13.	$\overline{\overline{\Psi}}'_{\alpha\mu\delta} = \sum_i {}^iQ\,{}^iP_\alpha\,{}^ir(\mu T_s)\,{}^iI_\delta$	
14.	$\overline{\overline{\Psi}}_{\alpha\delta\epsilon} = \sum_i {}^iQ\,{}^iP_\alpha\,{}^iI_\delta\,{}^iI_\epsilon$	

Note: Throughout these tables the position of a subscript defines its nature, the symbol appearing in this position defines the value of the subscript. For instance id in line 10 Table I denotes $i\delta$ from line 8 Table I with $\delta = d$, or $Md\delta$ in line 10 Table I denotes the number in row d and column δ of Table IV reference 2.

	Trigonometric orthogonal set	Legendre orthogonal set
1.	${}^{ij}s(t)={}^{i}\mathfrak{g}(t)\,{}^{j}s(t)$, signal input; a product of ${}^{i}\mathfrak{g}(t)$, the number i member of a set of time-varying gain functions, and ${}^{j}s(t)$, the number j member of an ergodic ensemble of signals. i and j ensembles statistically independent. Functions of j ensembles have zero mean. ${}^{i}\mathfrak{g}(t)=0$, $t<0$, $t>T$. ${}^{j}s(t)$ to be specified only through power spectral densities in line 6.	
2.	${}^{ij}n(t)={}^{i}\mathfrak{h}(t)\,{}^{j}n(t)$, noise input; a product of ${}^{i}\mathfrak{h}(t)$, the number i member of a set of time-varying gain functions, and ${}^{j}n(t)$, the number j member of an ergodic ensemble of noise functions. ${}^{i}\mathfrak{h}(t)=0$, $t<0$, $t>T$. See line 6.	
3.	${}^{ij}i(t)={}^{ij}s(t)$, desired output.	
4.	${}^{i}p(t)$, probability distribution of output utilization time, member i in ensemble of ${}^{i}\mathfrak{g}$, ${}^{i}\mathfrak{h}$, ${}^{i}p$.	
5.	${}^{i}Q$, probability of member number i in ensemble of ${}^{i}\mathfrak{g}$, ${}^{i}\mathfrak{h}$, ${}^{i}p$.	
6.	$\underset{ss}{\Phi}(s)=B^{I}\frac{\prod_\xi(s-w_\xi^{I})}{\prod_\lambda(s-q_\lambda^{I})}$, $1\le\lambda\le H^{I}$; $\underset{nn}{\Phi}(s)=B^{II}\frac{\prod_\xi(s-w_\xi^{II})}{\prod_\lambda(s-q_\lambda^{II})}$, $1\le\lambda\le H^{II}$; $\underset{sn}{\Phi}(s)=B^{III}\frac{\prod_\xi(s-w_\xi^{III})}{\prod_\lambda(s-q_\lambda^{III})}$, $1\le\lambda\le H^{III}$; $\underset{ns}{\Phi}(s)=B^{IV}\frac{\prod_\xi(s-w_\xi^{IV})}{\prod_\lambda(s-q_\lambda^{IV})}$, $1\le\lambda\le H^{IV}$; power spectral densities and cross-spectral densities of ergodic ensembles ${}^{j}s(t)$, ${}^{j}n(t)$. In general, $q_\lambda^{(\omega)}=q_\lambda^{I}$ if $u=I$.	
7.	K_λ^{I} = Residue at q_λ^{I} of $\Phi_{ss}(s)$, K_λ^{II} = Residue at q_λ^{II} of $\Phi_{nn}(s)$, K_λ^{III} = Residue at q_λ^{III} of $\Phi_{sn}(s)$, K_λ^{IV} = Residue at q_λ^{IV} of $\Phi_{ns}(s)$; $K_\lambda^{(\omega)}=K_\lambda^{I}$ if $u=I$.	
8.	${}^{i}\mathfrak{g}_x=\frac{1}{x!}\cdot\frac{d^x}{dt^x}\,{}^{i}\mathfrak{g}(t)\Big\vert_{t=0}$, $0\le x\le X$; ${}^{i}\mathfrak{h}_x=\frac{1}{x!}\cdot\frac{d^x}{dt^x}\,{}^{i}\mathfrak{h}(t)\Big\vert_{t=0}$, $0\le x\le X$.	
9.	$\Delta_1(q_\lambda^{(\omega)})=\begin{cases}1, & \mathrm{Re}\{q_\lambda^{(\omega)}\}>0\\ 0, & \mathrm{Re}\{q_\lambda^{(\omega)}\}<0\end{cases}$; $\Delta_2(q_\lambda^{(\omega)})=\begin{cases}0, & \mathrm{Re}\{q_\lambda^{(\omega)}\}>0\\ 1, & \mathrm{Re}\{q_\lambda^{(\omega)}\}<0\end{cases}$; $\Delta_3(b)=\begin{cases}1, & b=0\\ 0, & b\ne0\end{cases}$; $\Delta_4(b)=\begin{cases}0, & b=0\\ 1, & b\ne0\end{cases}$; $\delta_1(\Theta)=\begin{cases}1, & \Theta<0\\ 0, & \Theta\ge0\end{cases}$; $\delta_2(\Theta)=\begin{cases}0, & \Theta<0\\ 1, & \Theta\ge0\end{cases}$	
10.	$\overset{I}{V}(\xi,\eta,x,y)=\sum_{\lambda=1}^{H^I}K_\lambda^I\left\{\left[\frac{y!(-1)^\xi e^{-q_\lambda^I}\Delta_1}{(j\pi\eta-q_\lambda^I)^{y+1}}+\Delta_2\sum_{k=0}^{y}\frac{y!(-1)^{\xi+\eta}}{(y-k)!(j\pi\eta-q_\lambda^I)^{k+1}}\right]\cdot\left[\frac{-x!(-1)^\xi e^{q_\lambda^I}}{(j\pi\xi+q_\lambda^I)^{x+1}}+\sum_{\ell=0}^{x}\frac{x!}{(x-\ell)!(j\pi\xi+q_\lambda^I)^{\ell+1}}\right]+\sum_{k=0}^{y}\frac{y!}{(y-k)!(j\pi\eta-q_\lambda^I)^{k+1}}\cdot\left[\frac{\Delta_3}{x+y-k+1}+\Delta_4\left(\frac{(x+y-k)!}{(j\pi[\xi+\eta])^{x+y-k+1}}-\sum_{\ell=0}^{x+y-k}\frac{(x+y-k)!(-1)^{\xi+\eta}}{(x+y-k-\ell)!(j\pi[\xi+\eta])^{\ell+1}}\right)\right]\right\}$	$\overset{I}{V}(\xi,\eta,x,y)=\sum_{\lambda=1}^{H^I}K_\lambda^I\left\{\left[\frac{(y+\eta)!e^{-q_\lambda^I}\Delta_1}{(-q_\lambda^I)^{y+\eta+1}}+\Delta_2\sum_{k=0}^{y+\eta}\frac{(y+\eta)!}{(y+\eta-k)!(-q_\lambda^I)^{k+1}}\right]\cdot\left[\frac{-(x+\xi)!e^{q_\lambda^I}}{(q_\lambda^I)^{x+\xi+1}}+\sum_{\ell=0}^{x+\xi}\frac{(x+\xi)!}{(x+\xi-\ell)!(q_\lambda^I)^{\ell+1}}\right]+\sum_{k=0}^{y+\eta}\frac{(y+\eta)!}{(y+\eta-k)!(-q_\lambda^I)^{k+1}}\cdot\left[\frac{1}{x+\xi+y+\eta-k+1}\right]\right\}$
11.	$\overset{I}{J}(\delta,\epsilon,x,y)=\frac{1}{4}\left[\overset{I}{V}(\delta,\epsilon,x,y)+\overset{I}{V}(-\delta,\epsilon,x,y)+\overset{I}{V}(\delta,-\epsilon,x,y)+\overset{I}{V}(-\delta,-\epsilon,x,y)\right]$	$\overset{I}{J}(\delta,\epsilon,x,y)=\sum_{\xi=0}^{L}\sum_{\eta=0}^{L}\left[\sum_{b=0}^{L}\frac{M_{b\delta}M_{b\xi}}{(2b+1)^{-1}}\right]\cdot\left[\sum_{c=0}^{L}\frac{M_{c\epsilon}M_{c\eta}}{(2c+1)^{-1}}\right]\overset{I}{V}(\xi,\eta,x,y)$
12.	$\overset{(\omega)}{W}(\mu,\xi,x)=\sum_{\lambda=1}^{H^{(\omega)}}K_\lambda^{(\omega)}\left\{\Delta_1(q_\lambda^{(\omega)})\frac{-x!e^{-q_\lambda^{(\omega)}\mu T_s}}{(j\pi\xi-q_\lambda^{(\omega)})^{x+1}}+\Delta_2(q_\lambda^{(\omega)})\sum_{k=0}^{x}\frac{-x!(-1)^\xi e^{(1-\mu T_s)q_\lambda^{(\omega)}}}{(x-k)!(j\pi\xi-q_\lambda^{(\omega)})^{k+1}}+\Delta_3(\mu)\frac{x!}{(j\pi\xi-q_\lambda^{(\omega)})^{x+1}}+\Delta_4(\mu)\sum_{k=0}^{x}\frac{x!(-1)^{j\pi\xi\mu T_s}(\mu T_s)^{x-k}}{(x-k)!(j\pi\xi-q_\lambda^{(\omega)})^{k+1}}\right\}$	$\overset{(\omega)}{W}(\mu,\xi,x)=\sum_{\lambda=1}^{H^{(\omega)}}K_\lambda^{(\omega)}\left\{\Delta_1(q_\lambda^{(\omega)})\frac{-(x+\xi)!e^{-q_\lambda^{(\omega)}\mu T_s}}{(-q_\lambda^{(\omega)})^{x+\xi+1}}+\Delta_2(q_\lambda^{(\omega)})\sum_{k=0}^{x+\xi}\frac{-(x+\xi)!e^{q_\lambda^{(\omega)}(1-\mu T_s)}}{(x+\xi-k)!(-q_\lambda^{(\omega)})^{k+1}}+\sum_{k=0}^{x+\xi}\frac{(x+\xi)!(\mu T_s)^{x+\xi-k}}{(x+\xi-k)!(-q_\lambda^{(\omega)})^{k+1}}\right\}$
13.	$\mathcal{F}^{(\omega)}(\mu,\delta,x)=\frac{1}{2}\left[\overset{(\omega)}{W}(\mu,\delta,x)+\overset{(\omega)}{W}(\mu,-\delta,x)\right]$	$\mathcal{F}^{(\omega)}(\mu,\delta,x)=\sum_{\xi=0}^{L}\sum_{d=0}^{L}\frac{M_{d\delta}M_{d\xi}}{(2d+1)^{-1}}\overset{(\omega)}{W}(\mu,\xi,x)$
14.	$\mathcal{J}^{(\omega)}(\mu,\nu)=\sum_{\lambda=1}^{H^{(\omega)}}\left[\delta_2(\nu-\mu)\Delta_2(q_\lambda^{(\omega)})-\delta_1(\nu-\mu)\Delta_1(q_\lambda^{(\omega)})\right]K_\lambda^{(\omega)}e^{q_\lambda^{(\omega)}(\nu-\mu)T_s}$	
15.	$\overset{\cdots}{\Psi}''_{\alpha\mu\nu}=\sum_i {}^{i}Q\left\{{}^{i}p_\alpha\left[{}^{i}\mathfrak{g}(\mu T_s)\,{}^{i}\mathfrak{g}(\nu T_s)\mathcal{J}^{I}(\mu,\nu)+{}^{i}\mathfrak{h}(\mu T_s)\,{}^{i}\mathfrak{h}(\nu T_s)\mathcal{J}^{II}(\mu,\nu)+{}^{i}\mathfrak{g}(\mu T_s)\,{}^{i}\mathfrak{h}(\nu T_s)\mathcal{J}^{III}(\mu,\nu)+{}^{i}\mathfrak{h}(\mu T_s)\,{}^{i}\mathfrak{g}(\nu T_s)\mathcal{J}^{IV}(\mu,\nu)\right]\right\}$	
16.	$\overset{\cdots}{\Psi}'_{\alpha\mu\delta}=\sum_i {}^{i}Q\left\{\sum_{x=0}^{X}{}^{i}p_\alpha\left[{}^{i}\mathfrak{g}(\mu T_s)\,{}^{i}\mathfrak{g}_x\mathcal{F}^{I}(\mu,\delta,x)+{}^{i}\mathfrak{h}(\mu T_s)\,{}^{i}\mathfrak{g}_x\mathcal{F}^{IV}(\mu,\delta,x)\right]\right\}$	
17.	$\overset{\cdots}{\Psi}_{\alpha\delta\epsilon}=\sum_i {}^{i}Q\left\{\sum_{x=0}^{X}\sum_{y=0}^{X}{}^{i}p_\alpha\left[{}^{i}\mathfrak{g}_x\,{}^{i}\mathfrak{g}_y\mathcal{J}^{I}(\delta,\epsilon,x,y)\right]\right\}$	

Table II. The Optimum System

	Trigonometric orthogonal set	Legendre orthogonal set
1.	$\Psi''_{\alpha\mu\nu}=\overline{\overline{\overline{\Psi}}}{}''_{\alpha\mu\nu}+\dddot{\overline{\overline{\overline{\Psi}}}}{}''_{\alpha\mu\nu}$, $\Psi'_{\alpha\mu\delta}=\overline{\overline{\overline{\Psi}}}{}'_{\alpha\mu\delta}+\dddot{\overline{\overline{\overline{\Psi}}}}{}'_{\alpha\mu\delta}$, $\Psi_{\alpha\delta\epsilon}=\overline{\overline{\overline{\Psi}}}_{\alpha\delta\epsilon}+\dddot{\overline{\overline{\overline{\Psi}}}}_{\alpha\delta\epsilon}$, (See lines 12–14, Table I.A, and lines 15–17, Table I.B).	
2.	$G(s)=K\dfrac{\prod_{\xi}(s-u_{\xi})}{\prod_{\lambda}(s-v_{\lambda})}$, transfer function of continuous plant, simple poles only, $\mathrm{Re}\{v_{\lambda}\}<0,\ 1\le\lambda\le N;\ v_{\lambda}=0,\ \lambda=0.$ $A_{\lambda}=$ Residue at v_{λ} of $G(s)$; if $G(s)$ has no poles at origin, set $A_o=0$.	
3.	$G_{\chi}=\Delta_3(\chi)A_o+\sum_{\lambda=1}^{N}\dfrac{-A_{\lambda}v_{\lambda}}{(\pi\chi)^2+v_{\lambda}^2}\left[1-(-1)^{\chi}e^{+v_{\lambda}}\right],\ 0\le\chi\le L$	$G_{\chi}=\sum_{c=0}^{L}\sum_{\xi=0}^{L}M_{c\chi}M_{c\xi}(2c+1)\left\{\dfrac{A_o}{\xi+1}+\sum_{\lambda=1}^{N}A_{\lambda}\cdot\left[\dfrac{\xi!}{(v_{\lambda})^{\xi+1}}-\sum_{k=0}^{\xi}\dfrac{e^{v_{\lambda}}\,\xi!}{(\xi-k)!(v_{\lambda})^{k+1}}\right]\right\}$
4.	$\Phi''_{\alpha\mu\nu\chi\mathcal{H}}=\Delta_3(\alpha+\chi+\mathcal{H})\left\{\cos(\pi[\chi\mu+\mathcal{H}\nu]T_s)\cdot[1-\delta_1(\nu-\mu)\cdot\mu T_s-\delta_2(\nu-\mu)\cdot\nu T_s]\right\}$ $+\Delta_4(\alpha+\chi+\mathcal{H})\left\{\dfrac{\sin(\pi[\alpha+\chi\cdot(1-\mu T_s)+\mathcal{H}\cdot(1-\nu T_s)])-\delta_1(\nu-\mu)\sin(\pi[\alpha+\mathcal{H}(\mu-\nu)T_s])}{\pi(\alpha+\chi+\mathcal{H})}-\dfrac{\delta_2(\nu-\mu)\sin(\pi[\alpha+\chi(\nu-\mu)T_s])}{\pi(\alpha+\chi+\mathcal{H})}\right\}$	$\Phi''_{\alpha\mu\nu\chi\mathcal{H}}=\sum_{c=0}^{\chi}\sum_{k=0}^{\mathcal{H}}\dfrac{\chi!\mathcal{H}!(-1)^{c+k}}{(\chi-c)!(\mathcal{H}-k)!c!k!}\cdot\dfrac{(\mu T_s)^{c+k}-\delta_1(\nu-\mu)\cdot(\mu T_s)^{\alpha+\chi+\mathcal{H}+1}-\delta_2(\nu-\mu)\cdot(\nu T_s)^{\alpha+\chi+\mathcal{H}+1}}{(\alpha+\chi-c+\mathcal{H}-k+1)}$
5.	$\Phi'_{\alpha\delta\mu\chi}=\Delta_3(\alpha+\delta+\chi)\{\cos(\pi[\chi\mu T_s])\cdot[1-\mu T_s]\}$ $+\Delta_4(\alpha+\delta+\chi)\left\{\dfrac{\sin(\pi[\alpha+\delta+\chi\cdot(1-\mu T_s)])-\sin(\pi[\alpha+\delta]\mu T_s)}{\pi(\alpha+\delta+\chi)}\right\}$	$\Phi'_{\alpha\delta\mu\chi}=\sum_{c=0}^{\chi}\dfrac{\chi!(-1)^c}{(\chi-c)!c!}\cdot\dfrac{(\mu T_s)^c-(\mu T_s)^{\alpha+\delta+\chi+1}}{(\alpha+\delta+\chi-c+1)}$
6.	$F''_{\alpha\mu\nu}=\sum_{\chi=-L}^{L}\sum_{\mathcal{H}=-L}^{L}G_{\chi}G_{\mathcal{H}}\Phi''_{\alpha\mu\nu\chi\mathcal{H}}$	$F''_{\alpha\mu\nu}=\sum_{\chi=0}^{L}\sum_{\mathcal{H}=0}^{L}G_{\chi}G_{\mathcal{H}}\Phi''_{\alpha\mu\nu\chi\mathcal{H}}$
7.	$F'_{\alpha\delta\mu}=\sum_{\chi=-L}^{L}G_{\chi}\Phi'_{\alpha\delta\mu\chi}$	$F'_{\alpha\delta\mu}=\sum_{\chi=0}^{L}G_{\chi}\Phi'_{\alpha\delta\mu\chi}$
8.	$F_{\alpha\delta\epsilon}=\Delta_3(\alpha+\delta+\epsilon)$	$F_{\alpha\delta\epsilon}=\dfrac{1}{\alpha+\delta+\epsilon+1}$
9.	$f_{mn}=\sum_{\mu=m}^{M}\sum_{\nu=n}^{M}\sum_{\alpha=-L}^{L}\Psi''_{\alpha(\mu-m)(\nu-n)}F''_{\alpha\mu\nu}$	$f_{mn}=\sum_{\mu=m}^{M}\sum_{\nu=n}^{M}\sum_{\alpha=0}^{L}\Psi''_{\alpha(\mu-m)(\nu-n)}F''_{\alpha\mu\nu}$
10.	$f_m=\sum_{\mu=m}^{M}\sum_{\alpha=-L}^{L}\sum_{\delta=-L}^{L}\Psi'_{\alpha(\mu-m)\delta}F'_{\alpha\delta\mu}$	$f_m=\sum_{\mu=m}^{M}\sum_{\alpha=0}^{L}\sum_{\delta=0}^{L}\Psi'_{\alpha(\mu-m)\delta}F'_{\alpha\delta\mu}$
11.	$f=\sum_{\alpha=-L}^{L}\sum_{\delta=-L}^{L}\sum_{\epsilon=-L}^{L}\Psi_{\alpha\delta\epsilon}F_{\alpha\delta\epsilon}$	$f=\sum_{\alpha=0}^{L}\sum_{\delta=0}^{L}\sum_{\epsilon=0}^{L}\Psi_{\alpha\delta\epsilon}F_{\alpha\delta\epsilon}$.
12.	$k_1(nT_s)]=\left[f_{mn}\right]^{-1}f_m]$, $0\le m\le M$, $0\le n\le M$	
13.	$K_1^{\star}(z)=\sum_{n=0}^{M}k_1(nT_s)z^{-n}$	
14.	$\zeta=f-\sum_{m=0}^{M}k_1(mT_s)f_m$	

ly error sampled feedback system consting of a linear fixed plant and a alizable[5] linear digital compensator. s presented here the s-plane method ermits finding a system yielding miniium deterministic error only by cut d try. However, this method is apicable whether the duration of output ilization is finite or infinite. This ethod is useful for deterministic inputs.

The time-domain approach produces oth the value of the probabilistic error r a given linear system and the design a linear digital compensator or filter produce minimum mean-square error ith a given plant. Complete working uations are presented for obtaining on digital computer the design of the ptimum digital filter for a very general ass of input environments. This design applicable to cases where the duration output utilization is finite and prefably includes a limited number of mpling instants. On the digital comuter solutions are obtained in a matter minutes. Hand computation by this ethod is not visualized.

Appendix I

$$(s)=X_{ii}(s)+X_{ir}(s)+X_{ri}(s)+X_{rr}(s) \quad (57)$$

here

$$_{ii}(s)=I(s)^*I(s)$$
$$=\frac{1}{2\pi j}\int_{b-j\infty}^{b+j\infty} I(w)I(s-w)dw \quad (58)$$

$$_{ir}(s)=\frac{-1}{2\pi j}\int_{b-j\infty}^{b+j\infty} K_1^*(\epsilon^{wT_s})\times R^*(\epsilon^{wT_s})G(w)I(s-w)dw \quad (59)$$

$$_{ri}(s)=\frac{-1}{2\pi j}\int_{b-j\infty}^{b+j\infty} K_1^*(\epsilon^{(s-w)T_s})\times R^*(\epsilon^{(s-w)T_s})G(s-w)I(w)dw \quad (60)$$

$$_{rr}(s)=\frac{1}{2\pi j}\int_{b-j\infty}^{b+j\infty} K_1^*(\epsilon^{wT_s})K_1^*\times (\epsilon^{(s-wT)s})R^*(\epsilon^{wT_s})R^*(\epsilon^{(s-w)T_s})\times G(w)G(s-w)dw \quad (61)$$

here b is to be selected to the right in the plane of any singularities of functions of nly w within the integrals; s is to be elected so that all singularities lie to the ght of b for any function of $(s-w)$ within e integrals. Equations 58–61 can be educed by an application[4] of Poisson's mmation formula. Equation 59 will be iscussed as an example; the other three re quite similarly handled. The infinite tegral in equation 59 can be broken up to sections as follows

$$_{ir}(s)=\frac{-1}{2\pi j}\sum_{n=-\infty}^{n=+\infty}\int_{b+j(-\Omega/2+n\Omega)}^{b+j(+\Omega/2+n\Omega)}\times K_2^*(e^{wT_s})R^*(\epsilon^{wT_s})G(w)I(s-w)dw \quad (62)$$

where

$$\Omega=\frac{2\pi}{T_s} \quad (63)$$

set

$$v=w-jn\Omega$$

then interchanging summation and integration

$$X_{ir}(s)=\frac{-1}{2\pi j}\int_{b-j\Omega/2}^{b+j\Omega/2} K_1^*(\epsilon^{vT_s})R^*(\epsilon^{vT_s})\times \left[\sum_{n=-\infty}^{+\infty} G(v+jn\Omega)I(s-v-jn\Omega)\right]dv \quad (64)$$

Then by Poisson's summation formula with reference to equation 11

$$X_{ir}(s)=\frac{-T_s}{2\pi j}\int_{b-j\Omega/2}^{b+j\Omega/2} K_1^*(\epsilon^{vT_s})R^*\times (\epsilon^{vT_s})GI^*(\epsilon^{vT_s},s)dv \quad (65)$$

and expressing the integral in the $z=\epsilon^{vT_s}$ plane

$$X_{ir}(s)=\frac{-1}{2\pi j}\oint z^{-1}K_1^*(z)R^*(z)GI^*(z,s)dz \quad (66)$$

where the path of integration is now a circle around the origin of the z plane with a radius of $|z|=\epsilon^{bT_s}$.

Applying identical techniques to equations 58, 60, and 61

$$X_{ii}(s)=\frac{1}{2\pi j}\oint z^{-1}II^*(z,s)dz \quad (67)$$

$$X_{ri}(s)=\frac{-1}{2\pi j}\oint z^{-1}K_1^*(\epsilon^{sT_s}z^{-1})R^*\times (\epsilon^{sT_s}z^{-1})IG^*(z,s)dz \quad (68)$$

$$X_{rr}(s)=\frac{1}{2\pi j}\oint z^{-1}K_1^*(z)K_1^*(\epsilon^{sT_s}z^{-1})\times R^*(z)R^*(\epsilon^{sT_s}z^{-1})GG^*(z,s)dz \quad (69)$$

where the path of integration is the same as in equation 66. Applying contour integration on equations 66–69 and substituting these into equation 57, equation 10 results.

Appendix II

Equation 1 can be rephrased as

$$s=\int_0^T \overline{p(t)(i(t)-c(t))^2}dt \quad (70)$$

where $p(t)$ is the probability distribution of output utilization, $i(t)$ is the desired, and $c(t)$ the actual output.

With reference to Fig. 1, if the impulse response of the plant is $g(t)$, by real convolution (the t domain equivalent of equation (6)), there results

$$c(t)=\sum_{\nu=0}^{\infty} e_2(\nu T_s)g(t-\nu T_s) \quad (71)$$

Further, with reference to equation 6 and Fig. 1

$$e_2(T_s)=\sum_{n=0}^{\infty} k_1(nT_s)r((\nu-n)T_s) \quad (72)$$

With equations 70–72 and 34–36 after interchanging the sequence of summations and integrations

$$s=\Psi_{ii}(0,0)-2\sum_{m=0}^{\infty} k_1(mT_s)\Psi_{ig}'(0,-m)+\sum_{m=0}^{\infty}\sum_{n=0}^{\infty} k_1(mT_s)k_1(nT_s)\Psi_{gg}''(m,m-n) \quad (73)$$

which by the notations of equations 34–36 reduces to equation 32.

Now let it be assumed that the transform of the sampled impulsive response of the optimum system is

$$^\circ K_1^*(z)=\sum_{m=0}^{\infty} {}^\circ k_1(mT_s)z^{-m} \quad (74)$$

Then for the general system

$$K_1^*(z)=\sum_{m=0}^{\infty} k_1(mT_s)z^{-m}$$
$$=\sum_{m=0}^{\infty} [{}^\circ k_1(mT_s)+\epsilon^\epsilon k(mT_s)]z^{-m} \quad (75)$$

where ${}^\epsilon k(mT_s)$ is arbitrary. Now for ${}^\circ K_1^*(z)$ to be truly the optimum system it is necessary that after substituting equation 75 into equation 73

$$\left.\frac{\partial s}{\partial \epsilon}\right|_{\epsilon=0}=0 \quad (76)$$

for any selection of ${}^\epsilon k(mT_s)$. Carrying out the operation indicated in equation 76

$$\left.\frac{\partial s}{\partial \epsilon}\right|_{\epsilon=0}=-2\sum_{m=0}^{\infty} {}^\epsilon k(mT_s)\Psi_{ig}'(0,-m)+2\sum_{m=0}^{\infty} {}^\epsilon k(mT_s)\sum_{n=0}^{\infty} {}^\circ k_1(nT_s)\Psi_{gg}''(m,m-m)=0 \quad (77)$$

and since equation 77 must be satisfied for arbitrary ${}^\epsilon k(mT_s)$

$$\sum_{n=0}^{M} k_1(nT_s)\Psi_{gg}''(m,m-n)-\Psi_{ig}'(0,-m)=0, m=0,1,2\ldots M \quad (78)$$

Note that ${}^\circ k_1(nT_s)$ has been replaced by notation $k_1(nT_s)$ in equation 78, and further that a finite limit of summation M has been introduced in agreement with the assumption that $T=MT_s$ is the duration of output utilization: ${}^l p(t)=0$ if $t>T$. Considering the notation of equations 34–36, equation 33 is identical to equation 78.

Appendix III

With the notations of equations 39–43 and the definitions of equations 34–37

$$\Psi_{\alpha\delta\epsilon}={}^l p_\alpha{}^l i_\delta{}^l i_\epsilon \quad (79)$$

$$\Psi_{\alpha(\mu-m)\delta}'=\overline{{}^l p_\alpha{}^l r((\mu-m)T_s){}^l i_\delta} \quad (80)$$

$$\Psi_{\alpha(\mu-m)(\nu-n)}''=\overline{{}^l p_\alpha{}^l r((\mu-m)T_s){}^l r((\nu-n)T_s)} \quad (81)$$

$$F_{\alpha\delta\epsilon}=\Phi_{\alpha\delta\epsilon} \tag{82}$$

$$F_{\alpha\delta\mu}{}'=\sum_{\chi} G_\chi \Phi_{\alpha\delta\mu\chi}{}' \tag{83}$$

$$F_{\alpha\mu\nu}{}''=\sum_{\chi}\sum_{\kappa} G_\chi G_\kappa \Phi_{\alpha\mu\nu\chi\kappa}{}'' \tag{84}$$

Here

$$\Phi_{\alpha\delta\epsilon}=\int_0^T \phi_\alpha{}^I(t)\phi_\delta{}^{II}(t)\phi_\epsilon{}^{II}(t)dt \tag{85}$$

$$\Phi_{\alpha\delta\mu\chi}{}'=\int_{\mu T_s}^T \phi_\alpha{}^I(t)\phi_\delta{}^{II}(t)\phi_\chi{}^{III}(t-\mu T_s)dt \tag{86}$$

$$\Phi_{\alpha\mu\nu\chi\kappa}{}''=\begin{cases}\int_{\mu T_s}^T \phi_\alpha{}^I(t)\phi_\chi{}^{III}(t-\mu T_s)\times \\ \qquad \phi_\kappa{}^{III}(t-T_s\nu)dt, \ \nu\le\mu \\ \int_{\nu T_s}^T \phi_\alpha{}^I(t)\phi_\chi{}^{III}(t-\mu T_s)\times \\ \qquad \phi_\kappa{}^{III}(t-T_s\nu)dt, \ \mu\le \end{cases} \tag{87}$$

The coefficients G_χ, G_κ appearing in equations 83 and 84 are the Fourier coefficients of the impulse response, $g(t)=\mathfrak{L}^{-1}[G(s)]$, of the plant. If $\phi_\kappa{}^{III}(t)$ is a complete set of functions orthonormal on the interval $0<t<T$, these coefficients are given by

$$G_\kappa=\int_0^T \phi_\kappa{}^{III}(t)g(t)dt \tag{88}$$

For the purposes of Tables I, II and III, it has been assumed that the $\phi^I(t)$, $\phi^{II}(t)$, and $\phi^{III}(t)$ sets are identical, and that they are either trigonometric functions or Legendre polynomials.

Appendix IV

With the definitions and notations of Table I as explained under "A General Input Environment Selected for Detail Study" in reference 2 and in this paper the input and desired output can be written respectively

$$^{ij}r(t)={}^ir(t)+{}^i\mathfrak{g}(t){}^js(t)+{}^i\mathfrak{h}(t){}^jn(t) \tag{89}$$

$$^{ij}i(t)={}^ii(t)+{}^i\mathfrak{g}(t){}^js(t) \tag{90}$$

And by Taylor expansion

$$^i\mathfrak{g}(t)=\sum {}^i\mathfrak{g}_x t^x \tag{91}$$

$$^i\mathfrak{h}(t)=\sum {}^i\mathfrak{h}_x t^x \tag{92}$$

It is now assumed that the functions $\phi_\mu{}^I(t)$ and $\phi_\epsilon{}^{II}(t)$ are identical ($\phi_\mu{}^I(t)=\phi_\delta{}^{II}(t)$ if $\alpha=\delta$) and that they form a complete orthonormal set on $0<t<T$. Then with equations 89–92 the factors in equations 79–81 can be expressed in the following forms

$$^{ij}p_\alpha={}^ip_\alpha \tag{93}$$

$$^{ij}i_\delta={}^ii_\delta+\sum_x {}^i\mathfrak{g}_x{}^js_{x\delta} \tag{94}$$

$$^{ij}r(\mu T_s)={}^ir(\mu T_s)+{}^i\mathfrak{g}(\mu T_s){}^js(\mu T_s)+{}^i\mathfrak{h}(\mu T_s){}^jn(\mu T_s) \tag{95}$$

where

$$^ip_\alpha=\int_0^T \phi_\alpha(t){}^ip(t)dt \tag{96}$$

$$^ii_\delta=\int_0^T \phi_\delta(t){}^ii(t)dt \tag{97}$$

$$^js_{x\delta}=\int_0^T \phi_\delta(t)t^{x\,j}s(t)dt \tag{98}$$

Index l of equation 12 has been replaced by ij since the general ensemble l includes both the i and j ensembles of the present problem. If now the probability of function i within the i ensemble is ^iQ_j and the probability of the function j within the j ensemble is ^jQ, then substituting equations 89–98 into equations 79–82 there results

$$\Psi_{\alpha\delta\epsilon}=\overline{p_\alpha i_\delta i_\epsilon}+\sum_x\sum_y \overline{p_\alpha \mathfrak{g}_x\mathfrak{g}_y}\,\overset{\cdots\cdots}{s_{x\delta}s_{y\epsilon}} \tag{99}$$

$$\Psi_{\alpha(\mu-m)\delta}{}'=\overline{p_\alpha r((\mu-m)T_s)i_\delta}+ \sum\Big\{\overline{p_\alpha\mathfrak{g}((\mu-m)T_s)\mathfrak{g}_x}\,\overset{\cdots\cdots}{s(\mu-m)T_s)_{x\delta}}+ \overline{p_\alpha\mathfrak{h}((\mu-m)T_s)\,\mathfrak{g}_x}\,\overset{\cdots\cdots}{n((\mu-m)T_s)s_{x\delta}}\Big\} \tag{100}$$

$$\begin{aligned}\Psi_{\alpha(\mu-m)(\nu-n)}{}''=&\overline{p_\alpha r((\mu-m)T_s)r((\nu-n)T_s)}+\\ &\overline{p_\alpha\mathfrak{g}((\mu-m)T_s)\mathfrak{g}((\nu-n)T_s)}\times\\ &\overset{\cdots\cdots}{\Psi_{ss}((m-m-\mu+\nu)T_s)}+\\ &\overline{p_\alpha\mathfrak{g}((\mu-m)T_s)\mathfrak{K}((\nu-n)T_s)}\times\\ &\overset{\cdots\cdots}{\Psi_{sn}((m-n-\mu+\nu)T_s)}+\\ &\overline{p_\alpha\mathfrak{h}((\mu-m)T_s)\mathfrak{g}((\nu-n)T_s)}\times\\ &\overset{\cdots\cdots}{\Psi_{ns}((m-n-\mu+\nu)T_s)}+\\ &\overline{p_\alpha\mathfrak{h}((\mu-m)T_s)h((\nu-n)T_s)}\times\\ &\overset{\cdots\cdots}{\Psi_{nn}((m-n-\mu+\nu)T_s)}\end{aligned} \tag{101}$$

here the dashed line indicates averaging over the i ensemble; the dotted line indicates averaging over the j ensemble. Subscript x and ϵ were replaced where necessary by dummy subscripts, respectively y and δ. Notations $\Psi_{ss}(t)$, $\Psi_{sn}(t)$, $\Psi_{nn}(t)$, and $\Psi_{ns}(t)$ refer to the various autocorrelation and crosscorrelation functions of the stationary random processes which give rise to the $^{ij}s(t)$ and $^{ij}n(t)$ components of signal and noise. Of course these autocorrelation functions can be obtained by inverse two-sided Laplace transformations of the corresponding power spectral densities.

$$\Psi_{ss}(t)=\mathfrak{L}_2{}^{-1}[\Phi_{ss}(s)] \tag{102}$$

$$\Psi_{sn}(t)=\mathfrak{L}_2{}^{-1}[\Phi_{sn}(s)] \tag{103}$$

$$\Psi_{ns}(t)=\mathfrak{L}_2{}^{-1}[\Phi_{ns}(s)] \tag{104}$$

$$\Psi_{nn}(t)=\mathfrak{L}_2{}^{-1}[\Phi_{nn}(s)] \tag{105}$$

With these definitions and equation 98

$$\begin{aligned}\overset{\cdots\cdots}{s((\mu-m)T_s)s_{x\delta}} &=\overset{\cdots\cdots}{s((\mu-m)T_s)\int_0^T t^x s(t)\phi_\delta(t)dt}\\ &=\int_0^T t^x \overset{\cdots\cdots}{s(t)-s((\mu-m)T_s)}\phi_\delta(t)dt\\ &=\int_0^T t^x\Psi_{ss}(t-(\lambda\mu-m)T_s)\phi_\delta(t)dt\end{aligned} \tag{106}$$

Similarly

$$\overset{\cdots\cdots}{n((\mu-m)T_s)s_{x\delta}}=\int_0^T t^x\Psi_{ns}(t-(\mu-m)T_s)\phi_\delta(t)dt$$

This leaves to be evaluated $\overset{\cdots}{s_{x\delta}s_{y\epsilon}}$ in equation 99 but this latter evaluation has been done elsewhere.[2]

References

1. PROBABALISTIC ERROR AS MEASURE OF CONTROL-SYSTEM PERFORMANCE, **J. Zaborszky, J. W. Diesel.** *AIEE Transactions*, pt. II (*Applications and Industry*), vol. 78, July 1959, pp. 163–68.

2. DESIGN OF CONTINUOUS CONTROL SYSTEMS FOR MINIMUM PROBABILISTIC ERROR, **J. Zaborszky, J. W. Diesel.** *Ibid.*, see pp. 44–54 of this issue.

3. RANDOM PROCESSES IN AUTOMATIC CONTROL (book), **J. H. Lanning, R. H. Battin.** McGraw-Hill Book Company, Inc., New York, N. Y., 1956, Appendix D.

4. SAMPLED-DATA PROCESSING TECHNIQUES FOR FEEDBACK CONTROL SYSTEMS, **Arthur R. Bergen, John R. Ragazzini.** *AIEE Transactions*, pt. II (*Applications and Industry*), vol. 73, Nov. 1954, pp. 236–47.

5. ON CLOSED-FORM EXPRESSIONS FOR MEAN SQUARES IN DISCRETE-CONTINUOUS SYSTEMS, **J. Sklansky.** *Transactions*, Professional Group on Automatic Control, Institute of Radio Engineers, New York, N. Y., vol. PGAC-4, Mar. 1958, p. 21.

Design for Minimum Probabilistic Error of Continuous Linear Control Systems Subject to Constraints

J. ZABORSZKY
MEMBER AIEE

J. W. DIESEL
ASSOCIATE MEMBER AIEE

A NEWLY DEVELOPED approach to the synthesis of control systems as been based on "probabilistic" or "endgma" error.[1] These names denote the oncept of an average penalized error r such times when the output of the ontrol system is actually used. Detail esign processes for continuous[2] or samed-data[3] linear systems have been deeloped to yield linear systems operating ith minimum probabilistic square errors. his paper shows that constraints, specially an acceleration constraint on the utput, can be included in the design rocess for minimum probabilistic square rror. Only continuous systems are eated in this paper, but extension to ampled systems is straightforward.

An input environment has been selected r this study which is comparable in its xtensive scope to that used for the unonstrained case.[2,3]

onstraints

The constraint selected for illustration one of acceleration limiting on the output, $c(t)$, of the control system. While uch limits are usually nonlinear it is cusomary,[4] in order to preserve the linearity f the over-all problem, to constrain the ns value rather than the peak value of ne acceleration. In this sense then the onstraint is set up as:

$$\overline{t)^2} = \int_0^T \overline{{}^l\ddot{c}(t)^2\, {}^l{}_2p(t)\, dt} \leq {}_2a^2 \qquad (1)$$

here ${}_2a$ is the rms acceleration limit, the ouble dot denotes second derivative with espect to time, ${}^l{}_2p(t)$ is a weighting function or, potentially, a probability disibution function which defines the articular way in which the time averages f the square acceleration is taken. For ne special case of:

$$(t) = \begin{cases} 1/T & \text{if } 0<t<T \\ 0 & \text{if } T<t<\infty \end{cases} \qquad (2)$$

quation 1 yields the actual rms value of ne acceleration. The straight line deotes averaging over an ensemble of inuts indexed by l.

Subscripts preceding the function symbol will be uniformly used throughout the paper to distinguish quantities pertaining to the constraints.

Probabilistic Error

The probabilistic square error has been defined:[2]

$$s = \int_0^T \overline{{}^lp(t)({}^li(t) - {}^lc(t))^2 dt} \qquad (3)$$

where ${}^li(t)$ and ${}^lc(t)$ are, respectively, the desired and actual output created by ${}^lr(t)$; the number l member of the ensemble comprising the input environment of the system; ${}^lp(t)$ is the corresponding probability distribution of the utilization times of the output; and s is the end sigma.

The aim of the optimization is the system which produces the minimum, s, probabilistic square error, equation 3, under the constraint of equation 1.

Input-Output Environment

An input environment will be selected which can be described by:

$${}^{ij}r(t) = {}^ir(t) + {}^ig_0{}^js(t) + {}^ih_0{}^jn(t) \qquad (4)$$

This consists of a nonstationary ensemble of specific input functions, ${}^ir(t)$; an ergodic ensemble of random signal input functions ${}^js(t)$ which enter the system through a gain ${}^ig_0$ which may be correlated to the i ensemble; an ergodic ensemble ${}^jn(t)$ of random noise functions which will here be assumed uncorrelated to ${}^js(t)$ and which enters the system through a gain ${}^ih_0$. The latter, in turn, may be correlated to the i ensemble. This input environment is identical in its generality to the one studied for continuous systems[2] except that for the sake of brevity gains ${}^ig_0$ and ${}^ih_0$ are here restricted to be constant, and ${}^js(t)$, ${}^jn(t)$ are assumed uncorrelated. More details about this input environment are given in reference 2.

The desired output will be assumed to be:

$${}^{ij}i(t) = {}^ii(t) + {}^ig_0{}^js(t) \qquad (5)$$

where ${}^ii(t)$ derives in some specified way from ${}^ir(t)$. Since ${}^js(t)$ and ${}^jn(t)$ are uncorrelated ergodic ensembles they can be represented by rational power spectral densities as:

$$\Phi_{ss}(s) = B' \frac{\prod_{\xi}^{H'} (s - w_\xi')}{\prod_{\lambda}^{K'} (s - q_\lambda')} = \sum_{\lambda=1}^{H'} \frac{K_\lambda'}{s - q_\lambda'}; \qquad \begin{matrix} 1 \leq \xi \leq H' \\ 1 \leq \lambda \leq K' \end{matrix} \qquad (6)$$

$$\Phi_{sn}(s) = \Phi_{ns}(s) = 0 \qquad (7)$$

$$\Phi_{nn}(s) = B'' \frac{\prod_{\xi}^{H''} (s - w_\xi'')}{\prod_{\lambda}^{K''} (s - q_\lambda'')} = \sum_{\lambda=1}^{B''} \frac{K_\lambda''}{s - q_\lambda''}; \qquad \begin{matrix} 1 \leq \xi \leq H'' \\ 1 \leq \lambda \leq K'' \end{matrix} \qquad (8)$$

It will be assumed that $\Phi_{ss}(s)$ and $\Phi_{nn}(s)$ have zeros at infinity, that is, considering that these are even functions in s,

$$H' - K' = 2\theta' \quad H'' - K'' = 2\theta'' \qquad (9)$$

where θ' and θ'' are positive integers,

$$\theta' = 1, 2, 3 \ldots \quad \theta'' = 1, 2, 3 \ldots \qquad (10)$$

Then the power spectral densities of the second derivative of ${}^js(t)$ and ${}^jn(t)$ and cross-spectral densities of various other derivatives of these quantities can be reduced to the form:

$$\Phi_{\ddot{s}\ddot{s}}(s) = s^2 \sum_{\lambda=1}^{H'} K_\lambda' q_\lambda' + \sum_{\lambda=1}^{H'} K_\lambda' q_\lambda'^3 + \sum_{\lambda=1}^{H'} \frac{K_\lambda' q_\lambda'^4}{s - q_\lambda'} \qquad (11A)$$

$$\Phi_{\ddot{n}\ddot{n}}(s) = s^2 \sum_{\lambda=1}^{H''} K_\lambda'' q_\lambda'' + \sum_{\lambda=1}^{H''} K_\lambda'' q_\lambda''^3 + \sum_{\lambda=1}^{H''} \frac{K_\lambda'' q_\lambda''^4}{s - q_\lambda''} \qquad (11B)$$

$$\Phi_{s\ddot{s}}(s) = \sum_{\lambda=1}^{H'} K_\lambda' q_n' + \sum_{\lambda=1}^{H'} \frac{K_\lambda' q_\lambda'^2}{s - q_\lambda'} \qquad (12A)$$

$$\Phi_{n\ddot{n}}(s) = \sum_{\lambda=1}^{H''} K_\lambda'' q_\lambda'' + \sum_{\lambda=1}^{H''} \frac{K_\lambda'' q_\lambda''^2}{s - q_\lambda''} \qquad (12B)$$

Paper 60-29, recommended by the AIEE Feedback Control Systems Committee and approved by the AIEE Technical Operations Department for presentation at the AIEE Winter General Meeting, New York, N. Y., January 31–February 5, 1960. Manuscript submitted June 16, 1959; made available for printing November 12, 1959.

J. ZABORSZKY is with Washington University, St. Louis, Mo., and consultant to McDonnell Aircraft Corporation; J. W. DIESEL is with McDonnell Aircraft Corporation, St. Louis, Mo.

$$\Phi_{\dot{s}\dot{s}}(s) = -s \sum_{\lambda=1}^{H'} K_\lambda' q_\lambda' - \sum_{\lambda=1}^{H'} \frac{K_\lambda' q_\lambda'^3}{s - q_\lambda'} \tag{13A}$$

$$\Phi_{\dot{n}\dot{n}}(s) = -s \sum_{\lambda=1}^{H''} K_\lambda'' q_\lambda'' - \sum_{\lambda=1}^{H''} \frac{K_\lambda'' q_\lambda''^3}{s - q_\lambda''} \tag{13B}$$

Optimum System

Assuming a linear system with impulse response $k(t)$, the following superposition integral results for the output:

$$^l c(t) = \int_0^T k(t_1)\, ^l r(t-t_1) dt_1 \tag{14}$$

where $^l r(t)$ is the number l input to the system which may be discontinuous at $t=0$. That is:

$$r(0^-) = \dot{r}(0^-) = 0 \tag{15}$$

but potentially,

$$r(0^+) = r(0) \neq 0 \quad \dot{r}(0^+) = \dot{r}(0) \neq 0 \tag{16}$$

Consequently the output acceleration may be expressed generally as:

$$\ddot{c}(t) = r_{(0)} \dot{k}(t) + \dot{r}_{(0)} k(t) + \int_0^\infty dt_1 k(t_1) \ddot{r}(t-t_1) \tag{17}$$

where $k(o)=0$ was assumed, which is representative of practical systems. Substituting equations 14 and 17 into equations 1 and 3 the following two equations result:

$$\overline{\ddot{c}(t)^2} = \int_0^T dt_2 k(t_2) \int_0^T dt_1 k(t_1) \psi_{\ddot{r}\ddot{r}}(t_1, t_1 - t_2) + v_{OO} + 2v_{O\dot{O}} + v_{\dot{O}\dot{O}} + 2\int_0^T dt_1 k(t_1) v_{Or}(t_1) + 2\int_0^T dt_1 k(t_1) v_{\dot{O}r}(t_1) \tag{18}$$

and

$$s = \psi_{ii}(0, 0) - 2\int_0^T dt_1 k(t_1) \psi_{ir}(0, -t_1) + \int_0^T dt_3 k(t_3) \int_0^T dt_1 k(t_1) \psi_{rr}(t_3, t_3 - t_1) \tag{19}$$

where

$$\psi_{rr}(t_1, \tau) = \int_0^T \overline{dt_2 p(t_2+t_1) r(t_2) r(t_2+\tau)} \tag{20}$$

$$\psi_{ii}(t_1, \tau) = \int_0^T \overline{dt_2 p(t_2+t_1) i(t_2) i(t_2+\tau)} \tag{21}$$

$$\psi_{ir}(t_1, \tau) = \int_0^T \overline{dt_2 p(t_2+t_1) i(t_2) r(t_2+\tau)} \tag{22}$$

$$\psi_{\ddot{r}\ddot{r}}(t_1, \tau) = \int_0^T \overline{dt_2\, {}_2p(t_2+t_1) \ddot{r}(t_2) \ddot{r}(t_2+\tau)} \tag{23}$$

$$v_{OO} = \int_0^T dt\, \dot{k}^2(t)\, \overline{r^2(0)_2 p(t)} \tag{24}$$

$$v_{O\dot{O}} = \int_0^T dt\, k(t)\, \dot{k}(t)\, \overline{r(0)\dot{r}(0)_2 p(t)} \tag{25}$$

$$v_{\dot{O}\dot{O}} = \int_0^T dt\, k^2(t)\, \overline{\dot{r}^2(0)_2 p(t)} \tag{26}$$

$$v_{Or}(t_1) = \int_0^T dt\, \dot{k}(t)\, \overline{r(0)_2 p(t) \ddot{r}(t-t_1)} \tag{27}$$

$$v_{\dot{O}r}(t_1) = \int_0^T dt\, k(t)\, \overline{\dot{r}(0)_2 p(t)\, \ddot{r}(t-t_1)} \tag{28}$$

If, further, functions $p(t)$, $_2p(t)$, $r(t)$, $i(t)$ $k(t)$, and $\dot{k}(t)$ are expanded over:

$\phi_\alpha(t)$, $\alpha = 0, 1, 2 \ldots$

a complete set of orthonormal functions on the interval $0<t<T$, and the Fourier coefficients are computed and denoted as described by the following general case:

$$x(t) = \sum_y x_y \phi_y(t) \tag{29}$$

$$x_y = \int_0^T x(t) \phi_y(t) dt \tag{30}$$

Then, as is shown in Appendix I and reference 2 for the input environment described above, equations 18 and 19 take the form:

$$\overline{\ddot{c}(t)^2} = \sum_m \sum_n k_m k_n\, {}_0f_{mn} + \delta(0) \sum_m \sum_n k_m k_n\, {}_1f_{mn} \leq {}_2a^2 \tag{31}$$

$$s = f - 2\sum_m k_m f_m + \sum_m \sum_n k_m k_n f_{mn} \tag{32}$$

where $\delta(t)$ is a Dirac delta function, the f, f_m, f_{mn}, $_0f_{mn}$ and $_1f_{mn}$ coefficients will be discussed later and the k_m, k_n are Fourier coefficients of $k(t)$ as defined in equation 30. The delta function will be absent in equation 31 if $\Phi_{ss}(s)$ and $\Phi_{nn}(s)$ both have zeros of at least order 4 at $s=\infty$. Generally, however, when the delta function is present in equation 31, it will make this condition to a certain extent indefinite. For this reason equation 31 will, somewhat arbitrarily, be split into the following conditions:

$$_0c = \sum_m \sum_n k_m\, {}_0f_{mn} \leq {}_2a^2 \tag{33}$$

$$_1c = \sum_m \sum_n k_m k_n\, {}_1f_{mn} = 0 \tag{34}$$

The second condition is sufficient by the derivations of Appendix I and, if it is not necessary, at least it appears to be quite reasonable. The minimization of s then should be carried out under the twin constraints of equations 33 and 34 or, in other words, quantity:

$$s' = s + {}_0\lambda_0 c + {}_1\lambda_1 c = f - 2\sum_m k_m f_m + \sum_m \sum_n k_m k_n [f_{mn} + {}_0\lambda\, {}_0f_{mn} + {}_1\lambda\, {}_1f_{mn}] \tag{35}$$

must be minimized with respect to k_n. Here, $_0\lambda$ and $_1\lambda$ of course are the Lagrange multipliers established by equations 33 and 34. The result of the optimization is the optimum k_n or, by equation 25, a Fourier expansion of the impulsive response of the optimum system.

The minimization of equation 35 is carried out in Appendix II leading to the following three matrix equations to be solved for the optimum k_n matrix:

$$[\bar{f}_{mn} + {}_0\lambda\, {}_0\bar{f}_{mn} + {}_1\lambda\, {}_1\bar{f}_{mn}] k_n] = \bar{f}_m], \quad m \text{ and } n = 1, 2, \ldots M \tag{36}$$

$$\underbrace{k_m} [{}_0f_{mn}]\, k_n] \leq {}_2a^2, \quad m \text{ and } n = 0, 1, \ldots, M \tag{37}$$

$$\underbrace{k_m} [{}_1f_{mn}] k_n] = 0, \quad m \text{ and } n = 0, 1, \ldots, M \tag{38}$$

The first equation is linear in k_n but the last two are nonlinear so $_0\lambda$ and $_1\lambda$ will need to be established by cut-and-try.

Complete Computation Program

To carry out the solution indicated in equations 36 through 38 it will be necessary to evaluate first f, f_m, f_{mn}, $_0f_{mn}$ and $_1f_{mn}$. As in earlier cases[2,3] it develops that these have a general form:

$--f\ldots$ = rational function of

$$\sum_x \sum_y \sum_z --\Psi_{xyz} F_{xyz} \ldots \tag{39}$$

where the $F_{xyz}\ldots$ depend only on the selection of the orthonormal set on which expansions are obtained, so these can be precomputed for the few orthonormal sets which would be practically considered. On the other hand the $--\Psi_{xyz}$ factors (or in some cases Υ_{xyz} factors) represent the special characteristics of the input environment. Further, it develops that F, F_{abc}, and F_{abcmn} are identical to those obtained in reference 2 where complete computation programs are presented for three sets of orthogonal functions for the case of the unconstrained system. Similar programs can be produced for all three orthogonal sets with the constraints of this paper. In fact, the equations introduced here modify the program of reference 2 in a relatively minor way. To preserve the brevity of this presentation it will be left to the reader to introduce these modifications in the final areas of, respectively, Table I(B) and Table II of reference 2. It is significant that the most time-consuming parts of the program, those affecting the computations of the F_{abc}, F_{abcmn} and F_{abcmn} coefficients are not affected by the change since these coefficients are quite universal. In fact, once these coefficients are computed and recorded on tape they can be reused for any individual problem whether it involves constraints or not.

Conclusions

A design process is introduced to obtain the impulse response function of the

...ntinuous time-invariant linear system ...ich has the smallest average square ...or for such times when its output is ...ed, while maintaining a limited output ...celeration. To solve problems of a com...xity common in control-engineering ...actice it is necessary to utilize major ...ital computers, and the paper presents the necessary equations in an organized ...m for the programing of the computers.

Appendix I

With expansions as defined in equations ... and 30, the definitions of equations 31 ...d 32 take the form:

$$\sum_\alpha \sum_\beta \sum_\gamma \Psi_{\alpha\beta\gamma} F_{\alpha\beta\gamma} \qquad (40)$$

$$=\sum_\alpha \sum_\beta \sum_\gamma \Psi_{\alpha\beta\gamma}' F_{\alpha\beta\gamma m} \qquad (41)$$

$$_{n}=\sum_\alpha \sum_\beta \sum_\gamma \Psi_{\alpha\beta\gamma}'' F_{\alpha\beta\gamma mn} \qquad (42)$$

$$_{n}=\sum_\alpha \sum_\beta \sum_\gamma {}_0\Psi_{\alpha\beta\gamma} F_{\alpha\beta\gamma mn}+ \sum_\alpha \Upsilon_\alpha^{oo}\Big(\sum_\mu \sum_\nu \kappa_{\mu m}\kappa_{\nu n}F_{\alpha\mu\nu}\Big)+ \sum_\alpha \Upsilon_\alpha^{\dot o\dot o}F_{\alpha mn}+2\sum_\alpha \Upsilon_\alpha^{o\dot o}\Big(\sum_\mu \kappa_{\mu m}F_{\alpha m\mu}\Big)+ 2\sum_\alpha \sum_\beta \Upsilon_{\alpha\beta}^{o}\Big(\sum_\mu \kappa_{\mu n}F_{\alpha\mu\beta n}\Big)+ 2\sum_\alpha \sum_\beta {}_0\Upsilon_{\alpha\beta}^{\dot o}F_{\alpha m\beta n} \qquad (43)$$

$$_{n}=\sum_\alpha \sum_\beta \sum_\gamma {}_1\Psi_{\alpha\beta\gamma} F_{\alpha\beta\gamma mn}+ 2\sum_\alpha \sum_\beta {}_1\Upsilon_{\alpha\beta}^{\dot o}F_{\alpha m\beta n} \qquad (44)$$

Here the quantities $F_{\alpha\beta\gamma}, F_{\alpha\beta\gamma m}, F_{\alpha\beta\gamma mn}$, ...$_{\beta\gamma}, \Psi'_{\alpha\beta\gamma}, \Psi''_{\alpha\beta\gamma}$ have been previously de...ed in Tables I(B) and II of reference 2. ...should be remembered that in equations ...through 44 the F coefficients are assumed ...be based on expansions of all functions ...the same $\phi_x(t)$ orthonormal set as de...ed in equation 29 and 30. However, in ...erence 2, somewhat different function ...s were used for various functions in order ...shorten the computer program. Con...quently if $(F_{\alpha\beta\gamma m})_{tr}$ is the F factor de...ed[2] for trigonometric orthogonal sets, ...en for substituting into equations 43 or 44, $_{\mu\beta n}=1/2[(F_{\alpha\mu\beta n})_{tr}+(F_{\alpha(-\mu)\beta n})_{tr}]$. The ...me process applies when, but only when, n, μ, or ν appear in equation 43 or 44 at ...e of the first three indexes of F.)

Several additional definitions are needed, ...:

$$_{\alpha\beta\gamma}={}_0\Psi_{\alpha\beta\gamma}+\delta(t)_1\Psi_{\alpha\beta\gamma}=\overline{{}_2{}^ip_\alpha\,{}^{ij}\ddot r_\beta\,{}^{ij}\ddot r_\gamma}$$

$$=\overline{{}_2{}^ip_\alpha\,{}^i\ddot r_\beta\,{}^i\ddot r_\gamma}+\overline{{}^ip\ {}^ig_0^2}\ \overline{{}^j\ddot s_\beta\,{}^j\ddot s_\gamma}+\overline{{}^ip_\alpha\,{}^ih_0^2}\ \overline{{}^j\ddot n_\beta\,{}^j\ddot n_\gamma} \qquad (45)$$

...ere it has been considered that ${}^js(t)$ and ...(t) are uncorrelated ($\overline{{}^j\ddot s_\beta\,{}^j\ddot n_\gamma}=0$), with the ...shed line indicating averaging over the i ...semble and the dotted line averaging over the j ensemble. The first term on the right side of equation 45 poses no difficulty since it contains Fourier coefficients of known specific functions.

With reference to equation 30:

$$\overline{{}^j\ddot s_\beta\,{}^j\ddot s_\gamma}=\sum_j {}^jQ\int_0^T {}^j\ddot s(t_1)\phi_\beta(t_1)dt_1 \int_0^T {}^j\ddot s(t_2)\phi_\gamma(t_2)dt_2 \qquad (46)$$

where ${}^jQ$ is the probability of function number j within the j ensemble. Exchanging sums and integrals:

$$\overline{{}^j\ddot s_\beta\,{}^j\ddot s_\gamma}=\int_0^T dt_1\,\phi_\beta(t_1)\int_0^T dt_2\,\phi_\gamma(t_2)\,{}_2\psi_{\ddot s\ddot s}(t_2-t_1) \qquad (47)$$

considering that

$$\psi_{\ddot s\ddot s}(t_2-t_1)=\sum_j {}^jQ\,{}^j\ddot s(t_2)\,{}^j\ddot s(t_1) \qquad (48)$$

is the autocorrelation function of second derivatives taken on functions of the ergodic j ensemble. The latter can be obtained from the power spectral density of equation 11(A):

$$\psi_{\ddot s\ddot s}(t)=\mathfrak{L}_2^{-1}[\Phi_{\ddot s\ddot s}(s)]$$

$$=\delta_3(t)\sum_{\lambda=1}^{H'}K_\lambda' q_\lambda'+\delta_1(t)\sum_{\lambda=1}^{H'}K_\lambda' q_\lambda'^3+\sum_{\lambda=1}^{H'}\Delta_2(q_\lambda')K_\lambda' q_\lambda'^4\epsilon^{q_\lambda'|t|} \qquad (49)$$

where $\delta_1(t)$ or $\delta(t)$ is the Dirac delta function or impulse and $\delta_3(t)$ is the third-order impulse.[5] It should be remembered[5] that:

$$\delta_2(t)=\int_{-a}^{t}\delta_3(t)dt \qquad (50)$$

the second-order impulse, and:

$$\delta_1(t)=\int_{-a}^{t}\delta_2(t)dt \qquad (51)$$

$$u(t)=\int_{-a}^{t}\delta_1(t)dt \qquad (52)$$

where a is any finite positive real number and $t>0$. Then equation 49 can be substituted into equation 47 and the integration can be carried out. For a trigonometric orthonormal set as defined earlier there results:

$${}_2\Psi_{\alpha\beta\gamma}={}_0\Psi_{\alpha\beta\gamma}+\delta_1(0)_1\Psi_{\alpha\beta\gamma} \qquad (53)$$

where

$${}_0\Psi_{\alpha\beta\gamma}=\sum_i {}^iQ\Big\{{}_2P_\alpha\Big[{}_2{}^iR_\beta\,{}_2{}^iR_\gamma+{}^ig_0^2\Big(-\frac{\Delta_{\beta\gamma}}{2}(\pi\gamma)^2\sum_{\lambda=1}^{H'}K_\lambda'q_\lambda'+\frac{\Delta_{\beta\gamma}}{2}\sum_{\lambda=1}^{H'}K_\lambda'q_\lambda'^3+{}_2\mathfrak{J}'(\beta,\gamma)\Big)+{}^ih_0^2\Big(-\frac{\Delta_{\beta\gamma}}{2}(\pi\gamma)^2\sum_{\lambda=1}^{H''}K_\lambda''q_\lambda''+\frac{\Delta_{\beta\gamma}}{2}\sum_{\lambda=1}^{H''}K_\lambda''q_\lambda''^3+{}_2\mathfrak{J}''(\beta,\gamma)\Big)\Big]\Big\} \qquad (54)$$

$${}_1\Psi_{\alpha\beta\gamma}=\sum_i {}^iQ\Big\{{}_2P_\alpha\Big[{}^ig_0^2\sum_{\lambda=1}^{H'}K_\lambda'q_\lambda'(-(-1)^{\beta+\gamma}-1)+{}^ih_0^2\sum_{\lambda=1}^{H''}K_\lambda''q_\lambda''(-(-1)^{\beta+\gamma}-1)\Big]\Big\} \qquad (55)$$

where the following definitions have been made:

$$\mathfrak{J}^{(u)}(\xi,\eta)=\sum_{\lambda=1}^{H^{(u)}}\Delta_2(q_\lambda^{(u)})U(\xi,\eta,K_\lambda^{(u)},q_\lambda^{(u)}) \qquad (56A)$$

$$\mathfrak{J}^{(u)}(\xi,\eta)=\sum_{\lambda=1}^{H^{(u)}}\Delta_2(q_\lambda^{(u)})U(\xi,\eta,K_\lambda^{(u)}q_\lambda^{(u)4},q_\lambda^{(u)}) \qquad (56B)$$

$$U(\xi,\eta,K,q)=K\frac{q}{q^2+(\xi\pi)^2}\Big\{-\Delta\xi\eta+\frac{q}{q^2+(\eta\pi)^2}([(-1)^\xi+(-1)^\eta]\epsilon^q-[(-1)^{\xi+\eta}+1])\Big\} \qquad (56C)$$

$$\Delta_2(q)=\begin{cases}0, & Re[q]>0\\ 1, & Re[q]<0\end{cases};\quad \Delta\xi\eta=\begin{cases}0, & |\xi|\ne|\eta|\\ 1, & |\xi|=|\eta|\ne0\\ 2, & |\xi|=|\eta|=0\end{cases} \qquad (57)$$

$${}_2P_0={}_2p_0 \qquad {}_2{}^iR_0={}^i\ddot r_0$$

$${}_2P_\alpha=\frac12({}_2p_a)\ a=|\alpha|\ne0;\ {}_2{}^iR_\beta=\frac12{}^i\ddot r_b,$$

$$b=|\beta|\ne0 \qquad (58)$$

By similar processes:

$$\Upsilon_\alpha^{oo}=\sum_i {}^iQ\Big\{{}_2p_\alpha\Big[{}^ir^2(0)+{}^ig_0^2\sum_{\lambda=1}^{H'}\Delta_2(q_\lambda')\times K_\lambda'+{}^ih_0^2\sum_{\lambda=1}^{H''}\Delta_2(q_\lambda'')K_\lambda''\Big]\Big\} \qquad (59)$$

$$\Upsilon_\alpha^{o\dot o}=\sum_i {}^iQ\Big\{{}_2p_\alpha\Big[{}^ir(0)\,{}^i\dot r(0)+{}^ig_0^2\sum_{\lambda=1}^{H'}\Delta_2(q_\lambda')K_\lambda'q_\lambda'+{}^ih_0^2\sum_{\lambda=1}^{H''}\Delta_2(q_\lambda'')K_\lambda''\Big]\Big\} \qquad (60)$$

$$\Upsilon_\alpha^{\dot o\dot o}={}_0\Upsilon_\alpha^{\dot o\dot o}+\delta_1(0)_1\Upsilon^{\dot o\dot o} \qquad (61)$$

where

$${}_0\Upsilon_\alpha^{\dot o\dot o}=\sum_i {}^iQ\Big\{{}_2p_\alpha\Big[{}^i\dot r^2(0)-{}^ig_0^2\sum_{\lambda=1}^{H'}\Delta_2(q_\lambda')K_\lambda'q_\lambda'^2-{}^ih_0^2\sum_{\lambda=1}^{H''}\Delta_2(q''_\lambda)K_\lambda''q_\lambda''^2\Big]\Big\} \qquad (62)$$

$$
{}_1\Upsilon_{\alpha}{}^{\dot{o}\dot{o}} = \sum_i {}^iQ \left\{ {}_2p_\alpha \left[-{}^ig_0{}^2 \sum_{\lambda=1}^{H'} K_\lambda' q_\lambda' - {}^ih_0{}^2 \sum_{\lambda=1}^{H''} K_\lambda'' q_\lambda'' \right] \right\} \quad (63)
$$

$$
\Upsilon_{\alpha\beta}{}^{o} = \sum_i {}^iQ \left\{ {}_2p_\alpha \left[{}^ir(0)\,{}^i\ddot{r}(0) + {}^ig_0{}^2 \left(\sum_{\lambda=1}^{H'} K_\lambda' q_\lambda' + \sum_{\lambda=1}^{H'} \Delta_2(q_\lambda') K_\lambda' q_\lambda'^3 \frac{(-1)^\beta \epsilon^{q_\lambda'} - 1}{(q_\lambda')^2 + (\beta\pi)^2} \right) + {}^ih_0{}^2 \left(\sum_{\lambda=1}^{H''} K_\lambda'' q_\lambda'' + \sum_{\lambda=1}^{H''} \Delta_2(q_\lambda'') K_\lambda'' q_\lambda''^3 \times \frac{(-1)^\beta \epsilon^{q_\lambda''} - 1}{(q_\lambda'')^2 + (\beta\pi)^2} \right) \right] \right\} \quad (64)
$$

$$
\Upsilon_{\alpha\beta}{}^{\dot{o}} = {}_0\Upsilon_{\alpha\beta}{}^{\dot{o}} + \delta_1(0)\,{}_1\Upsilon_{\alpha\beta}{}^{o} \quad (65)
$$

where

$$
{}_0\Upsilon_{\alpha\beta}{}^{\dot{o}} = \sum_i {}_iQ \left\{ {}_2p_\alpha \left[{}^i\dot{r}(0)\,{}^i\ddot{r}(0) + {}^ig_0{}^2 \sum_{\lambda=1}^{H'} \Delta_2(q_\lambda') K_\lambda' q_\lambda'^4 \times \frac{(-1)^\beta \epsilon^{q_\lambda'} - 1}{(q_\lambda')^2 + (\beta\pi)^2} + {}^ih_0{}^2 \sum_{\lambda=1}^{H''} \Delta_2(q_\lambda'') K_\lambda'' q_\lambda''^4 \times \frac{(-1)^\beta \epsilon^{q_\lambda''} - 1}{(q_\lambda'')^2 + (\beta\pi)^2} \right] \right\} \quad (66)
$$

$$
{}_1\Upsilon_{\alpha\beta}{}^{o} = \sum_i {}^iQ \left\{ {}_2p_\alpha \left[-{}^ig_0{}^2 \sum_{\lambda=1}^{H''} K_\lambda' q_\lambda' - {}^ih_0{}^2 \sum_{\lambda=1}^{H''} K_\lambda'' q_\lambda'' \right] \right\} \quad (67)
$$

Finally, for the general orthonormal sets as in equations 29 and 30:

$$
\kappa_{xy} = \int_0^T \phi_x(t)\phi_y(t)dt \quad (68)
$$

and for the specific trigonometric set defined in Table I(A) of reference 2:

$$
\kappa_{xy} = 0, \quad x+y \text{ even} \quad (69)
$$

$$
\left.\begin{aligned} \kappa_{oy} &= -2, \quad x=0 \\ \kappa_{xy} &= \frac{-4y^2}{(y+x)(y-x)}, \quad x \neq 0 \end{aligned}\right\} x+y \text{ odd} \quad (70)
$$

Appendix II

The condition $k(0)=0$ can, in view of equation 29, be equivalently expressed as:

$$
\sum_{y=0}^{M} k_y \phi_y(o) = 0 \quad (71)
$$

or

$$
k_o = -\frac{1}{\phi_0(0)} \sum_{y=1}^{M} k_y \phi_y(o) \quad (72)
$$

To find the system which operates with the minimum probabilistic error the Fourier coefficients ${}^0k_n$ are needed which minimize ς as expressed in equation 35. If ${}^\epsilon k_n$ is a set of arbitrary coefficients the general impulse response has coefficients:

$$
k_n = {}^0k_n + \epsilon\,{}^\epsilon k_n \quad (73)
$$

so a necessary condition of ${}^0k_n$ being the coefficients of the optimum system is:

$$
\left.\frac{\partial \varsigma}{\partial \epsilon}\right|_{\epsilon=0} = 0 \quad (74)
$$

Substituting equation 73 into equation 35 and applying equations 72 and 74, there results equation 36 with the definitions:

$$
\bar{f}_{mn} = f_{mn} - f_{mo} - f_{on} + f_{oo} \quad (75)
$$

$$
{}_0\bar{f}_{mn} = {}_0f_{mn} - f_{mo} - f_{on} + {}_0f_{oo} \quad (76)
$$

$$
{}_1\bar{f}_{mn} = {}_1f_{mn} - {}_1f_{mo} - {}_1f_{on} + {}_1f_{oo} \quad (77)
$$

$$
\bar{f}_m = f_m - f_o \quad (78)
$$

References

1. PROBABILISTIC ERROR AS MEASURE OF CONTROL SYSTEM PERFORMANCE, J. Zaborszky, J. W. Diesel. *AIEE Transactions*, pt. II (*Applications and Industry*), vol. 78, July 1959, pp. 163–68.

2. DESIGN OF CONTINUOUS CONTROL SYSTEMS FOR MINIMUM PROBABILISTIC ERROR, J. Zaborszky, J. W. Diesel. *Ibid.*, see pp. 44–54 of this issue.

3. DESIGN OF SAMPLED-DATA CONTROL SYSTEMS FOR MINIMUM PROBABILISTIC ERROR, J. Zaborszky, J. W. Diesel. *Ibid.*, see pp. 54–62 of this issue.

4. ANALYTICAL DESIGN OF LINEAR FEEDBACK CONTROLS (book), G. C. Newton, Jr., L. A. Gould, J. F. Kaiser. John Wiley & Sons, Inc., New York, N. Y., 1957.

5. MATHEMATICS OF CIRCUIT ANALYSIS (book), E. A. Guillemin. John Wiley & Sons, Inc., New York, N. Y., 1951.

Investigation of the Feasibility of Designing Homing Aircraft Flight Control Systems for Minimum Probabilistic Error

J. ZABORSZKY
MEMBER AIEE

JOHN W. DIESEL
ASSOCIATE MEMBER AIEE

AN EARLIER paper[1] introduced the concept of the "probabilistic" or "end-sigma" error and proposed it as a measure of control system performance and as a basis for control system design. The probabilistic square error conceptually is the average of the squared error for only those times when the output is used.

A subsequent group of papers[2–4] presents detailed design processes to find continuous or sampled-data control systems which are optimum in the sense of having minimum probabilistic error. Optimization of systems subject to constraints is also considered.[4] All these papers are general in nature; the techniques proposed are broad in scope and not tied to any specific control situation.

It is the purpose of the present paper to explore the feasibility of solving an important and complex practical control problem, flight control of a homing aircraft, by the proposed techniques. The discussion of necessity has to be of an exploratory nature, since the space limitations of a technical paper prevent the inclusion of detailed analysis of all the many aspects of a specific missile system. What is accomplished here is a demonstration of the fact that homing systems can be described in terms of concepts which are directly accessible to the design techniques[2–4] which have been developed.

The probabilistic error as a performance measure seems broader in scope than conventional performance criteria applied to the design of missile control systems since it summarizes in a single measure the various operating and input environments. The exploration is limited here to the type of homing navigation usually referred to as "Constant Bearing."

Paper 59-1152 recommended by the AIEE Feedback Control Systems Committee and approved by the AIEE Technical Operations Department for presentation at the AIEE Fall General Meeting, Chicago, Ill., October 11–16, 1959. Manuscript submitted June 16, 1959; made available for printing July 31, 1959.

J. ZABORSZKY is with Washington University, St. Louis, Mo., and Consultant to McDonnell Aircraft Corporation, St. Louis, Mo.; JOHN W. DIESEL is with McDonnell Aircraft Corporation, St. Louis, Mo.

ntrol to a Constant Bearing Course

In ideal homing the missile can be ned at the instant when homing is tiated in such a way that if both the get and missile velocity vectors re- in unchanged (no maneuvers) they will ually collide. Assuming that hom- is initiated at $t=0$, and at this time get and missile are respectively, in ints T_0 and M_0 at a range $\mathcal{R}(0)$, see Fig. a collision course will clearly have been tiated if the velocity components pendicular to the line of sight for both get and missile are equal. Thus, with speeds constant the line of sight will intain a constant bearing up to colli- n.

In an actual situation there will be th target maneuvers and errors in the tial aiming of the missile on a collision urse. Yet if the bearing of the line of ht were maintained constant, eventual lision would result. Accordingly, the ntrol system is designed to reduce to o any deviations in the bearing of the e of sight from missile to target. Only 2-dimensional problem will be treated this paper.

finitions and Reference Systems

The geometry of homing on a constant aring course will be described using the ordinate system of Fig. 1. T_0 and M_0 e are the respective positions of target d missile at $t=0$, the instant of initiation homing. V_M and V_T are the meas- ed velocity vectors of, respectively, target and the missile at $t=0$. V_{Ta} d V_{Ma} are the corresponding actual ctors. At $t=0$, the y-axis of the co- dinate system is selected to connect nts, T_0 and M_0, with the origin 0 at . Also, the origin of the co-ordinate tem is assumed to travel with con- nt speed V_M so that at time t it reaches sition O(t) with the x and y axes keeping eir original orientation. If $V_{Ma}=V_M$, $_a=V_T$, and no maneuver occurs $_M=$constant, $V_T=$constant), and fur- r, if

$$\sin[\beta(0)]=V_T\sin[\sigma(0)] \tag{1}$$

en target and missile would be, respec- ely, at points T_t' and O(t) at time t. rther, at $t=t_f$ they would collide at nt O(t_f). During the entire run, $t<t_f$, the line-of-sight from missile target would maintain a constant entation. In reality, because of initial ors and maneuvers, the missile and get will be located respectively in nts T_t and M_t at time t. If the range stance from target to missile) is $\mathcal{R}(t)$

at time t, and if the angle of the line of sight at t with the line of sight at $t=0$ is $\Delta\sigma(t)$, a small angle (from Fig. 1)

$$e(t)=X_T(t)-X_M(t)\cong\mathcal{R}(t)\Delta\sigma(t) \tag{2}$$

If, further, the actual missile speed $V_{Ma}(t)$ is maintained constant and $|V_{Ma}(t)|=|V_M|$, and if the deviation between the actual direction of $V_{Ma}(t)$ and the initial direction of V_M is $\Delta\gamma(t)$, then from Fig. 1

$$d_M(t)=V_M\int_0^t\Delta\gamma(t)dt \tag{3}$$

Further, from Fig. 1,

$$x_M(t)=d_M(t)\cos\beta_0=V_M\cos\beta_0\int_0^t\Delta\gamma(t)dt \tag{4}$$

since by the definition of the co-ordinate system, $x_M(0)=0$. Laplace transformed equations 2 and 4 become

$$E(s)=X_T(s)-X_M(s)=\mathcal{L}\{\mathcal{R}(t)\Delta\sigma(t)\} \tag{5}$$

$$X_M(s)=V_M\cos\beta_0\frac{1}{s}\Delta\Gamma(s) \tag{6}$$

Representation of Homing Navigation System with Geometry Cancellation

A simplified block diagram of a typical homing system is shown in Fig. 2. Here $G(s)$ represents the transfer function of the airframe and the servomechanism plus whatever compensating networks are to be applied. It is assumed that this transfer function is time invariant linear or at least it can be approximated as such.

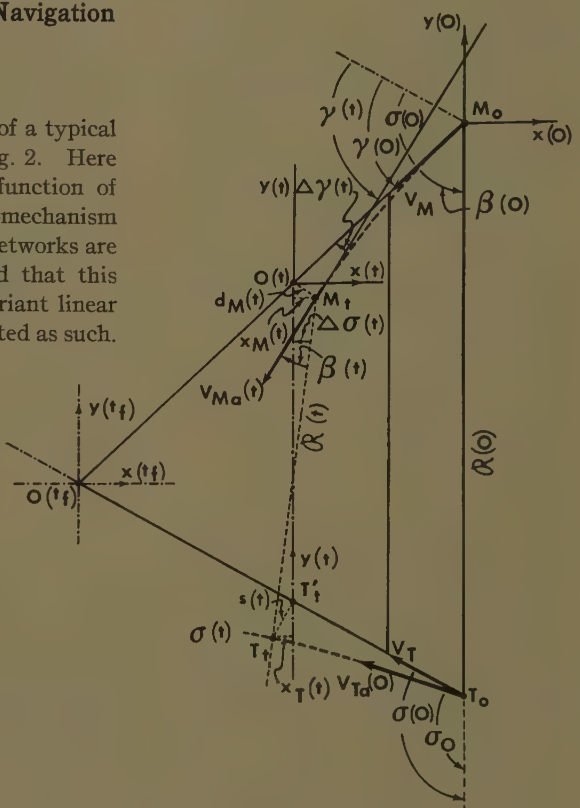

Fig. 1 (right). Geometry of homing

For feedback purposes, the output of this transfer function is $d^k\Delta\gamma(t)/dt^k$, that is, the order k derivative of the change in missile heading. Of course the eventual output of the missile is its actual heading ($k=0$), but the instrumentation may be such that the control system can only sense rates ($k=1$) or accelerations ($k=2$). The input to the transfer function $G(s)$ is a manipulated variable $\mu(t)$ produced by a computer which receives information on $d^k\Delta\sigma(t)/dt^k$, the number k (and possibly numbers higher than k) derivatives, or integral for negative k, of the change of line-of-sight angle, and information on range $\mathcal{R}(t)$, and possibly of its derivatives. The computer is permitted to be nonlinear and is able to compute derivatives of the quantities fed to it but in computing integrals of such quantities would lack information on the initial values of these integrals. Range and range rate are assumed to be approximately independent of the action of the control system, the

Fig. 2 (below). Block diagram of homing computer

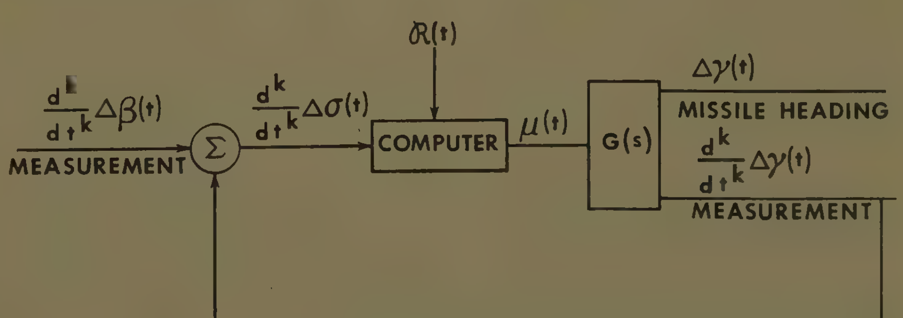

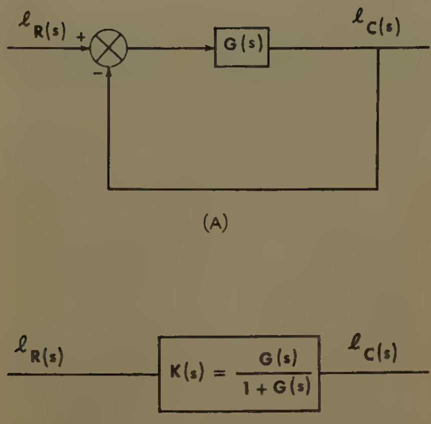

Fig. 3. Reduced block diagram

second derivative of $\mathcal{R}(t)$ is usually negligible. The computer is included in the control system in order to manipulate its output, $\mu(t)$, in a manner giving some desirable adaptive characteristics to the flight control system. Advantages in adaptive characteristics, in the sense of geometry cancellation, are exhibited by a class of computers instrumenting one of the following equations

$$\mu(t)=\frac{1}{V_M \cos\beta_0}\frac{d^{k+1}}{dt^{k+1}}(\mathcal{R}(t)\Delta\sigma(t)) \qquad k=-1,0,1,\ldots \quad (7)$$

Of chief interest are the cases $k=0$ and $k=1$. Then, from Fig. 2,

$$s^k\mathcal{L}\{\Delta\gamma(t)\}=\frac{1}{V_M \cos\beta_0}\times \mathcal{L}\left\{\frac{d^{k+1}}{dt^{k+1}}(\mathcal{R}(t)\Delta\sigma(t))\right\}G(s) \quad (8)$$

or by equations 5 and 6

$$s^{k+1}X_M(s)=\left\{s^{k+1}[X_T(s)-X_M(s)]-\sum_{i=0}^{k}s^{k-1}[x_T^{(i)}(0)-x_M^{(i)}(0)]\right\}G(s) \quad (9)$$

where superscript (i) means time derivative of order i. Defining

$$^{\ell}R(s)={}^{\ell}X_T(s)-\sum_{i=0}^{k}s^{-i-1}[{}^{\ell}x_T^{(i)}(0)-{}^{\ell}x_M^{(i)}(0)] \quad (10)$$

$$^{\ell}C(s)={}^{\ell}X_M(s) \quad (11)$$

from equation 9

$$^{\ell}C(s)=K(s)^{\ell}R(s)=\frac{G(s)}{1+G(s)}{}^{\ell}R(s) \quad (12)$$

A corresponding block diagram is shown in Figs. 3(A) or 3(B). The index ℓ refers to the number ℓ member in an ensemble of input functions, that is, to one specific input function from an ensemble.

Block Diagram with Geometry Cancellation

It should be noted that equation 12 describes a time invariant system with ordinary Laplace transfer function. Furthermore, this is a conventional unity feedback control system, Fig. 3. This means that the "geometry cancellation" is complete. The forward-loop transfer function $G(s)$ in this system, as previously described, is just the Laplace transfer function of compensating networks, servomechanism and airframe.

The output $c(t)$ of this system is the missile position along the x co-ordinates: $x_M(t)$. The $r(t)$ is the target position, $x_T(t)$ with the following quantity subtracted (equation 10)

$$e_T(t)=\sum_{h=0}^{k}\frac{1}{h!}t^h[x_T^{(h)}(0)-x_M^{(h)}(0)], \qquad k\geq 1 \quad (13)$$

$$e_T(t)=0,\ k=-1$$

Equation 13 represents part of the accumulated effect of errors in the initial aiming of the missile. The fact that this is subtracted from the input is an expression of the fact that if the control is based on rates or higher derivatives, it will not be able to eliminate some of the initial errors since it never receives information on these. Of course instrumentation considerations will frequently determine what derivatives can be used. Because of the way the co-ordinate system is selected there will always be (see Fig. 1),

$$x_M(0)=0 \qquad x_T(0)=0 \quad (14)$$

$$x_M^{(1)}(0)=0 \qquad x_T^{(1)}(0)=-V_{Ta}\sin\sigma_0+V_T\sin\sigma(0) \quad (15)$$

The last relation of course gives the initial measuring errors of target speed and heading. It can be observed from equations 13 through 15 that for $k=-1$ or $k=0$, all errors present at the time of transition to homing can be corrected, but for $k=1$ the error associated with $x_T^{(1)}(0)$ is in the blind spot of control.

While the equations are in terms of $x_T(t)$ and $x_M(t)$, it should not be forgotten that the transfer function $G(s)$ is in missile heading (or its derivatives) over manipulated input. In turn the computer requires an input consisting of range and its derivatives together with line-of-sight angle and its derivatives. These are then the quantities which must be measured or otherwise instrumented. $x_T(t)$ and $x_M(t)$ need not be instrumented in any way. These, in effect, are transitory concepts used in the course of the analysis only.

Up to this point no noise was assumed to be present; this assumption however is dropped in what follows.

The Total Input

The input, $^{\ell}r(t)$, to the computer can now be separated into a number of components

$$^{\ell}r(t)={}^{ij}r(t)={}^{i}r(t)+{}^{ij}s(t)+{}^{ij}n(t) \quad (16)$$

where

$$^{i}r(t)={}^{i}x_T(t)+{}^{i}x_e(t) \quad (17)$$

and

$$^{ij}s(t)={}^{ij}x_T(t) \quad (18)$$

The over-all ensemble is split here into two ensembles, i and j which are statistically independent. Functions $^{i}x_T(t)$ and $^{ij}x_T(t)$ represent ensembles of actual target maneuvers $^{i}x_e(t)$ is the fictitious target maneuver representing initial errors, and $^{ij}n(t)$ is the fictitious target maneuver representing noise.

The Deterministic Target Maneuvers

The $^{i}x(t)$ ensemble is assumed to be a set of possible, known deterministic target maneuvers each having a probability within the ensemble of ^{i}Q. The ergodic hypothesis does not apply to this ensemble.

Random Target Maneuvers

The $^{ij}x_T(t)$ ensemble is assumed to be a representation of random lateral maneuvers of the target. These being lateral, will fall essentially in a direction perpendicular to the initial target heading (Fig. 1) with an elongation $^{j}s(t)$. The ergodic theorem applies to the j ensemble so that $^{j}s(t)$ can be represented by a rational power spectral density of the form[2,3]

$$\Phi_{ss}(s)=B^I\frac{\prod_{\xi}(s-w_\xi^I)}{\prod_{\lambda}(s-q_\lambda^I)} \quad (19)$$

It is not necesary to label this power spectral density by j, since the j ensemble is ergodic.

Now since $^{j}s(t)$ is perpendicular to the initial target heading the corresponding component in the x direction will be established as

$$^{ij}s(t)={}^{ij}x_T(t)={}^{i}g_0{}^{j}s(t) \quad (20)$$

where

$$^{i}g_0=\cos[^{i}\sigma(0)] \quad (21)$$

is a gain that is properly a member of the i ensemble since it depends on the initial

et heading. The latter is clearly elated with the deterministic ieuvers of the target.

e Fictitious Target Maneuver

t follows from the way the co-ordinate tem is selected that any measuring or at the time of transition to homing 0) will, in latter portions of the run, ear as a fictitious target maneuver. ilar effects result from an initial turn- rate $(x_M^{(2)}(0)\neq 0)$ of the missile. has been explained in connection with ations 13 through 15 that, depending the selection of the computer, the con- system may be blind (if $k>0$) to e of this fictitious input and conse- ntly unable to correct it. The part he fictitious input which the system ble to see will be with reference to ation 13

$$t)=\sum_{h=0}^{\infty}\frac{1}{h!}t^h[x_T^{(h)}(0)-x_M^{(h)}(0)]-e_T(t)$$

$$=\sum_{h=k}^{\infty}\frac{1}{h!}t_h[x_T^{(h)}(0)-x_M^{(h)}(0)]\quad k\geq 0 \tag{22}$$

course there will be a finite practical er limit of the summation as higher ivatives of a system of given order are).

he part $e_T(t)$ of the fictitious target ieuvers which are in the blind spot of trol will produce additional square rs which can be simply added to end na if this part of the fictitious target ieuver is statistically independent of actual target maneuver and the rest he fictitious target maneuver.

e Noise Input

here will be random noise entering the ht control system. The main source he noise would be the radar. Most of noise would be directly entering (see . 1) into the information on the line- ight angle $\sigma(t)$. In equation 16, t) is the fictitious target maneuver ivalent of the noise. The angular se amplitude would approximately be ersely proportional to range $\mathcal{R}(t)$; the other hand, such changes in x_T ear as products of range and of changes $\sigma(t)$. Consequently, the noise in- nation referred to in equation 16 will independent of range or time, and in , can be considered stationary

$$t)={}^ih_0{}^jn(t) \tag{23}$$

ere ${}^ih_0$ is a constant gain determined by constants of the system and of the geometry and ${}^jn(t)$ is a stationary random process that can be described by a rational power spectral density[2,3]

$$\Phi_{nn}(s)=B^{II}\frac{\prod_{\xi}(s-w_{\xi}^{II})}{\prod_{\lambda}(s-q_{\lambda}^{II})} \tag{24}$$

There may be other noise components which vary in different ways with the range. These too can be approximated in the form of equation 23 except that ${}^ih_0$ would be time varying. Such time variation is permissible in the proposed method.

Depending on the value of k in equation 7, it may be necessary to introduce a correction of the nature of equation 22 for the initial values of the noise and its derivatives.

In most cases random signal and noise will be uncorrelated.

$$\Phi_{ns}(s)=\Phi_{sn}(s)=0 \tag{25}$$

The Desired Output

The aim of the control action is to keep the bearing of the line-of-sight constant. So the desired output[2,3] is inherently the actual target position

$$^{ij}i(t)={}^ix_T(t)+{}^{ij}s(t) \tag{26}$$

where ${}^ix_T(t)$ and ${}^{ij}s(t)$ are respectively defined under "the deterministic target maneuver." and "random target maneuvers," equations 16 through 22.

The Actual Output

With reference to Fig. 3(B) and equation 16, this is obtained in the s domain

$$^{ij}C(s)=K(s)\ {}^{ij}R(s) \tag{27}$$

or in the t domain

$$^{ij}c(t)=\int_0^{\infty}k(t)\ {}^{ij}r(t-\tau)d\tau \tag{28}$$

The Error

This is defined[2-4] as the difference between the desired and actual outputs,

$$^{ij}e(t)={}^{ij}i(T)-{}^{ij}c(t) \tag{29}$$

or with equations 13 and 26,

$$^{ij}e(t)={}^ix_T(t)+{}^{ij}s(t)-{}^{ij}x_M(t) \tag{30}$$

Probability Distribution of Output Utilization Times

The control action will not be fully successful in keeping the bearing of the line-of-sight constant or the error ${}^{ij}e(t)$ (equation 29) zero, but it will keep it small. Should ${}^{ij}e(t)$ be zero or $x_M(t)=x_T(t)$, then target and missile would collide (see Fig. 1) in point $O(t_f)$ at time,

$$^it_f(\mathcal{R}(0))=\frac{\mathcal{R}(0)}{V_M\cos{}^i\beta(0)-{}^iV_T\cos{}^i\sigma_0} \tag{31}$$

These times are shown here as functions of initial range $\mathcal{R}(0)$ and of i, the index of the i ensemble of functions. This ensemble is to be interpreted here as an ensemble of sets or matrices of functions and quantities which are statistically interrelated to each other; specifically: function ${}^ix_T(t)$, the deterministic target maneuver, function ${}^ix_e(t)$, the fictitious target maneuver caused by initial measuring errors, and quantities ${}^i\beta(0)$ and ${}^i\sigma_0$, the initial headings of missile and target. If $\mathcal{R}(0)$ is statistically dependent on these members of the i ensemble it too should be considered a member of this ensemble. Conversely, initial measuring errors condensed in ${}^jx_e(t)$ are actually a subensemble in i which could be statistically independent of ensemble i. The actual distance of the target and missile (Fig. 1) would of course be

$$d(t)=[(x_T(t)-x_M(t))^2+(y_T(t)-y_M(t))^2]^{1/2} \tag{32}$$

However, if $x_T(t)-x_M(t)$ changes relatively little when t is near t_f then the minimum distance will occur when $y_T(t)-y_M(t)=0$ that is at about $t=t_f$. Now the missile will be exploded about the time of minimum distance. This means that for given initial range $\mathcal{R}(0)$ and target maneuver number i, the ${}^iq(t|\mathcal{R}(0))$ conditional probability density of time interval t from transition to homing to explosion will exhibit a more or less narrow peak centering around ${}^it_f(\mathcal{R}(0))$, For example

$$^iq(t|\mathcal{R}(0))=\frac{1}{2a\sqrt{\pi}}e^{-\frac{[t-{}^it_f(\mathcal{R}(0))]^2}{2a^2}} \tag{33}$$

Frequently, say in the case of a missile used against an approaching attacker, it will be possible to assume that the target maneuver, initial error, and initial bearings of missile and target are statistically independent of the initial range $\mathcal{R}(0)$, and further, that the initial ranges have a probability distribution $q(\mathcal{R}(0))$. This distribution may be influenced, for instance, principally by the way salvos or sequences of missiles would be fired at an attacker. Then the over-all probability distribution of time elapsing from the activation of the system; that is, the initiation of homing to the output utilization (explosion) takes the form

$$^ip(t)=\int_0^{\infty}q({}^i\mathcal{R}(0)){}^iq(t)d\mathcal{R}(0) \tag{34}$$

Naturally this probability density is still dependent on i. In other words, a different distribution will belong to every member set of the i ensemble including

initial headings, ${}^i\beta(0){}^i\sigma(0)$, initial error ${}^ix_e(t)$, and deterministic target maneuver ${}^ix_T(t)$. Conversely, if the range $\mathcal{R}(t)$ is statistically a member of the i ensemble, the probability density of output utilization will be from equation 33

$$ {}^ip(t)=\int_0^\infty q({}^i\mathcal{R}(0))\,\frac{1}{2\sqrt{\pi}\sigma}\times e^{-\frac{[t-{}^it_f({}^i\mathcal{R}(0))]^2}{2a^2}}\,d\,{}^i\mathcal{R}(0) \quad (35) $$

If, further, the i ensemble is restricted to one member, and $a\rightarrow 0$ so that ${}^ip(t)=\delta(t-{}^it_f)$, a Dirac delta function, then the special case of a final value system[5–7] results.

Design for Minimum Probabilistic Error of Homing Flight Control System with Geometry Cancellation

The flight control system of a homing aircraft with geometry cancellation has now been reduced to the concepts, terminology, and notations of references 2, 3, and 4. The functions defined in equations 16 through 26 feed directly, with identical notations, into lines 1 through 4 of Table I(A) and lines 1 through 6 of Table I(B) of references 2, 3, or 4. Furthermore, this provides all the necessary information to carry out the computations in Tables I and II of references 2, 3, and 4. The result of the computation (lines 9 and 10, Table II, reference 2) is the impulse response $k(t)$, Fig. 4(B), of the flight control system which has the smallest probabilistic error (ε is also obtained from this calculation) among all time invariant linear systems. The geometry compensated homing system was shown previously to be time invariant linear as shown in Fig. 3(B). The optimum time-invariant closed-loop transfer function $K(s)=\mathcal{L}\{k(t)\}$ can then be easily converted into the corresponding open-loop transfer function $G(s)$ of Figs. 3(B) or 2. This latter contains the existing "plants" of the servomechanisms and airframe. Comparing the transfer functions of these latter existing components with the desired optimum open-loop transfer function $G(s)$, it is easy to establish the transfer function of necessary compensating computers. This process of optimization has been introduced in detail[1–4] and extensively illustrated by numerical examples.[2,3] The purpose of the present paper is only to show that the geometry compensated homing flight control system is one case of a control system to which these processes apply. Application of these techniques results in a control system which gives minimum mean square miss performance in a broadened sense, over an extended class of input and range environments.

In reality, the discussions in preceding sections of this paper establish merely the definitions and concepts and outline the determination of the various functions and quantities which are necessary inputs to the computations of references 2, 3, or 4 in order to optimize the flight control system in the minimum probabilistic error sense. For an individual case it still may require substantial effort to carry out the required determinations of the various functions, to analyze inputs, etc. Space and other restrictions make i[t] clearly impossible to include the detail[s] within the confines of a technical paper.

Conclusions

It is shown that the general problem of the homing aircraft can be expressed in terms of concepts which make it amenable to computations developed[2–4] for designing control systems to operate with minimum probabilistic square errors.

The probabilistic error[1] extends the generality of conventional measures of performance because it summarizes the performance of a system over its entire operating environment.

References

1. Probabilistic Error as Measure of Control System Performance, J. Zaborszky, J. W. Diesel. *AIEE Transactions*, pt. II (*Applications and Industry*), vol. 78, July 1959, pp. 163–68.

2. Design of Continuous Linear Control Systems for Minimum Probabilistic Error, J. Zaborszky, J. W. Diesel. *Ibid.*, see pp. 44–5[3] of this issue.

3. Design of Sampled Data Control Systems for Minimum Probabilistic Error, J. Zaborszky, J. W. Diesel. *Ibid.*, see pp. 54–62 of this issue.

4. Design for Minimum Probabilistic Error of Continuous Linear Control Systems Subject to Constraints, J. Zaborszky, J. W. Diesel. *Ibid.*, see pp. 63–66 of this issue.

5. Optimum Design and Miss Distribution of Homing Missiles, R. C. Booton, Jr. Dynamic Analysis and Control Laboratory, Massachusetts Institute of Technology, Cambridge, Mass., 1950.

6. An Optimization Theory for Time-Varying Linear Systems with Nonstationary Statistical Inputs, R. C. Booton, Jr. *Proceedings*, Institute of Radio Engineers, New York, N. Y., vol. 40, Aug. 1952, p. 977.

7. Final Value Controller Synthesis, M. V. Mathews, C. W. Steeg. *Transactions*, Professional Group on Automatic Control, Institute of Radio Engineers, vol. PGAC-2, Feb. 1957, p. 6.

Transient Decay of Current Through Paralleled Mercury-Arc and Silicon Rectifiers

W. R. HODGSON
MEMBER AIEE

THE ADVENT of silicon semiconductor rectifier applications to large potlines has brought about application problems heretofore not significant. Many of the users of large amounts of d-c power wish to try a large power silicon rectifier in actual service before the purchase of a complete potline. Since the greater majority of the existing potlines have mercury-arc rectifiers providing the d-c power, it is only natural to put a silicon rectifier on a potline in parallel with the mercury-arc rectifiers. Fig. 1 is a single-line diagram of a modern electrochemical potline. The normal method of de-energizing the line is to trip the master a-c circuit breaker feeding all units. The problem of magnitude of potline decay current which must be handled by [a] single silicon rectifier in parallel with several mercury-arc rectifiers under these conditions requires analysis.

Comprehensive analytical solutions t[o] many engineering problems have bee[n] occasionally bypassed in favor of les[s] time-consuming approximate solutions. Noteworthy among such problems ar[e] those classified as being of the distributed parameter type. From the standpoint o[f] definition a distributed parameter problem can be one in which the descriptive components are distributed in time. Fo[r] example, a study of the effects of a decay

Paper 60-36, recommended by the AIEE Industrial Power Rectifiers Committee and approved by the AIEE Technical Operations Department for presentation at the AIEE Winter General Meeting, New York, N. Y., January 31–February 5, 1960. Manuscript submitted November 2, 1959; made available for printing December 1, 1959.

W. R. Hodgson is with the Westinghouse Electric Corporation, East Pittsburgh, Pa.

1. Typical single-line
ram of mercury-arc rectifier
ine with single silicon
rectifier in parallel

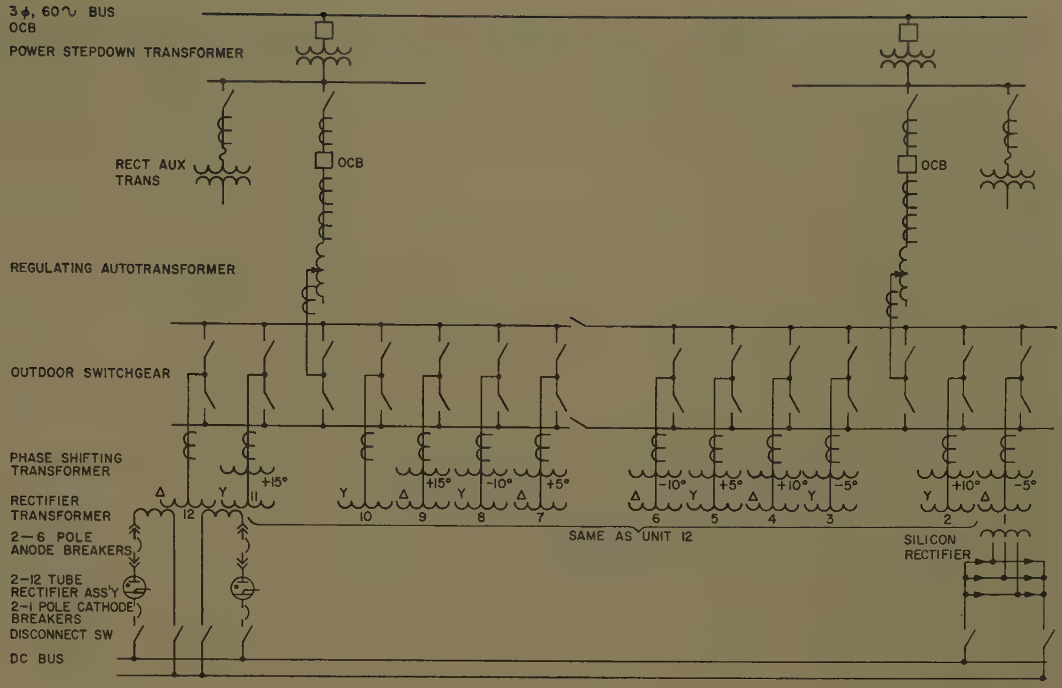

d-c potline current on a silicon recti- in parallel with ignitron rectifiers is a blem of this type.

he approximate solutions to these blems involve the application of sim- ying assumptions and limited number solutions in order to obtain results by d-solution techniques in a reasonable iod of time. However, with the aid of nputer equipment a minimum number implifications need be made. With this hnique the parameters of the problem be changed at will in order to deter- e their effect on the fixed parameter ng studied. This allows a more rough study of the problem more ckly and at less cost than the corre- nding solution by hand

his paper will discuss this problem, method of using computers to obtain lution, and the results and conclusions his study in analyzing the decay of a e electrochemical potline d-c distri- ion under trip of a main a-c circuit aker.

menclature

₁=impedance mercury-arc rectifier in- cuding transformer, mercury-arc tube, and bus
=impedance silicon rectifier including silicon cells and bus
=bus impedance between units
=impedance nth mercury-arc rectifier
=impedance low-voltage potline bus loop
=equivalent impedance of n mercury- arc rectifiers
=equivalent impedance of silicon rectifier
=potline back emf
=potline current total
=silicon rectifier current
=mercury-arc rectifier current
L = inductance
R = resistance

System Considerations

A typical potline may consist of 30,000 to 120,000 amperes d-c at 300 to 800 volts. In the past this has generally been supplied by several mercury-arc rectifiers operating in parallel as shown in Fig. 1. Each of the mercury-arc rectifier sections have cathode and anode breakers. In general, a single a-c circuit breaker will feed the entire potline rectifier group. Load tests[1,2] in the field have been made which show that the most satisfactory method of removing a rectifier line from service is to trip the master a-c breaker, thus removing a-c power simultaneously from all units. The potline current will then decay through the mercury-arc tubes and rectifier transformers dividing between the paralleled units. Field tests have shown this method to be quite suitable for mercury-arc rectifiers.

The situation is somewhat changed when a silicon unit is paralleled on the bus with mercury-arc units. This is due to the fact that a 6-phase double-way circuit is used with silicon rectifiers whereas a 6-phase double-Y single-way circuit is used on the mercury-arc unit. Reference

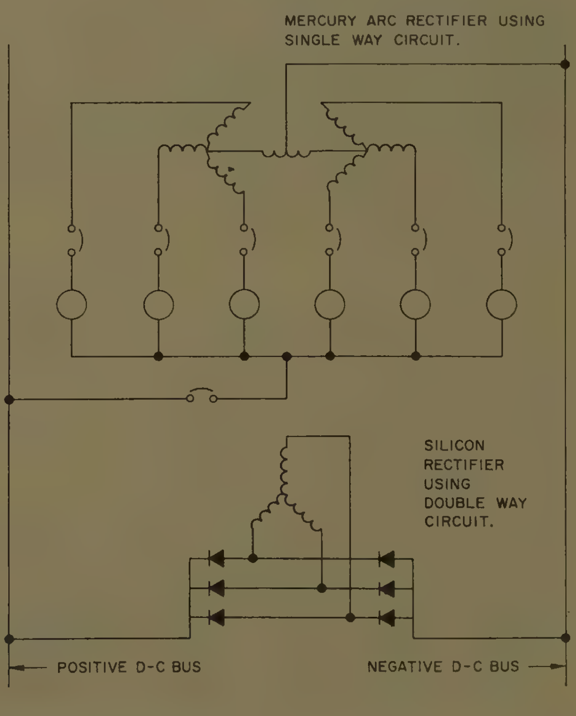

Fig. 2. Six-phase double-Y single-way mercury-arc circuit and 6-phase Y double-way silicon rectifier d-c circuits

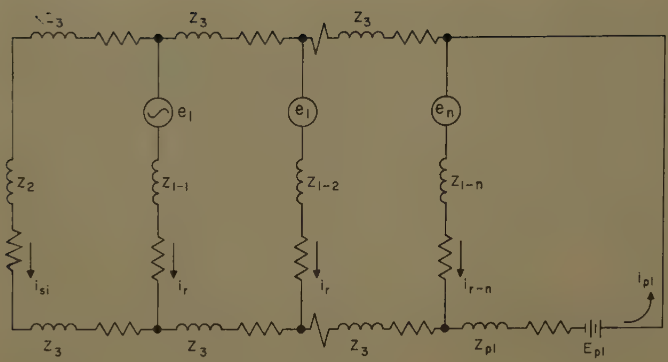

Fig. 3. Equivalent circuit d-c system

to Fig. 2 will show the difference in the circuits. The mercury-arc rectifier has a transformer winding impedance in series with the tube, while the silicon rectifier cell with its double-way circuit is connected directly between the d-c busses are shown in Fig. 2.

The impedance of the circuit will determine the division of current flow under transient conditions. Since the silicon rectifier section has a much lower impedance than the mercury-arc rectifier sections, it is necessary to determine how much of the potline decay current will flow through the silicon rectifier and to analyze this as to its effect on the silicon cell itself. Reference to the silicon unit shown in Figs. 1 and 2 shows that when there is no a-c power on the silicon unit, the diodes in all three phases in series with the diodes on the other side of the bridge circuit are in parallel across the bus. In effect, this increases the current-carrying capability of the silicon rectifier. This immediately indicates that the unit can handle more than its normal short-time rating for the short period of time required until the potline current decays to zero. This, coupled with the fact that the time constant of most potlines is only a matter of a few cycles (approximately 6 to 10 cycles), greatly increases the safe current-handling capacity of a silicon rectifier unit and lessens the probability of silicon rectifier cell destruction due to large currents handled during potline decay.

Normal short-time current-carrying curves provided by silicon cell manufacturers cannot be utilized to determine the capability of the rectifier under these conditions. This is due to the fact that the short-time rating curves are generally based on 180-degree conduction whereas with the rectifier discharge current from the potline 360-degree conduction results. Due to the configuration of the phases in which all three are in parallel, unbalance will result between paralleled silicon cells which must be taken into account in the final analysis. With 180-degree conduction cycles the alternate nonconducting cycles will generally allow some cooling of the junction and in effect provide a different temperature excursion from that experienced with 360-degree conduction which has no alternate nonconducting cycle. For these reasons final analysis must be made on the basis of the heat which can be stored or dissipated by the silicon cell during the short conducting period during current discharge At no time during the decay can the amount of heat generated in the diode from the current flowing through it exceed the capabilities of the silicon cell or failure of the cell would result.

It appeared advisable to analyze the resultant decay of direct current on a potline to determine if any special precautions must be taken to protect the silicon cells during potline current decay in applications where parallel operatio with mercury-arc rectifiers is conten plated.

A typical system of the type being cor sidered is shown in Fig. 1. The primar consideration is to determine the current in the d-c section of the silicon rectifier therefore only the impedances in th secondary side are considered. A lump ing of common d-c loads and source connected to the d-c bus was made to ob tain the equivalent circuit.

This equivalent circuit for the d-c sys tem is shown in Fig. 3.[1,2] The componen parts contain impedances of low-voltag secondary conductors and mercury-ar tubes or silicon rectifiers and, in the cas of the mercury-arc rectifier, the trans former winding impedances. The resist ance and inductance of conductors can b obtained by fundamental formulas. Th resistance of the rectifiers was assume constant and obtained by ratio of rect fier cell or tube voltage drop to tube cur rent for a number of load conditions. Th breaker impedance was neglected sinc it is negligible with the breaker contact closed.

The impedance Z_R for the mercury-ar rectifiers and Z_s in the simplified equiva lent circuit in Fig. 4 for the silicon rect fiers is a summation of the impedance between the low-voltage side of the rect fier transformer and the cathode bus or i case of silicon rectifier between the d- bus. Included in these two impedanc values is impedance Z_3 (Fig. 3) for the d- bus system. Impedance Z_R for th mercury arc represents several parall units. This Z_R impedance is the equiva lent impedance of each of the norma mercury-arc rectifiers in steady state an accordingly only one phase of the Y conducting at a time. The impedanc therefore includes transformer and inte phase impedances plus bus-bar and tub impedances. On this basis the potlin mercury rectifiers can be simplified a shown in Figs. 3 and 4. The mercury-a

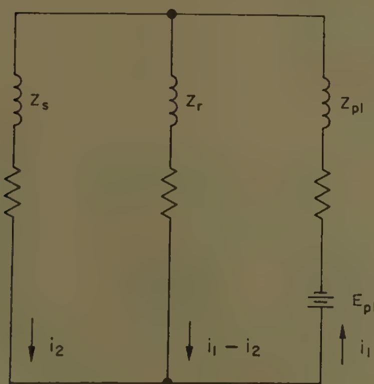

Fig. 4 (left). Simplified equivalent circuit of d-c system as entered into computer

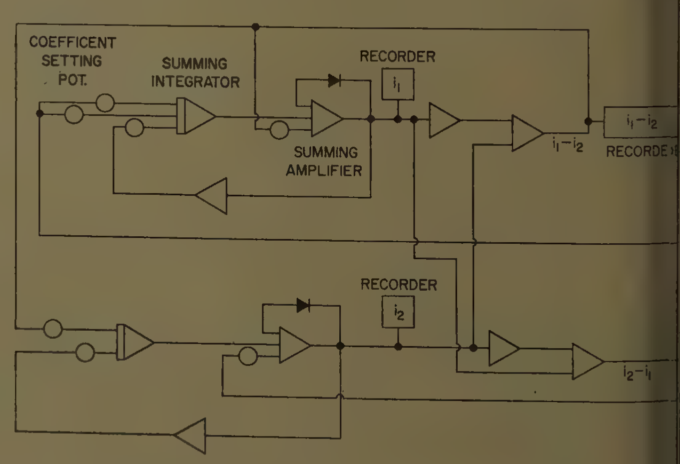

Fig. 5 (right). Block diagram of analog computer for study of potline currents

ifier circuit can be further simplified hout affecting results by lumping all he impedances into a single equivalent t as shown in Fig. 4.

mpedances in the silicon section since transformer windings are not in the charge path consist simply of the imlances in the rectifier sections and in bus bar. The simplified circuit of . 4 shows the lumped silicon paramrs.

Tests have been run in the field to ermine resistance and inductances of line circuits.[1,2] Since these values y quite considerably, a series of imlance values (Z_p) for the potline was inated in order to study the problem. the usual system the potline inductance relatively large compared with other tem components.

mputer Analysis

For the purpose of this study it was ermined that a compound *RL* circuit sts as shown in Fig. 4, and that steadyte conditions had been reached before circuit was de-energized by opening the circuit breaker. The resulting nsient must then restore the circuit normal conditions, that is, $I=0$. The tching operation takes place at time 0 and the analysis was made to estigate the current at subsequent es during the transient period. Since ady state has been reached prior to the tching operation the current flowing at 0 is

$$= \frac{E-B_{emf}}{R}$$

s current will serve as a boundary dition. After the switching operation urs, the differential equation, which lies is as follows:

$$+Ld_i/dt=0$$

s must, however, be modified due to back electromotive force (emf) of the s and since two parallel paths exist shown in Fig. 5 two simultaneous loop ations result. Referring to Fig. 4, equations to be solved are

$$+i_1(R_{pl}+R_r)+di/dt(L_{pl}+L_r)- L_rdi_2/dt-R_ri_2=0 \quad (1)$$

$$+L_r)di_2/dt+(R_r+R_s)i_2- L_rdi_1/dt-R_ri_1=0 \quad (2)$$

ince these equations have the first erential *di/dt* of the current, it leads an ideal solution for the differential lyzer. For this reason all solutions e made on the differential analyzer actually plotted rather than tabulated. Fig. 5 is a computer block schematic of equations 1 and 2 entered to obtain the required solution from the differential analyzer. Fig. 6 shows the results in plotted form as taken from the the differential analyzer as a solution to one set of parameters.

Only *R* and *L* were considered in this analysis and only the overdamped solution in which the current will rise to a maximum and die away gradually, has been considered as a solution. Experience indicates that this is reasonable for potline d-c circuits.

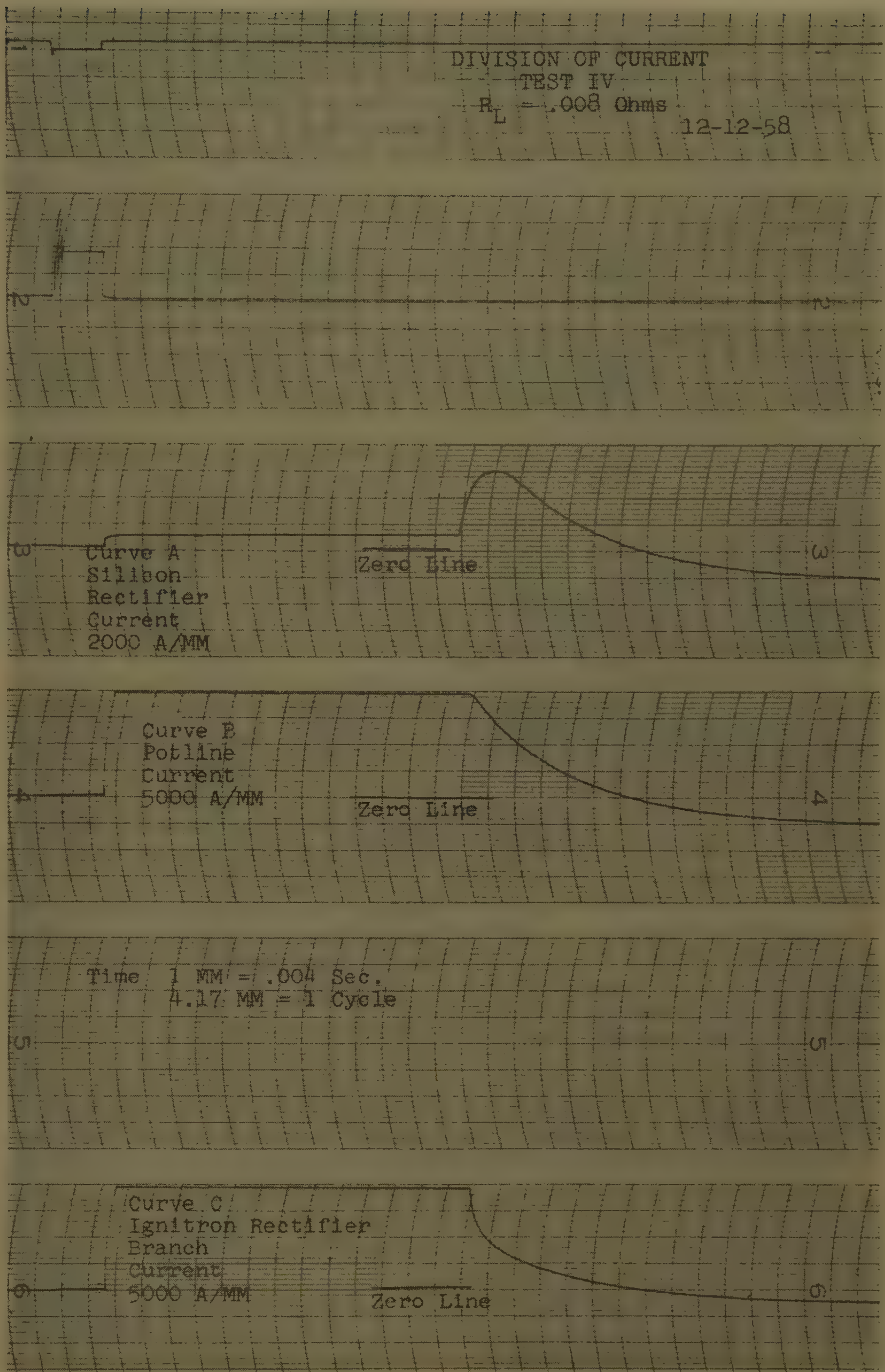

Fig. 6. Typical solution as obtained from differential analyzer

In order to obtain definite information from the foregoing equations it is necessary to know the variables at the start of the conditions, that is, at time zero. These values then allow the input voltages of each integrator at the start of computation to be defined. Each of the integrators as shown in Fig. 5 has a provision for setting initial conditions into the computing device. It is not the purpose of this paper to describe the machine to do the computing since many papers and articles have been written on that subject. Normally there is more

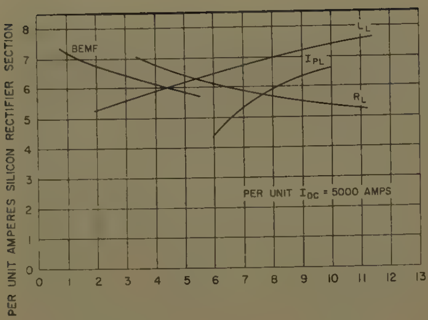

Fig. 7. Variation of silicon rectifier current under various potline parameter conditions

L_L=potline inductance, microhenrys $\times 10^2$
R_L=potline resistance, ohms$\times 10^{-8}$
BEMF=back emf of potline, volts$\times 10^2$
I_{pL}=potline current, kiloamperes$\times 10$

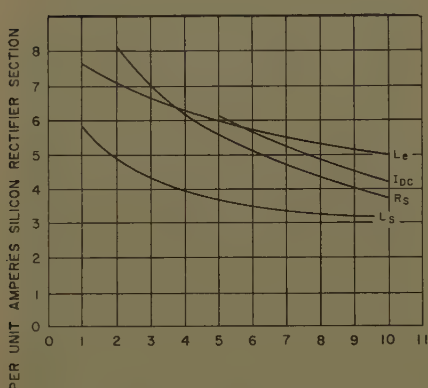

Fig. 8. Variation of silicon rectifier current under various silicon rectifier, mercury-arc rectifier, and bus parameter conditions

L_s=silicon unit inductance, microhenrys$\times 10$
R_s=silicon unit resistance, ohms$\times 10^{-4}$
I_{dc}=silicon unit rating, kiloamperes
L_e=parallel inductance of mercury-arc rectifier and system, microhenrys

than one computer setup for a given problem and the selection of one over the other is generally made for reasons of economy, better accuracy, or because of scale factor advantages. In simplifying the problem, computer setups involving more integrations than absolutely needed were not considered.

Analysis of Results

Fig. 6 depicts a typical run as taken from the computer information. This figure graphically shows the decay of potline current, the decay of current through the paralleled mercury-arc rectifiers, and the initial increase in current and final decay through the silicon rectifier. At the instant the breaker is tripped the potline current is 100,000 amperes and the silicon rectifier is carrying 5,000 amperes. The mercury-arc rectifier provides the remaining 95,000 amperes. One cycle after the circuit has been interrupted the potline current has decayed to 85,000 amperes while the mercury-arc rectifiers have fallen to 52,000 amperes. The remaining 33,000 amperes is now flowing through the silicon rectifier. The maximum current in the silicon rectifier is reached at approximately one cycle from which time it begins to decay to zero.

Since the effect of various parameters was desired, a given parameter was varied over a fixed range and several runs made on the computer. These computer runs were made changing one variable and holding all others constant to determine the effect of changing any circuit impedance values. Several runs were made with two variables being changed in order to determine if interpolation between curves could be made with several variables changed. Results of these tests indicate that if a given set of potline conditions is known, interpolation between curves has shown that the results can be accurately predicted to any given set of conditions. The results of the various runs thus provide a curve which has been reproduced in Figs. 7 and 8. These figures provide a visual indication of the effect of changing a parameter on the amount of current which must be handled by the silicon rectifier during potline decay.

Fig. 7 plots the effect of potline parameter conditions. The effect of increasing the back emf or potline resistance is to lessen the discharge current in the silicon section. Decreased size of the potline, since the silicon rectifier is now a larger percentage of the potline current, decreases the per-unit transient current in the silicon rectifier section. An increase in potline inductance tends slightly to increase the duty on the silicon rectifier section.

Fig. 8 shows that an increase in inductance or resistance in the silicon potline section will decrease current in the silicon section. Therefore, in physical placement of the unit on the potline bus the geometry of the bus should be taken into consideration to obtain maximum permissive reactance between it and the paralleled mercury-arc units. Increasing the size of the silicon section also decreases its per unit current for two reasons: 1. It is a larger percentage of potline size. 2. It has a higher short-time capability since more silicon cells are available to share the load.

As previously indicated the capability of the silicon rectifier to carry the high potline discharge must be analyzed from

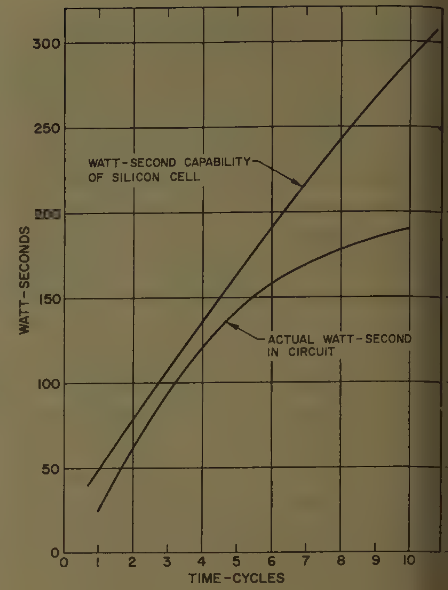

Fig. 9. Comparison of watt-seconds of typical silicon cell and watt-seconds in silicon rectifier during potline decay

the standpoint of the heat developed in the silicon cell due to the losses generated from this current. This has been analyzed as shown in Fig. 9. The curves in this figure are all reduced to the capabilities of a single cell. The watt-seconds which must be dissipated are determined from the number of diodes in parallel, a derating factor due to unbalance between parallel cells on a single phase, and the fact that for discharge of a direct current all three phases are in parallel. Reasonable unbalance factors were taken into consideration in determining how much current would be divided between the three parallel phases. As indicated in Fig. 9, the silicon cell is capable of handling the total watt-seconds for this particular case. If the complement of cells or the size or type of cell are changed, or configuration is to be changed the capabilities of the cell must be rechecked.

Conclusions

The program described in this paper has proved capable of predicting the current that a silicon rectifier must handle when operating in parallel with mercury-arc rectifiers during the transient phenomena associated with master trip of the a-c breaker to de-energize the potline. From Figs. 7 and 8 the effect of various parameters on the magnitude of current handled by the silicon rectifier can be summarized. The values on the curve cover a wide range of parameters and should give indication of the current expected once the potline parameters are known.

)n a given potline, the back emf, the uctance and resistance of the potline, l the ampere size are a fixed param-r. The amount of potline discharge rent can therefore be predicted from s. 7 and 8 once the rating and physical figuration of the silicon rectifier unit etermined.

'he proper placement on the potline can be predicted to give impedance ues in the silicon branch to obtain rents within the capabilities of the s being used. Thus assurance can obtained that the silicon rectifier unit can satisfactorily handle the potline discharge current. Even considering the most severe set of conditions that the present limit of practical potlines imposes, the transient currents are well within the short-time capabilities of silicon units investigated as shown in Fig. 9.

With the program as followed on the computer sufficient data were obtained to assist in analysis of paralleled mercury-arc rectifiers and silicon rectifiers during the transient phenomena associated with potline decay.

References

1. Field Tests on a 100-Megawatt Rectifier Installation, J. K. Dillard, John Kiefer, C. S. Hague. *AIEE Transactions*, pt. I (*Communication and Electronics*), vol. 74, May 1955, pp. 245–53.

2. Load-Dropping Tests in a Large Ignitron Rectifier Installation, S. J. Pope, J. K. Dillard, C. R. Marcum. *Ibid.*, vol. 72, May 1953, pp. 164–75.

3. Mathematical Model and Procedure for Arc-Back Current Calculations for Paper Rectifiers, H. P. Fullerton, J. Teno. *Ibid.*, pt. II (*Applications and Industry*), vol. 77, Nov. 1958, pp. 456–64.

4. Comparison of Calculated and Measured Arc-Back Current in Large Power Rectifier Systems, J. Teno, C. H. Titus, R. N. Wagner. *Ibid.*, 1958 (Jan. 1959 section), pp. 585–89.

Series Capacitors Applied to Power Rectifiers

L. J. HIBBARD
MEMBER AIEE

T. J. BLISS
MEMBER AIEE

HE SERIES CAPACITOR for a number of years has been a recognized ans of reducing the regulation of power smission circuits. This paper is oted to a study of its application to le-phase power rectifiers supplying uctive loads. It is shown here that es capacitors may be of significant p in reducing the voltage regulation the d-c load. Recommendations are red for the selection of the appropriate acitor rating and for capacitor proion. Data are given concerning the ct of the series capacitor on the k inverse voltages experienced by the ifier elements. Laboratory data are mitted to demonstrate what degree uccess may be anticipated in achieving theoretically predicted performance n the series capacitor is applied. The hors hope this study will further the eptance of series capacitor applications encourage others to extend the lysis to include multiphase rectifiers.

'he authors became interested in this investigation several years ago during a study of the feasibility of converting the facilities of electrified railroads from the use of 25-cps (cycle per second) power to 60-cps power. Where recent locomotive additions were of the rectifier type, it appeared desirable to determine if a simple means existed to make them operate satisfactorily at the higher frequency. This required that the regulation be reduced from the otherwise undesirably high level which would result from the increased supply system and rectifier transformer reactance at the higher frequency. The series capacitor appeared a hopeful means of accomplishing this end and so this study was initiated. Recognizing that this application is so limited as to interest but a few engineers, the authors have made the following material entirely general so that it is applicable to a much wider variety of rectifier applications.

The elements of the circuit studied are shown in Fig. 1. A single-phase a-c power source is assumed connected to terminals *a-d*. The series capacitor is represented by C. The inductance L_1 represents the leakage inductance of the rectifier transformer plus the inductance of the supply circuits and the power source itself. The inductances L_2 represent any inductance between the transformer terminals and the rectifiers. Direct current is produced in the load having resistance R_L and inductance L_L. Point n in the *e-f* winding is a center tap, of course.

Significant voltage and current relationships for the circuit of Fig. 1 are shown in Fig. 2. In preparing this figure it was assumed that load inductance L_L is so high that the d-c load current I_d is constant, i.e., has no "ripple." This makes analysis simpler and is not a poor approximation of the effects of practical inductive loads.

Two points of significance should be brought out in connection with Fig. 2. First, the presence of the capacitor causes commutation (that period designated by angle u in Fig. 2 when both rectifying elements are conducting as the load current is alternately transferred from one to the other) to commence in each half-cycle at an angle leading the instant when the supply voltage goes through zero. Without the series capacitor this angle, defined as δ and indicated in Fig. 2, is zero, and it is this difference plus the fact that the angle δ is referred to in latter portions of this paper which make it of interest.

er 60-39, recommended by the AIEE Industrial er Rectifiers Committee and approved by the E Technical Operations Department for prestion at the AIEE Winter General Meeting, York, N. Y., January 31–February 5, 1960. uscript submitted November 2, 1959; made lable for printing December 9, 1959.

. Hibbard was with Westinghouse Electric poration, East Pittsburgh, Pa., until his recent ement; T. J. Bliss is with Westinghouse Elec-Corporation, Boston, Mass.

authors wish to acknowledge their debt to Mr. . Dillard for his initial help in the investigation to Mr. M. K. Enns for carrying out the reed computations and preparing the curves.

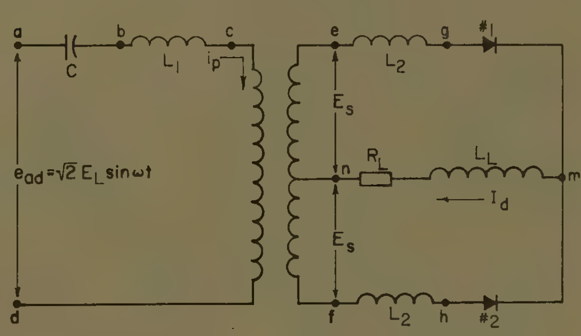

Fig. 1. Basic idealized circuit of a single-phase full-wave rectifier with series capacitator

More significant is the effect of the capacitor on the d-c voltage plot e_{nm}. Note that during the intervals when the rectifier elements are not commutating that the voltage e_{bd} measured on the rectifier side of the series capacitor is greater than the supply voltage since e_{bd} is equal to the supply voltage e_{ad} less the capacitor voltage e_{ab}. During the same noncommutating intervals, the voltage drops across the inductance L_1 and L_2 are zero since the currents through them are constant (because I_d was assumed constant). Thus, since e_{bd} is higher than it would be without the series capacitor so also is the d-c load voltage e_{mn}. It is exactly this ability of the series capacitor to increase the d-c load voltage that is the subject of this paper.

It now remains to report the details and results of the investigation made as to the practical benefits obtained and problems, if any, incurred in such applications of series capacitors. The investigation was conducted in three steps reported in the following sections: a theoretical analysis; a laboratory study using analog circuitry; and a full-scale laboratory study.

Analytical Study

The mathematical analysis was carried out using the assumptions stated or implied in the introductory discussion, namely:

1. The entire circuit is free of resistance except the load having resistance R_L.

2. Load inductance L_L is so large that load current I_d is absolutely constant. Thus the rms, the average, and the crest value of I_d are identical.

3. Rectifiers *1* and *2* are theoretically perfect rectifying elements having zero resistance to the flow of current in one direction and infinite resistance to reverse flow.

4. Applied voltage e_{ad} is a perfect sinusoidal function of time.

The average value of the load voltage e_{mn} is denoted as E_d, and by definition E_{d0} is the value of E_d at zero load. The rms value of the a-c voltage appearing between transformer terminal e (or f) and midpoint n at no load is defined as E_s and the rms value of the applied a-c voltage e_{ad} is defined as E_L.

For the purpose of generalization and to avoid confusion over transformer turns-ratio, the concept of commutating reactance is employed. This reactance is identified as X_L rather than X_c as prescribed in standards[1] to avoid possible confusion with capacitive reactance, and for the purposes, of this paper X_L will represent the inductive commutating reactance only, i.e., total commutating reactance with no series capacitor. With this reservation, the commutating reactance X_L for the circuit of Fig. 1, as defined by the American Standards[1] is

$$X_L=\frac{2\pi f}{2}\left[\left(\frac{E_s}{E_L/2}\right)^2 L_1+2L_2\right]$$

$$=\pi f\left[\left(\frac{E_s}{E_L/2}\right)^2 L_1+2L_2\right] \quad (1)$$

where f is the frequency of applied voltage e_{ad}.

Similarly, X_C is defined as the capacitive commutating reactance and is

$$X_C=\frac{1}{2}\left(\frac{E_s}{E_L/2}\right)^2\frac{1}{2\pi fC} \quad (2)$$

The nomenclature gives appropriate units for all quantities in the foregoing equations and subsequent material.

The ratio of X_C to X_L or in other words, the value of X_C expressed in per unit (pu) of X_L represents the pu compensation provided by the series capacitor and was found to be a most convenient means of generalizing the results. Similarly, the currents were placed in a generalized or pu form by defining the base current I_b as the rms value of the steady-state a-c current which would flow in the transformer secondary with $X_C=0$ and both diodes short-circuited. Thus

$$I_b=\frac{E_s}{X_L} \quad (3)$$

If $I_{d\ pu}$ is defined as the pu value of the load current, then

$$I_{d\text{pu}}=\frac{I_d}{I_b}=\frac{I_dX_L}{E_s} \quad (4)$$

While this definition of pu load current appears to contain s strange combination of average and rms values, it was found a convenient device since all curves plotted as a function of $I_{d\ pu}$ are demonstrative of the effect of varying any of the three quantities I_d, X_L or E_s. Indeed to avoid losing sight of this, pu load current is hereafter identified in both text and curves by the ratio I_dX_L/E_s rather than the somewhat less cumbersome symbol $I_{d\ pu}$. Those familiar with rectifier terminology will recognize the pu load current expressed in this form as identical to the commutating reactance factor inasmuch as direct current commutated by each rectifier device is identical to the load current I_d.

The mathematical analysis conducted is detailed in Appendix I. The desired goal was to obtain curves of d-c load voltage E_d versus d-c load current I_d, or more generally, curves of the ratio E_d/E_{d0} against pu load current I_dX_L/E_s for various degrees of compensation, i.e., values of the ratio X_C/X_L. Three sets of equations requiring sequential solution are derived in Appendix I. The first set relates the angle of overlap u to the angle by which commutation precedes zero value of source voltage (angle δ, see Fig. 2) for any selected value of X_C/X_L. This set is comprised of equations 34 for $X_C/X_L\neq 1$ and 35 for $X_C/X_L=1$. The second set solves for I_dX_L/E_s given u, δ, and X_C/X_L: equation 36 for $X_C/X_L\neq 1$ and 37 for $X_C/X_L=1$. The third set, comprised of equation 43 only (good for all values of X_C/X_L), then relates E_d/E_{d0} to u, δ, and I_dX_L/E_s for any X_C/X_L.

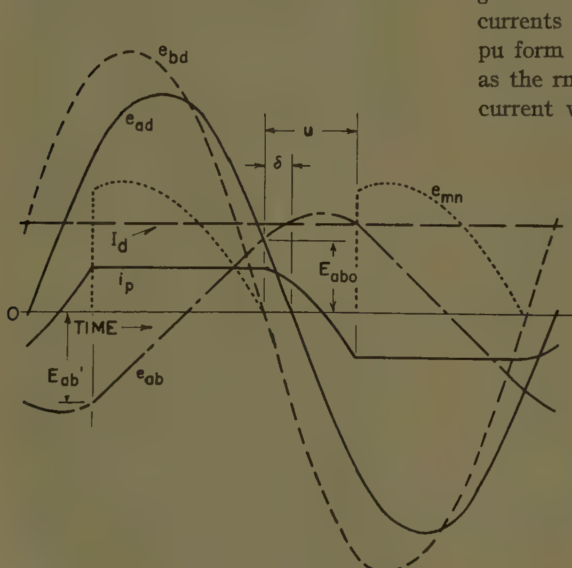

Fig. 2 (left). Voltage and current relationships in circuit of Fig. 1

Fig. 3 (right). Derived curves of angle δ as function of angle of overlap u

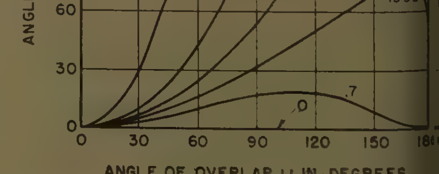

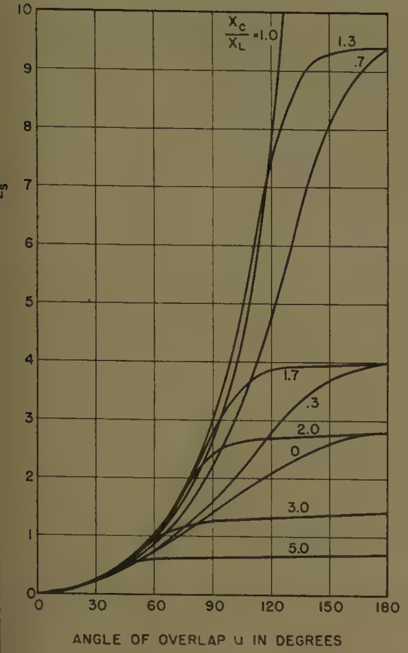

4. **Derived curves of pu load current as function of the angle of overlap u**

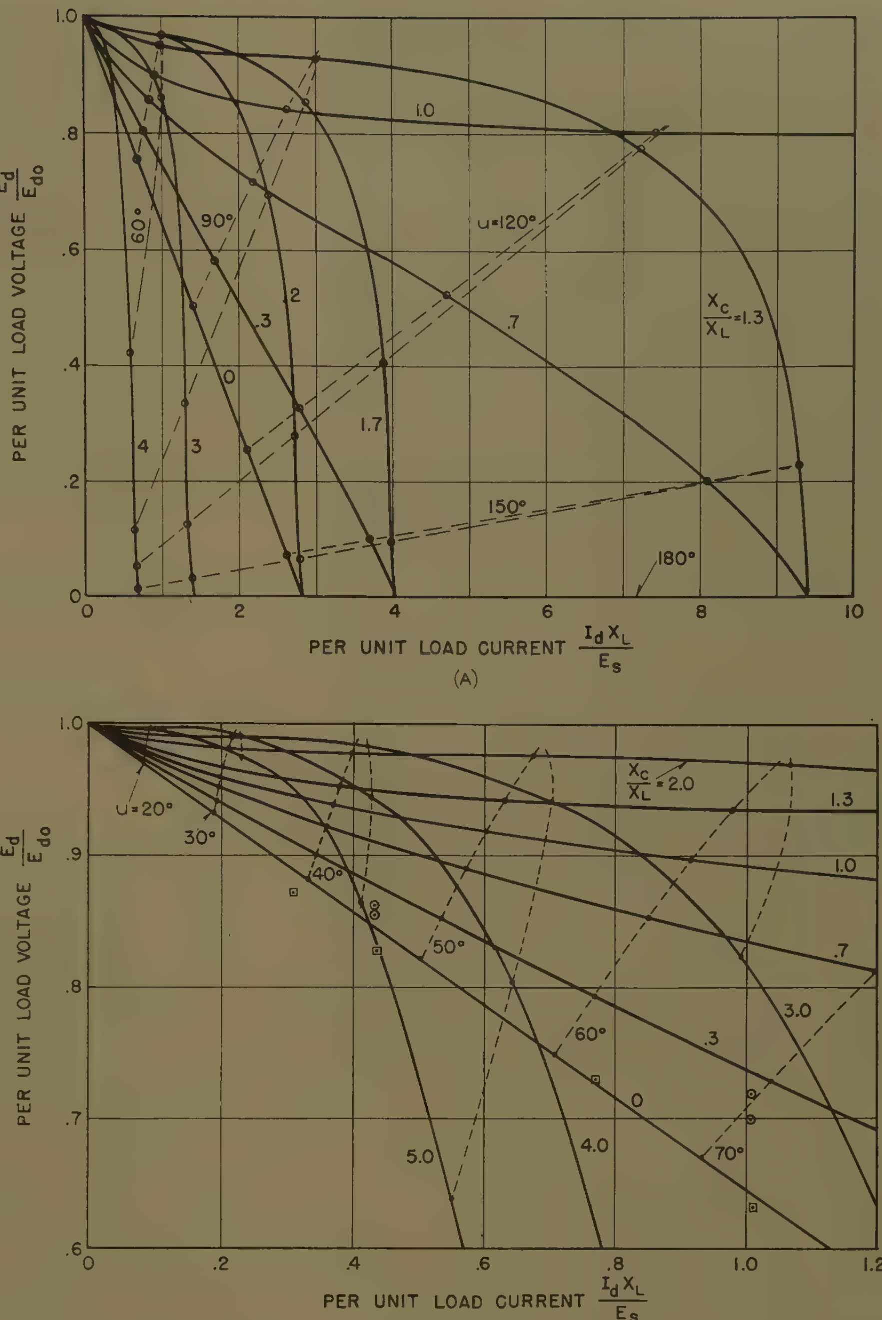

(A)

(B)

Fig. 5. Derived curves of pu load voltage as function of pu load current

A—For wide range of load currents

B—For a limited range of load currents. Railway laboratory data also plotted

Value of X_C/X_L	Symbol
0	⊡
0.26	●

Having obtained the derivations, the ded computations were carried out on International Business Machines rporations *704* computer and the re-s are plotted in a series of curves dis-sed in the following paragraphs.

ig. 3 demonstrates how the angle δ ies as a function of u for various values X_C/X_L.

ig. 4, relating I_dX_L/E_s to u for various ues of X_C/X_L, shows that for constant $_L/E_s$, as the amount of capacitive re-ance is increased up to $X_C/X_L=1.0$, angle of overlap decreases. At some her value of capacitive reactance de-ding on I_dX_L/E_s, this trend reverses.

ig. 5(A) shows how E_d/E_{d0} varies r a wide range in I_dX_L/E_s for different ues of X_C/X_L. Points on each curve which the angle of overlap is the same connected by dashed curves. Fig.) shows the same data over a more ctical range. These curves are the red regulation curves and, depending the magnitude of I_dX_L/E_s, they offer siderable theoretical promise of re-ed regulation to be achieved by using es capacitors. For example, assume ctifier loaded to 0.4 pu load current. h zero compensation ($X_C/X_L=0$), d-c load voltage is read from Fig. 5(B) bout 0.86 pu of its no-load value. The e figure shows that with sufficient es capacitance to make $X_C/X_L=0.7$, d-c voltage at the same load current 92 pu of its no-load value.

s noted, the curves of Fig. 5 are based derivation. To test their usefulness the ability of practical circuitry to deliver the improvements in regulation indicated by them, the earlier mentioned laboratory tests were conducted and are described in the following paragraphs.

Analog Study

The analog study was made by essentially setting up a model of Fig. 1 using small silicon diodes as the rectifying elements and components of the Anacom[2] to provide the remainder of the circuitry. As a matter of interest, the actual magnitudes of the load current I_d in the analog setup were on the order of tenths of amperes and E_{d0} was about 10 volts. A very large inductance was used to represent L_L to minimize ripple in the load

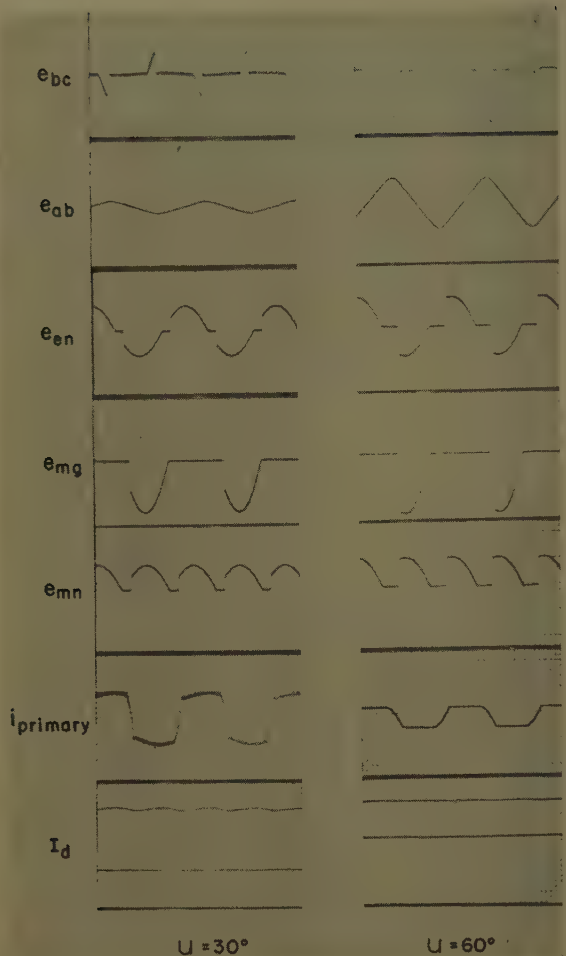

Fig. 6. Oscillograms of analog circuit quantities for $X_C/X_L=1.0$. Amplification of vertical scale of current traces 10 times greater for u=30 degrees than for u=60 degrees. All voltage traces to a common scale

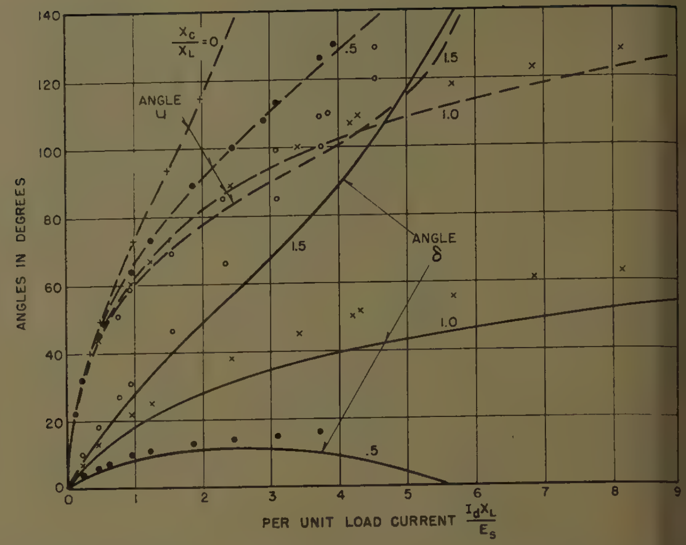

Fig. 7. Angles u and δ obtained from analog study as function of p[u] load current. The analog data are plotted; the curves are calculate[d]

Anacom data value of X_C/X_L	Symbol
0	+
0.5	●
1	×
1.5	○

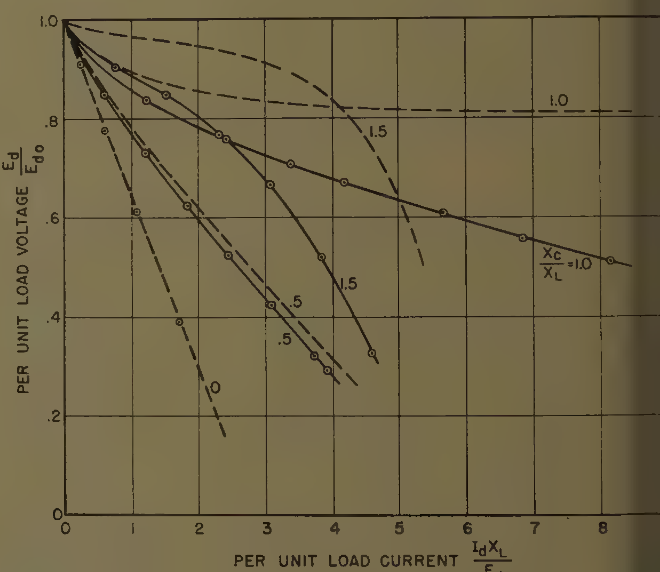

Fig. 8. Analog data—pu load voltage as a function of pu load curre[nt]

Anacom data —⊙—⊙—
Calculated data - - - -

current and so approximate the assumed condition of constant load current on which the theoretical derivations were based. Typical oscillograms obtained are shown in Fig. 6. The extent of success in obtaining a constant I_d may be judged from the indicated traces.

Efforts were made in reducing the data to compensate for the effects of resistance in the circuit by noting that during any half-cycle there is voltage across the load only when the rectifiers are not commutating. During this same period the current is constant in the a-c portion of the circuit as must be the voltage drop across the resistance of the circuit. Such drop, therefore, reduces the average d-c voltage by an amount equal to

$$\frac{1}{\pi}\int_0^{\pi-u}\frac{R_pI_d}{4}d(\omega t)+\frac{1}{\pi}\int_0^{\pi-u}R_sI_dd(\omega t)$$
$$=I_d\left(1-\frac{u}{\pi}\right)\left(\frac{R_p}{4}+R_s\right) \quad (5)$$

where R_p was the resistance of the primary circuit measured between terminals a and d while R_s was that measured between point n and either anode. The coefficient of one-fourth in the first integral is a result of the fact the transformer used had a one-to-one turns ratio between windings c-d and e-f. As each test was made the angle of overlap u, and the magnitude of I_d were obtained so that this voltage drop could be calculated from this equation in each case. This voltage plus the forward drop of the diodes measured with a cathode-ray oscilloscope was added to the reading of the voltmeter connecte[d] from m to n to determine E_d.

The more important generalized data [o]f the analog study was given in Figs. 7 an[d] 8. Fig. 7 demonstrates a fair agreeme[nt] between measured and calculated values [of u] and δ for various load currents. Fig. [8] compares the regulation curves obtaine[d] from the analog with the calculate[d] curves. Apparent discrepancies are di[s]cussed in a subsequent section.

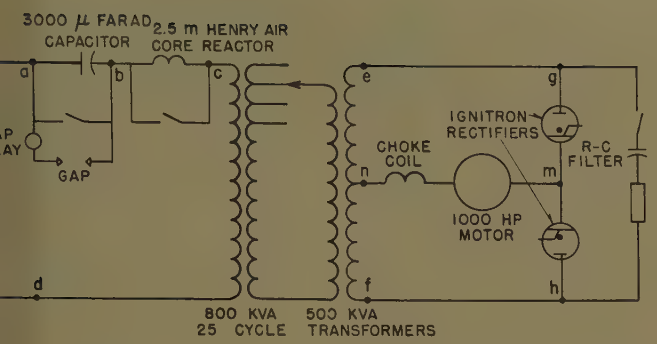

. 9. **Simplified schematic of full-scale railway laboratory circuit**

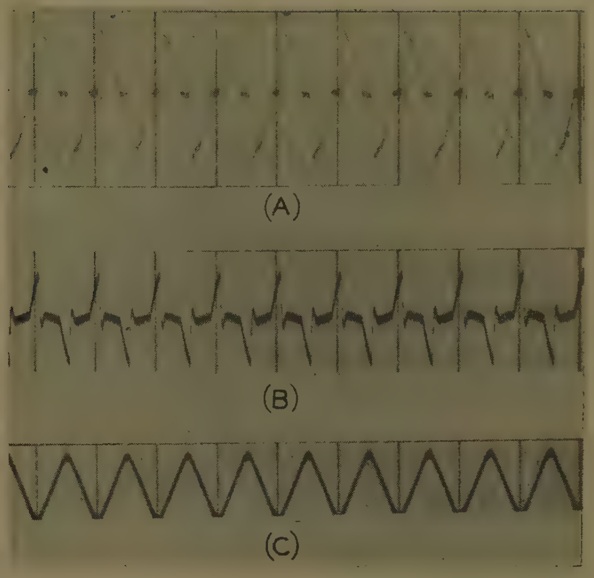

. 10 (right). **Typical railway laboratory data—magnetic oscillographic traces of voltage waves**

A—e_{gh}, anode-to-anode voltage
B—e_{bo}, voltage across 2.5 microhenrys inductance
C—Series capacitor voltage

ll-Scale Tests

n addition to the theoretical and ana- studies, a full-scale setup was made in Westinghouse Railway Laboratory, st Pittsburgh, Pa. The schematic gram of the test circuit is shown in Fig. While all the the a-c equipment was igned for 25-cps operation, a 60-cps ver source was used. The *370* type tor is approximately rated 1,000 horse- ver at 1,000 volts d-c and is identical motors presently in operation in recti- units.

3y switching, four different test condi- ns were readily investigated:

'est Condition no. 1. Series capacitor rt-circuited, series reactor short-cir- ed, and a-c filter open.

'est Condition no. 2. Series reactor in uit, series capacitor short-circuited and filter open.

'est Condition no. 3. Series capacitor series reactor in circuit and a-c filter n.

'est Condition no. 4. Series capacitor and es reactor in circuit and one 23.5-micro- d a-c circuit filter circuit closed.

'ypical data taken are shown in Table id Fig. 10 shows some of the magnetic llographic records. The traces may dentified by reference to Fig. 9.

'he d-c voltage regulation data of Table ere reduced to the generalized form are indicated in Fig. 5(B) along the theoretical curves. It is in- sting to note the good agreement so ained.

luation of Regulation Curves

he full-scale laboratory date and the log data tend to confirm the validity he derived curves of Fig. 5 for the lower values of X_C/X_L. However, there may be some question on this point since data was not obtained for values of X_C/X_L greater than 0.26 in the full-scale setup, and the analog data does not agree too well with the derived curves for $X_C/X_L \geq 1$ as seen from Fig. 8. It is the authors' opinion that the discrepancy is not the result of erroneous derivation or solution, but is caused by the fact that the diodes used in the analog setup did not have infinite resistance to flow of current in the reverse direction. As will be shown later, the peak inverse voltage across the rectifying devices is increased by the presence of the series capacitor and without question conduction in the reverse direction would tend to reduce the load voltage. An ignitron rectifier, on the other hand, would much more nearly meet the theoretical condition of having infinite resistance to the reverse flow of current in the rectifier devices, and would therefore be expected to achieve more nearly the theoretical results. In any event, it should be noted the derived curves neglect the effect of losses and arc drop in the case of ignitron rectifiers which tend to increase regulation. However, the series capacitor will not significantly affect these, so that the relative improvement in regulation in an actual rectifier obtained by a series capacitor application is expected to agree closely with the relative improvement shown by the derived curves of Fig. 5 for practical values of I_dX_L/E_s at least.

Recognition should be given to the fact that the ranges of I_dX_L/E_s explored and indicated in Figs. 4, 5, and 8 are relatively extreme to what would be normally encountered in common rectifier practice. To demonstrate this let $\underline{X_T}$ represent the per-unit reactance of the transformer expressed on a base equal to the rated volt-amperes at the line terminals of the transformer a-c winding, and let X_T represent the ohmic value of this reactance as measured on the a-c winding side. Of course,

$$X_T = \underline{X_T} \times \frac{E_L^2}{VA} \tag{6}$$

where VA is the volt-ampere rating of the a-c winding of the transformer. Let it be assumed there is no other reactance in

Table I. Railway Laboratory Test Data

Test Condition	E_{ad}	$i_{primary}$	E_{cd}	E_{ab}	E_{bc}	Motor, Rpm	E_{en}	E_d	I_d	Filter Current
1	2,270	147				1,360	808	664	400	
1	2,240	350				729	743	554	1,000	
1							845		0	
2	2,264	145	2,200		180	1,310	788	630	400	
2	2,240	345			350	618	688	480	1,000	
2							842		0	
3	2,260	145	2,246	101	160	1,330	800	650	400	
3	2,240	350	2,200	245	360	686	740	532	1,000	
3							845		0	
4	2,260	145	2,250	100	200	1,345	815	656	400	20.25
4	2,240	345	2,220	242	380	695	759	546	1,000	33
4							845		0	

All a-c quantities are expressed in rms volts or amperes.

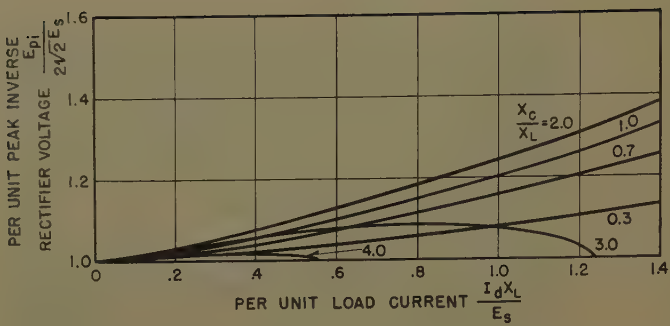

Fig. 11. Derived of peak inverse voltage on rectifier elements in pu of peak inverse voltage with no series capacitor as function of pu load current

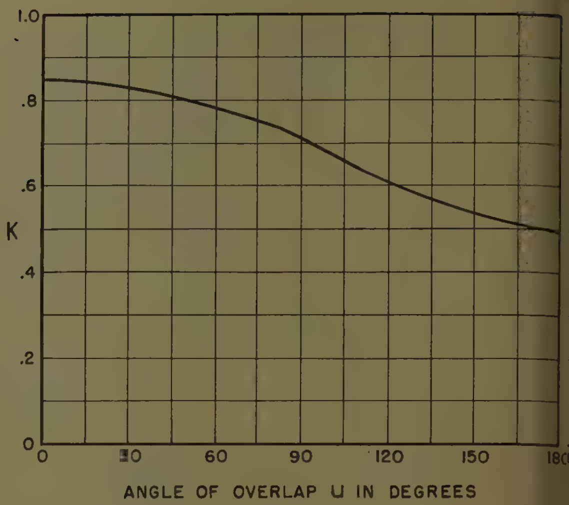

Fig. 12 (right). Relation between coefficient K and angle of overlap u

the circuit, in which case, the commutating reactance is obtained as

$$X_L=\frac{1}{2}\left(\frac{E_s}{E_L/2}\right)^2 X_T \tag{7}$$

The volt-ampere rating of the a-c winding may be obtained from standard works on rectifiers as

$$VA=E_s I_{dR} \tag{8}$$

where I_{dR} is the rated value of the d-c load current. Substituting equations 6 and 8 in 7, then yields

$$X_L=2\underline{X_T}\,\frac{E_s}{I_{dR}} \tag{9}$$

and the expression for pu load current used throughout this paper becomes

$$\frac{I_d X_L}{E_s}=2\,\frac{I_d}{I_{dR}}\,\underline{X_T} \tag{10}$$

If the rectifier is delivering rated load current, then the pu load current is

$$\frac{I_d X_L}{E_s}=2\underline{X_T} \tag{11}$$

Values of $\underline{X_T}$ for single-phase rectifiers do not typically exceed about 0.10 pu so that it is seen from equation 2 that rectifiers operating at rated load or less will normally be operating at values of $I_d X_L/E_s$ of less than 0.2 pu if the reactance of the supply system is negligible. Abnormally high supply system reactance plus the possibility of operating at higher than rated currents for limited periods of time extend the possible values of $I_d X_L/E_s$ which might be encountered to as high as perhaps one pu.

Peak Inverse Voltage

The rectifier devices of a single-phase full-wave rectifier experience a peak inverse voltage of $2\sqrt{2}E_s$ if no series capacitor is used. A derivation is carried out in Appendix II to obtain the ratio of the peak inverse voltage with a series capacitor to that without it, as a function of $I_d X_L/E_s$ and for given values of X_C/X_L. Solutions of the equations obtained are plotted in Fig. 11. These demonstrate plainly the effect of the capacitor on the peak inverse voltage and will permit the necessary co-ordination in making a capacitor application to avoid the possibility of exceeding the peak inverse voltage rating of the rectifying devices.

Series Capacitor Rating

Having selected a desired value of X_C/X_L based on the amount of improvement required in load voltage regulation, attention must be given to specifying the complete capacitor rating. The ohmic value value X_{CR} of the capacitive reactance to be actually inserted in the a-c supply circuit is obtained from the relation

$$X_{CR}=\frac{1}{4}\left(\frac{E_L}{E_s}\right)^2\left(\frac{X_C}{X_L}\right)X_L \tag{12}$$

where X_L, as before is the inductive commutating reactance.

Standards for series capacitors[3] do not require that the capacitor volt-ampere rating be specified, but require among other quantities that the reactance and the continuous current be specified. This is based on the assumption that the current is sinusoidal, which of course, is not the case when the series capacitors are applied to rectifiers serving inductive loads. Therefore Appendix III is devoted to a solution of the volt-amperes developed in a capacitor of reactance X_{Cp} when an alternating current having a square-wave shape and crest value I_p is passed through it. It is shown there that the total volt-amperes developed are equal to 0.85 $I_p^2 X_{Cp}$. Were the current sinusoidal, the volt-amperes would, of course, be but 0.50 $I_p^2 X_{Cp}$ where I_p is still the crest value. The actual waveshape of the rectifier a-c current is somewhere between a square shape and a sinusoid depending on the angle of overlap u. The capacitor volt-amperes developed by passage of the rectifier a-c current i_p having crest value I_p may thus be taken as $KI_p^2 X_{cp}$ where K is a coefficient varying from $K=0.85$ for $u=0$ to $K=0.5$ for $u=180$ degrees. Indeed for the case with no series capacitor it is not too difficult to obtain the curve of the coefficient K as a function of the angle of overlap u. This curve was calculated and is shown in Fig. 12. It demonstrates that for angles of overlap up to 60 or 80 degrees, K does not drop significantly below 0.85. While this curve of K versus u may vary (though not in the limits) somewhat when a series capacitor is applied, it appears reasonable to base the capacitor kilovolt-ampere (kva) rating on the 0 85 coefficient making no allowance for the fact it is somewhat less at currents corresponding to full load on the rectifier. Therefore, the capacitor requires as a minimum a volt-ampere rating corresponding to rated d-c load current I_{dR} as follows

Minimum capacitor volt-ampere rating

$$=0.85\left(\frac{E_L}{E_s}\right)^2 I_{dR}^2 X_{CR} \tag{13}$$

This is stated as a minimum since two other factors must be taken into account: 1. voltage across the capacitor and 2. co-ordination between short-time overload capabilities of rectifier and series capacitor.

The first of these items requires investigation since series capacitor standards define the maximum current for continuous operation as restricted to a "substantially sinusoidal waveform such that the maximum rms voltage between terminals does not exceed 1.10 times the

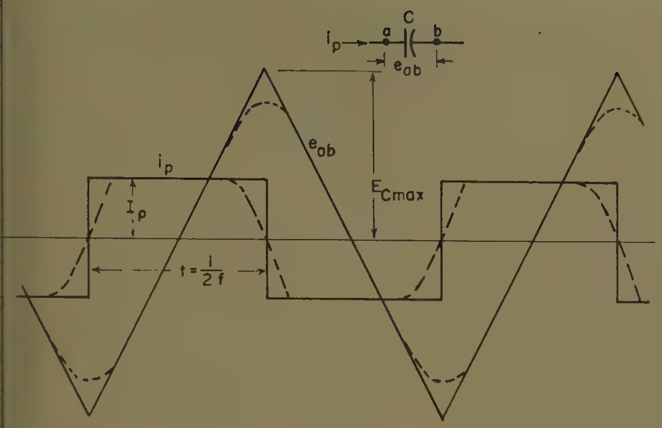

Fig. 13. Series capacitor current and voltage relationships

ted voltage."[3] If the capacitor volt-
npere rating is obtained by equation 13,
e rated voltage V_{CR} of the capacitor will

$$_{CR}=\sqrt{Q_{CR}X_{CR}} \tag{14}$$

om the familiar relation

$$_{R}=\frac{V_{CR}^2}{X_{CR}} \tag{15}$$

here Q_{CR} is the rated volt-amperes of
e capacitor. Substituting equations 13
14 yields

$$_{CR}=0.922\frac{E_s}{E_L}I_{dR}X_{CR} \tag{16}$$

Voltage V_{CR} represents the sinusoidal
oltage which would develop Q_{CR} if im-
essed across X_{CR}. The actual rms volt-
e developed across the capacitor must
w be developed and compared against
Assuming alternating current i_p as a
uare wave, the voltage across the capaci-
r will be triangular as shown in Fig. 13.
e change in voltage from one peak to
other (positive to negative or vice versa)
ll be equal to the area under the corre-
onding half-cycle of the current wave,
, the change in charge Δq on the capaci-
r in one half-cycle, divided by the
pacitance. Thus

$$_{\max}=\frac{1}{2}\frac{\Delta q}{C}=\frac{1}{2}\left(\frac{I_p}{2f}\right)2\pi fX_{CR}=\frac{\pi}{2}I_pX_{CR} \tag{17}$$

t rated rectifier load current, the crest
lue of the alternating current is

$$=\frac{E_s}{E_L}I_{dR} \tag{18}$$

The amplitude factor (ratio of maxi-
um value to rms value) of a triangular
ave[4] is $\sqrt{3}$ so that the rms value of the
iangular-shaped capacitor voltage may
obtained as

$$_{Crms}=\frac{1}{\sqrt{3}}\frac{\pi}{2}X_{CR}\frac{E_s}{E_L}I_{dR}=0.907\frac{E_s}{E_L}I_{dR} \tag{19}$$

Comparison of equations 16 and 19 then show that the rms voltage resulting from the passage of the a-c current of the rectifier when at rated load through the capacitor is somewhat less than the rated voltage of the capacitor. Since the capacitor current will not actually have a square shape with rated load on the rectifier, neither will the voltage wave have a pure triangular shape. Rather, the voltage wave will be rounded off at the peaks, as shown in Fig. 13 causing its rms value with full load on the rectifier to be even less than the value obtained in equation 19.

The second area to be investigated is that of co-ordination between the overload capabilities of the capacitor and of the rectifier. Rectifiers, depending on the specified service, are assigned various short-time overload capabilities as shown in Table II.[1] Series capacitors are permitted to operate "at 135% of rated current for periods not exceeding 30 minutes and at 150% for periods not exceeding 5 minutes."[3] Another paragraph of the same standards[3] states that series capacitor units shall be capable of withstanding a maximum rms momentary overvoltage of 1.7 times the rated rms voltage for a period of one minute and goes on to point out this limit applies "for power frequencies where high-frequency transients are not superimposed," and "the crest voltage should not exceed 1.41 times the foregoing rms values." From the latter restriction, it appears reasonable to interpret the 5-minute overload capability as permitting 150% of rated current providing the crest voltage does not exceed 1.5 times the crest value of the rated rms voltage. Concerning the 1.7 multiplying factor for one-minute overloads it should be noted that the standards[3] go on to note for this factor and others given for shorter overload duration, "The capacitor shall be capable of withstanding 300 applications of overvoltage indicated in the foregoing table," and "Normal service conditions associated with regular use of the series capacitor shall not result in currents in excess of 150 per cent of rated current." Inasmuch as there exists no comparable restrictions in rectifier application as to the number of times the rectifier may be operated at its one-minute rating (if assigned), it must be concluded that the appropriate way to rate the capacitor is to make its current rating such that at the maximum short-time rectifier rating (be it one- or 5-minute duration) the crest voltage across it does not exceed 1.5 times the crest of the corresponding voltage rating.

The last conclusion may be stated mathematically using equations 17 and 18 to obtain

$$1.5\sqrt{2}V_{CR}\geqq E_{C\max}=\frac{\pi}{2}I_{dR}\frac{E_s}{E_L}X_{CR}\underline{I_{doL}} \tag{20}$$

where $\underline{I_{doL}}$ is the maximum short-time overload rating of the rectifier expressed in per unit of its continuous rating. From the fact that $V_{CR}=I_{CR}X_{CR}$, it is then obtained that

$$I_{CR}\geqq 0.742I_{dR}\frac{E_s}{E_L}\underline{I_{doL}} \tag{21}$$

If M is defined as a factor equal to 0.742 $\underline{I_{doL}}$, equation 21 reduces to

$$I_{CR}\geqq MI_{dR}\frac{E_s}{E_L} \tag{22}$$

For convenience, the values of M ap-

Table II. Standard[1] Rectifier Short-Term Overload Capabilities and Multiplying Factors to Obtain Series Capacitor Current Ratings

Service	Overload Ratings in % of Rated Current	M
Electrochemical	150% current for 1 minute	0.98
Industrial	125% current for 2 hours 200% current for 1 minute	1.31
Class I—Railway or Mining	150% current for 2 hours 200% current for 1 minute	1.31
Class II—Railway or Mining	150% current for 2 hours 300% current for 1 minute	1.96
Class III—Railway	150% current for 2 hours 300% current for 5 minutes	2.22

Notes: 1. All overload ratings given above are following 100% load.
2. See equation 22 of text for use of M.

plicable for each recognized rectifier application are set forth in Table II.

For the sake of comparison, the value of I_{CR} obtained if the capacitor volt-ampere rating obtained in equation 13 were used is determined as

$$I_{CR}=\left(\frac{Q_{CR}}{X_{Cp}}\right)^{1/2}=0.922\frac{E_L}{E_s}I_{dR} \tag{23}$$

As will be noted, the value of M for every application shown in Table II is greater than 0.922. Thus the short-time overload requirements dictate the capacitor size, and equation 22 must be used to obtain the current rating of the capacitor rather than equation 13.

In summary, then, having determined the desired X_C/X_L ratio and presuming the value of X_L is known, the series capacitor reactance is obtained from equation 12 and its current rating from equation 22. The nominal system voltage, the basic insulation level, and system frequency must also be specified. The permissible short-time working current and duration are specified in accordance with the earlier quoted standards.[3] Finally, recognition must be given the possibility of a fault occurring from line-to-line on the rectifier side of the capacitor which will subject the capacitor to the system fault current at that point. For this reason, the fault current and duration must also be specified.

Series Capacitor Protection

The use of a protective gap (such as described in reference 5) in parallel with the series capacitor as shown in Fig. 9 is recommended. This gap protects the capacitor from dangerous voltages which might occur as a result of faults in either the d-c circuit or in the a-c circuit on the load side of the capacitor. The gap will also operate in the event of an arc back in the rectifier.

To avoid possible damage to the capacitor dielectric, it is suggested that the gap-crest flashover voltage E_{gap} be not greater than approximately 2.5 times the peak value of the rms voltage across the capacitor corresponding to its rated current, i.e.

$$E_{gap\,(max)}\leqq 2.5\sqrt{2}\,I_{CR}X_{CR}=3.54I_{CR}X_{CR} \tag{24}$$

Of course, the crest voltage appearing across the capacitor for which it is undesirable to have the gap operate is that when the rectifier is at its maximum permissible short-time overload. From the means by which the capacitor rating was obtained in the preceding paragraphs, this voltage is seen to be 1.5 $\sqrt{2}\,I_{CR}X_{CR}$ and allowing for margin, gives a lower limit to the gap flashover of

$$E_{gap(min)}\geqq 1.25(1.5\sqrt{2}\,I_{CR}X_{CR})=2.65I_{CR}X_{CR} \tag{25}$$

Thus, equations 24 and 25 provide limits within which the protective gap should be set.

During the full-scale laboratory tests the gap fired each time an arc back occurred. The effect of this operation was excellent in that it greatly restricted the arc-back current. The rectifier designer must occasionally introduce inductive reactance in the circuit by intent to limit arc-back currents to values which are harmless to the rectifiers. This is undesirable from the standpoint of voltage regulation. The gapped series capacitor thus offers a means of reducing voltage regulation but not increasing arc-back crest currents

Conclusions

1. The series capacitor offers a workable method of decreasing the voltage regulation of single-phase diametric rectifiers supplying inductive loads.
2. Theoretical data have been presented which permit estimating the effects of series capacitor compensation on the performance of single-phase diametric rectifiers supplying inductive loads over a wide range in variables.
3. Analog and full-scale laboratory results have been reported which support the theoretical data for practical angles of overlap and degrees of compensation. Lacking data to the contrary, it must be assumed that the full theoretical improvements in regulation with greater amounts capacitive compensation cannot be obtained practically.
4. A simple, yet conservative means of rating the series capacitor and its associated protective device has been presented.

Appendix I. Derivation of Expression for E_d/E_{do}

Referring to Figs. 1 and 2, the following relations may be obtained. It is assumed that time $t=0$ at the instant commutation starts as the end of a positive half-cycle of primary current i_p is approached, and for convenience, that $L_2=0$.

The capacitor voltage at time $t=0$ is

$$E_{ab0}=\sqrt{2}\,E_L\sin(\pi-\delta)=\sqrt{2}\,E_L\sin\delta \tag{26}$$

The expression for the primary current i_p during commutation $(0\leqq t\leqq u/\omega)$ is

$$i_p=\frac{1}{L_1}\int_0^t e_{bc}dt+I_d\frac{E_s}{E_L} \tag{27}$$

The expression for the voltage e_{bc} across inductance L_1, during commutation $(0\leqq t\leqq u/\omega)$ is

$$e_{bc}=\sqrt{2}\,E_L\sin(\omega t+\pi-\delta)-e_{ab} \tag{28}$$

The expression for the voltage e_{ab} across the capacitance C during commutation $(0\leqq t\leqq u/\omega)$ is

$$e_{ab}=E_{ab0}+\frac{1}{C}\int_0^t i_p\,dt \tag{29}$$

Through a Laplace transform operation and substitution of equations 1, 2, 26, 28, and 29, equation 27 may be solved to yield for $0\leqq t\leqq u/\omega$

$$i_p=\frac{2\sqrt{2}E_s^2}{E_LX_L}\left(\frac{1}{1-\frac{X_C}{X_L}}\right)\times\left\{\left[\sin\omega t-\frac{1}{k}\sin\omega_0 t\right]\sin\delta+[\cos\omega t-\cos\omega_0 t]\cos\delta\right\}+\frac{I_dE_s}{E_L}\cos\omega_0 t \tag{30}$$

where

$$\omega_0=\omega\sqrt{\frac{X_C}{X_L}}\quad\text{and}\quad k=\sqrt{\frac{X_C}{X_L}}$$

The following relations may also be written from Figs. 1 and 2 based on the fact the voltage on a capacitor is equal to the charge divided by the capacitance and the change in charge on a capacitor during an interval that a current is forced through it is equal to the time integral of the magnitude of the current over the duration of the interval.

$$-E_{ab}'=E_{ab0}-\frac{I_d}{C}\left(\frac{\pi-u}{\omega}\right)\frac{E_s}{E_L} \tag{31}$$

$$E_{ab}'=E_{ab0}+\frac{1}{C}\int_0^{u/\omega}i_pdt \tag{32}$$

where E_{ab}' is the magnitude of voltage on the capacitor at the instant commutation ceases. The sum of equations 31 and 32 yields

$$2E_{ab0}=\frac{I_d}{C}\left(\frac{\pi-u}{\omega}\right)\frac{E_s}{E_L}-\frac{1}{C}\int_0^{u/\omega}i_pdt \tag{33}$$

The current i_p given in equation 30 was integrated as required and with equations 2 and 26 substituted in equation 29 to obtain after eliminating I_dE_s/E_L

$$\delta=\tan^{-1}\frac{(\pi-u)(\cos ku-\cos u)-(1+\cos ku)\sin u+\frac{1}{k}(1+\cos u)\sin ku}{(\pi-u)\left(\sin u-\frac{1}{k}\sin ku\right)-\frac{1}{k}(\sin u)\sin ku+\left(\frac{2}{k^2}-\cos u-1\right)(1+\cos ku)} \tag{34}$$

for $X_C/X_L\neq 1$.

For the case $X_C/X_L=1.0$, it is necessary to take the derivative of the numerator and

nominator of equation 34 and let X_C/X_L 1.0 to yield

$$\tan^{-1}\frac{(\pi-u)\sin u+(1+\cos u)\times\left(\frac{\sin u}{u}-1\right)}{(\pi-u)\left(\cos u-\frac{\sin u}{u}\right)+(\sin u)\times\left(1-\frac{\sin u}{u}\right)+\frac{4}{u}(1+\cos u)} \qquad (35)$$

Now i_p as given by equation 30 may be aluated at $t=u/\omega$ where it is known to ual $-I_dE_s/E_L$. From this I_dX_L/E_s is nd to be

$$\frac{X_L}{s}=2\sqrt{2}\frac{\left(\frac{1}{k}\sin ku-\sin u\right)\sin\delta+(\cos ku-\cos u)\cos\delta}{(1+\cos ku)\left(1-\frac{X_C}{X_L}\right)} \qquad (36)$$

$X_C/X_L\neq 1$.

Again the derivatives of the numerator d denominator of this expression must be ken and letting $X_C/X_L\to 0$ then gives

$$\frac{X_L}{s}=\frac{\sqrt{2}\,u\left(\frac{\sin u}{u}-\cos u\right)\sin\delta+(\sin u)\cos\delta}{1+\cos u} \qquad (37)$$

$X_C/X_L=1$.

The average load voltage E_{d0} for $I_d=0$ is

$$_0=\frac{\omega}{\pi}\int_0^{\pi/\omega}\sqrt{2}E_s\sin\omega t\,dt=\frac{2\sqrt{2}E_s}{\pi} \qquad (38)$$

d the average load voltage E_d at load cur- nt i_d is

$$=\frac{\omega}{\pi}\int_0^{\pi/\omega}e_{mn}dt \qquad (39)$$

ow the expression for the load voltage e_{mn} ay be written from Figs. 1 and 2 with the ne $t=0$ now defined as the instant com- utation ceases as

$$_n=\sqrt{2}E_s\sin(\omega t+u-\delta)+\left(E_{ab}'-\frac{I_d}{C}\frac{E_s}{E_L}t\right)\frac{E_s}{E_L} \qquad (40)$$

for $0<t\leq\frac{\pi-u}{\omega}$

d $e_{mn}=0$

$$\text{for } \frac{\pi-u}{\omega}\leq t<\frac{\pi}{\omega} \qquad (41)$$

Substituting equations 40 and 41 in 39, rrying out the indicated integration and bstituting equation 2 yields

$$_l=\frac{\sqrt{2}E_s}{\pi}[\cos\delta+\cos(u-\delta)-(\pi-u)\sin\delta]+\frac{I_dX_C}{2\pi}(\pi-u)^2 \qquad (42)$$

ividing equation 42 by 38 then gives

$$=\frac{1}{2}\left[\cos\delta+\cos(u-\delta)-(\pi-u)\sin\delta+\left(\frac{I_dX_L}{E_s}\right)\left(\frac{X_C}{X_L}\right)\frac{(\pi-u)^2}{4\sqrt{2}}\right] \qquad (43)$$

Note that letting $X_C\to 0$ in equation 34 yields $\delta=0$ as would be expected. Doing the same in equation 36 then gives

$$\frac{I_dX_L}{E_s}=\sqrt{2}(1-\cos u)\text{ for }\frac{X_C}{X_L}=0 \qquad (44)$$

Letting $X_C/X_L\to 0$ in equation 43 and substituting equation 44 then gives

$$\frac{E_d}{E_{d0}}=1-\frac{I_dX_L}{2\sqrt{2}\,E_s}\text{ for }\frac{X_C}{X_L}=0 \qquad (45)$$

which may be checked with any standard work on rectifiers (reference 6, equation 9-3, for example,) as the expression for the load voltage of the rectifier circuit under consideration when $X_C=0$.

Appendix II. Derivation of Effect of Capacitor on Peak Inverse Voltage

From Figs. 1 and 2, the inverse voltage experienced by rectifying device number 2 while number 1 is conducting is found to be

$$e_{\text{inverse}}=e_{mh}=2(e_{ad}-e_{ab})\frac{E_s}{E_L} \qquad (46)$$

Letting time $t=0$ be the instant applied voltage e_{ad} passes through zero as it changes from negative to positive and using the same reasoning concerning the voltage across the capacitor as in obtaining equation 31 permits equation 46 to be written.

$$e_{\text{inverse}}=2\sqrt{2}\,E_s\sin\omega t-2\left[-E_{ab}'+\frac{I_d}{C}\frac{E_s}{E_L}\left(t-\frac{u-\delta}{\omega}\right)\right]\frac{E_s}{E_L} \qquad (47)$$

The maximum inverse voltage occurs when

$$\frac{de_{\text{inverse}}}{dt}=0 \qquad (48)$$

Substituting equations 2 and 47 in 48, taking the derivative, solving for t, and multiplying by X_L/X_L yields

$$t=\frac{\cos^{-1}\frac{I_dX_L}{2\sqrt{2}E_s}\left(\frac{X_C}{X_L}\right)}{\omega} \qquad (49)$$

This equation and equations 2, 26, and 31 here then substituted in 47 to obtain the peak inverse voltage E_{pi}. The result was then divided by the peak inverse voltage for $X_C=0$, commonly known to be $2\sqrt{2}E_s$ to obtain

$$\frac{E_{pi}}{2\sqrt{2}E_s}=\sin\left[\cos^{-1}\left(\frac{I_dX_L}{2\sqrt{2}E_s}\right)\left(\frac{X_C}{X_L}\right)\right]-\sin\delta+\left(\frac{I_dX_L}{2\sqrt{2}E_s}\right)\left(\frac{X_C}{X_L}\right)\times\left[\pi-\delta-\cos^{-1}\left(\frac{I_dX_L}{2\sqrt{2}E_s}\right)\left(\frac{X_C}{X_L}\right)\right] \qquad (50)$$

This equation is good only for

$$0\leq\frac{I_dX_L}{E_s}\leq\frac{2\sqrt{2}}{X_C/X_L}$$

since the value of a cosine cannot exceed unity. For values of $I_dX_L/E_s>2\sqrt{2}/X_C/X_L$ no point exists where the derivative of e_{mn} is zero. The maximum value E_{pi} occurs at the instant commutation ceases, i.e., at $t=(u-\delta)/\omega$, which may be substituted together with equations 2, 26, and 31 in 47 to obtain

$$\frac{E_{pi}}{2\sqrt{2}E_s}=\sin(u-\delta)-\sin\delta+\left(\frac{I_dX_L}{2\sqrt{2}E_s}\right)\left(\frac{X_C}{X_L}\right)(\pi-u) \qquad (51)$$

Appendix III. Derivation of Volt-Amperes Developed in the Series Capacitor

Referring to Fig. 1, let $L_1=L_2=0$ and let $X_C\to$ zero. The commutating angle, u, goes to zero and primary current becomes a square wave of crest value I_p. The Fourier expansion of i_p is then

$$i_p=\frac{4}{\pi}I_p\left(\sin\omega t+\frac{1}{3}\sin 3\omega t+\frac{1}{5}\sin 5\omega t+\ldots\right) \qquad (52)$$

The rms value of the $(2n-1)$th harmonic is simply

$$i_{\text{rms}(2n-1)}=\frac{4I_p}{\sqrt{2}\pi(2n-1)} \qquad (53)$$

The volt-amperes developed in the series capacitors is the sum of the products of the square of each harmonic of the current times the reactance of the capacitor at the corresponding frequency. Thus, if X_{CR} is the reactance of the capacitor at the fundamental frequency, the volt-amperes Q_C developed in it is

$$Q_C=\sum_{n=1}^{\infty}\left[(i_{(\text{rms})(2n-1)})^2\frac{X_{CR}}{2n-1}\right] \qquad (54)$$

Substituting equation 53 in 54 yields

$$Q_C=\frac{8}{\pi^2}I_p^2X_{CR}\left[1^3+\left(\frac{1}{3}\right)^3+\left(\frac{1}{5}\right)^3+\ldots\right]=0.85I_p^2X_{CR} \qquad (55)$$

Nomenclature

C = designates capacitor, also value of capacitance, farads

E_{ab0} = magnitude of capacitor voltage e_{ab} at instant commutation commences, volts

E_{ab}' = magnitude of capacitor voltage e_{ab} at instant commutation ceases, volts

$E_{C\max}$ = maximum value of capacitor voltage e_{ab}, volts

$E_{C\text{rms}}$ = rms value of capacitor voltage e_{ab}, volts

E_d = average value of d-c voltage, volts

E_{d0} = average value of d-c voltage at zero load, volts

E_{gap} = crest voltage at which protective device should operate, volts

E_L = rms value of applied a-c voltage, volts

E_s = rms value of voltage appearing between transformer d-c terminals and midtap at zero load, volts

e_{pi} = peak inverse voltage on rectifying devices, volts
e_{xy} = designates voltage between points x and y identified in Fig. 1, also instantaneous value of this voltage as a function of time, volts
f = frequency, cps
I_b = rms value base current, amperes
I_d = average value of d-c load current, amperes
I_{CR} = rated rms current of series capacitor, amperes
I_{dR} = rated average value of d-c load current, amperes
I_{d0L} = value of average d-c load current at overload, pu of rated average d-c load current
$I_{d\ pu}$ = value of average d-c load current expressed, pu
I_p = peak magnitude of current on a-c side of transformer, amperes
i_p = instantaneous value of current on a-c side of transformer as a function of time, amperes
K = coefficient by which the product $I_p{}^2X_{CR}$ is multiplied to obtain voltamperes developed in series capacitor
k = coefficient equal to $\sqrt{X_C/X_L}$
L_1 = inductance on a-c side of transformer representing transformer leakage inductance of a-c source and supply circuit, henrys
L_2 = inductance between d-c terminals of transformer and rectifier anodes, henrys
L_L = inductance of d-c load, henrys
M = coefficient by which the term $I_{dR}E_s/E_L$ is multiplied to obtain I_{CR}
Q_C = reactive power developed in series capacitor, volt-amperes
Q_{CR} = volt-ampere rating of series capacitor
q = charge on capacitor, coulombs
R_L = resistance of d-c load, ohms
R_p = resistance of a-c supply, circuits, and a-c transformer winding, ohms
R_s = resistance in one-half of d-c winding plus that of anode lead, ohms
t = instantaneous value of time, seconds
u = commutating angle or angle of overlap, degrees or radians
VA = volt-ampere rating of transformer a-c winding, volt-amperes
V_{CR} = rms voltage rating of series capacitor, volts
X_C = commutating reactance due to capacitive reactance of series capacitor only, ohms
X_{CR} = rated reactance of series capacitor, ohms
X_L = commutating reactance due to inductive reactance only of complete circuit, ohms
δ = angle by which start of commutation precedes next subsequent zero value of supply voltage, degrees or radians
ω = angular velocity of supply voltage, radians/second ($\omega = 2\pi f$)

References

1. American Standard for Pool Cathode Mercury-Arc Power Converters. *ASA C34.1 1949*, American Standards Association, New York, N. Y., Jan. 1949.

2. A Large-Scale General-Purpose Electric Analog Computer, E. H. Harder, G. D. McCann. *AIEE Transactions*, vol. 67, pt. I, 1948, pp. 664–73.

3. Series Capacitors. *Standard no. CPZ-1957*, National Electrical Manufacturers Association, New York, N. Y., 1957.

4. Standard Handbook for Electrical Engineers (book). McGraw-Hill Book Company, Inc., New York, N. Y., fifth edition, 1922, p. 101.

5. The Series Capacitor and the High-Voltage Line, R. E. Marbury. *Westinghouse Engineer*, Pittsburgh, Pa., Sept. 1951, pp. 134–43.

6. Standard Handbook for Electrical Engineers, (book). McGraw-Hill Book Company, Inc., eighth edition, 1949, p. 862.

Determination of Ground-Fault Current on Common A-C Grounded-Neutral Systems in Standard Steel or Aluminum Conduit

J. A. GIENGER
MEMBER AIEE

O. C. DAVIDSON
ASSOCIATE MEMBER AIEE

R. W. BRENDEL
ASSOCIATE MEMBER AIEE

A NEED has been indicated in the electrical industry for information which will enable the design engineer to predict the magnitude of fault current that will flow in a circuit enclosed by metal conduit when subjected to ground fault conditions. The purpose of this paper is to present usable data, obtained by laboratory tests, for the improved design of grounded-neutral circuits in rigid steel or aluminum conduit.

Previous studies have been made of the unexpected characteristics of grounded circuits in steel conduit which clearly demonstrate the powerful influence of inductive reactance, caused by the presence of an encircling magnetic duct, upon current flowing in the faulted conductor.[1,2] The magnetic conduit introduces inductive reactance in the enclosed faulted conductor which is greatest when the fault current returns in a remote path, substantial when it returns over the conduit itself, and still appreciable when an internal bonding conductor is utilized. The higher reactance associated with a remote return circuit influences the ground-fault current to seek the conduit path for return flow. With a conventional conduit system having tightly assembled conduit fittings and properly installed bonding jumpers, all of the ground-fault current may be considered to return on the conduit; even bonding to low-resistance ground paths, such as heavy building steel, has a negligible influence upon the ground circuit impedance.[2] Only the use of an internal bonding conductor or nonmagnetic conduit is effective. The inductive reactance is more likely to be troublesome in the common grounded-neutral systems having 120, 240, or 277 volts to ground. This study is limited to the usual conduit construction and to the common systems mentioned.

The consequences of underestimating or ignoring this high ground-fault impedance are especially precarious when long circuits are installed through hazardous areas or buildings storing combustible materials. One plant has had four instances in which standard rigid conduit or fittings were burned through during a ground fault on circuits protected by properly applied conventional circuit breakers or fuses. Fig. 1 shows the results of one such ground fault on a 208-volt 3-phase 3-wire grounded-neutral circuit to a 20-horsepower scrubber pump motor. The length of the feeder and branch circuit, all in steel conduit, limited the fault current to less than the magnetic instantaneous tripping value of its branch circuit breaker. An arc was established at the location of the fault and was sustained until the time-delay overload element tripped the circuit breaker. All this time (about 15 seconds) hot metal was spewed into a hazardous area. Apparently the arc did not develop into a phase-to-phase fault which, with its higher voltage and lower circuit impedance, would have operated the instantaneous trip element.

Method of Tests

A series of laboratory tests were performed with copper conductors in sizes 1-, $1^1/_4$-, $1^1/_2$-, 2-, $2^1/_2$-, 3-, and 4-inch

Paper 60-12, recommended by the AIEE Industrial and Commercial Power Systems Committee and approved by the AIEE Technical Operations Department for presentation at the AIEE Winter General Meeting, New York, N. Y., January 31–February 5, 1960. Manuscript submitted September 4 1959; made available for printing October 2, 1959.

J. A. Gienger, O. C. Davidson, and R. W. Brendel are all with the Eastman Kodak Company, Rochester, N. Y.

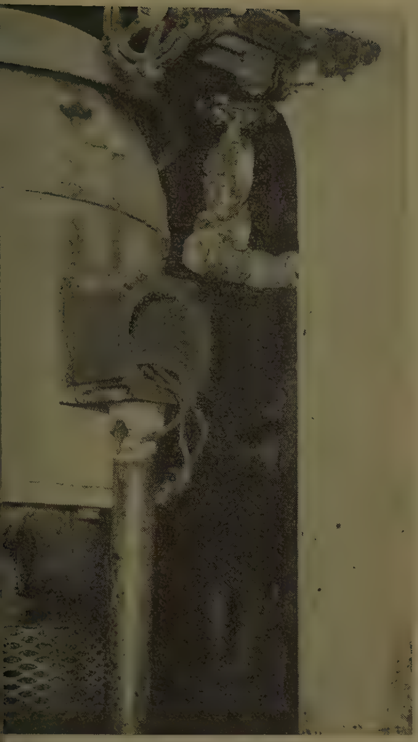

. 1. Example of a conduit burn-through
ulting from a sustained arcing ground fault

nmercial electrical steel conduit and 2$^1/_2$-, 3-, and 4-inch commercial elec-cal aluminum conduit. On all tests 60-cle current was caused to flow through outgoing cable within a 10-foot length conduit. In one case the voltage drop s read with the current return path ng the conduit to simulate a typical bund-fault condition; see Fig. 2 (case

In the second case the voltage drop s read with the current return path ng the conduit paralleled with a cable thin the conduit to simulate an internal nding conductor; see Fig. 2 (case 2).

In every test the voltage drop and cur-nt flow were read on a low reading indi-ing voltmeter and an indicating am-ter at various currents up to approxi-tely 12 times the rated current-carry-capacity of the conductor under test. mitations of space and capacity of the pply transformer necessitated making tests on 10-foot lengths of conduit. ltage drop per 100 feet of conduit was lculated by simply multiplying the asured voltage drop by the factor of . All readings were taken at a line ble temperature of approximately 60 C egrees centigrade) and a conduit tem-rature of approximately 27 C. These nperatures were measured by means of thermocouple imbedded between the ands of the line cable and another ermocouple taped in direct contact th the conduit.

Results of Tests

The ground-fault impedance occurring at all values of current flow tested is presented as four families of voltage-drop curves. Fig. 3(A) displays the voltage drop resulting with a phase-to-ground fault in commercial electrical steel conduit and the fault current return along the conduit. Fig. 3(B) depicts a ground-fault condition in steel conduit with the current return on the conduit plus an internal bonding conductor connected in parallel with the conduit. The family of curves in Fig. 3(C) represents phase-to-ground conditions in commercial electrical aluminum conduit with the enclosing conduit as the return circuit. Fig. 3(D) displays the resulting voltage drop as it occurs with the line conductor in aluminum conduit when the fault flow returns along the conduit plus a parallel internal bonding conductor.

It should be pointed out that the curves presented here represent the symmetrical steady-state current values. The initial asymmetrical value of fault current will vary with the resistance and reactance of the circuit, the instantaneous voltage, and the impedance of the arc at the instant the fault is started. Since the problem, as presented here, is to determine the minimum ground-fault current instead of the maximum, it is the steady-state value that should be considered.

Experience at one plant has indicated that circuits protected at 30 amperes or less will not burn through standard rigid steel conduit or fittings when faulted. However, feeders protected by fuses or circuit breakers rated greater than 30 amperes have permitted high-current arcing to continue for a sufficient period to burn through a steel enclosure.

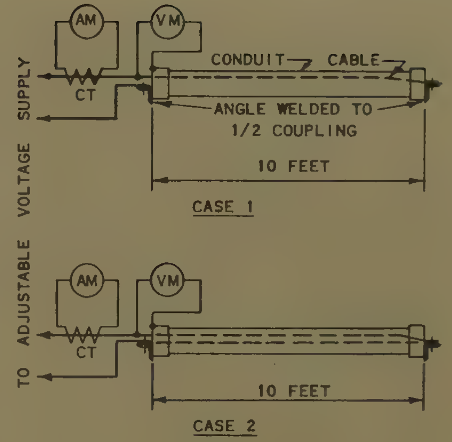

Fig. 2. Test connections

Table I is a study of the curves representing a size 4/0 circuit in 2$^1/_2$-inch conduit and indicates the limitations of feeder length that must be observed during design if the feeder protective device is to be expected to trip instantaneously. Assumptions have been made that the circuit-breaker instantaneous-trip device will operate at 2,300 amperes and that the conditions of system voltage and arcing potential will be as specified in Table I.

A comparison of the limitations outlined in Table I reveals the marked advantage resulting when an internal equipment bonding conductor is provided in a steel conduit installation. The resulting reduction of impedance in the faulted line conductor will permit feeder distance to

Table I. Maximum Lengths of a Size 4/0 Feeder

Fault Return Path	Maximum Length of Feeder* 208/120-Volt System	480/277-Volt System
2$^1/_2$-inch steel conduit	130	386
2$^1/_2$-inch steel conduit + 4/0 cable	222	660
2$^1/_2$-inch aluminum conduit	385	1,140
2$^1/_2$-inch aluminum conduit + 4/0 cable	392	1,160

* Maximum lengths have been calculated assuming: 1. The instantaneous tripping value equals 2,300 amperes. 2. Full voltage, as shown, will be sustained at the protective device during the fault. 3. A potential having a 40-volt component in phase with the line-to-neutral source voltage will occur at the arcing fault.

Table II. Fault Tests on an Actual 500-MCM Feeder

Trial No.	Return Path	Voltage Drop, Volts*	Fault Current, Amperes Predicted	Actual
1	3-inch steel conduit	230	1,290	1,362
2	3-inch steel conduit	230	1,290	1,355
3	3-inch steel conduit + size 4/0 cable	190	2,280	2,350
4	3-inch steel conduit + size 4/0 cable	192	2,300	2,260

* Voltage drop measured 700 feet from fault.

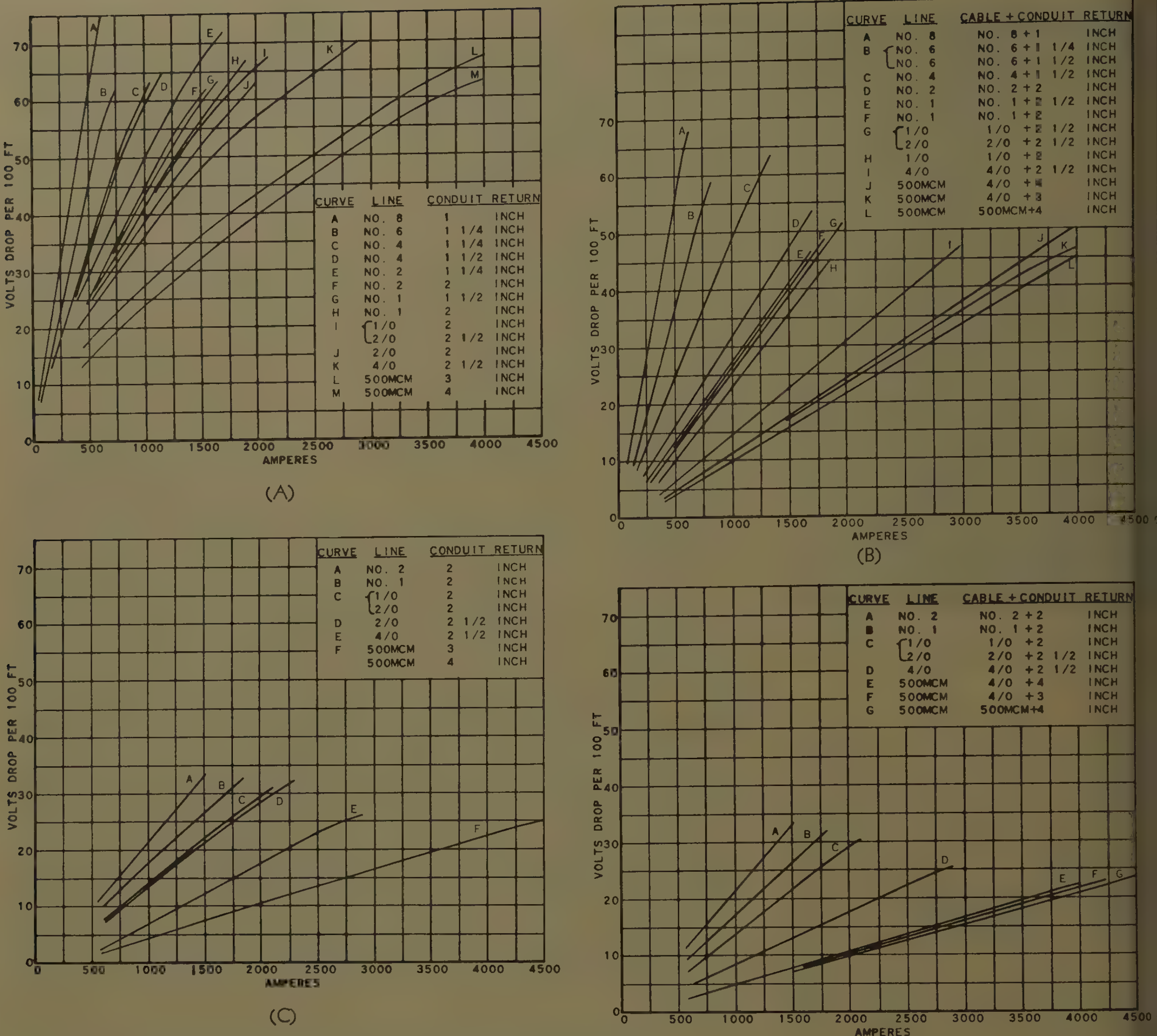

Fig. 3. Voltage-drop curves for various ground-fault return conditions

A—On steel conduit
B—On internal bonding cable plus steel conduit
C—On aluminum conduit
D—On internal bonding cable plus aluminum conduit

be increased 1.7 times the permissible length of the same capacity feeder which relies entirely upon its steel conduit for a return path.

A greater advantage is displayed by the installation of aluminum conduit. The same size *4/0* circuit can be safely utilized to serve an electric load at a location 2.96 times further distant than its steel counterpart. The nonmagnetic property and relatively high electrical conductivity of this material may provide an inexpensive and justifiable solution for the design engineer to avert a potential ground-fault hazard even though it is more susceptible than steel to arcing damage. Table I and the voltage-drop curves disclose little or no advantage to providing an additional internal bonding conductor in an aluminum conduit system.

It is reasonable to assume that the fault impedances presented in this report are also applicable for determining the currents that could flow in an ungrounded system when two phase-to-ground faults occur simultaneously. Although the fault potential imposed upon this type of "ground" fault is equal to phase-to-phase voltage, the conduit paths may be appreciably longer. The hazards of sustained high currents during faults such as this are no less important than on grounded neutral systems. However, a good program of ground detection, tracing, and clearing will greatly reduce the probability of sustained high fault currents on the ungrounded system.

Verification of Data

For the purpose of verifying the data obtained by laboratory tests, an actual feeder was selected and subjected to a phase-to-ground fault. The feeder consisted of three 500-MCM (thousand-circular-mil) cables and one size *4/0* conductor installed in 3-inch steel conduit. It normally supplied 480-volt 3-phase 60-cycle power on a grounded-neutral system and was chosen for its unusual length and because the conduit run is conveniently exposed and installed in a reasonably safe area. The size *4/0* cable is a bonding conductor in-

led for the prime purpose of reducing und-fault impedance. To simulate a t, one phase was bolted to the conduit. als 1 and 2 were performed with the ding conductor disconnected and insu-d from the conduit path. The bond-cable was reconnected for trials 3 and provide a return path in parallel with conduit. Fault current and voltage p along the ground-fault circuit were sured at a point 700 feet from the lo-on of the fault by means of both indi-ng instruments and oscillograph re-lers.

he results are indicated in Table II compared with the magnitudes of cur-predicted by use of the test curves at same value of voltage drop. The l numbers are for reference and indi-e the sequence in which the tests were ormed. For a duration of 16 hours or to the tests, the feeder carried a y light or negligible load. A shut-n period varying from 1/2 to 2 hours preceded each of the first three tests, king it reasonable to assume that the ductor temperature was below 60 C ing trials 1, 2, and 3. This would ex-n the slightly higher currents meas-d as compared with the curves which based on a 60 C conductor tempera-e. A period of only a few minutes nspired between trials 3 and 4. It is ly that the conductor reached a tem-ature greater than 60 degrees during l 4 as a result of the accumulative perature rise that accompanied the closely spaced fault tests. This would account for the measured current decreasing from 70 amperes above the predicted value to 40 amperes below the predicted current in trial 4.

After trial 1, an electrician stationed along the conduit route reported that he observed an emission of sparks at a pull-box assembly. It should be noted here that all pull-box covers were removed for the duration of the experiment and the conduit installation was located within a darkened building. Close inspection of the spark-producing area revealed a "hand-tight" conduit locknut and evidence of arcing. The loose locknut was tightened before trial 2 and in the following experiments no visible sparking could be detected. The sparking had occurred even though the pull-box installation was properly provided with a bonding jumper around the assembly and bolted to the pull box itself to assure electrical continuity. This emphasizes the importance of tightly assembled fittings in a conduit system.

Conclusions

1. The choking effect induced into a ground-faulted line cable by a magnetic conduit enclosure should be considered in the design of long grounded-neutral circuits.

2. The voltage-drop curves presented in this paper can be used to determine the following:

(*a*) The impedance of a grounded-neutral circuit in commercial electrical steel or aluminum conduit under ground-fault conditions.

(*b*) The maximum allowable setting of an instantaneous tripping device to assure adequate protection under ground-fault conditions.

(*c*) The maximum allowable length of a grounded-neutral circuit when the instantaneous tripping value of the circuit protective device is not adjustable or cannot be lowered without creating a co-ordination problem.

3. When a proposed or existing feeder in steel conduit exceeds its maximum allowable length, the following alternatives should be explored:

(*a*) Installation of an internal equipment bonding conductor which should be bonded to the conduit system at regular intervals.

(*b*) Installation of aluminum conduit instead of steel.

4. The low ground-fault impedance exhibited by feeders in aluminum conduit is an important design feature which, under certain conditions, could provide a decided advantage over steel conduit.

5. There is little or no advantage to be gained by installing an internal bonding conductor in a 2-inch or larger aluminum conduit feeder.

References

1. Iron Conduit Impedance Effects in Ground Circuit Systems, A. J. Bisson, E. A. Rochau. *AIEE Transactions*, pt. II (*Applications and Industry*), vol. 73, July 1954, pp. 104–07.

2. Some Fundamentals of Equipment-Grounding Circuit Design, R. H. Kaufmann. *Ibid.*, pp. 227–32.

Discussion

H. Kaufmann (General Electric Comy, Schenectady, N. Y.): This paper kes signal contributions to a better under-nding of the behavior of a-c system unding circuits. A sufficiently broad roach has been used which permits respondingly far reaching interpretations be made.

he test reported in the paper involved passage of a 60-cycle alternating current r a single internal power conductor with return current flowing on the enclosing duit. The magnitude of current and the ressed driving voltage were documented. e circuit examined represents that pre-ted by a single line-to-ground fault on a hase circuit.

he relationship between voltage and rent in the test case involved positive, ative, and zero sequence impedances. e magnitude and character of the posi-e and negative sequence impedances are te well known. This discussion will sent an analysis of the relative magnitude he zero sequence impedance, Z_0, or rather, ratio of zero sequence impedance to posi-e sequence impedance Z_0/Z_1. The analytical steps by which this can be accomplished are detailed in Fig. 4. In addition to the measured values of voltage E and current I, there is needed a value of the positive sequence impedance Z_1. (The equality of Z_2 and Z_1 for cable circuits in conduit avoid the need for impedances other than Z_1.) Values of Z_1 used in this analysis (representative of conductors in steel conduit) are given in Table III.

No measure of the circuit power factor was made by the authors. In the absence of this information, analysis has been made on the assumption that the ratio X_0/R_0 is about the same as X_1/R_1. Examination of the tabulated values of Z_1 discloses that in all except the largest conductor size, R is greater than X; that is, the power factor angle is less than 45 degrees. In reference 2 of the paper there is described on page 4 and illustrated in Fig. 2 the manner in which the magnetic properties of the steel conduit tend to confine the return current flow to a thin shell along the inner surface of the conduit at low to moderate current values. The effect is an additional impedance component in Z_0 which is largely of resistive character. This will tend to make the power factor angle of Z_0 also low, approaching near equality with that of Z_1. Thus, for the most part, the assumption of near equal X/R ratios is realistic. In the case of the largest conductor size, the impedance angle difference might be substantial but would not exceed 45 degrees. Even if the impedance angles differ by 45 degrees, the true ratio of Z_0/Z_1 for an indicated value of 10 on the graph would be 10.5. At higher ratios of Z_0/Z_1 the percentage error would be less than 5%.

The results of the analysis are given in Figs. 5–7. The impedance variation being directly a function of current makes it desirable to use current magnitude as the

Table III. Assumed Values for $Z_1=Z_2$

Conductor Size	Ohms Per 100 Feet: X	R	Z	X/R
8	0.0075	0.0811	0.0814	0.90
6	0.0068	0.051	0.0515	0.13
4	0.0063	0.0321	0.0327	0.20
2	0.0058	0.0203	0.021	0.29
1	0.0057	0.0163	0.017	0.35
1/0	0.0054	0.0131	0.0139	0.41
2/0	0.0053	0.0102	0.0115	0.52
4/0	0.005	0.0064	0.0081	0.78
500 MCM	0.0047	0.0039	0.0055	1.2

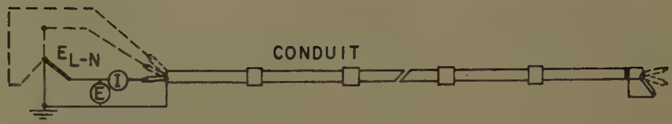

Fig. 4. Current-voltage-impedance relationships involved in a single line-to-ground fault

$$I_G = 3I_0 = \frac{3E_{L-N}}{Z_1+Z_2+Z_0} = \frac{3E_{L-N}}{2Z_1+Z_0}$$

Note: In test measurements

$$E_{L-N} = E$$

$$I_G = I$$

$$I = I_G = \frac{3E}{2Z_1+Z_0}$$

From which can be derived:

$$Z_0 = \frac{3E}{I} - 2Z_1$$

$$Z_0/Z_1 = 3\left(\frac{E}{I}\right) \div Z_1 - 2$$

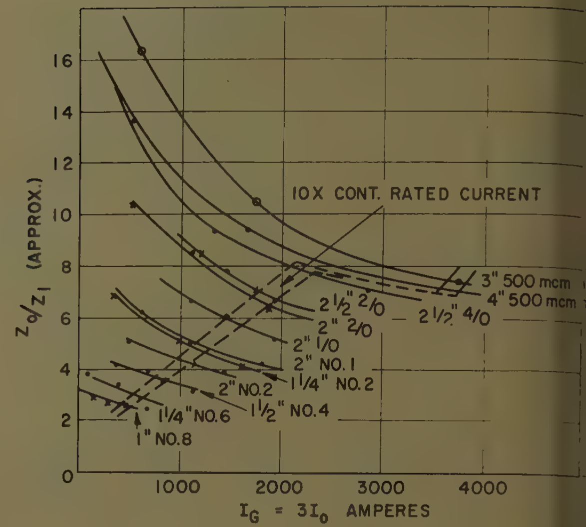

Fig. 5. Z_0/Z_1 ratios applicable to power conductors in steel conduit without internal ground wires

abscissa. Fig. 5 includes a line at the "10 times continuous rated current" value. It is evident that substantial elevation in the value of Z_0 due to magnetic effects in steel conduit are still present at currents as high as 10 times the continuous rating. This is a most significant observation.

Fig. 6 shows that a full-size internal ground wire markedly reduces the value of Z_0 and makes it comparable with that obtained with aluminum conduit. (Furthermore, the internal ground wire picks up a sizeable fraction of the return current flow thus easing the tendency to spark and flash at conduit joints and terminations.) Had the Z_1 values for the aluminum conduit case been adjusted downward slightly to compensate for the absence of magnetic enclosure, the reflected values of Z_0/Z_1 in Fig. 7 would have been elevated slightly. The authors concede that steel conduit with a full-size internal ground conductor is comparable with aluminum conduit in so far as Z_0 values are concerned. The behavior of aluminum conduit in transferring large-magnitude ground-fault currents at joints and terminations has not appeared in the technical literature.

E. J. Rutan (Consulting Engineer, New York, N. Y.): The value of this paper lies in the extensive data which are now made available for application to the design of safe conduit enclosed wiring systems. The possibilities of serious damage and resulting fires occurring due to faults on 208- and 240-volt a-c circuits have not been fully realized by designers. Code-making committees also have not recognized the hazards which exist (see my discussion of the paper by Bisson and Rochau).[1]

The present authors, and others before them, have been pointing out the current-limiting effects of steel conduit on fault currents. The National Electric Code approves the conduit as the return path for ground currents; in fact, it has no requirement for other ground return circuits for conduit enclosed wiring.

The authors, in Table I, give circuit limits for obtaining instantaneous tripping. There are other conditions which may be more serious. These apply to circuits operating at 208 or 240 volts with 120 volts to neutral.

If one refers to the Underwriters' Laboratories Standard for Fuses, he will find that the allowable blowing time for acceptable fuses at 200% rated current is surprisingly long. For example, a 200-ampere fuse can take 8 minutes to blow at 400 amperes, and a 400-ampere fuse can take 10 minutes at 800 amperes.

Reference to tripping curves of larger molded-case breakers will show maximum tripping times of 8 to 10 minutes for 200- to 400-ampere breakers at 200% rated current. The minimum times may be of the order of 2 to 3 minutes for 200% rated current.

When a fault occurs in a steel conduit system, the reactance due to the conduit not only limits the so-called short-circuit current, but helps to maintain the arc. I know of one failure which resulted in a serious fire due to the molten steel dropping from the conduit.

In Table IV, several typical installations are computed, using the author's data, which might be a hazard if a fault developed. From this table it is seen that there can be arcing of long duration on circuits between 200 and 350 feet long. Such circuits can occur in tall buildings 15 or more stories high. (The circuit length must be taken from the service because this is the point at which the neutral is grounded and therefore the location where both sides of the circuit are within the conduit.)

Other illustrations include the following: The 30-horsepower motor circuit with a 225-

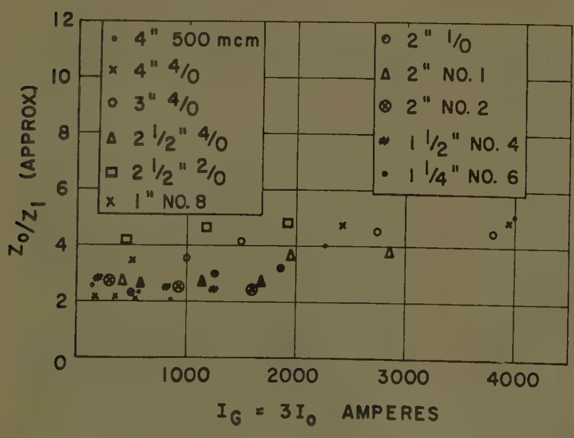

Fig. 6. Z_0/Z_1 ratios applicable to power conductors plus one full-size ground conductor in steel conduit

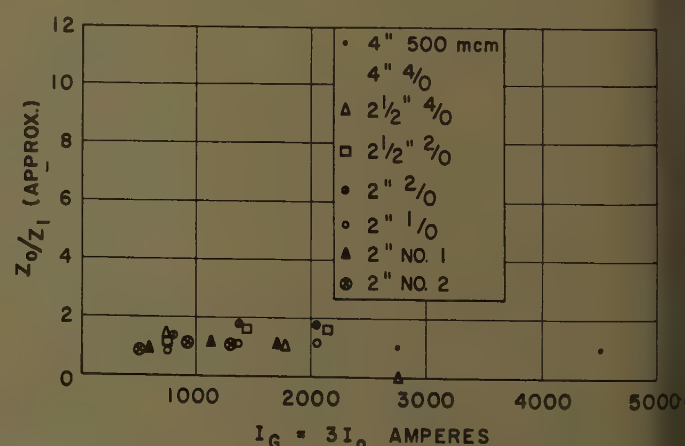

Fig. 7. Z_0/Z_1 ratios applicable to power conductors in aluminum conduit without internal ground wires

Table IV. Possible Hazardous Installations

Characteristic	Case 1	Case 2	Case 3
Installation 208/120 volts	30-horsepower, 3-phase motor	75-horsepower, 3-phase motor	500-MCM feeder
Rated current	83	196	380
Conductor size	no. 3	4/0	500 MCM
Conduit size, inches	$1^1/_2$	$2^1/_2$	3
Permissible fuse, amperes (National Electric Code Table 430-146)	250	500	400
Maximum fuse blowing time in minutes at 200% (and amperes)	10 (500)	12 (1,000)	10 (800)
Permissible circuit breaker, amperes	225	400	400
Breaker tripping time in minutes (and amperes)	1.5–6 (500)	1.5–5 (1,000)	1.5–10 (800)
Author's curve, Fig. 3(A)	*D*	*K*	*L*
Circuit length in feet for currents in items 6 and 8 (40–50 volts at arc)	250–280	220–250	300–370

Table VI. Circuit Impedances Obtained from Table V

Case	Return Path	Impedance, Milliohms per 100 Feet: Go	Return	Total
1	Steel structure, no conduit	12+	1+*j*50	52
2	Steel conduit	12+	24+*j* 2	36
3	Steel conduit plus internal return conductor	12+	8+*j* 2	20
4	Aluminum conduit	12+	2+*j* 2	14
5	Aluminum conduit plus internal return conduit	12+	1.7+*j* 2	13.8

ere circuit breaker in conduit 185 feet might arc for 1/3 to 1 minute with a current of 750 amperes before the ker will trip. The 500-MCM feeder, 0 feet long, might sustain an arc of) amperes for 0.9 to 1.5 minutes before reaker will trip.

one takes the time, it will be found that t the same circuit lengths and clear-imes apply for most of the cable and uit conditions tabulated by the authors.

ne foregoing examples illustrate the e of the paper, which points out the lvantages of steel conduit for long runs the advantages of aluminum conduit. hould also lead fuse manufacturers to ove fuse performance, and induce cir- breaker designers to try to narrow ripping limits.

more importance, it should suggest to responsible code committees that they n consider constructions to reduce these rds.

ERENCE

ee reference 1 of the paper, p. 107.

. Roehmann (Kaiser Aluminum and nical Corporation, Spokane, Wash.): larify matters, one may calculate, as an nple, the circuit impedances for *2/0* Awg erican Wire Gage) copper conductor and h steel and aluminum conduit. These, d on the figures in Table V, are given Table VI.

ne first case in Table VI assumes that entire return current flows over the structure. This may occur when there poor (open) joint in the conduit, or n the conduit is nonmetallic, or when e is no conduit at all. The value of eactance is somewhat arbitrary depend-on the width of the loop, i.e., the sep-ion of go and return path. For direct current, this case would offer the smallest resistance; for alternating current, it offers the highest impedance. In the second case of Table VI as in all following cases, reactance is at a minimum: A coaxial conductor has the lowest reactance of all possible arrangements. Conduit a-c resistance is high, however, due to the high losses. Paralleling the internal return conductor reduces the resistance materially, cutting impedance from 36 to 20 milliohms. These figures check reasonably well with the impedances obtained from the appropriate voltage–current curves in Figs. 3(A) and 3(B) of the paper. Substitution of the aluminum for the steel conduit reduces impedance to 14 milliohms, which is in accordance with the data from Fig. 3(C). The paralleling return conductor helps now very little, again in accordance with the authors' findings, Fig. 3(D).

The impedance ratio of the circuit with steel conduit (case 2) and circuit with aluminum conduit (case 4) is 36 to 14 or 2.6. For a *4/0* Awg conductor in $2^1/_2$-inch conduit, the authors report a ratio of 2.96. Perhaps the authors would give, in their closure, a curve or table of this ratio versus conductor size, based on their test data, Figs. 3(A) and 3(C), and assuming the maximum conduit fill permitted by the National Electric Code. We expect that for all commonly used sizes, this ratio will be above 2; i.e., permit, with aluminum conduit, extension of the feeder length to twice that permitted for steel conduit. This length is based on considerations of safe fault clearance but has nothing to do with the feeder length as determined by voltage drop. Before feeder length is doubled, or more than doubled, by changing from steel to aluminum conduit, one should check whether voltage drop during normal operation will remain within acceptable limits.

ble V. Sixty-Cycle A-C Resistance

Conductor Enclosure	Resistance, Milliohms per 100 Feet
wg copper conductor, warm	12
h steel conduit	24
conduit plus *2/0* copper in parallel	8
h aluminum conduit	2
inum conduit plus *2/0* copper in allel	1 7

H. E. House and P. D. Tuttle (Aluminum Company of America, Massena, N. Y.): The authors have presented information that is of great value for designers of industrial distribution systems in which long conduit runs are becoming common.

Of interest is the fact that steel conduit, with an internal grounding conductor adding to the construction cost, does not permit the same length of run as aluminum conduit alone for the same voltage drop, as defined in the paper. Or, from the other point of view, the same minimum fault current can be expected from a much longer run of aluminum conduit than from steel.

For industrial distribution circuit breakers having time delay tripping, a similar ground fault on identical steel and aluminum conduit runs will cause the circuit breaker on the aluminum-clad feeder to trip out much more quickly than that on the steel clad feeder. If instantaneous trip devices are also incorporated in the breaker, the difference may mean an instantaneous trip on

Table VII. Impedance Values

60-Cycle-Current, Amperes	Temperature Rise, C: Cable	Temperature Rise, C: Conduit	Resistance, Ohms per 100 Feet	Reactance, Ohms per 100 Feet: Actual Value	Reactance, Ohms per 100 Feet: Equivalent X_a at 1 Foot
In Steel Conduit					
100	12	8	0.0458	0.0248	0.0299
200	40	26	0.0422	0.0240	0.0291
300	77	47	0.0400	0.0231	0.0282
	(ambient 23.6–24.3)				
In Aluminum Conduit					
100	6	3	0.00550	0.0042	0.0093
200	21	9	0.00582	0.0042	0.0093
300	47	18	0.00630	0.0042	0.0093
	(ambient 30.6–31.2)				
Isolated Cable*					
100	4		0.00527		0.0093
200	14		0.00547		0.0093
300	30		0.00580		0.0093
	(ambient 23.1–23.5)				

* Laid on wooden runner.

the aluminum conduit run and a delayed trip on the steel conduit feeder. Hence the susceptibility of aluminum to somewhat more arcing damage is more than overcome by the faster clearing time, and, in addition, conductor damage is minimized.

The low voltage drop of aluminum conduit ground faults will tend to minimize the possibility of sparking at any poorly made joints or box connections. Furthermore, the hazard to personal safety of high ground-fault voltages is mitigated.

As a matter of interest, the impedance values of a *4/0* Awg copper *RHH* cable in $2^1/_2$-inch steel and aluminum conduit runs are given in Table VII from recent experiments conducted by the Electrical Engineering Division of Alcoa Research Laboratories. With current in the cable returning through the conduit the entire reactance is reflected in the cable. These values are for equilibrium temperature conditions for the 60-cycle-per-second currents.

J. A. Gienger, O. C. Davidson, and **R. W. Brendel:** The comments presented have added to the knowledge of the subject and we wish to thank the discussers.

Our approach to the problem of conduit burn-throughs was to obtain experimental data to determine the minimum current to be expected on a severe phase-to-ground fault. An attempt was then made to put the information in some simple graph which could be easily used to co-ordinate the design of the line with the time-current characteristic of the protective device so that the fault would be cleared in a few cycles. With circuit breakers it seems advisable to use the "instantaneous trip" value since the time required to burn through various conduits at all values of current has not yet been determined. However, limited tests indicate that 2-inch steel conduit can be burned through in about 1 seconds with 500 amperes, or in 5 seconds with 350 amperes. For 3-inch steel conduit the times are about 4 seconds and 8 seconds. Aluminum conduit can be burned through in somewhat less time.

Application of Accepted Cable-Heating Principles to Unequally Loaded Underground Duct

R. D. CHAMLEE
MEMBER AIEE

D. E. McCALL
NONMEMBER AIEE

A NUMBER of factors influence the selection of wire and cable sizes in an industrial power system. The more important factors are load requirements, codes, plant design specifications, voltage regulation, short-circuit levels, economics, and cable heating.

This paper is limited to one of the factors: cable heating. In particular, the paper outlines a solution to the problem of making a design check for overheating in unequally loaded underground ducts. Existing papers on cable heating are written primarily for equally loaded ducts. The basic intent of this paper is to present a solution that is easy to use and gives results of acceptable accuracy for unequally loaded ducts.

General Considerations

Loaded cables generate heat. The heat comes from losses within the conductor, sheath, and surrounding magnetic enclosure. The magnitude of the losses depends on circuit characteristics, cable construction, and physical environment. This generated heat is dissipated from the conductor to ambient earth in a multipath thermal flow. The resultant temperature rise of the conductor is a function of the amount of generated heat and the thermal resistance of the heat-flow paths.

Industry has adopted temperature limitations to control the rate of deterioration of cable insulation. In general, the deterioration increases with temperature. Recommended values of maximum allowable conductor temperatures are published in the specifications issued by the Association of Edison Illuminating Companies (AEIC) and the Insulated Power Cable Engineers Association (IPCEA). These temperature ratings are based on the type of insulation, operating voltage, and general application.

Current Calculations

Current ratings of insulated cables are calculated on the basis of temperature limitations. In the 1930's, the cable industry adopted an empirical calculation method which included standard duct-bank heating constants.[1,2] These constants, theoretically based on typical conditions, have become known as National Electric Light Association (NELA) constants. The use of duct-bank constants avoided the very difficult evaluation of the thermal resistance between the duct structure and ambient earth. Some of the many complex variables accounted for in the NELA constants are as follows:

1. Size, number, and spacing of ducts.
2. Configuration of duct banks.
3. Material of duct and duct structure.
4. Depth of duct below grade.
5. Type of soil and moisture content.
6. Type of ground surface.
7. Atmospheric temperature variations.

Many papers have been written on the subject of cable heating and circuit loading. A comprehensive study of present practices has been published by the Edison Electric Institute.[3] Of noteworthy interest, among many AIEE papers on cable heating, is one by Neher and McGrath that includes a compilation of engineering formulas and constants for the calculation of current-carrying capacities. The calculation procedure outlined by Neher and McGrath is based on actual thermal resistances rather than on an over-all empirical duct constant. Existing tables will be recalculated by a similar solution.[4] Such a recalculation is not expected to make significant changes in existing tables.

In 1943 the IPCEA published a series of tables covering current-carrying capacities of paper, rubber, and varnished cambric cables.[5] These and similarly calculated tables published by cable manufacturers have become accepted industry standards. Thus, they are basic data used in the development of this paper.

The IPCEA tables for underground ducts are calculated for 3, 6, 9, and 1[illegible] ducts, and 30, 50, 75, and 100% load factor. Interpolation is used for intermediate ducts and load factors.

The NELA constants used for calculations by IPCEA were based on nonmetallic ducts 3 to 4 inches in diameter.

Paper 60-38, recommended by the AIEE Petroleum Industry Committee and approved by the AIEE Technical Operations Department for presentation at the AIEE Winter General Meeting, New York, N. Y., January 31–February 5, 1960. Manuscript submitted September 16, 1959; made available for printing November 19, 1959.

R. D. Chamlee and D. E. McCall are with C. F. Braun and Company, Alhambra, Calif.

tables were prepared for equally ed cables of similar size, all located utside ducts. The calculations as- ed an unspecified average soil condi- with no extraneous heat sources.

he authors studied a series of homo- ous duct banks to investigate the t of cable size on duct-bank losses idle duct temperature. The homo- ous banks were each composed of lly loaded cables of the same type size. The studies were based on EA tables. The studies showed the wing results for the conditions given re, in each case, cable size was in- sed and 100% load factor maintained.

For a given number of loaded ducts: l duct-bank loss increases, idle duct perature increases.

For a given total duct-bank loss: Num- of loaded ducts decreases, idle duct tem- ture increases.

For a given idle duct temperature: Num- of loaded ducts decreases, total duct- k loss decreases.

CTICAL CASE

he typical duct bank in an industrial t comprises cables of unequal size and loading. Hence it does not agree with the assumptions used for IPCEA tables. The IPCEA states, however, that current ratings for such a bank can be estimated from their tables with a fair degree of approximation by selecting the symmetrical arrangement that most nearly corresponds, gives approximately the same total watts loss in the duct bank, and gives the same group ambient (idle duct) temperature.[5] These conditions imply some compromise solution for determining current-carrying capacities and resultant duct-heating effect in a mixed bank of underground ducts.

SOLUTIONS FOR MIXED BANKS

The authors investigated three solutions for checking duct heating in mixed banks. Solution *A* utilized IPCEA current-capacity charts plotted in curve form. Maximum current-carrying capacities for wires of the same type but different size were determined on the basis of equivalent ducts. It was assumed that the differences in duct heating effect were negligible for various sizes of wire in duct banks with the same number of equivalent ducts. An equivalent duct represented a duct whose cables carried 100% of allowable current. The mechanics of the solution were trial and error.

Solution *B* was based on the total duct-bank losses. As an approximation, it was assumed that current ratings for groups of cables of unequal size and unequal loading could be established by basing the maximum rating of each cable on a homogeneous bank of the same size cable. Each such homogeneous bank would have the same total duct-bank losses as the original bank. Solution *B* is the method proposed by the authors and is described in detail elsewhere in this paper.

Solution *C* was similar to *B* except that the basis was idle duct temperature rather than total duct losses. In the solution, duct temperature was based on total duct losses.

Solutions *A*, *B*, and *C* gave the same results for a given homogeneous duct bank. As the duct bank became mixed, however, the results began to differ slightly. For a given mixed bank, solution *A* gave the highest relative current ratings for

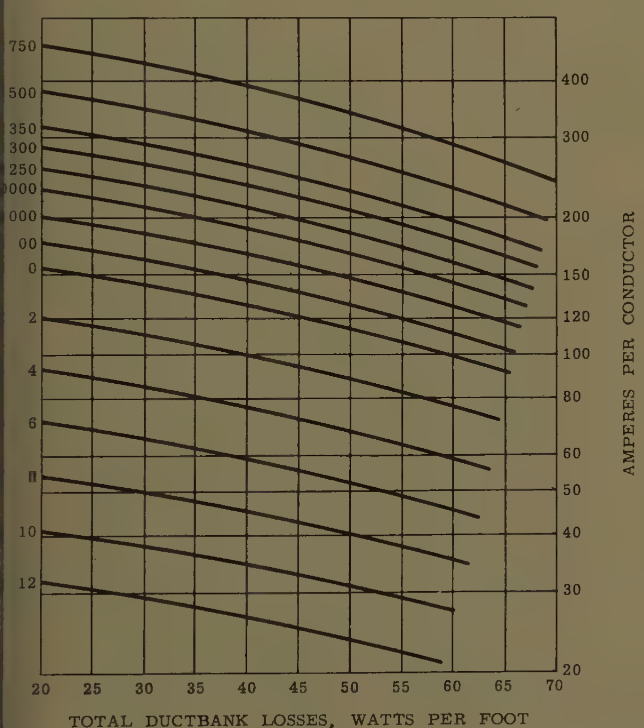

CORRECTION FACTORS

	60 C COPPER	75 C COPPER	85 C COPPER
20 C Ambient	.87	1.00	1.07
30 C Ambient	.75	.90	.99

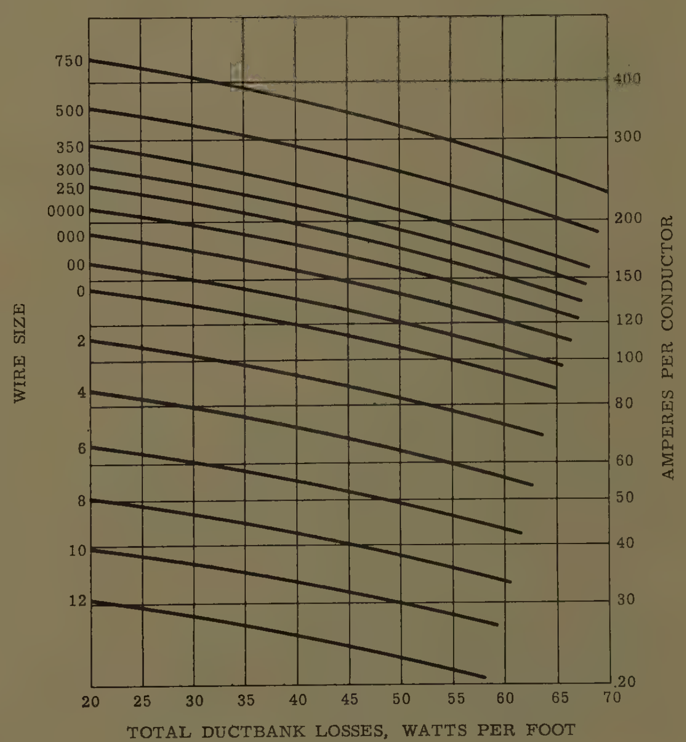

CORRECTION FACTORS

	60 C COPPER	75 C COPPER	85 C COPPER
20 C Ambient	.87	1.00	1.07
30 C Ambient	.75	.90	.99

Fig. 1. Current-carrying capacity of thermoplastic- and rubberlike-insulated cable, 0–6,000 volts, 75 C copper, 20 C ambient

A—Three single-conductor shielded, one 3-conductor shielded, or three single-conductor nonshielded
B—One 3-conductor nonshielded

small wires and lowest relative ratings for large wires. For the same bank, solution C gave the lowest ratings for small wires and highest ratings for large wires. The authors had no firm basis to determine which of the solutions gave the more nearly correct results. Since the results were very close, a prime factor in the recommendation of solution B was the simplicity in mechanics of solution.

Proposed Solution

Assumptions

The proposed solution for making a design check for overheating in underground ducts is based on the following assumptions and conditions.

1. The maximum current ratings for various sized cables are based on total duct-bank losses.

2. Duct-bank temperature is assumed constant for determining maximum current ratings.

3. Within a given bank, the individual ducts vary in their ability to dissipate heat. This is taken into account by locating loaded cables in outside ducts, with the largest heat generators in corner positions.

4. The data included in this paper are based on 100% load factor. Load factor is the ratio of the average load to maximum 1-hour load during a 24-hour period.

5. In order to establish data for duct-bank loss curves, it was necessary to calculate current-carrying capacities for duct banks in excess of IPCEA tables. These calculations were based on extended curves values of the NELA constant. A sample calculation is included in the Appendix.

6. The change of a-c resistance in cables not fully loaded is assumed negligible.

7. It is assumed that the over-all accuracy of the solution is not decreased by basing maximum current-carrying capacities of different types of wires on the same value of total duct-bank losses. This assum tion is based on data calculated fro Figs. 1–4.

Fig. 2. Current-carrying capacity of rubberlike-insulated cable, 10,000–15,000 volts, 75 C copper, 20 C ambient, three single-conductor shielded or one 3-conductor shielded

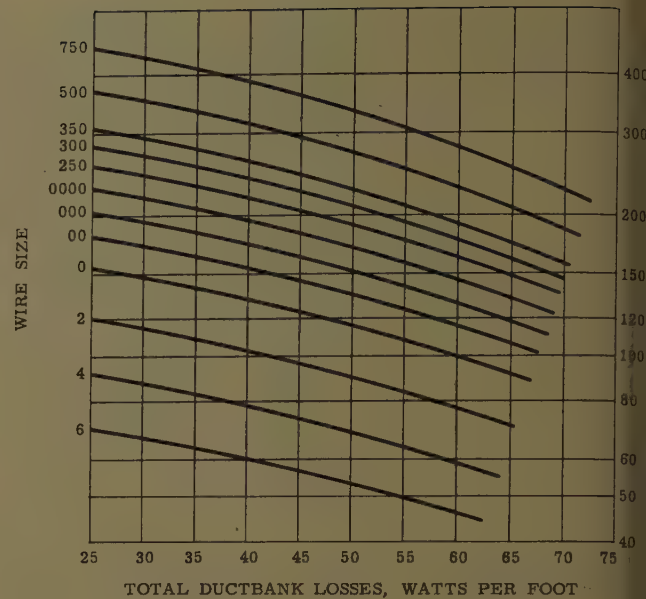

CORRECTION FACTORS

	60 C COPPER	70 C COPPER	75 C COPPER	85 C COPPER
20 C Ambient	.86	.96	1.00	1.08
30 C Ambient	.73	.85	.90	.99

Curves

Figs. 1–4 were plotted from data tak from homogeneous banks where all cabl were the same size and type and we equally loaded. The curves apply to mo than one cable type where results are e sentially the same. Correction factors a

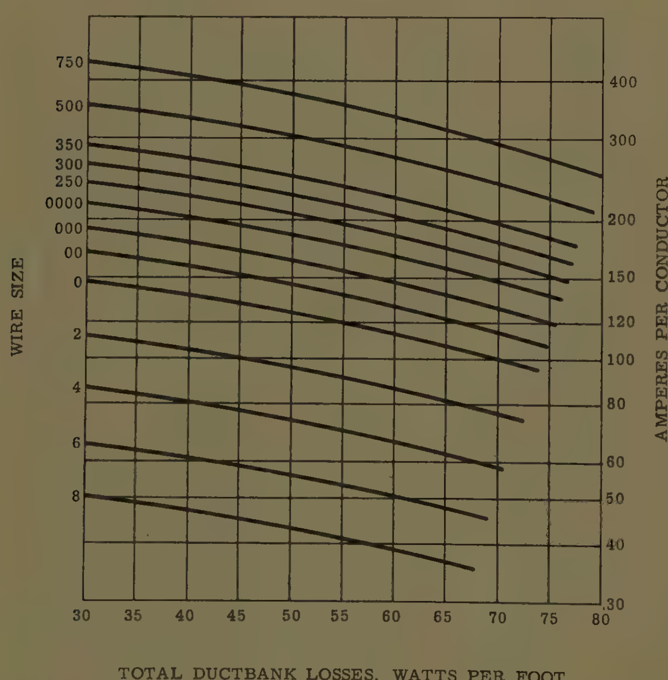

Fig. 3. Current-carrying capacity of varnished-cambric-insulated cable, 0–5,000 volts, 85 C copper, 20 C ambient, three single-conductor nonshielded or one 3-conductor nonshielded

For 30 C ambient, multiply by 0.92

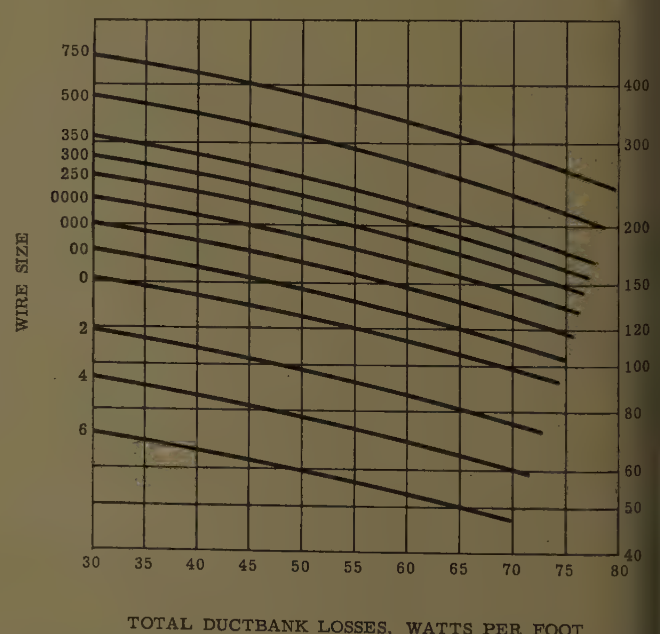

Fig. 4. Current-carrying capacity of paper-insulated cable, 15,0 volts, 81 C copper, 20 C ambient, three single-conductor shielded one 3-conductor shielded

For 30 C ambient, multiply by 0.91

Table I. Example of Duct-Bank Heating Check

Duct Bank From	Sw-Hse 24	Cables	600 v RHW, 3-1/C	Spares	2
To	Manhole 241		5,000 v VC, 3/C, Nonshielded	Ambient	20°

cuit	Hp or Kva Rating	Name Plate, Amps	Load, Amps I	Wire Size	Use Figure	Circuit μ-Ohm/Ft R	Circuit Loss, I^2R	Dielectric Loss, W_D	I, Max.	Not OK	Adjustments: Wire Size	Adjustments: R	Adjustments: I^2R	Adjustments: Δ, I^2R	Adjustments: I, Max.
1	2	3	4	5	6	7	8	9	10	11	12	14	14	15	16
	7.5	11	9	12	1A	5,800	0.47		22						23
	7.5	11	9	12	1A	5,800	0.47		22						23
	7.5	11	11	12	1A	5,800	0.70		22						23
	7.5	11	11	12	1A	5,800	0.70		22						23
	25	32	25	8	1A	2,340	1.46		37						40
	25	32	30	8	1A	2,340	2.10		37						40
	25	32	30	8	1A	2,340	2.10		37						40
	40	52	40	6	1A	1,470	2.35		48	X	4	925	1.48	−0.87	67
	40	52	50	6	1A	1,470	3.68		48	X	4	925	2.31	−1.37	67
0	75	93	75	0	1A	372	2.09		103						112
1	75	93	85	0	1A	372	2.68		103						112
2	100	123	100	00	1A	300	3.00		118	X					127
3	100	123	120	00	1A	300	4.32		118	X					127
4	500	63	60	4	3	955	3.44	0.11	68						72
5	500	63	60	4	3	955	3.44	0.11	68						72
6	2,000	242	215	350	3	123	5.68	0.24	230	X				−0.87	243
G-1	45	54	40	6	1A	1,470	2.35		48	X	4	925	1.48	−0.87	67
G-2	45	54	54	6	1A	1,470	4.28		48	X	4	925	2.70	−1.58	67
R-1	100	120	85	0	1A	372	2.68		103	X	00	300	2.17	−0.51	127
R-2	750	104	90	0	3	384	3.11	0.17	118						123
							51.10							−5.20 watts/ft	
							0.63	0.63							
							51.73							56.90	
						2 spares, each at 1/20×51.73	5.17							−5.20	
						Total duct-bank losses, W=56.90 watts/ft								W= 51.70 watts/ft	

Table II. Circuit Constants for Use With Figs. 1–4 and Table I in Duct-Bank Calculations*

e Size	Fig. 1(A) R at 75 C	Fig. 1(A) W_d at 5 Kv	Fig. 1(B) R at 75 C	Fig. 1(B) W_d at 5 Kv	Fig. 2 R at 75 C	Fig. 2 W_d at 15 Kv	Fig. 3 R at 85 C	Fig. 3 W_d at 5 Kv	Fig. 4 R at 81 C	Fig. 4 W_d at 15 Kv
750	63	0.13	63	0.10	63	0.75	64	0.31	64	0.38
500	88	0.11	88	0.10	88	0.63	90	0.27	89	0.34
350	119	0.10	119	0.08	119	0.57	123	0.24	121	0.29
300	138	0.09	138	0.07	138	0.54	143	0.22	140	0.27
250	164	0.08	164	0.07	164	0.51	169	0.21	167	0.25
000	191	0.08	191	0.07	191	0.47	197	0.22	195	0.24
000	240	0.08	240	0.06	240	0.43	246	0.20	244	0.22
00	300	0.07	300	0.06	300	0.40	309	0.19	305	0.20
0	372	0.07	372	0.05	372	0.37	384	0.17	380	0.19
2	585	0.05	585	0.04	585	0.30	605	0.14	600	0.15
4	925		925		925	0.23	955	0.11	945	0.12
6	1,470		1,470		1,470	0.17	1,510	0.08	1,500	0.09
8	2,340		2,340				2,410	0.04		
10	3,660		3,660							
12	5,800		5,800							

=circuit a-c resistance in microhms per foot at specified temperature. W_d = circuit dielectric loss in watts per foot at specified operating voltage. Omit dielec- loss for cables below 3 kv.

luded for variations in ambient and oper temperatures which are given in grees centigrade (C). The correction tors are based on the formulas used IPCEA in calculating their current-rying capacity tables.[5]

ADS

The duct-heating calculations are based load currents. The recommended thods of handling the more common es of loads are as follows:

tor Feeders. The normal operating rent of the motor is used. This value approximately equal to

$$\frac{\text{operating brake horsepower}}{\text{nameplate horsepower}} \times \text{nameplate amperes}$$

Lighting and Power Feeders. These feeders are usually sized to handle some expansion. The load currents used should represent the ultimate load. For transformers, this is nameplate current.

Intermittent Loads. Circuits such as controls, alarms, and welding feeders normally supply little or no load and therefore are negligible. If an operating and a spare motor feeder are in the same duct bank, the operating motor only is included in the calculations. If the operating and spare feeders are in separate banks, both are considered as operating.

Spare Empty Ducts. Spare empty ducts are considered as possible future loaded ducts. If the future load is known, its value is used in the calculations. Otherwise each empty duct is assumed to contribute an average value of watt loss to duct heating.

Procedure

The procedure is a tabular step-by-step method of determining duct losses, obtaining maximum current capacities, and revising cable sizes as required to eliminate overheating. The procedure is best explained by following through an example of a typical bank. Table I sets up

the problem. The solution follows these steps:

Columns 1 and 2. Enter the number and rating of each circuit. Include only those feeders that contribute to heating.

Column 3. Enter the nameplate or maximum current of each circuit.

Column 4. Enter the value of normal operating currents. These are the values used as a basis for duct heating.

Column 5. Enter the minimum wire size as determined from code or voltage drop requirements, whichever is greater.

Column 6. Designate the governing current-carrying chart for each circuit based on wire type.

Column 7. Enter the circuit a-c resistance from Table II.

Column 8. Calculate the I^2R loss based on operating loads and totalize.

Column 9. Enter the dielectric losses from Table II and totalize. These values will be zero for all 600-volt wire.

Add Column 8 Plus Column 9. Add the allowance for spare ducts. This gives total duct-bank losses for checking maximum current-carrying capacities.

Column 10. Enter the maximum allowable current-carrying capacities from Figs. 1–4, using temperature correction factors as required.

Column 11. Indicate those circuits for which the allowable currents are low. The maximum allowable current should equal nameplate current from column 3. This will allow any one load to operate at its nameplate capacity. The increased losses for operation of one such load above normal operating conditions are assumed negligible.

Columns 12–16. If allowable currents are too low, wire sizes must be changed on some of the feeders. It is not usually necessary to change all affected circuits. The change in a few circuits may decrease the total watts loss sufficiently to increase other ratings to an acceptable value. Inspection of the affected circuits and current-carrying capacity graphs will give a good indication of what total change in watts loss is needed. In some cases, it may be more economical to reduce the watts loss by changing circuits that initially are satisfactory. For example, a change from no. *6* to no. *4* American Wire Gage at 600 volts might accomplish the same result as a change from 350 MCM (thousand circular mils) to 500 MCM at 5 kv.

Conclusions

A solution has been outlined for checking cable heating in mixed underground duct banks. The simplicity of the solution makes it readily usable as a design tool. The solution contains certain assumptions and variables. It is believed that refinements to the solution would not greatly affect over-all accuracy because of the inherent inaccuracies in estimating basic quantities such as ambient temperature, ultimate loads, and extraneous heat sources. Refinements, or entirely new solutions, will come as more knowledge is gained in the field of buried cables and pipes.

Appendix. Sample Calculation

The following sample calculation is for duct banks larger than considered in IPCEA tables:

Sample calculation is for 500-MCM wire, Fig. 1(A)

T_c = copper temperature = 75 C

T_a = ambient temperature = 20 C

N = loaded ducts = 15

H = NELA duct constant = 0.70 for 15 ducts based on extended curve of NELA constants versus loaded ducts

R_c = thermal resistance of circuit = 2.35 thermal ohms per foot based on back-check of IPCEA table

R_d = thermal resistance of duct bank = NH = 10.50 thermal ohms per foot

W = total circuit losses = $T_c - T_a/R_c + R_d$ = 4.28 watts per foot

NW = total duct-bank losses = 64.2 watts per foot

R = circuits a-c resistance in microhms per foot = 87.5 from Table II

W_d = circuit dielectric loss in watts per foot = 0.11 from Table II

$$I=\sqrt{\frac{W-W_d}{R\times 10^{-6}}}=\sqrt{\frac{4.28-0.11}{87.5\times 10^{-6}}}=218 \text{ amperes}$$

References

1. Determination of Ratings for Underground and Aerial Cable. *Publication no. 28*, National Electric Light Association (now the Association of Edison Illuminating Companies), New York, N. Y., Mar. 1932.

2. Current Carrying Capacity of Impregnated Paper Insulated Cable. *Publication no. A14*, Edison Electric Institute, New York, N. Y., July 1933.

3. Underground Systems Reference Book. *Publication no. 55-16*, Edison Electric Institute, 1957, chap 10.

4. The Calculation of the Temperature Rise and Load Capability of Cable Systems, J. H. Neher, M. H. McGrath. *AIEE Transactions*, pt. III (*Power Apparatus and Systems*), vol. 76, Oct. 1957, pp. 752–72.

5. Current-Carrying Capacity of Impregnated Paper, Rubber and Varnished Cambric Insulated Cable. *Publication no. P-29-226*, Insulated Power Cable Engineers Association, Montclair, N. J., Dec. 1943.

Discussion

A. R. Kelly (Esso Research and Engineering Company, Madison, N. J.): The authors and their company are to be complimented on their continuing effort to sharpen the calculating method for current ratings in mixed duct banks. When they introduced their solution *A* some years back, they recognized that partially loaded cables do not contribute to mutual heating as much as fully loaded cables do. Now, in their solution *B*, they allow for the fact that a no. *12* Awg (American wire gage) conductor emits fewer watts per foot than its *4/0* Awg neighbor at the same temperature, and that this affects the relative contribution of each to the duct-bank mutual heating problem.

In solution *B*, an orderly extension is attempted of the IPCEA tables for homogeneous duct banks to cover duct banks with mixed cable sizes, mixed cable loadings, (in per cent of individual cable "full" loads), and mixed cable constructions and copper temperatures. Of the two criteria listed by IPCEA for approximate duct bank equivalence, that of equal total duct-bank loss is respected while that of equal group ambient appears to be neglected.

Appraisal of solution *B* leads quickly to the conclusion that proper means have not yet been included to account for rated copper temperatures other than those for which the curves and Table II were derived. This is shown by the following example:

Two duct banks are assumed, one with four ducts and one with ten. Each duct bank dissipates 38.1 watts per foot, and ambient earth temperature is 20 C in both cases. Each duct contains one fully loaded low-voltage cable, and all cables are identical in wire size and construction, so as to have an identical thermal resistivity R_c (including surface radiation to the inside of the duct wall) of 3.1 thermal ohms per foot. The only differences is that in duct bank no. *1*, with ten ducts, the cable insulation is suitable for conductor temperature of only 60 C, while in duct bank no. 2, with four ducts, the insulation is suitable for 85 C conductor temperature. To find the relative current-carrying capacities according to solution *B*, one presumably enters the appropriate Figs. 1–4 at 38.1 watts per foot, reads the ampere rating corresponding to the wire size (not fixed for this example), and applies the proper correction factors below the curves. This shows the current rating at 85 C to be 23% above that at 60 C. Using the IPCEA calculation method

Table III. Example Based on IPCEA

Symbols (see Appendix)	Duct Bank 1	Duct Bank 2
T_c*	60	85
T_a*	20	20
N	10	4
H	0.74	0.93
R_c†	3.1	3.1
R_d†	7.4	3.72
W‡	$\frac{60-20}{3.1+7.4}=3.81$	$\frac{85-20}{3.1+3.72}=9.53$
NW‡	38.1	38.1
R	r	$1.085r$
W_d	0	0
I	$(3.81\times 10^6/r)^{1/2}$	$(9.53\times 10^6/1.085r)^{1/2}$

from which $I_2/I_1=(9.53/1.085\times 3.81)^{1/2}=1.52$

* Degrees C.

† Thermal ohms per foot.

‡ Watts per foot.

trated in the Appendix of the paper, ever, the 85 C current is 52% above for 60 C as shown in Table III.

can thus be inferred that solution annot be applied directly in those cases re copper temperature differs from that med in Figs. 1–4. Perhaps some modi-ion is possible, short of expanding these es to cover all possible copper tempera-s.

he above example can be carried further lustate the neglect, by solution B in its ent form, of the requirement for equal ip ambient (idle duct) temperature be-en equivalent duct banks. Let T_d be the perature of the inner surfaces of the ts. Then

$$\frac{-T_d}{-T_a}=\frac{R_c}{R_d}$$

	Duct Bank 1	Duct Bank 2
	3.1*	3.1*
	7.4*	3.72*
	60 C	85 C
	20 C	20 C
	48.2C	55.5 C

ermal ohms per foot.

difference in T_d for the two cases should n indication of the difference in idle duct peratures.

ssuming additional curves, or some other hod of properly allowing for various ed" copper temperatures, there is still the stion as to whether solution B allows quately for mixing of rated copper tem-itures, cable loadings, cable sizes, or le constructions in the same duct bank. the results by solution B truly an ex-ion of the IPECA method? One answer his is that the IPCEA method cannot igorously extended to cover nonhomo-eous duct banks. This is due to the imption implicit in the IPCEA method t the inner surfaces of all ducts are at same temperature T_d, where

$$=T_a+WR_d \quad (1)$$

$$=T_a+(NW)H \quad (1A)$$

ile there may be an isothermal envelope arating the "inside" of the duct bank n the "outside," it seems clear for a ed duct bank that it neither includes inner duct surfaces nor is at tempera-T_d as defined by equation 1(A).

nother approach is to ask whether, for special cases of homogeneity, solution B es the same results as the corresponding CEA bases; the "weighted averaging" of ition B could be considered as having an erent possibility of error as great as that the extreme values between which it rages. Differences in wire size, and in le construction (affecting R_c), are perly allowed for. The treatment of tial loading is questionable, however. A form load reduction in a homogeneous t bank would, per IPCEA, cause a uction in T_d due only to the reduction in n equation 1(A). With the assumption ed by the authors under column 11, the ilting change in individual cable rating is portional to the change in

$$[_c-T_d)/R_c]^{1/2}$$

with T_d. In solution B, on the other hand, the rating is found by entering Figs. 1–4 at a reduced total duct loss, NW. But since these illustrations were derived from IPCEA tables for fully loaded cables, a reduced value of NW implies in general a reduced value of N and some increase in H, in equation 1(A). The implied temperature T_d is therefore different in solution B from that per the IPCEA method, for partially loaded cables. There is a resulting dis-crepancy in the "new" ratings obtained by each method.

Next consider the averaging basis itself, namely, the assumption of fully loaded homogeneous duct banks of such configura-tion (different from the actual) that the value NW is held constant. As demon-strated by the authors, this is a tenable basis. However, H is known for any particular duct bank, and the values NH and T_d are then easily obtainable from NW. One might prefer entering curves similar to Figs. 1–4, except plotted against T_d instead of NW; this would presumably be similar to solution C of the authors.

The discussion so far has been kept within the authors' stated acceptance of NELA duct-bank heating constants, which were derived for 3- and 4-inch conduits. Just how IPCEA allows for this, in listing ratings for cables as small as *14* Awg, it not clear. Perhaps the authors could clarify this point. If no allowance was made, then the ratings for these smaller wire sizes would be too high for the normal industrial practice, where conduit size is tailored to cable size. This is because the density of heat sources (cables) in the duct cross section is greater than assumed by the NELA constants. In such an event, the reduction in rating of small wire sizes from solution A to B should probably be carried further.

Going further afield, other areas for fur-ther refinement, aside from duct-bank con-figurations, soil resistivities, etc., could be:

1. Additional derating factors for cables in inside ducts.
2. Credit for improved heat-flow pattern in duct banks with metallic ducts over those with nonmetallic ducts.

It would be an interesting and possibly useful addition to this paper if quantitative results were presented giving the bases for the qualitative results listed under "homo-geneous duct banks."

Finally, it is recognized that the authors' treatment, as would any other imaginable treatment short of one requiring a com-puter for solution, must make some kind of simplifying assumptions, which, in them-selves, limit the accuracy theoretically attain-able. Thus, in Table I the effect of chang-ing the wire size of five cables is uniformly distributed as a credit among the other 15 cables, regardless of relative position in the duct bank. Similarly, no allowance is made for the heat-flow pattern in the earth, which would result for a homogeneous duct bank in the bottom center cable being the hottest. Considering these and other limitations to exact solution, any future solution which treats the problem more rigorously should be at least as simple to apply as the authors' solutions A or B.

R. D. Chamlee and **D. E. McCall**: Mr. Kelly utilized an example for homogeneous ducts to illustrate inconsistencies in the application of solution B. It was stipulated that duct bank *1* and duct bank *2* each dis-sipate 38.1 watts per foot. It should be noted that the 38.1 watts occur when the conductors are operating at rated tempera-ture. This is 60 C for duct bank *1* and 85 C for duct bank *2*. To find the relative current-carrying capacities according to solution B, you should not select current values on the basis of 38.1 watts per foot. Instead, you must use a watt-per-foot value that corresponds to the base temperature rating of the appropriate Figs. 1–4. This is 75 C for Figs. 1 and 2, 85 C for Fig. 3, and 81 C for Fig. 4.

We have revised the example outlined in the discussion. It now shows that the current ratings obtained by the two methods compare favorably. To obtain specific results, we limited the comparison to Fig. 1(A) and chose a wire size of *3/0* Awg.

In the IPCEA method of calculation, H is an empirical constant based on equally loaded cables of similar size, all located in outside ducts. In his discussion of T_d, Mr. Kelly assumes that H is known for any par-ticular duct bank. We do not feel that H can accurately be determined or estimated for mixed banks. Thus, T_d cannot easily be determined. The discussion of T_d illustrates that solution B does not give exact results.

As a matter of interest, we particularly like solution C from a theoretic basis. From

Table IV. Revised Example

Symbols	Calculation Basis: Duct Bank 1	Calculation Basis: Duct Bank 2	Solution B: Duct Bank 1	Solution B: Duct Bank 2
T_c	60	85	75*	75*
T_a	20	20	20	20
T_c-T_a	40	65	55	55
N	10	4	10	4
H	0.74	0.93	0.74	0.93
R_c	3.25	3.25	3.25	3.25
R_d	7.40	3.72	7.40	3.72
R_c+R_d	10.65	6.97	10.65	6.97
W	$\frac{40}{10.65}=3.76$	$\frac{65}{6.97}=9.33$	$\frac{55}{10.65}=5.16$	$\frac{55}{6.97}=7.89$
NW	37.6	37.3	51.6	31.6
R	228×10^{-6}	248×10^{-6}		
I	$\sqrt{\frac{3.76\times10^6}{228}}=128$	$\sqrt{\frac{9.33\times10^6}{248}}=194$	$145\times0.87=126$	$182\times1.07=195$

* Base.

a practical view, however, we were not able to arrive at an acceptable and simple method of solution. The difficulty centered around the determination of idle duct temperature. The approach used by the authors made use of the total duct bank losses. The solution required two sets of curves: one to arrive at specified cable size and current rating for determining idle duct temperature, and a second set of curves which gave current rating based on idle duct temperature.

We do not claim that any of the solutions, *A*, *B*, or *C*, give exact results. This was never the intent, due to the complexity of the problem and the inherent inaccuracies in quantitatively estimating the necessary data to arrive at an exact solution. The basic intent was to prepare a reasonably accurate solution that was easy to use and, therefore, would be used. Some of the possible refinements mentioned in the paper and discussions are themselves subjects of controversy and are difficult to apply on a general basis. With the solution outlined in the paper, a particular user may modify or refine the solution so as best to fit his needs.

Rapid Determination of Approximate Closed-Loop Poles of Feedback Control Systems

S. K. BASU
NONMEMBER AIEE

Synopsis: In a control system, the transient response can be determined accurately only when the closed-loop poles of the system are known. The determination of the closed-loop poles involves in general a solution of a high-degree equation, which is difficult when the degree of the equation exceeds two. While mathematicians have attempted to solve such equations analytically, the control engineers have preferred approximate graphical solutions. The present paper suggests an extension of an already existing graphical method. The technique followed requires an asymptotic gain-frequency plot of the given open-loop transfer function. The plot is divided into three regions, viz., the high-gain region, the low-gain region, and the region near the crossover frequency. The closed-loop real poles are determined for high-gain and low-gain regions from known relationships of closed-loop and open-loop functions. From the knowledge derived therefrom, the complex-conjugate roots (along with real roots, if any) are determined for the crossover frequency region.

THE KNOWLEDGE of the transient response forms a very important part in the study of the performance of a feedback control system. The transient response can be approximately determined from a knowledge of the frequency response of the given open-loop transfer function. Though several methods of correlating the two exist, hardly any give reliable results. The Laplace transformation, on the other hand, is a correct analytical method of determining transient response from known system transfer functions, provided the locations of their closed-loop poles are known. Unfortunately, the determination of the closed-loop poles is rather difficult because it involves solution of a polynomial characteristic equation of the form $1+G(S)=0$, where $G(S)$ is the given open-loop transfer function of the complex frequency S. In general $G(S)$ is a third to fifth order polynomial in S. It is also known that, while straightforward solutions exist for quadratic equations, no such direct equations are available for higher degree equations. Special methods are therefore necessary for solving them.

Many workers have found solutions of such high-degree polynomials by numerical methods, e.g., Graeffe[1] and Lin.[2,3] By nature such methods are laborious, and satisfactorily accurate only when sufficient rigor is imposed. The control engineers, on the other hand, prefer approximate but quick graphical methods for the solution of such equations.

Evans[4] was one of the workers who had attempted to find the closed-loop poles graphically. His "root locus" method was published in 1947 and since then it has opened to later workers an approach full of possibilities. While giving due credit to Evans for his novel approach, it must be admitted that plotting a root locus is not an easy job. Because of this, many have since worked either on the simplification of his method or in finding other parallel methods, notably the following: Kusters and Moore,[5] Russel and Weaver[6] (an extension of the method developed by Profos[7]), Chu,[8] Yeh,[9] Biernson,[10] and Chen.[11]

The present paper follows closely the methods adopted by Biernson[10] and Chen[11] as regards the determination of the closed-loop real poles, and aims at further simplification and rapidity in obtaining the closed-loop complex poles of a feedback control system.

Rough Approximation of Closed-Loop Pole Locations

Fig. 1 represents a typical feedback control system, where $G(S)$ is the open-loop transfer function, R the reference input, C the response, and E the error R-C. Thus, the open-loop transfer function

$$\frac{C}{E}=G(S) \tag{1}$$

the closed-loop system function

$$\frac{C}{R}=\frac{G(S)}{1+G(S)} \tag{2}$$

and the error transfer function

$$\frac{E}{R}=\frac{1}{1+G(S)} \tag{3}$$

In general $G(S)$ may be represented as, say,

$$G(S)=\frac{K(S+a_1)(S+a_2)}{S(S+b_1)(S+b_2)(S+b_3)(S+b_4)} \tag{4}$$

where $b_4>b_3>a_2>a_1>b_2>b_1$, K is the gain factor, a_1 and a_2 are the open-loop zero locations, and b_1, b_2, b_3 and b_4 the open-loop pole locations, together with a pole at the origin ($S=0$). The asymptotic gain-frequency plot of $G(S)$ is next obtained easily[12] and is represented in Fig. 2. It is clear from this plot that at a certain frequency ω_c, known as the cross-

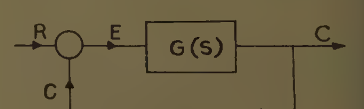

Fig. 1. Symbolic representation of feedback control system

Paper 60-105, recommended by the AIEE Feedback Control Systems Committee and approved by the AIEE Technical Operations Department for presentation at the AIEE Winter General Meeting, New York, N. Y., January 31–February 5, 1960. Manuscript submitted June 3, 1959; made available for printing December 23, 1959.

S. K. BASU is with the University College of Technology, Calcutta, India.

Thanks are expressed to Prof. A. K. Sen Gupta, D.Sc., and Dr. A. K. Choudhury, both of Calcutta University, for their encouragement and suggestions in the preparation of this paper.

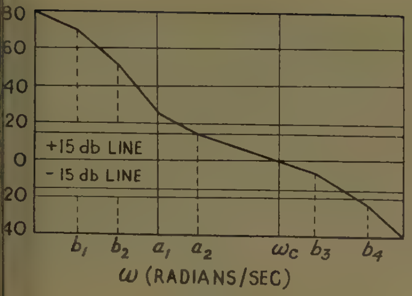

2. Asymptotic gain-frequency plot of equation 4

r frequency, the gain becomes 0 db cibels), i.e., $|G(S)|=1$; on one side of the gain increases with diminishing quency and on the other side the gain reases with increasing frequency. badly, the whole plot can be divided three regions:

High-frequency low-gain region.
Low-frequency high-gain region.
Crossover frequency region.

Though there are no sharp lines of marcation between these regions, the 5-db lines have been arbitrarily chosen Chen[11] for approximate studies, inly because these lines can be conered as sufficiently away from the ssover frequency ω_1.

Now, for the low-gain region (i.e., be- -15 db), $G(S)<<1$; therefore

$$\frac{G(S)}{1+G(S)}\cong G(S)=\frac{C}{E}$$

, the open-loop transfer function. The sed-loop poles therefore correspond to open-loop poles, i.e., poles of $G(S)$ of s region ($S=-b_4$).

For the high-gain region (i.e., above 5 db), $G(S)>>1$; therefore

$$\frac{1}{1+G(S)}\cong\frac{1}{G(S)}=\frac{1}{C/E}$$

, the reciprocal of the open-loop nsfer function. The closed-loop poles refore correspond to the open-loop os, i.e., zeros of $G(S)$ of this region, $=-a_1$). Since the other zero at $S=$ $_2$ lies very near to the +15-db line, can also be approximately considered another closed-loop pole. It is to be ed here that the poles of E/R are sidered in this treatment instead of se of C/R. In practice, since the poles E/R and those of C/R are identical, h a treatment should be valid.

Considering the region of $G(S)$ within $\pm$15-db lines, the existence of a sed-loop pole can be expected near crossover frequency. In fact, the minant closed-loop complex poles of the system function which are responsible for the quality of the transient response are located near ω_c. Determination of the closed-loop poles in this region is therefore of prime importance, though simple approximate relationships like the other two regions are not available here. However, a knowledge of the locations of closed-loop poles determined in the other two regions can help in reducing the order of the characteristic equation $1+G(S)=0$. For example if $G(S)$ of equation 4 is taken, it may be seen at once from Fig. 2 that $S=-a_1$, $S=-a_2$, and $S=-b_4$ are the locations of the approximate closed-loop poles and, further, that for the frequency region considered (the $\pm$15-db region) $b_1<b_2<a_1<<|S|<<b_4$. The new reduced form of $G(S)$ is then

$$G(S)\cong\frac{KS(S+a_2)}{SSS(S+b_3)b_4}=\frac{K(S+a_2)}{b_4S^2(S+b_3)} \tag{5}$$

The closed-loop system function is therefore

$$\frac{C}{R}=\frac{G(S)}{1+G(S)}=\frac{K(S+a_2)}{K(S+a_2)+S^2(S+b_3)b_4} \tag{6}$$

and the characteristic equation

$$1+G(S)=S^2(S+b_3)b_4+(S+a_2)K=0 \tag{7}$$

Evidently it is a third-degree equation, whereas the original polynomial was of fifth order. The solution of this third-degree equation is not really difficult when one considers that the approximate value of its only real root has already been located (at $S=-a_2$). If equation 7 is now divided by the known real root factor $(S+a_2)$, the resulting equation is a quadratic and hence the conjugate complex roots are immediately obtained.

Shift of Approximate Pole Locations From Actual Closed-Loop Poles

The closed-loop poles so far determined are only approximate because the open-loop poles coincide with the closed-loop poles only at zero gain, and the open-loop zeros coincide with the closed-loop poles only at infinitely high gain. Since in practice these two extreme limits of gain are not involved, the actual closed-loop poles must be situated in slightly different locations.

Direction of Shifts

The direction of shifts of the approximate real poles can easily be determined if a simple application of the root locus method[1] is considered.

It is known that a closed-loop root is determined by a point defined by $1+G(S)=0$, so that $|G(S)|=1$ and $\angle G(S)=$ 180 degrees$+n$ 360 degrees, where n is any integer including zero. If, now, the pole-zero configuration of $G(S)$ in equation 4 is represented in Fig. 3, it may be seen from the consideration of $\angle G(S)$ that there are no possibilities of the existence of real poles to the left of a_1 or to the right of a_2 and b_4. The approximate closed-loop pole located at a_1 must therefore move to the right and the poles at a_2 and b_4 to the left, in order to reach the actual closed-loop real pole locations.

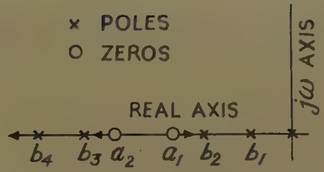

Fig. 3. Pole-zero configuration of G(S) of equation 4 on S-plane

Magnitude of Shifts

The magnitude of shifts, as has been determined by Biernson,[10] applying a numerical reiteration process, is reasonably accurate. If the magnitudes of shifts at $S=-a_1$, $S=-a_2$, and $S=-b_4$ are denoted respectively by δa_1, δa_2, and δb_4, then

$$\delta a_1=\left[(S+a_1)\frac{1}{G(S)}\right]_{S=-a_1} \tag{8}$$

If δa_1 indicates a large percentage shift, a second approximation is applied where

$$\delta a_1'=\left[(S+a_1)\frac{1}{G(S)}\right]_{S=-a_1\pm\delta a_1} \tag{8A}$$

The correct sign of $\pm\delta a_1$ in equation 8(A) obviously depends on the direction of shift of a_1, as determined in the foregoing section.

If, still, $\delta a_1'$ shows a large percentage shift, a third approximation or, as necessary, more successive approximations may be made until the difference between two consecutive shifts as δa_1 and $\delta a_1'$, or $\delta a_1'$ and $\delta a_1''$, etc., almost vanish. At this stage the value of δa_1 obtained is reasonably correct.

Similarly,

$$\delta a_2=\left[(S+a_2)\frac{1}{G(S)}\right]_{S=-a_2}$$

$$\delta b_4=[(S+b_4)G(S)]_{S=-b_4}$$

In like manner, the magnitude of shifts δa_2 and δb_4 can be determined with increasing accuracy from successive approximations.

The accurate locations of the closed-loop real poles have now been obtained at $S=-a_1+\delta a_1$, $S=-a_2-\delta a_2$, and $S=-b_4-\delta b_4$; see Fig. 3.

Shift of Closed-Loop Complex Poles

It is not possible to determine the magnitude and direction of shifts of closed-loop complex poles in the same manner as those for real poles. However, once the approximate locations of the complex conjugate poles have been obtained, and equation 7 and a known real root factor $S+a_2$ applied, the generalized frequency response plot[5,10] can be conveniently applied for a restricted region of the S-plane where the closed loop complex poles have been located. This very restricted plot would greatly save the labor involved in Biernson's method[10] of plotting an extensive region in the S-plane. A complex pole in the S-plane can be defined in terms of $|S|$ and ζ, the damping ratio of the pole; see Fig. 4(A). $G(S)$ is calculated for a few values of $|S|$ corresponding to a few values of ζ and the gain (db) and phase angle of $G(S)$ are plotted against $|S|$ for several values of ζ. Then a point on the constant ζ curve which corresponds to $G(S)=0$ db (magnitude 1) and $\angle G(S)=180$ degrees$+n$ 360 degrees represents accurately the location of a closed-loop complex pole; see Fig. 4(B). The other complex pole is its conjugate.

Example

An example is taken from Biernson[10] and Chen.[11] Here

$$G(S)=\frac{500\left(\frac{S}{0.2}+1\right)(S+1)}{S\left(\frac{S}{0.04}+1\right)^2\left(\frac{S}{16}+1\right)^2} \quad (9)$$

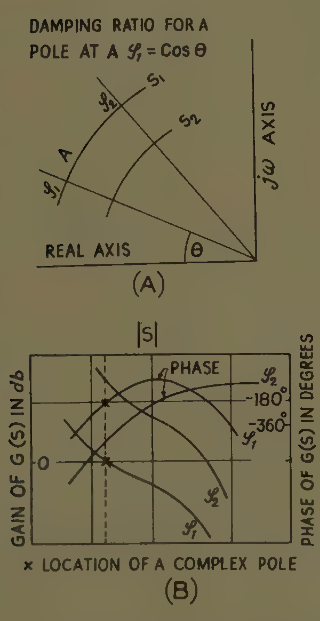

Fig. 4. A—Location of complex poles in S-plane. B—Generalized frequency response plot

The asymptotic gain-frequency plot of equation 9 is given in Fig. 5. The plot is divided into three gain regions as suggested. In the high-gain (above $+15$ db) region a closed loop pole is located at $S=-0.2$ and another is located approximately at $S=-1$ (because it is almost on the $+15$-db border line). No closed-loop poles can be immediately located for the low-gain (below -15 db) region. However, the open-loop double-order pole at $S=-16$ may be considered to be made up of two single-order poles located at $S=-16\ K$ and $S=-16/K$, where the constant K, though arbitrary, should not be greater than 2.[11] The value of $K(=1.4)$ was so chosen that the higher frequency open-loop pole at $S=-16\ K=-16\times1.4=-22.4$ may be located in the low-gain region, resulting in a probable location for a closed-loop pole. The other pole is then located at $S=-16/1.4=-11.4$ and is well within the ±15-db region. Thus

$$\left(\frac{S}{16}+1\right)^2=\frac{1}{16^2}(S+16)^2\approx$$

$$\frac{1}{16^2}(S+11.4)(S+22.4) \quad (10)$$

and a closed-loop pole is located approximately at $S=-22.4$. The approximate locations of the closed-loop real poles are therefore at $S=-0.2$, $S=-1$ and $S=-22.4$.

A pole-zero configuration of $G(S)$ of equation 9 interpreted in the manner of Fig. 3 indicates that the shift of the approximate pole at $S=-0.2$ is in a decreasing direction and the shifts for poles at $S=-1$ and $S=-22.4$ in an increasing direction.

The magnitude of shifts is:

At $S=-0.2$, $\delta_{-0.2}=+0.0016$.

At $S=-1.0$, $\delta_{-1.0}=-0.25$.

Considering this to be a large percentage shift, successive approximations are applied in a way already discussed. The magnitudes of shifts are obtained as

$$\delta_{-1.0}'=-0.37,\ \delta_{-1.0}''=-0.45,\ \delta_{-1.0}'''=-0.47$$

Because the shifts are rapidly converging $\delta_{-1.0}'''=-0.47$ may be considered as sufficiently accurate.

At $S=-22.4$, $\delta_{-22.4}=-4.0$, and in the next successive approximations $\delta_{-22.4}'=-2.5$, $\delta_{-22.4}''=-2.9$. The shift $\delta_{-22.4}''=-2.9$ may be considered as sufficiently accurate.

The accurate closed-loop real poles can now be said to be located at

$S=-0.2+0.0016=-0.198$

$S=-1.0-0.47=-1.47$

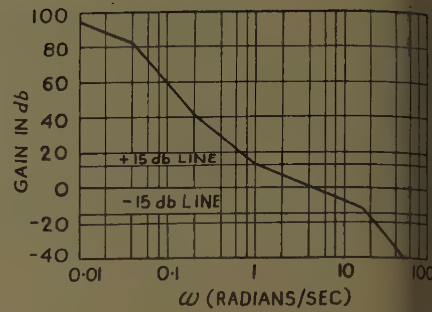

Fig. 5. Asymptotic gain-frequency plot of equation 9

$S=-22.4-2.9=-25.3$

The approximate closed-loop complex poles will now be discussed. Rewriting equation 9 yields

$$G(S)=\frac{4\times256(S+0.2)(S+1)}{S(S+0.04)^2(S+16)^2}$$

$$\approx\frac{4\times256(S+0.2)(S+1)}{S(S+0.04)^2(S+11.4)(S+22.4)} \quad (11)$$

Again, in the frequency region now being considered (the ±15-db region), $0.04<<0.2<<|S|<<22.4$, and equation 11 reduces to

$$G(S)\approx\frac{4\times256S(S+1)}{SS^2(S+11.4)\times22.4}=\frac{45.6(S+1)}{S^2(S+11.4)} \quad (12)$$

Therefore, the characteristic equation follows:

$$1+G(S)=S^2(S+11.4)+45.6(S+1)=0 \quad (13)$$

If $S=-1.47$ is considered to be the only real root of this third degree equation, then dividing equation 13 by $(S+1.47)$ yields quadratic

$$S^2+2S(4.97)+31=0 \quad (14)$$

So that $S=-4.97\pm j2.53$, showing the location of the closed-loop complex poles.

Also

$S=\sqrt{31}=5.57$

$\zeta=\frac{4.97}{5.57}=0.89$

The locations of closed-loop complex poles as defined by equation 14 are only approximate, and to obtain the accurate values a generalized frequency response plot is drawn for $|S|=5$, 6, and 7, and for $\zeta=0.7$, 0.8 and 0.9.

Fig. 6 shows the plot for $G(S)$ of equation 9 for the aforesaid values of $|S|$ and ζ. A careful study of Fig. 6 reveals that only for values of $\zeta=0.73$ and $|S|=5.65$ the required gain and phase conditions are satisfied. The corresponding complex pole locations are $S=-4.12\pm j\,3.86$.

The final results are:

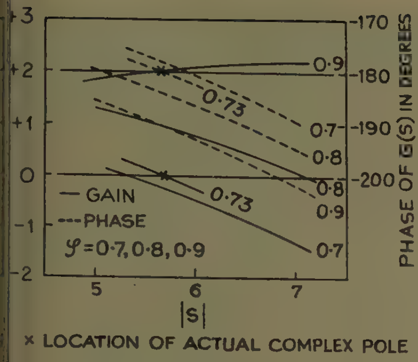

. 6. Generalized frequency response plot of G(S) of equation 9

cation of closed loop real poles at $S=$).198, $S=-1.47$, and $S=-25.3$.

cation of closed loop complex conjugate es at $S=-4.12+j3.86$ and $S=-4.12-$ .86.

e results compare well with those deter- ned by Biernson[10] and Chen.[11]

nclusions

The methods suggested in this paper tempt further simplification over those esented by Biernson[10] and Chen[11] in e determination of closed-loop poles near e region of crossover frequency. For e sake of comparison it may be stated at Biernson used an extended general- d frequency response plot in place of a alized one as presented here, because e approximate closed-loop complex pole ations were not readily available by s method. On the other hand, Chen ed the charts due to Yeh[9] in the final ages of analysis to determine the closed-loop complex poles. The methods of Biernson and Chen thus require templates or extensive charts. Considering these facts, the approach presented here seems less laborious, though sacrificing a little in accuracy.

Regarding the determination of closed-loop poles in the high-gain and low-gain regions, along with the determination of magnitudes of shifts of the approximate closed-loop poles, the method of Biernson has been followed. Whereas, in determining the direction of shifts, a more general viewpoint using the S-plane plot of the pole-zero configuration of the open-loop transfer function $G(S)$ has been employed.

It is known that the transient behavior of a control system is generally guided by the location of its closed-loop poles near the crossover frequency region. The number of such closed-loop poles lies generally between two and three in this region for all stable control systems. Thus either a pair of complex conjugate poles, or a real pole together with the pair of complex conjugate poles, will in general be obtained in this region. This striking phenomenon, that not more than three closed-loop poles would normally exist in the crossover frequency region of a stable control system, makes the determination of the closed-loop poles easy by the approximate method presented in this paper. It is to be noted further that the low-frequency closed-loop poles have an effect on the settling time and also add long tails to the transient response, whereas the high-frequency closed-loop poles do not. It is apparent therefore that while the low-frequency poles should be determined accurately, a rough determination of the high-frequency poles is sufficient.

References

1. MATHEMATICS OF MODERN ENGINEERING (book), R. E. Doherty, E. G. Keller. John Wiley & Sons, Inc., New York, N. Y., vol. I, 1936, pp. 98–128.

2. A METHOD OF SUCCESSIVE APPROXIMATIONS OF EVALUATING THE REAL AND COMPLEX POLES OF CUBIC AND HIGHER ORDER POLYNOMIALS, S. N. Lin. *Journal of Mathematics and Physics*, Cambridge, Mass., vol. 20, Aug. 1941, pp. 231–42.

3. A METHOD OF FINDING ROOTS OF ALGEBRAIC EQUATIONS. *Ibid.*, vol. 22, June 1943, pp. 60–77.

4. CONTROL SYSTEM SYNTHESIS BY ROOT LOCUS METHOD, Walter R. Evans. *AIEE Transactions*, vol. 69, pt. I, 1950, pp. 66–69.

5. GENERALIZATION OF THE FREQUENCY RESPONSE METHOD FOR THE STUDY OF FEEDBACK CONTROL SYSTEMS, N. L. Kusters, W. F. Moore. *Proceedings*, Conference on Automatic Control, Butterworths Scientific Publications, London, England, 1952.

6. SYNTHESIS OF CLOSED LOOP SYSTEMS USING CURVILINEAR SQUARES TO PREDICT ROOT LOCATION, D. W. Russel, C. H. Weaver. *AIEE Transactions*, pt. II (*Applications and Industry*), vol. 71, Jan. 1952, pp. 95–104.

7. A NEW METHOD FOR THE TREATMENT OF REGULATION PROBLEMS, P. Profos. *Sulzer Technical Review*, New York, N. Y., vol. 2, 1945, pp. 1–5.

8. SYNTHESIS OF FEEDBACK CONTROL SYSTEMS BY PHASE ANGLE LOCI, Yaohan Chu. *AIEE Transactions*, pt. II, vol. 71, Nov. 1952, pp. 330–39.

9. SYNTHESIS OF FEEDBACK CONTROL SYSTEMS BY GAIN-CONTOUR AND ROOT-CONTOUR METHODS, Victor C. M. Yeh. *Ibid.*, vol. 75, May 1956, pp. 85–96.

10. QUICK METHODS FOR EVALUATING THE CLOSED LOOP POLES OF FEEDBACK CONTROL SYSTEMS, George Biernson. *Ibid.*, vol. 72, May 1953, pp. 53–70.

11. A QUICK METHOD FOR ESTIMATING CLOSED-LOOP POLES OF CONTROL SYSTEMS, Kan Chen. *Ibid.*, vol. 76, May 1957, pp. 80–87.

12. SERVOMECHANISMS AND REGULATING SYSTEMS DESIGN, Vol. I (book), H. Chestnut, R. W. Mayer. John Wiley & Sons, Inc., New York, N. Y., 1951.

The Selection of Electric Winder Drives for the Paper Industry

M. H. FISHER
MEMBER AIEE

ELECTRIC winder drives are used universally throughout the paper in- stry, and electric backstand brakes e being used in increasing numbers as ese winder drives are required to service e new wider and faster-speed paper- aking machines. D-c adjustable volt- e winder drives are used on all modern gh-speed winders. Although some all, slow-speed winders utilize a-c ives, this paper will concern itself with d-c drives having either mechanical or electric backstand brakes.

The paper mill winder must be fast enough to keep ahead of the paper-making machine which it serves. To do this, the winder must operate at two to three times the maximum speed of the paper machine. Difficulty in keeping up with the paper machine production increases with paper machine speed and the number of shipping rolls desired from each machine roll. Paper machines designed to operate at 2,000 and 2,500 fpm (feet per minute) are followed by winders able to operate at 5,000 to 6,000 fpm. Of course, as the speed and width of the winder and the tension in the sheet between the unwind stand and the winder increases, the hp (horsepower) required to drive the winder increases, and the drive performance requirements are more stringent.

With few exceptions, paper winders are of the 2-drum surface type with the shipping rolls being wound on top and between

Paper 60-106, recommended by the AIEE General Industry Applications Committee and approved by the AIEE Technical Operations Department for presentation at the AIEE Winter General Meeting, New York, N. Y., January 31–February 5, 1960. Manuscript submitted March 21, 1956; made available for printing January 7, 1960.

M. H. FISHER is with the Westinghouse Electric Corporation, East Pittsburgh, Pa.

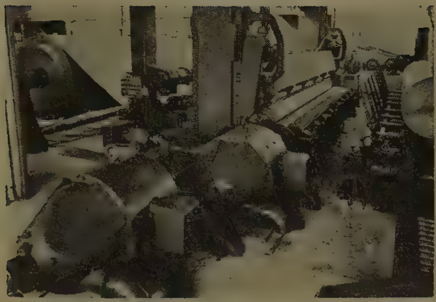

Fig. 1. Direct-connected 2-motor winder drive for 226-inch-wide 4,000-fpm, kraft paper winder with mechanical brake

the two drums. The drums may be driven by individual motors or a single motor direct-connected to one drum, and geared or belted to the other drum. The belting may be of the fixed or adjustable ratio type. The winder builder and/or the user decide whether a single-motor drive or a 2-motor drive is the better suited for a given application. The electrical manufacturer can build either type with equal success. A 2-motor winder drive is shown in Fig. 1.

Experience has shown that if two motors are used the load on the motors is not generally divided equally; thus the sum of the hp ratings must be about 1.25 times the rating of a single motor, as shown in Table I. The additional cost of two motors and excess hp is offset by a saving in mechanical parts. When two motors are used, ammeters in the motor armature circuits indicate load, and a shunt field rheostat in series with one motor field allows the load to be proportioned between the motors as directed by the operator.

Table I. Rotating Equipment Ratings Winders with Mechanical Brakes

Single-Motor, Hp	Two-Motor, Hp*	Power Supply Generator, Kw†	Packaged Drive Rating, Hp*
15	2-10	15	15
20	2-15	20	20
25	2-15	25	25
30	2-20	30	30
40	2-25	40	40
50	2-30	40	50
60	2-40	50	60
75	2-50	60	75
100	2-60	75	100
125	2-75	100	125
150	2-100	125	150
200	2-125	150	200
250	2-150	200	
300	2-200	250	
350	2-250	300	
400	2-250	300	

* Four-motor winders require 4 motors each rated the same as the 2-motor winders.

† Do not change rating when slitters and/or rider roll are motor driven.

Winder Control Features, Automatic Accelerating and Decelerating Methods

Speed control of the winder can be achieved by operation with a single-rheostat handle; see Fig. 2. Zones of OFF, THREAD SPEED, and RUN are provided. The thread speed zone provides a constant operating speed of 50 to 100 fpm for the operator to check the straightness of the paper, the operation of the slitters, and the trim disposal system, before accelerating to high speed. Turning the rheostat into the run zone initiates operation at any speed selected by the operator. Conversely, returning the rheostat to the off position initiates a stopping action under controlled regenerative braking conditions. Smooth transitions from thread speed to acceleration and from acceleration to run speed are necessary for successful operation. Acceleration or deceleration at a slower rate than that dictated by the automatic control can be achieved by turning the speed control rheostat at a slow rate. Speed control of a winder is the same either with or without an electric brake.

The use of automatic accelerating and decelerating means provides the highest performance from the electric equipment automatically, without depending on the operator's judgment of the drive capacity. With automatic control the operators can give their full attention to other winder requirements, thus increasing production as well as improving its quality. Limitations to the maximum rate of acceleration are:

1. Commutating ability of the rotating machines.
2. Strength of the paper sheet (maximum ability to transmit energy to the backstand).
3. Ability to hold constant tension during acceleration.

Electric winder drives are accelerated automatically on a time-limit or a current-limit basis. Time limit may be provided by the use of a motor-operated rheostat with buttons arranged to provide constant change of speed per degree of travel. When the motor-operated rheostat is used, generator excitation is obtained from the constant potential exciter bus. Owing to the necessity for excessive maintenance, motor-operated rheostats have not adequately met winder drive requirements.

Time-limit acceleration can also be provided in high-gain regulator circuits by the use of electrical time delay schemes such as capacitor discharge circuits. The regulator used in these circuits supplies the generator excitation. The use of a regulator of this type allows provision for a constant threading speed, as well as time-limit acceleration, and it reduces the complexity of the problem of holding constant tension during the acceleration and deceleration periods.

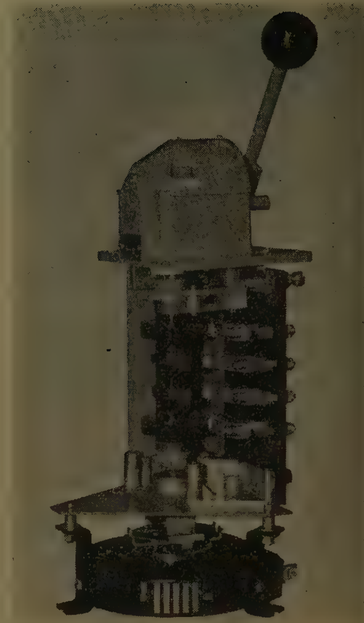

Fig. 2. Winder speed control rheostat. Note lever operation and rugged construction including cams used in setting up circuits for thread and run operations

For most large winder drives, the current-limit accelerating method is most desirable, since a minimum accelerating time within the capability of the drive is utilized. To provide current-limit acceleration and deceleration, a regulator is provided to excite the generator. Threading speed is regulated as well as constant current acceleration and deceleration. Fig. 3 shows the performance of a large winder drive during current-limit acceleration and deceleration. Calculations to establish the minimum accelerating time are developed later in this article.

Mechanical Features of Winder Drives

Rotating equipment located at the winder should be protected from entry of falling dirt and paper fibers. Experience indicates that the minimum successful enclosure is the National Electrical Manufacturers Association dripproof protected enclosure. Application of 60-degree-centigrade rise in open motors with covers added is usually acceptable.

Of course, forced ventilation for the rotating equipment located at the winder is best, since air taken from outside

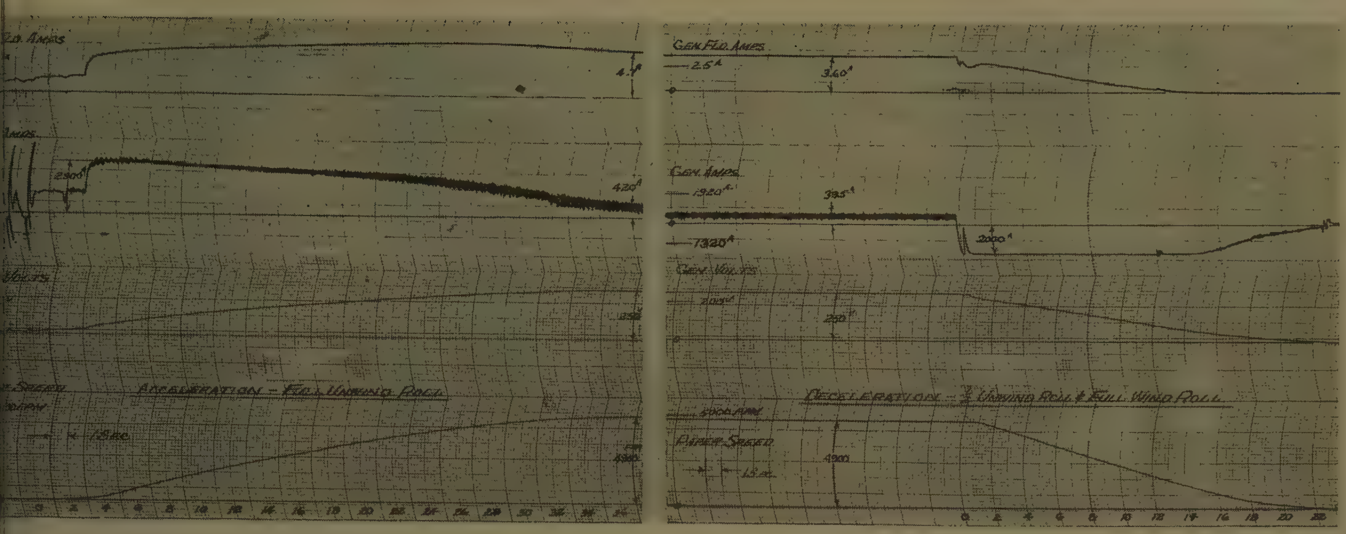

ig. 3. Current limit acceleration and deceleration performance tests from 240-inch-wide 5,000-fpm heavy kraft paper winder with electric braking generator

nill is clean. Also, full ventilation is ined at all times regardless of whether ot the drive motors are operating. iction of the continuous rating may ossible with forced ventilation, since cooling is available during the entire cycle.

times, when two motors are used to the winder drums, space considera- is necessary in selecting the motors, use of the diameter of the drums. arrangements are shown in Fig. 4. direct-connected arrangement is pre- d when paper speed and drum eter make this arrangement feasible. omics and available space usually te the arrangement.

e use of ball-bearing motors mini- s the losses of rotating equipment, icularly at breakaway. On the larger of equipment there is an economic cost consideration in favor of sleeve ings that cannot be overlooked.

perators' desks are ordinarily pre- d to wall or pedestal-mounted opera- stations. When mechanical back-

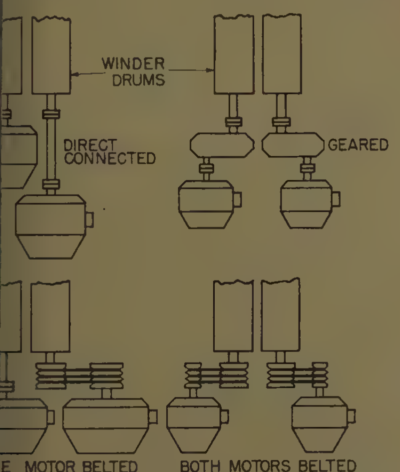

4. Motor arrangements for 2-motor winder drives

stand brakes are used, the electric and pneumatic controls can be mounted on the same desk, as shown in Fig. 5. A barrier between the two controls prevents damage to the electric controls, should a pneumatic or hydraulic control line break.

Nomenclature

C = cost of electric power, dollars per kw-hour
D = diameter, inches
E = electromotive force (volts)
eff = efficiency of backstand
ft-lb/hp = foot-pounds per horsepower
hp = sheet horsepower
IC = inertia compensation
IR = voltage drop
K = paper machine availability factor
L = length, feet
s = fpm top sheet speed
S = paper-machine speed, fpm, corresponding to average weight of manufactured paper
SE = stored energy of backstand, hp-sec (hp-seconds)
t = accelerating time in sec
T = tension, lb/inch sheet width corresponding to average weight of paper manufactured
W = width, inches

Selecting Winder Drive Ratings

As previously mentioned, ratings of the winder drive are selected chiefly on the winder width, the maximum operating speed, and the maximum sheet tension requirements of the winder. Desired rate of acceleration and deceleration as well as the type of braking (mechanical or electrical) used on the backstand must also be considered. Fig. 6 shows the power requirements of the winder motors and braking generators as determined by a study of new winders. These curves include friction and windage losses of the winder as well as the electric losses of the braking generator.

The winding tension utilized by individual mills varies. Data taken in numerous mills indicate that the tension values shown in Fig. 7 meet the requirements of most mills. The values are for sheet tension at the winding rolls, and the tension at the backstand may be less, depending on stationary surfaces, spreaders, or spiked rolls.

If the desired tension in the sheet and the width and speed of the winder are known, the hp rating of the components of the drive may be calculated by use of the curves of Fig. 6. The following relation gives the hp required to hold the desired tension in the sheet with no consideration for the efficiency of any part of the winder or the drive, and this relation may be used as a check:

$$\text{hp in sheet} = \frac{\text{TWs}}{33{,}000 \text{ ft-lb/hp}}$$

If a mechanical braking system is used on the unwind stamd, the generator size

Fig. 5. Operator's control desk for 2-motor winder drive with mechanical braking. Pneumatic controls are combined in desk with electric controls. Barrier inside of desk protects electric control should pneumatic control line break

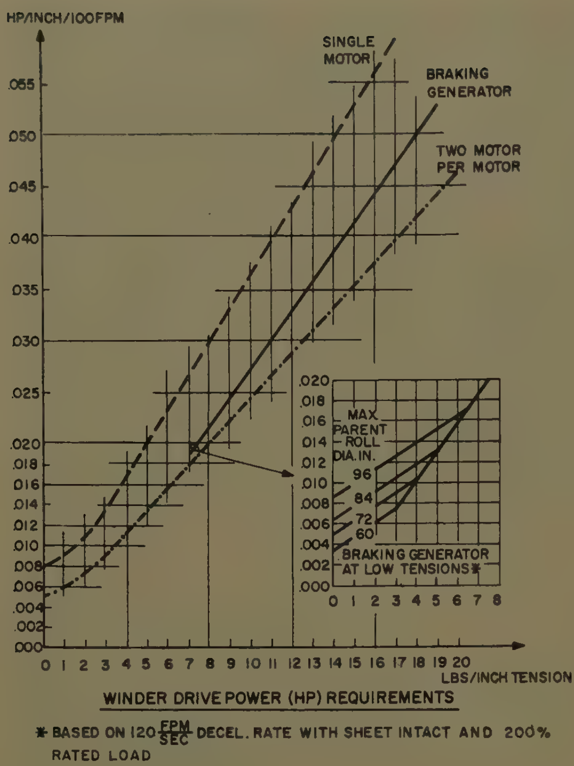

Fig. 6 (left). Power requirements of winder motors and braking generators. Departure from linearity at lower end is result of friction and inertia losses

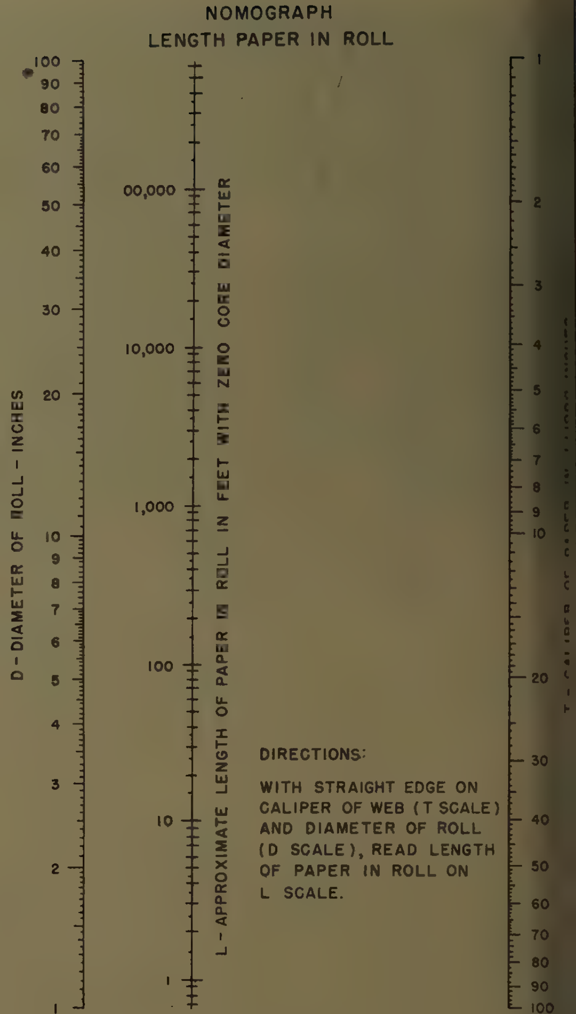

Fig. 8 (right). Nomograph for determining length of paper in roll

must be selected to be compatible with the motor size. For example, if the drum drive motor is rated 350 hp, a 300-kw generator should be used; see Table I.

The motor and the generator rating having been selected without regard to acceleration requirements, the time required for acceleration should be checked by calculating the stored energy in the entire system (horsepower-seconds is a handy unit to use). The hp rating and overload capacity of the motor is known, but this value must be reduced by the efficiency of the winder and the hp required to hold tension in the sheet. The two extremes are considered here: 1. acceleration with full tension set on the mechanical brake, and 2. acceleration with the mechanical brake released. Examples to illustrate follow.

Consider a 240-inch-wide, 5,000-fpm winder for kraft paper of weights up to 43 lb/1,000 sq ft (square feet) with an 84-inch-diameter machine roll.

The WK^2 of each steel and paper roll is first obtained from the machinery manufacturer or determined by calculation. Then, the following equation is used to calculate the SE:

$$\text{SE, hp-sec} = \frac{WK^2\,(\text{change in rpm})^2}{3.23\times10^6}$$

SE at 5,000 fpm, with a full roll on the unwind stand and an empty core on the winder:

	Hp-Sec
Unwind roll of 84-in. diameter	3,710
Wind drums of 18.5-in. diameter	2,280
Idler roll	263
Sleeve shaft	605
Drive motor	352
Total	7,210

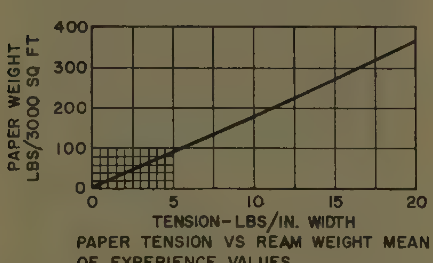

Fig. 7. Relation of paper weight and winding tension. Practical experience curves

From Fig. 7, 43-lb board will require 8.5 lb tension/inch width. From Fig. 6, 0.031 hp/in./100 fpm is required, which indicates that the drive motor will be required to deliver 372 hp for tension and friction requirements. Assume that the winder duty cycle allows the use of a 350-hp motor good for 225% load on acceleration, and suppose that the operator does not reduce his tension-setting during acceleration:

	Hp
Total hp available acceleration 2.25×350	790
Needed for friction and tension (no IC provided)	372
Maximum hp available for acceleration	418

Time for acceleration:

$$\frac{7{,}210\text{ hp-sec}\times2}{418\text{ hp}}=34\text{ sec}$$

Beyond the tension of 8.5 lb/inch width exerted by the brake, additional tension is necessary to accelerate the payout reel to 5,000 fpm linear speed in 34 sec. This additional tension may be calculated as follows:

$$T=\frac{\text{hp}\times33{,}000\text{ ft-lb/hp}}{W\times s}$$

$$\text{hp}=\frac{SE_{bs}\times2}{t\times\text{eff}}$$

Combining these yields

$$T=\frac{SE_{bs}\times2\times33{,}000}{Wst\times\text{eff}}$$

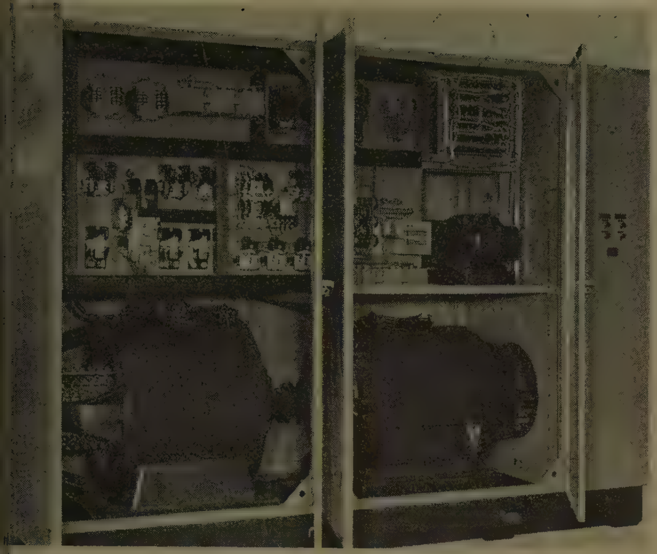

Fig. 9. Package drive with 200-hp power supply and booster for slitters. Panels from left to right: Upper—Static exciter, a-c breaker, and reference. Lower—Magnetic control panel and magnetic amplifier for generator control

Fig. 11. Single 350-hp motor drum drive and 250-hp electric braking generator for large kraft paper winder capable of exerting 8.5-lb/inch width tension on a 240-inch-wide sheet at 5,000 fpm

n

$$\frac{3,710\times2\times33,000}{240\times5,000\times34\times0.95}$$

6.3 lb/inch width

The 8.5-lb/inch width exerted by the kstand brake plus 6.3-lb/inch width sion required to accelerate the back-nd and reel of paper, results in a net sion of 14.8-lb/inch width in the sheet ing acceleration.

Now, take the other extreme and ume that paper tension is held at the ired final value during the accelerating l decelerating periods. This recalibra-n of the braking effort during the rate of change-of-speed period is called ertia compensation" (IC). The mini-m accelerating with a mechanical ke on the backstand and with a stant tension of 8.5-lb/inch width in sheet may be calculated as follows is consideration would not apply when electric brake is used since it can be caused to act as a motor and supply accelerating power): Assume $eff_{bs}=0.95$. Then

$$t=\frac{SE_{bs}\times2\times33,000}{TWs\times eff_{bs}}$$

$$t=\frac{3,710\times2\times33,000}{8.5\times240\times5,000\times0.95}=25.3\text{ sec}$$

The drum roll drive motor rating required to get 25.3 sec, considering 90% efficiency of the entire winder is

$$hp=\frac{SE_w\times2}{t\times eff_w}$$

$$=\frac{7,210\times2}{25.3\times0.9}=659\text{ hp}$$

But 790 hp is available for acceleration; therefore the time required will be

$$t=\frac{SE_w\times2}{hp\times eff}$$

$$=\frac{7,210\times2}{790\times0.9}=20.3\text{ sec}$$

and the tension to accelerate in 20.3 sec will be

$$T=\frac{SE_{bs}\times2\times33,000}{tWs\times eff}$$

$$=\frac{3,710\times2\times33,000}{20.3\times240\times5,000\times0.95}$$

$$=10.6\text{-lbs/inch width}$$

If the calculated accelerating time is unacceptably long, then larger apparatus must be used to get a shorter time. The generator which must be selected to supply the motor requirements would be rated 300 kw, good for 200% load on acceleration. The 300-kw base rating is set by steady-state running requirements of the 350-hp motor.

Actual operating conditions would probably be somewhere between the two extreme cases described. The operator would be expected to reduce the tension somewhat during acceleration; thus the 34-sec acceleration is pessimistic. The 20.3-sec acceleration is optimistic and hard to achieve.

Modern newsprint winders present a special problem in that the newsprint machine roll is usually as large as the kraft machine roll, say, 72 to 84 inches in diameter, and 250 to 300 inches wide. Newsprint is wound at speeds up to 6,000 fpm with tensions ranging from 1 to $1^1/_2$ lb/inch width. While newsprint has a tensile strength in the machine direction in the order of 10-lb/inch width, the 42-lb kraft board considered in the above example has a tensile strength in the machine direction of about 85-lb/inch width, and it is wound at 8.5-lb/inch width tension. The newsprint winder must be provided with extraordinarily good tension control during the acceleration and deceleration periods to prevent breaking the sheet; thus a critical regulation problem is created demanding a good inertia-compensating system. (IC is defined as

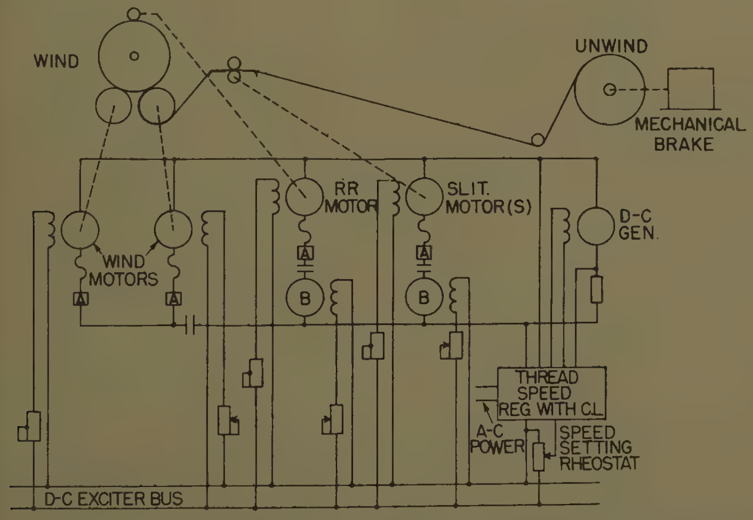

Fig. 10. Schematic diagram showing basic control scheme for winder with mechanical backstand brake. Circuits for rider roll and slitter drives shown

recalibration of the tension-regulating device to maintain constant tension during the accelerating and decelerating period.)

The relatively light tension requirements of newsprint dictate the use of relatively light hp drive motors. Accelerating and decelerating times are increased owing to the reduced hp available, and this tends to reduce the severity of the problem of holding tension during the rate of change periods. With mechanical braking on the unwind stand, the minimum accelerating time is dependent on the sheet tension required to accelerate the unwind stand. This results in relatively long accelerating periods when mechanical brakes are used. When an electric brake is used and a good IC system is provided, this time is reduced since the braking generator can act as a motor during the accelerating period. The decelerating time is also minimized since the braking generator removes the stored energy and regulates tension as the speed is reduced. Successful IC systems have been devised for use with the lighter papers, but further improvements are needed to meet the demand of wider and higher speed winders.

The duty cycle required of the apparatus may be determined by calculation. For a given paper grade, the maximum speed of the paper machine itself and the desired winder operating speed should be known. The total per-cent operating time can now be calculated:

$$\frac{S}{s\ (\text{fpm winder})} = \text{per-cent operating time}$$

Usually, maximum fpm for both should be used, although it is rare that a winder is operated at maximum tension when a paper machine makes light paper at fast speeds. For this case, assume the paper machine operates at 2,000 fpm.

$$\frac{2{,}000\ \text{fpm}}{5{,}000\ \text{fpm}} = 40\%\ \text{operating time}$$

Now, assuming 10% additional time for acceleration and deceleration, the rms hp, as a per cent of the selected motor rating, can be calculated by conventional means:

$$\text{rms hp} = \sqrt{0.4\left(\frac{372}{350}\right)^2 + 0.1\left(\frac{790}{350}\right)^2}$$
$$= \sqrt{0.962}$$
$$= 0.985$$

This calculation indicates that the motor rating is satisfactory. If, however, the rms hp thus calculated is greater than 1.0, a more detailed calculation utilizing the nomograph of Fig. 8 to get the exact length of paper in a given roll and calculation of the exact accelerating and decelerating time to determine the operating cycle would yield a more nearly correct calculation.

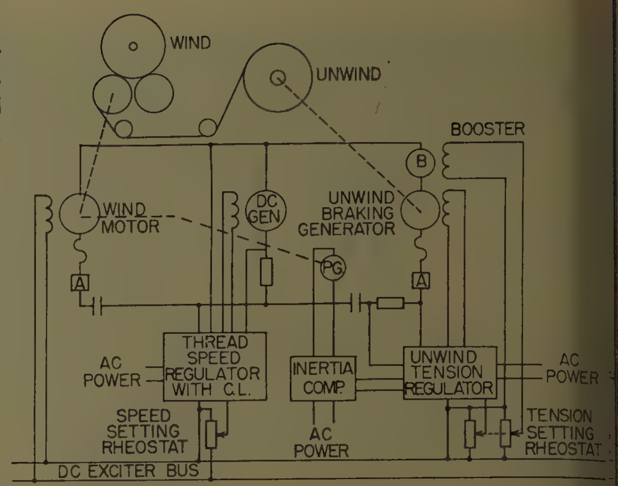

Fig. 12. Schematic diagram showing single motor winder drive with current-limit acceleration and deceleration, and constant tension regulation on electric backstand brake

Rider Roll and Slitter Drives

Some winder manufacturers utilize electric drives for rider rolls and slitters; others mechanically power these auxiliaries. Since the motors for driving rider rolls are usually quite small as compared to the drum drive motors, boosters having the same ampere rating and a voltage rating equivalent to the *IR* drop of the rider roll motors are supplied in series with the rider roll motors. The booster adds sufficient volts to the generator supply to make the counter emf for the rider roll motor and the winder drive motors equal over the entire speed range, thus the rider roll motors exert approximately constant torque from stall to full operating speed. Fig. 9 shows details of a package drive.

It is usually desirable to operate shear cut slitters at a speed exceeding the paper speed. A fixed speed of 5% to 15% above maximum operating speed is used. Considering a fixed speed above top operating speed, on a 5,000-fpm winder, the cutting edges are run at 5,250 fpm when the paper is traveling at 5,000 fpm and at 250 fpm when the winder is standing still. Thus, a booster in series with the cutter motor or motors is required to supply not only the *IR* drop of the slitter motors, but also a fixed voltage of 5% to 15% of the maximum generator voltage. Fig. 10 shows schematically the circuit arrangement for slitter and rider roll drives.

Winders With Electric Brakes

Winders with electric unwind stand brakes as shown in Fig. 11, are being used in increasing numbers as their performance, convenience, and economy become recognized by the paper industry. Following are the principal advantages of the electric winder drive with electric braking:

Performance

1. Automatic constant tension.
2. IC during acceleration and deceleration.
3. Minimum acceleration and deceleration time within the full capacity of the drive.

Convenience

1. Unwind payout and slack take-up.
2. Single-handle speed control.
3. Braking generator easily reversed to wind paper "wire-side in" or "wire-side out."

Economy

1. Less man power required.
2. Braking power recovered.
3. No brake linings to maintain.
4. Smaller main motor-generator set required.

The features of automatic constant requires a regulator capable of maintaining constant hp. The regulator adjusts the shunt field of an adjustable speed motor to hold field flux proportional to the reel diameter by regulating constant current in the motor armature circuit. (hp = a constant ($E \times I$))

Because of the tension error introduced by friction and windage, it is desirable to minimize the friction loads of the unwinding stand and the drive. Antifriction bearings should be used on the unwind stand and in the braking generator. The braking generator preferably should be direct-coupled to the reel core without belts, chains, or gears interposed. The range of tension adjustment is necessarily limited since the friction losses become a greater portion of regulated current as tension is reduced. Tension ranges not exceeding four to one are satisfactory with a minimum tension of about one pound per inch.

The continuous rating of a braking

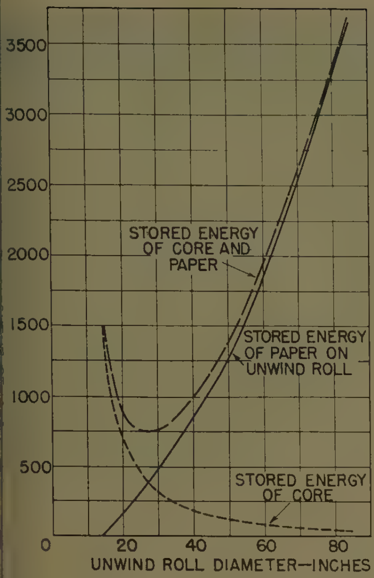

13. Variation in SE as 240-inch wide
nt roll changes from 84-inch diameter
imum to 14-inch minimum at 5,000 fpm

erator (usually rated in hp because
istable speed motors are so rated) is
cted to provide the tension require-
its of the winder, as given in Fig. 7.
king units may be given a dual hp
ng such as 75/100 hp: but in practice
unit is successfully used at top hp
ng without exceeding temperature
ts due to the duty cycle operation.
m Fig. 7, for 8.5-lb/inch width, a
stant of 0.022 hp/inch/100 fpm is
iired. Therefore, the rating of the
king generator for a direct-connected
king generator, for a 240-inch-wide
5,000-fpm winder using a 14-inch diameter core and an 84-inch diameter parent roll, calculates to be 264 hp, 227/1,364 rpm. Accordingly a 250-hp 225/1,350-rpm motor would be specified. For economic reasons, final selection of the base rating of the braking generator should not be decided upon until accelerating requirements are considered.

When electric braking is provided for a winder, a booster generator is used in series with the braking generator; see Fig. 12. This booster may provide power for payout, slack take-up and stall tension, as well as the *IR* drop of the braking generator armature circuit. The rating of the booster should be adequate to supply the *IR* drop of the braking generator armature circuit at maximum overload. For example, the booster rating for the 240-inch-wide 5,000-fpm winder previously considered would be 33 volts, 900 amperes, good for 200% load.

There is a limitation in the change in diameter that can be accomplished at the backstand with the center wind reel. This limitation is imposed by the maximum possible speed range by shunt field control of a d-c adjustable speed motor which is 6 to 1. This limitation is usually no serious handicap since the use of larger cores makes paper handling easier. Use of the nomograph of Fig. 8 will show that there is very little additional paper on the small diameter cores. Reel diameter changes beyond 6 to 1 can be accomplished in special cases, but such control is unduly expensive and requires a mechanical diameter or tension-measuring device with its problems of physical interference and maintenance.

Regulation of tension at constant speed is a relatively easy task for electrical control. Conversely, maintenance of constant tension during the accelerating and decelerating period, IC, is probably the most difficult problem encountered in the electric winder drive. If a constant rate of change of speed can be maintained during the accelerating period, the magnitude of the problem is somewhat reduced. The wide variation in the kinetic energy as the reel diameter changes presents the most difficult problem.

Fig. 13 shows the change in stored energy of the unwind roll as the reel diameter changes on a 240-inch-wide 5.000-fpm kraft paper winder. Fig. 14 shows the tension variation encountered during acceleration and deceleration when four 9,000-ft rolls of 0.0126-inch-thick paper, 42 inches in diameter, are wound from one 84-inch-diameter machine roll, and IC is accomplished by a stepped recalibration of the regulated tension.

With the stepped system, relays that sense the change in speed indicated by movement of the speed-adjusting rheostat are used for initiating IC; and these relays remain actuated as long as the drive speed is changing. Calibration of the IC circuit is different for acceleration and deceleration. Although Fig. 13 shows a considerable change in the amount of SE in the unwind reel, the tension variations shown in Fig. 14 are not sufficiently great to prevent the use of the stepped recalibrating system. As the desired sheet tension is reduced, however, the tension variation during acceleration becomes a greater proportion of the sheet tension.

A more accurate signal for IC can be obtained by measuring the rate of rise of the power supply generator voltage. A further improvement in the IC signal is obtained by use of a rate of rise of voltage from a pilot generator driven by the braking unit, as shown in Fig. 12.

Control schemes utilizing motor-operated rheostats to follow the diameter change can be used to adjust the unwind-braking generator shunt field current with the IC signal strength calibrated by an additional rheostat plate. Frequent operation of the rheostat and its relay-sequencing and resetting system necessitates maintenance unnecessary with other systems, and optimum adjustment of such rheostats is difficult to attain.

When current-limit acceleration and deceleration are used, the acceleration and the deceleration time is essentially

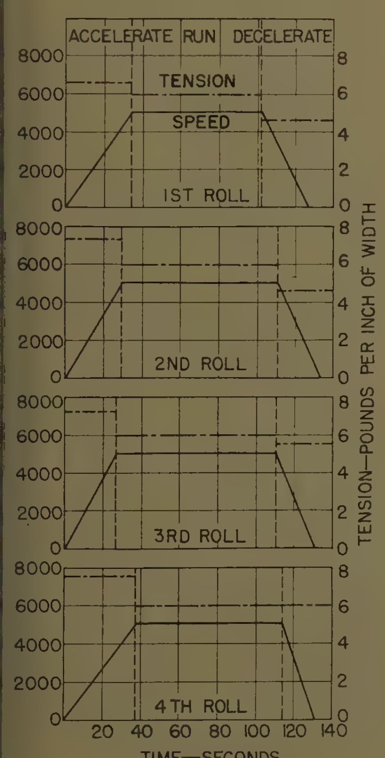

Fig. 14 (left). Time cycles for winding four 9,000-ft rolls of 0.0126-inch-thick (42 lb) board, each 42 inches in diameter from one 84-inch-diameter machine roll

Fig. 15 (right). Dynamic performance of winder drive with current-limit acceleration and deceleration. Plotted from the oscillograph record shown in Fig. 3

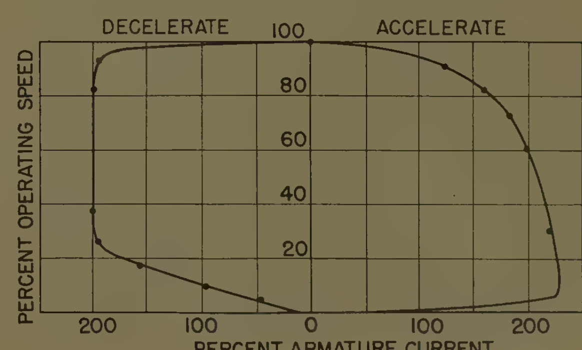

independent of the tension setting, since the braking generator power is returned to the d-c system. The time is limited by the overload capacity of the power supply generator. To get a balanced drive system, the drum drive motor or motors should be selected to accommodate all available power on acceleration. The overload capacity of the braking generator should be selected to generate all power that can be absorbed by the power supply generator on deceleration. Note the dynamic current-limit characteristics of the drive shown in Fig. 15, which is taken from the tests on the large kraft winder, as shown in Fig. 3.

Selection of a suitable power supply generator to provide the same time of acceleration for the 240-inch-wide 5,000-fpm winder previously considered with a mechanical brake, will now be considered with an electric brake which returns power to the d-c system. The total stored energy at 5,000 fpm is approximately the same, so that the value of the 7,210 hp-sec previously calculated will again be used. The time for acceleration is taken to be the same but the generator rating can be reduced because, during steady-state running, the braking generator will return power to the system.

The time required to get the entire winder mass into motion is very nearly independent of tension when the braking generator is used. Assuming an over-all winder mechanical efficiency of 90% and a motor efficiency of 92%, the power required from the generator for 34-sec acceleration will be

$$\frac{7{,}210 \text{ hp-sec} \times 2}{34 \text{ sec} \times 0.9 \times 0.92} = 512 \text{ hp}$$

$$= 382 \text{ kw}$$

The actual steady-state running load was found to be about 100 kw. Therefore, a 200-kw generator with 200% overload capacity on acceleration can be used instead of the 300-kw generator with 200% overload capacity required for the same winder with a mechanical brake. Of course, the motor-generator set drive motor size can be reduced accordingly. Savings in the motor-generator set and the omission of the mechanical brake somewhat offset the cost of the braking generator.

Note that the use of the current-limit acceleration and deceleration results in the minimum accelerating and decelerating time utilizing the power supply generator to top capacity.

The convenience of operating an all-electric drive is unexcelled by other types of drives. Rolls weighing 35,000 pounds are not easy to turn by hand; the electric brake makes hand turning unnecessary. Paper is paid out from the parent roll by pushing a payout push button. Payout occurs only as long as the button is held down. The paper is threaded through the winder and on to the shipping core. There may be some slack in the sheet immediately following the parent roll. This slack is undesirable since the winder may start the parent roll with a sufficient jerk to break the sheet especially when it is not threaded exactly straight. A slack-takeup push button is provided to remove the slack conveniently and insure a smooth start with the paper under tension. Use of the electric drive in turning the backstand roll reduces the man power required to thread the winder. Fig. 16 shows a panel providing current-limit and electric-brake control.

Sometimes it is desirable to wind shipping rolls wire-side in and at other times wire-side out. The magnetic control can be arranged to reverse the braking generator easily, or a reversing knife switch can be provided in the field circuit or the armature circuit of the braking generator, to permit its operation in either direction.

Recovering of the braking power is an economic consideration that is particularly valuable on the larger and faster winders. The following equation can be used to calculate power savings: Annual power savings = 0.178 TWSKC. The annual power savings for several typical winders is shown in Table II.

Conclusions

Development of regulator circuitry has played a large part in the success of the d-c adjustable voltage winder drive. The continuous operation of a paper machine demands reliability of the winder drive and recent developments in magnetic-amplifier regulators has provided the necessary continuity of service.

D-c adjustable voltage systems for winder drives have the performance characteristics and the flexibility of arrangement necessary for the application. Care in the proper selection of ratings, and electrical as well as mechanical features of d-c adjustable voltage winder drives will insure their continued acceptability to the paper industry.

Fig. 16. Modern magnetic-amplifier panel, which can provide either current-limit acceleration and deceleration or automatic tension control with an electric brake. Note static components used, providing high dependability and low maintenance

Table II. Annual Savings Operating with Braking Generator

K=0.92; C=$0.006 Assumed

Type of Paper	Weight, Lb/3,000 Sq Ft	Tension, Lb/Inch	Speed, Fpm	Width, Inches	Annual Savings, Dollars
News	32	1	2,500	252	615
Book	45	4.5	1,500	180	1,187
Kraft	207	10.5	1,350	240	3,324

Appendix. Data for Estimating Winder Drives

Ream measure

- Standard—500 sheets, 24 by 36 inches (3,000 sq ft).
- Book paper—500 sheets, 25 by 38 inches.
- Board—1,000 sq ft.

Density of paper

- Kraft—45 lb/cubic ft.
- Coated book—55 lb/cubic ft.

Caliper versus weight

- Newsprint—32 lb/3,000 sq ft = 0.0032 inch thick.
- Kraft—43.5 lb/1,000 sq ft = 0.014 inch thick.

Length paper in roll

$$L = \frac{0.0654\,(D_0^2 - D_1^2)}{\text{Thickness, inches}}$$

The usual winding tension = 10% ultimate tension.

Winding tension

$$\text{Paper} = \frac{\text{lb}/3{,}000 \text{ sq ft}}{9} \times 4 \times 0.1$$

$$= \underline{\quad\quad} \text{lb/inch width}$$

$$\text{Board} = \frac{\text{lb}/1{,}000 \text{ sq ft}}{3} \times 4 \times 0.1$$

$$= \underline{\quad\quad} \text{lb/inch width}$$

The Pennsylvania Railroad Class GG-1 Electric Locomotives

J. W. HORINE
MEMBER AIEE

H. S. OGDEN
MEMBER AIEE

A LARGE GROUP had gathered on the upper platform of The Pennsyl-[v]ia Railroad Thirtieth Street Station in [Ph]iladelphia on Sunday morning, May 17, [19]59. Standing at the head of a train of [ste]aming coaches they watched a very [spe]cial locomotive back down the track [an]d couple to the leading car. The oc-[cas]ion was the 25th anniversary of the [con]struction of the first class-*GG-1* elec-[tri]c locomotive for The Pennsylvania [Ra]ilroad. It was this locomotive, num-[ber] *4800*, fresh from the paint shop and [pro]udly displaying a 25th anniversary [bro]nze plaque beneath the engineman's [wi]ndow (Fig. 1), that was to haul the [Na]tional Railway Historical Society [spe]cial train. A brief ceremony with its [att]endant picture-taking climaxed the [occ]asion and the train departed for New [Yo]rk.

Thus, by marking the completion of a [qu]arter-century of successful operation of [loc]omotive number *4800*, the Railroad [wa]s highlighting the excellent record that [the] *GG-1* locomotive fleet had established [in] 25 years of intensive service. From an [eng]ineering standpoint, therefore, it is [hig]hly appropriate to review briefly the [dev]elopment and characteristics of this [des]ign.

[De]velopment of Design

At the time the *GG-1* locomotive design [pro]ject was started, the Railroad was con-[sid]ering designing and building an elec-[tri]c locomotive with tracking character-[isti]cs and general appearance that would [con]stitute a worthy replacement for the [ear]lier class *P5A* locomotives then in [pa]ssenger service.

The combined efforts of The Pennsyl-[va]nia Railroad, the Baldwin Locomotive [W]orks (now Baldwin-Lima-Hamilton), [the] Westinghouse Electrical and Manu-[fac]turing Company (now Westinghouse Electric Corporation), and the General Electric Company were focused on the project.[1] Design criteria were carefully established in the light of previous experience, and full advantage was taken of the most advanced technological developments of that time.[2,3]

Track Tests

The tracking qualities of the *P5A* locomotives then operating were not up to expectations, particularly at high speeds, and improvements were necessary. Management of The Pennsylvania Railroad took a forward-looking step by instituting a testing program to determine why some locomotive designs possessed good tracking qualities and others did not.[4] To obtain the necessary data it was decided to use special test ties capable of measuring the track stresses induced by passage of the locomotive wheels. Some years previously the Railroad had made approximately 300 special cast-iron ties, each provided with means for measuring horizontal impact forces on the rail. Essentially, this was accomplished by the running rail forcing a hardened steel ball into a renewable soft iron bar, in a manner similar to the Brinell hardness tester. Measuring the diameter of the indention in the bar would give an indication of the force applied to the rail. These ties were installed in the westbound high-speed track near the Claymont, Del., station on the Philadelphia–Washington main line; Fig. 2.

When the ties were first installed the track surface was carefully aligned. It was not surprising, therefore, that there was no discernible difference in test tie readings, regardless of the type of locomotive operated over the track. To obtain measurable differences, the running rails were displaced laterally and vertically at a location near the entering end of the test section. The induced oscillations damped out as the locomotive traversed the remainder of the test section, and a stress record was obtained.

By this time, the techniques of using strain gages for making stress measurements had advanced sufficiently to enable the electrical manufacturers to build and install a system of "weigh bars" on the locomotives. Combining these with specially built journal boxes, Fig. 3, made it possible to obtain continuous records of the lateral forces on the ends of the locomotive axles. Multielement oscillographs and long rolls of sensitized paper provided permanent records of the results, Fig. 4. Thus the riding characteristics of any locomotive, as indicated by the Brinell ties under the rail, could be directly correlated with flange forces generated on the locomotive and indicated by the weigh bars. Such instrumentation required that the locomotive pull a test car containing the oscillographs and auxiliary apparatus required to make the measuring system function, Fig. 5.

An analysis of results obtained from tests on the *P5A* locomotives with their 2-C-2 wheel arrangement quickly told what was happening during operation at passenger-train speeds. Changes were made in the truck equalization system to

Fig. 1. Locomotive 4800, May 17, 1959

[Pap]er 60-48, recommended by the AIEE Land [Tra]nsportation Committee and approved by the [AI]EE Technical Operations Department for [pre]sentation at the AIEE Winter General Meeting, [Ne]w York, N. Y., January 31–February 5, 1960. [Ma]nuscript submitted November 2, 1959; made [av]ailable for printing November 27, 1959.

[J.] W. Horine is with The Pennsylvania Railroad [Com]pany, Philadelphia, Pa., and H. S. Ogden is [wit]h the General Electric Company, Erie, Pa.

Fig. 2. Test ties installed in main-line track at Claymont, Del.

correct the poor operation, and a short series of test runs with a locomotive verified that acceptable operation had been achieved, Fig. 6.

Assuming that even better operation was possible, the investigations of riding quality were continued by The Pennsylvania Railroad management. For this purpose a locomotive having a 2-C+C-2 wheel arrangement was borrowed from the New York, New Haven and Hartford Railroad and gearing installed to permit operation at speeds up to 120 mph (miles per hour). When this locomotive was run over the test ties, substantial reductions in the lateral forces were indicated. Two tenable explanations of this were offered: first, that the reductions were due entirely to the lower axle weights inherent in this design, and second, that wheel arrangement exerted a predominant influence on tracking characteristics and that axle weights were relatively unimportant. The solution of this problem was evidently fundamental to further progress in locomotive design and a decision was reached to build two sample locomotives and make exhaustive tests upon each. The one showing best over-all results would be the basis for future electric locomotive designs.

Sample Locomotives

The General Electric Company was called upon to build a locomotive with the 2-C+C-2 wheel arrangement to be known as locomotive *4899*, Fig. 5. At the same time an order was placed with the Baldwin Locomotive Works and Westinghouse Electrical and Manufacturing Company for a rigid-frame locomotive patterned after the *P5A*, but with a 2-D-2 wheel arrangement. This was to be known as locomotive number *4800*, Fig. 7. Both locomotives were to have motors and control of the same general type, differing only in the number and size of the motors.

Mechanical design work on both locomotives was carried out on a 3-way basis, engineers of Baldwin, Westinghouse, and General Electric working in co-operation with The Pennsylvania Railroad. The 2-D-2 locomotive was designed to have lower axle weights than those of the *P5A* after its modification, and the 2-C+C-2 locomotive was designed to have higher axle weights than the original test locomotive borrowed from the New Haven Railroad. Both locomotive cabs were streamlined to give the appearance characteristic of the Pennsylvania electric locomotive fleet today.

Immediately upon completion of the two locomotives comparative testing was started. They were run over the Claymont test ties at speeds up to 115 mph and both designs performed exceptionally well; Fig. 8. During the many test runs, locomotive *4899* and its trailing car were repeatedly accelerated to 100 mph in 64.5 seconds, or at an average rate of 1.55 mphps (mph per second). This accomplishment required peak outputs of 9,300 hp (horsepower) at the rail, equivalent to 11,000 diesel locomotive horsepower. To complete the test program both locomotives were equipped with weigh bars and continuous oscillographic records were taken while operating between New York and Philadelphia at sustained speeds of 100 mph wherever track conditions would permit this velocity.

To handle the photographic records that came from the two 6-channel oscillographs required for recording axle thrusts, elaborate darkroom facilities were installed in the basement of The Pennsylvania Railroad office building at the Wilmington, Del., station. Here the rolls of exposed paper were processed after each day's operation and the results were ready for analysis the next morning.

Careful scrutiny of the voluminous mass of paper records and a review of the Brinell measurements from the test ties showed that locomotive *4899* had the better over-all tracking characteristics and developed lower lateral impact forces, although the difference between the two test locomotives was not great.

History

Taking into consideration the evidence of all the data accumulated as well as other pertinent factors, The Pennsylvania Railroad management decided that the 2-C+C-2 locomotive should form the basis for the design of their new electric passenger locomotives; see Fig. 9. In accordance with the Railroad's established system of designating classes of locomotives, the symbol *GG* was assigned to this design to indicate the wheel arrangement: 2 truck axles, 3 drivers, 3 drivers and 2 truck axles. The numeral 1 was added to indicate the first locomotives built on this design, and thus the famous *GG-1* was christened.

The original locomotive number, *4899*, became number *4800*. As the first of 139 units of the same general type, it has carried this number down to the present moment. The 2-D-2 rigid-frame locomotive, originally numbered *4800*, was eventually renumbered *4999*. Although it gave years of reasonably satisfactory service, it developed the habit of leaving the rails on sharp curves in yards and was finally retired.

Development of the Fleet

Number *4800* made its first scheduled run in passenger service between New York and Wilmington, Del., on May 16, 1934. Other locomotives of the same design followed rapidly until the number finally totaled 139. Although designed primarily for passenger service (Fig. 10), 57 of the fleet of 139 are assigned to freight service (Fig. 11), where they turn in an excellent performance record. They are used interchangeably, however, in passenger service when required. The conversion from one type of service to the other is a simple operation requiring less than 5 minutes. A brake selector handle (Rotaire Valve) is turned to its appropriate position and the brake-pipe feed

Fig. 3. Application of weigh bar to locomotive journal box

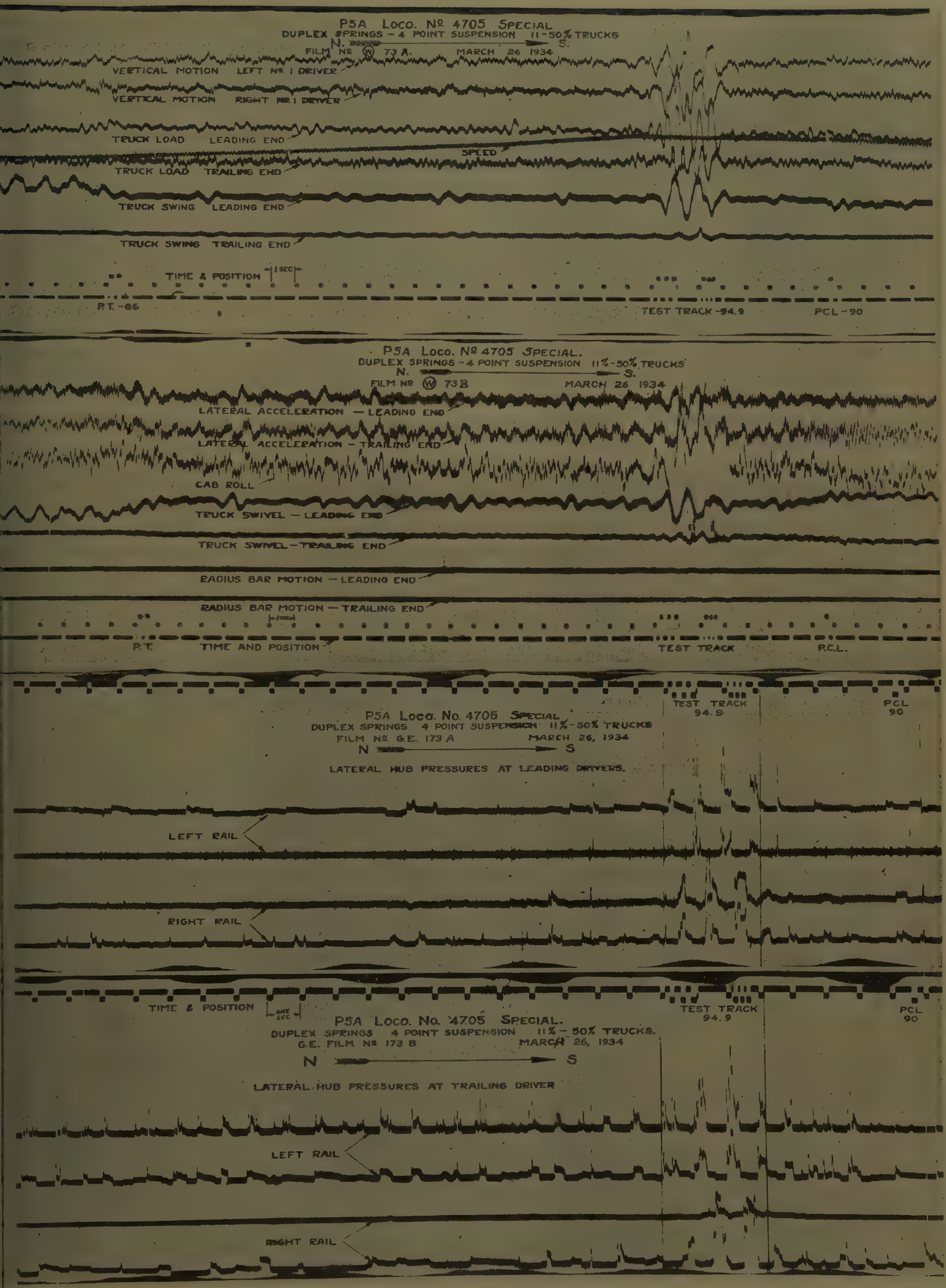

ig. 4. Sample oscillogram traces of axle thrusts made on modified P5A locomotive 4705 fitted with weigh bars operating on test track, Claymont, Del.

Fig. 5. First class-GG-1 locomotive fitted with weigh bars and hauling test car

valve is adjusted for the appropriate pressure. For freight service, the master controller is restricted to 17 of its 22 notches.

Originally the locomotives were equipped with a vertical fire-tube boiler of Pennsylvania Railroad design to supply steam for train heating. Age and obsolescence have dictated a change to the type of steam generator commonly used on diesel-electric locomotives. Cost of repairs to the original boilers made the change more economical. Water tanks with a total capacity of 2,755 gallons are divided between the two ends of the locomotive. A 390-gallon fuel-oil tank is within and surrounded by the water tank in the forward, or no. 1, end.

The locomotives are equipped with no. *8EL* air-brake apparatus, including the *D-24* type of brake valves. They have 4-aspect continuous-indication cab signals and automatic train-speed control.

Something of the magnitude of the task being performed by these locomotives may be judged by the following statistics. The system over which they operate comprises approximately 2,200 miles of track. In passenger service, they produce an average of 125,000,000 car miles per year, or the equivalent of a 10-car train circling the globe 500 times. In freight service, they ably supplement the older locomotives of the *P5* class. Together, this motive power produces approximately 15-billion ton miles, the equivalent of a train of 150 40-ton cars circling the globe 100 times in a year.

Case Histories

As the years passed, locomotive number *4800* accumulated an impressive mileage total. By August 1, 1959, it had operated 2,795,577 miles, equivalent to 112.3 trips around the world at the equator. Dividing this distance by the total time elapsed since the locomotive was placed in service reveals that number *4800* has had a continuous running speed of 13 mph for its entire life. During the quarter-century of its life it has hauled an average of 13 cars and produced 36,342,501 passenger-car miles. Assuming an average of 30 passengers per car, this is over 1 billion passenger miles, more than sufficient to transport the entire population of New York City all the way to Philadelphia. In performing this vast amount of work, number *4800* consumed 122,214,240 kilowatt-hours of electric energy costing $1,582,297, or more than six times the original cost of the locomo-

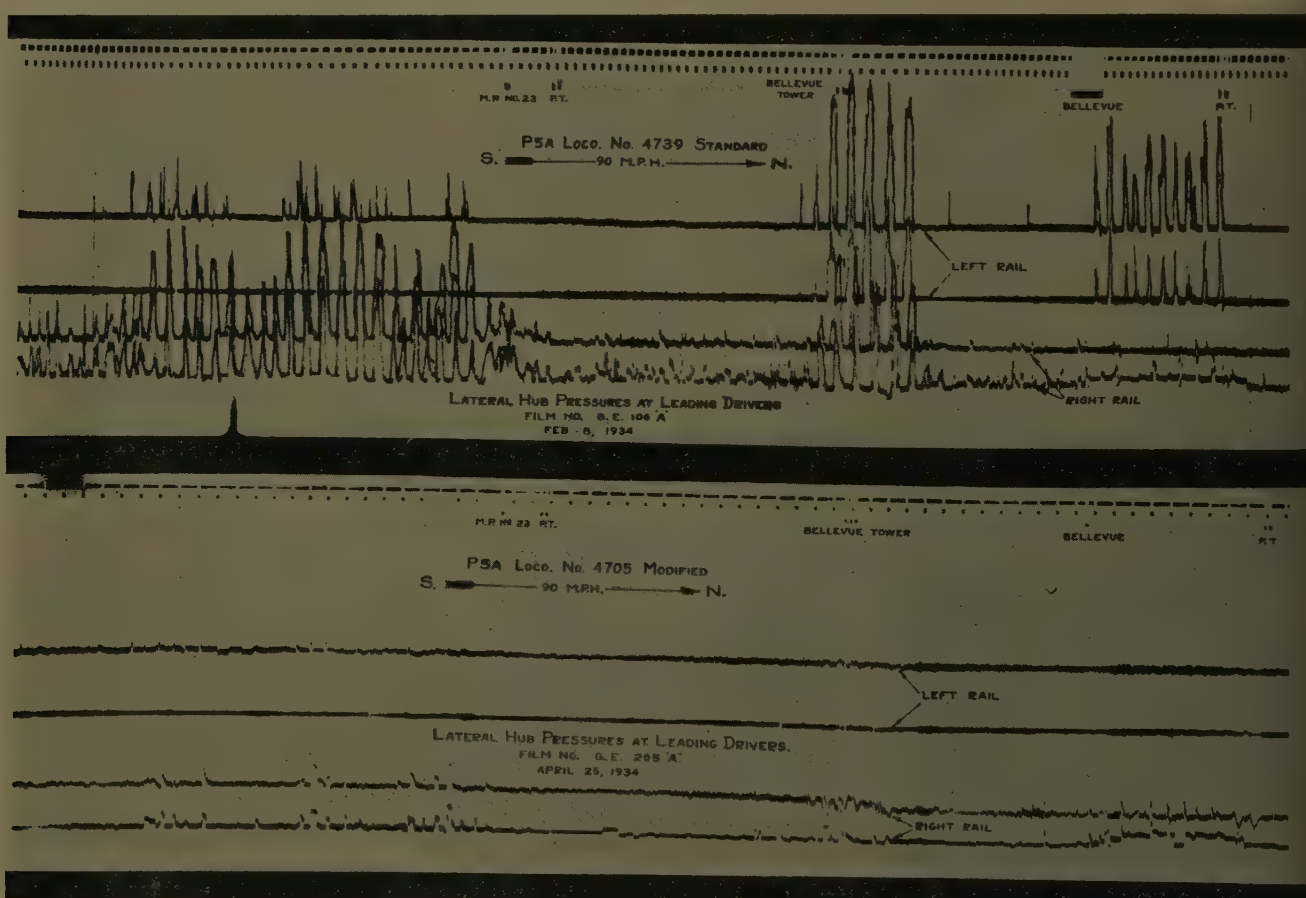

Fig. 6. Axle thrusts showing effect of modification on P5A locomotive when operating at 90 mph over crossovers at Bellevue Tower, Del.

Although designed for a maximum
d of 100 mph, this locomotive was re-
edly brought up to 128 mph during
ries of braking tests in 1935.

sters of locomotive number *4800* in *GG-1* family have achieved notoriety. operation of the fleet has, on the le, been relatively free from serious dents although there have been a few. omotive number *4823* was the first to nvolved in an en-route accident result- in two fatalities. Shortly thereafter same locomotive was struck by light- and lost a transformer. This was owed in a few months by the first in- ce of a *GG-1* crew member suffering a l heart attack. The locomotive was featured on The Pennsylvania Rail- d calendar for 1936. This honor ap- ently caused it to forsake its evil ways, since then *4823* has not been involved ny unfortunate incidents.

umber *4840*, after 10 years of service, ved that a *GG-1* is a rugged locomo- . While traveling at 80 miles an hour ncountered a bulldozer crossing the ks at Stanton, Del., and threw the hine across four tracks. Total dam- to the locomotive consisted of a ted nose and one pair of engine truck els derailed.

ossibly the greatest notoriety ever achieved by any locomotive fell to the lot of number *4876* in January 1952. Failure of the train brakes caused it to crash into the concourse at Union Station, Washington, D.C., where it fell through the floor into the baggage room below. Removing this locomotive presented a serious problem. It could not be reached by a wreck crane to either lift or drag it out, as it was surrounded by building columns spaced at 6-foot intervals that could not well be removed. Accordingly, the locomotive was dismantled in place and cut into pieces slightly less than 6 feet in any dimension. Parts were trucked out of the station baggage room and shipped to The Pennsylvania Railroad Company's shops at Altoona, Pa. In November 1952, 10 months later, the rebuilt number *4876* was returned to service.

Fig. 7. Class R1 2-D-2 locomotive on test run. Note instrumentation on trucks

Snow Trouble

The outstandingly successful operation of this fleet of locomotives has not been

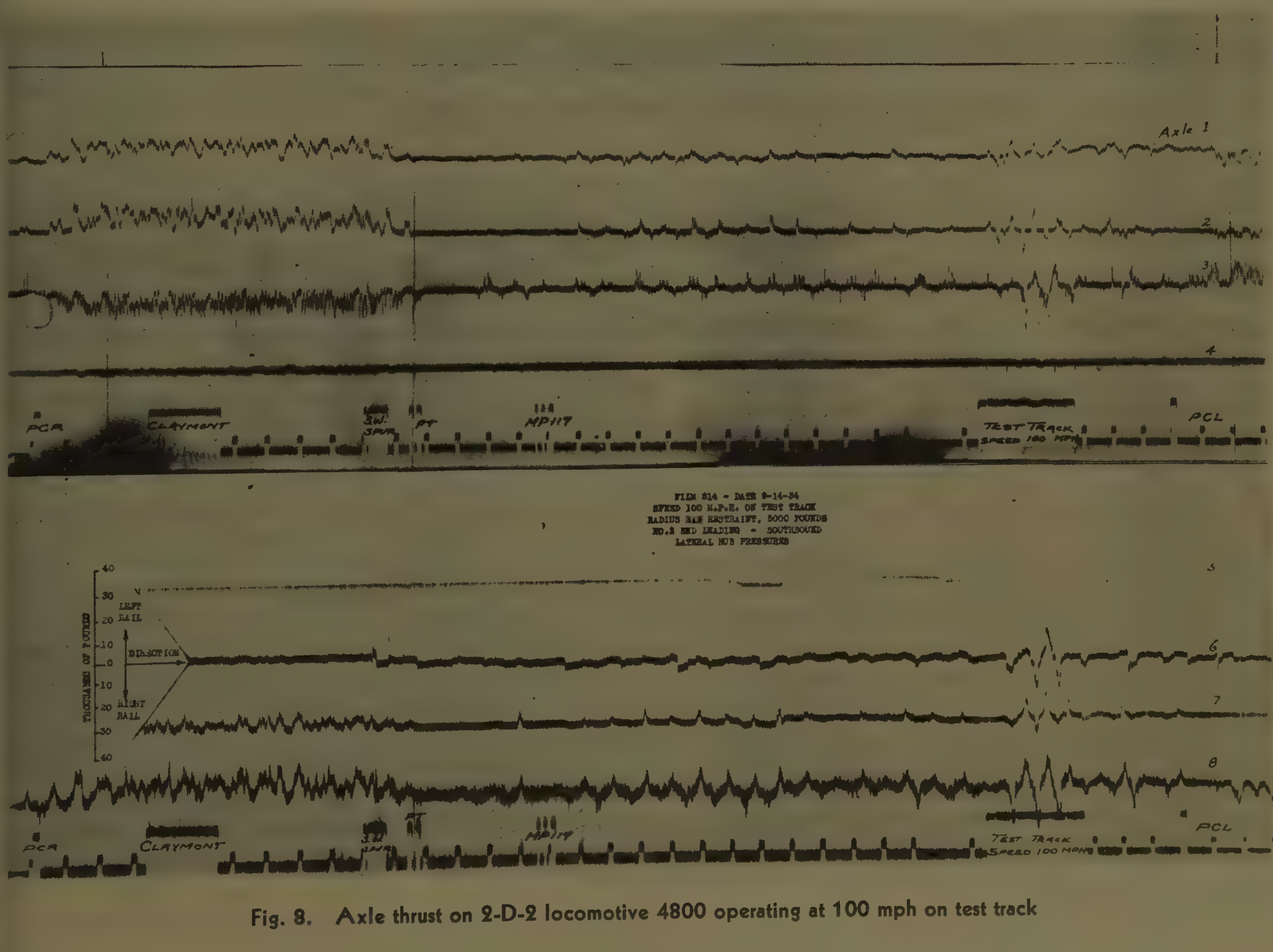

Fig. 8. Axle thrust on 2-D-2 locomotive 4800 operating at 100 mph on test track

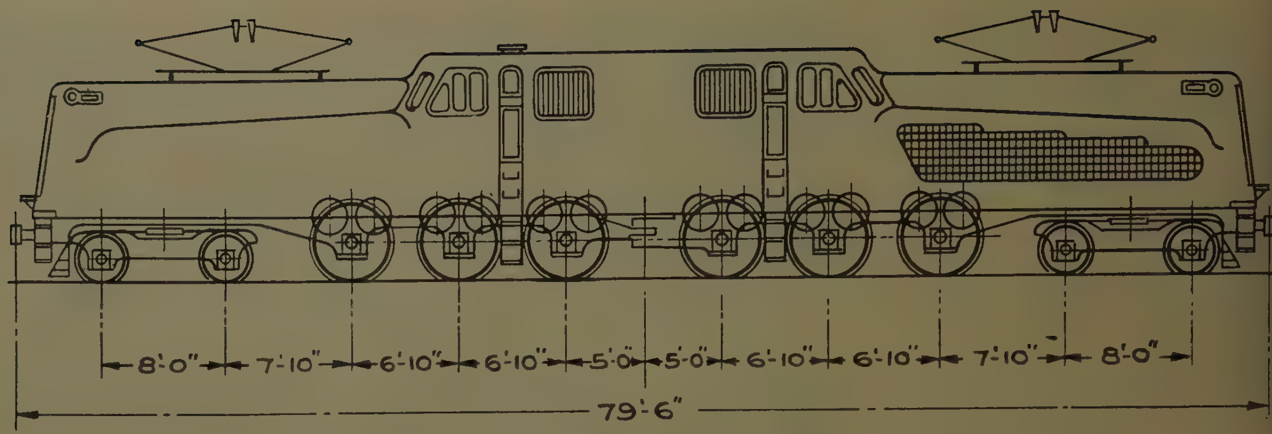

Fig. 9. General dimensions and statistics of class GG-1 locomotives, 100-mph gears

Total weight, 477,000 pounds
Weight on drivers, 303,000 pounds
Weight on driving axle, 50,500 pounds, average
Weight on each truck, 87,000 pounds
Starting tractive effort, 70,700 pounds

Maximum speed, 100 mph
Continuous tractive effort, 17,300 pounds
Continuous speed, 100 mph
Continuous horsepower, 4,620

Fig. 10. Early GG-1 locomotive in passenger service crossing the Susquehanna River, Havre de Grace, Md.

Fig. 11. Class GG-1 locomotive in main-line freight service

without blemish. The weatherman and snow were almost the fleets undoing. Snow protection consists of fine mesh linen screens applied over the air inlet louvers during snow storms and kept in place as long as the snow continues to blow. It is usual to lose a few motors in a snow storm, since there are always locomotives en route without screens in place when the snow starts. In February 1958, however, a freak snowstorm occurred. Locomotives not only continued to lose motors after the screens were in place, but locomotives taken into the shop, repaired, and returned to service promptly lost more motors. This continued until passenger service was badly crippled.

The source of the trouble was finally identified when inquiry at the Weather Bureau developed the fact that the snow was of a peculiar type that had not fallen in that area during the life of the *GG-1* locomotives. It is known as "diamond" or "arctic" snow. The flakes are of extremely small size and, because of the lack of surface tension, or meniscus effect, in snow, they are capable of passing through openings and crevices that would not pass water. Hence, the linen screens offered no protection and the snow passed right through them. Moreover, after the snowfall ceased, the temperature continued to hover around 8 to 12 degrees Fahrenheit with high winds. This meant that the snow neither crusted nor packed, but continued to drift and swirl with the passage of trains.

Oddly enough, the same territory experienced another unusual snow storm in March of the same year. This was of a diametrically opposite type: the temperature was barely below freezing, there was very little wind, and the snowflakes were huge and wet. Deposits as large as 12 to 14 inches in diameter built up on overhead wires; power and communication lines were badly damaged, and many areas were without electric service for weeks. The *GG-1* locomotive fleet, however, did not lose a single motor.

Protection of the locomotives against snow presents a twofold problem. First, what expenditure can be economically justified in view of the rarity of the condition encountered in 1958? Second, what practical means are available to prevent entry of this type of snow? Partially corrective measures have already been taken, and research to develop fully effective measures at reasonable cost is being carried on.

Conclusions

In the 25 years since number *4800* went into service, the *GG-1* locomotive fleet has accumulated a total of 337,000,000 locomotive miles. This is equivalent to 13,536 trips around the world at the equator, or an average of 97.4 times around the world for each of the 139 locomotives in the fleet. The outstanding performance that has characterized this operation is a living tribute to the fore

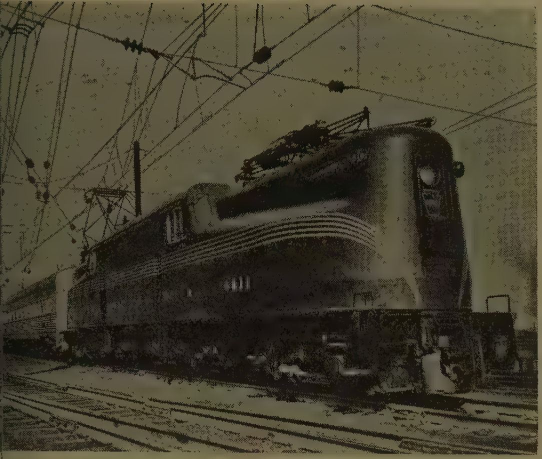

Fig. 12. Class GG-1 locomotive hauling stainless steel Congressional Limited

...edness and good judgment of The ...nsylvania Railroad management and ...locomotive builders responsible for ...nception and perfecting of the design ...e early 1930's.

...he geographic location of the elec-trified lines, coupled with the fact that the passenger traffic over them has been handled almost exclusively by *GG-1* locomotives for 25 years, has resulted in world-wide popularity for these locomotives.

The handling of "famous name" trains, such as the Broadway Limited, The Congressional Limited (Fig. 12), the Spirit of St. Louis, and the fleet of popular trains between New York and the deep South, as well as the "clockers" of the New York-Philadelphia-Washington service, has served to fix the image of the *GG-1* as "the electric locomotive."

References

1. ELECTRIC PASSENGER LOCOMOTIVES. *Railway Age*, New York, N. Y., vol. 100, no. 7, Feb. 15, 1936, pp. 278–82.

2. ELECTRIC LOCOMOTIVE OPERATION, H. C. Griffith. *Mechanical Engineering*, New York, N. Y., vol. 63, June 1941, pp. 456–60.

3. SINGLE-PHASE A-C ELECTRIC LOCOMOTIVES ON THE PENNSYLVANIA RAILROAD—PROTECTION AND TONNAGE RATING, H. C. Griffith. *AIEE Transactions (Electrical Engineering)*, vol. 61, Apr. 1942, pp. 224–28.

4. TRACK TESTS OF ELECTRIC LOCOMOTIVES. *Railway Age*, vol. 101, no. 11, Sept. 12, 1936, pp. 374-80; no. 12, Sept 19, pp. 412–18.

Discussion

...**. Lessmann** (Westinghouse Electric ...oration, East Pittsburgh, Pa.): It is ...fying to read this paper summarizing ...ears' experience with the *GG-1* electric ...notive, covering, as it does, its concep... construction, tests, and many years of ...ation. The authors should be highly ...nended.

...e *GG-1* locomotives, although designed ...ears ago, still rank as the best passenger ...notives in the country since probably ...her could meet railroad schedules with ...s as large as those handled by the *GG-1* ... During the war years, these loco...ves did an outstanding job in handling ...nger trains under perhaps more diffi... conditions than ever encountered any...e at any time. It has been said that ...success of The Pennsylvania Railroad ...rification during the last war was one of ...deciding factors against possible opera... of the railroads in the United States by ...Government.

...r personnel is proud to have had the ...rtunity to take part in this joint de...pment. As is frequently the case, some ...es of such an effort may at times re... more recognition than others. One ...ibution made almost exclusively by ...inghouse engineers was the develop... of the quill drive which permitted ... of the motor weight to be spring...orted and which was instrumental in ...ning good tracking performance.

...e paper mentions briefly that these ...notives are also used in freight service. ...n the question concerning freight ...ce was raised, both electrical manu...rers' representatives advised against it ...ood grounds: 1. the low adhesion to ...h the *GG-1*'s could be worked, about ..., which was inherent in the design of the ...ric equipment, and 2. the character... of the traction motors, namely, the a-c ...nutator motors. However, after a ...hy discussion, the decision to use the ... locomotives in this type of service was made by Mr. Duer, who was then Electrical Engineer of The Pennsylvania Railroad. The decision proved to be correct and the locomotives have performed well in freight service.

In order to analyze schedules in freight service and arrive at a satisfactory solution, a co-operative effort between the electrical manufacturers produced a new and unique method of calculating and predicting the performance of the locomotives in any service and with any desired tonnage on the basis of the expected temperature of the motors which, of course, should be kept within acceptable limits. This method was described in a paper by Felix and Jungk.[1] I shall quote one paragraph from Part I of this paper:

"The only boundaries which these single-phase locomotives recognize are those defined by the maximum permissible speed, the maximum tractive effort, and the top speed–tractive effort curve along which maximum horsepowers are developed. In addition, many of the high-speed passenger locomotives demonstrate their adaptability to different types of service by pulling freight trains weighing up to 5,500 tons at speeds between 30 and 50 miles per hour where operating points can be chosen, from many of the 60 available notches, as freely as in the 60- to 80-miles-per-hour passenger speed range."

It is interesting to know that for freight service, the effect of the momentum was taken into account. Downgrades were utilized to build up momentum to help in scheduling uphill grades. This was possible because these locomotives were capable of high hp output at high speeds. Schedules laid out on this basis were met without difficulties. Tonnage calculations never had to be reduced; in some instances, they could even be increased. Careful calculation of the New York to Washington run of the Congressional trains brought the time of these trains down from 4 hours and 25 minutes to 3 hours and 35 minutes.

I would like to mention here that the electrical engineering staff of The Pennsylvania Railroad has always been of the highest caliber. This fact accounts in a large measure for the success of the Railroad's electrification. I consider myself fortunate to have worked with these men, some of whom have retired.

Such men as Jacob Stair, Jr., and Ken Gordon have left an excellent record also in their work with the AIEE Land Transportation Committee.

The design, manufacture, and operation of the *GG-1* locomotive show what is possible, since it is, as it were, a living example of the result of teamwork between manufacturers and users. We can and should look forward to a continuation of such teamwork in a not-too-distant future which is foreshadowed by the development of superior equipments, e.g., the new locomotives and multiple-unit cars using ignitron or even silicon rectifiers to produce the current for d-c traction motors, with their superior tractive effort characteristics. We would be proud to be part of this team.

REFERENCE

1. COMPLETE ANALYSIS OF MOTOR TEMPERATURE RISE, Fremont Felix, H. G. Jungk. *AIEE Transactions*, vol. 60, 1941, pp. 578–86.

D. R. MacLeod (General Electric Company, Erie, Pa.): This paper is a tribute to a most unusual and dramatically successful peacetime effort in engineering co-operation when the best available talent in the United States was brought together under the leadership of J. V. B. Duer, a Fellow of the Institute since 1929 and, at the time this locomotive was born, Chief Electrical Engineer of The Pennsylvania Railroad. It is probably unfair to single out any one engineer for particular mention from among the many from all the companies who co-operated in this project, but it is my belief that the greatest individual contribution came from Basil Cain who conceived the running gear that gave this locomotive such excellent tracking characteristics.

It is interesting to speculate on what

might have been the logical development of the *GG-1* had not further extension of The Pennsylvania Railroad system ceased before the fleet of 139 locomotives was completed. When the extension to Pittsburgh was being studied, 7,500-hp and 10,000-hp locomotives were designed for high-speed passenger service and to move freight over the 1% ruling grades at 50 mph. The 7,500-hp locomotive would have been named the *GG-2* and would have had the 2-C+C-2 running gear with 60-inch wheels to accommodate the larger motors. These motors were to have been a modernized version of the motors used on the 2-D-2 locomotive mentioned in the paper that bore the number *4800* originally. The so-called 7,500-hp locomotive was designed to develop 14,000 hp at 61 mph and 8,500 hp at 100 mph. The 10,000-hp locomotive was to have been used for freight service only. The Pennsylvania Railroad electrification system was designed to deliver 36,000 hp to a single train and these superpower locomotives were to take advantage of this huge source of power.

H. S. Ogden: I wish to thank Mr. Lessmann and Mr. MacLeod for their discussions and their interest in this paper which is largely historical.

Mr. Lessmann has emphasized the quality of the locomotives and drawn attention to aspects of their operation not covered elsewhere. In doing this, he has also commented on some of the personalities that were involved in the *GG-1's* development.

Mr. MacLeod takes us into the realm of speculation and comments on what might have happened if The Pennsylvania Railroad electrification had been extended. He also mentions some rather large powers for single-cab locomotives.

Train Performance Calculated by Digital Computer—Supplemental Programs

J. E. HOGAN
MEMBER AIEE

THE CALCULATION OF TRAIN performance, i.e., the speed, the distance traveled, and the running time of a given train over a given route, provides useful information to railroad management and to manufacturers of railroad traction equipment. These calculations are tedious and time consuming when performed manually. For this reason several special-purpose machines have been constructed to perform the computations more rapidly.[1] Recently the use of high-speed digital computers has resulted in a much greater saving of time.

Since its development in 1957 the Pennsylvania Railroad digital computer program[2] for calculating train performance on the International Business Machines (IBM) Model *650* data processing machine has been used extensively. It has saved many man-hours and has facilitated the study of the performance of several proposed new trains and locomotives. Time for much of this work might not have been available with previous slower calculating methods.

The rate at which the digital computer accurately calculates train performance is amazing. Nevertheless, the preparation of the essential preliminary data still takes time. Now, however, a part of this preparatory work can be performed rapidly by the digital computer with considerable saving in time through the use of two new programs:

1. A program to calculate MALT (maximum acceleration on level, tangent track)
2. A program to finalize track data

MALT Calculating Program

By the use of the MALT Calculating Program, the digital computer calculates and stores the necessary tables of the maximum acceleration on level tangent track or MALT, the tractive effort and the tractive resistance. These tables are then used in the aforementioned train performance calculating program to calculate the performance and the energy or fuel consumption of:

1. Freight trains
2. Passenger trains (locomotive hauled)
3. Trains of multiple-unit cars

With this program, only one punched card is required for the pertinent data of each train consist. This is a noteworthy time-saving feature. Into the train data card is punched the following information:

1. Number of cars
2. Total weight of cars
3. Number of cars with mechanical axle-driven air-conditioning apparatus
4. Cross-sectional (frontal) area of cars
5. Number of locomotive units, or motored multiple-unit cars
6. Weight per locomotive unit
7. Axles per locomotive unit
8. Cross-sectional area of locomotive unit
9. Locomotive identification
10. Train identification
11. Code:
    - 88 Freight train
    - 98 Passenger train (locomotive hauled)
    - 89 Multiple-unit train
    - 99 Helper locomotive

After one train data card has been punched, a card for another train differing by only one or two items can be prepared quickly. This reduces the preparatory time for subsequent runs.

In addition to the train data card, two to four punched cards are required for tabulating the tractive effort or tractive force for each 5-mile-per-hour increment of speed. However, as tractive effort data are constant for each class of locomotive unit or multiple-unit car, these tractive effect cards are prepared only once and may be used repeatedly.

By the use of special control cards inserted in the deck of train data cards, the following changes in train data can be made automatically during a run without stopping the calculations:

1. Changing train consist (cars and/or locomotive)
2. Adding helper locomotive
3. Cutting off helper locomotive

In the calculation of a run, the increase in machine-time developing the stored tables is less than 6 seconds. In these few seconds the following work is performed by the digital computer.

1. Store train data on memory drum
2. Store table of tractive effort per unit
3. Compute and store a table of total tractive effort
4. Compute and store a table of the tractive resistance of the locomotive
5. Compute the tractive resistance of the cars, add the locomotive resistance and store the sum, forming a table of total resistance

Paper 60-25, recommended by the AIEE Land Transportation Committee and approved by the AIEE Technical Operations Department for presentation at the AIEE Winter General Meeting, New York, N. Y., January 31–February 5, 1960. Manuscript submitted September 28, 1959; made available for printing October 26, 1959.

J. E. Hogan is with the Pennsylvania Railroad Company, Philadelphia, Pa.

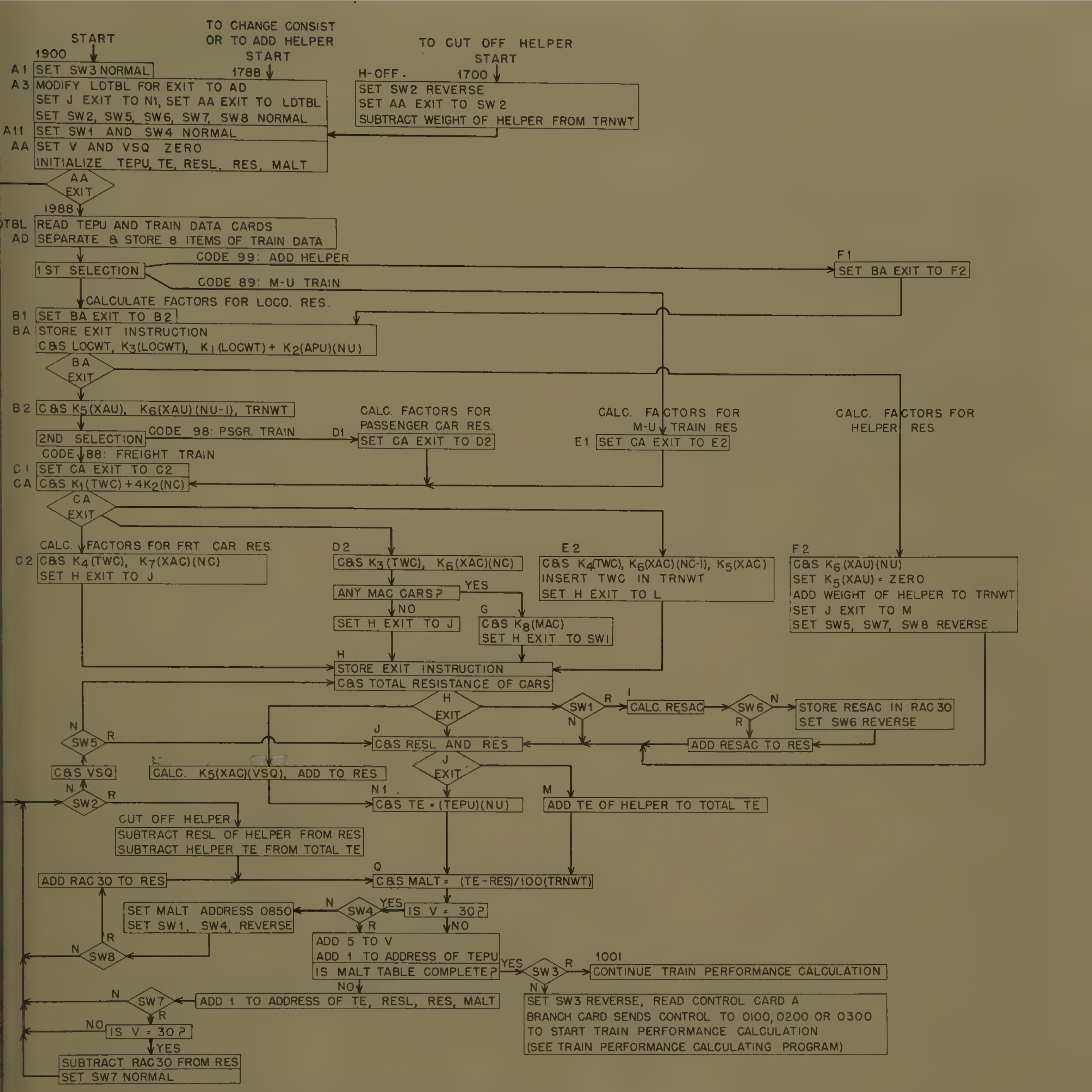

Fig. 1. Flow diagram, program to calculate maximum acceleration on level tangent track

From values of tractive effort, resistance train weight, compute and store a of maximum acceleration on level ent track from the equation:

$$LT = (TE\text{-}RES)/100(TRNWT) \qquad (1)$$

hich

LT = Maximum acceleration on level tangent track (miles per hour per second)

= Tractive effort (pounds)

= Total resistance (pounds)

WT = Train weight (tons)

hen done manually, this work, in-ing punching and checking the data s, takes about one man-hour.

The methods used in developing the several tables may become evident from a study of the flow diagram of the program logic, Fig. 1, in which the following abbreviations or symbols are used.

APU = Axles per unit
C&S = Calculate and store
CODE = Train code
LDTBL = First instruction of stored routine for loading data into the IBM *650*
LOCWT = Locomotive weight, total, tons
$K2$ = Constant No. 2
MAC CARS = Mechanically air-conditioned cars, apparatus axle-driven
MALT = Maximum acceleration on level tangent track
M-U = Multiple-unit
N = Outlet of switch set normal; R, reverse
NC = Number of cars
NU = Number of locomotive units or motored M-U cars
RAC30 = Resistance caused by air-conditioning at 30 miles per hour
RES = Tractive resistance, total, pounds
RESAC = Resistance caused by air-conditioning, pounds
RESL = Resistance of locomotive, pounds
SW2 = Switch No. 2
SW2 N = Switch No. 2 set normal; SW2 R, reverse
TE = Tractive effort or tractive force, pounds
TEPU = Tractive effort per unit, pounds
TRNWT = Train weight including weight of locomotive, tons

TWC = Total weight of cars and lading, tons
V = Speed, miles per hour
VSQ = Speed squared
XAC = Cross-sectional area of cars, square feet
XAU = Cross-sectional area of locomotive unit, square feet

In a manner typical of digital computer programing each value of resistance is calculated when needed by the use of stored equations. This is in contrast to the usual method of reading values from tables or charts when performing the calculations manually. To minimize computer time, the program is arranged efficiently so that factors which are to be used repeatedly are computed and stored first, thereby reducing the number of multiplications. Locomotive resistance, total resistance, tractive effort, and maximum acceleration on level tangent track are calculated for each tabular speed before proceeding to the next speed.

Tractive resistances calculated by this program are based on the Davis equations[3] as follows:

Locomotive:

$$RESL = k_1(LOCWT)+k_2(APU)(NU)+k_3(LOCWT)(V)+k_5(XAU)(VSQ)+k_6(XAU)(NU-1)(VSQ) \quad (2)$$

Freight cars:

$$RES = k_1(TWC)+4k_2(NC)+k_4(TWC)(V)+k_7(XAC)(NC)(VSQ) \quad (3)$$

Passenger cars:

$$RES = k_1(TWC)+4k_2(NC)+k_3(TWC)(V)+k_6(XAC)(NC)(VSQ) \quad (4)$$

Train of multiple-unit cars:

$$RES = k_1(TWC)+4k_2(NC)+k_4(TWC)(V)+k_5(XAC)(VSQ)+k_6(XAC)(NC-1)(VSQ) \quad (5)$$

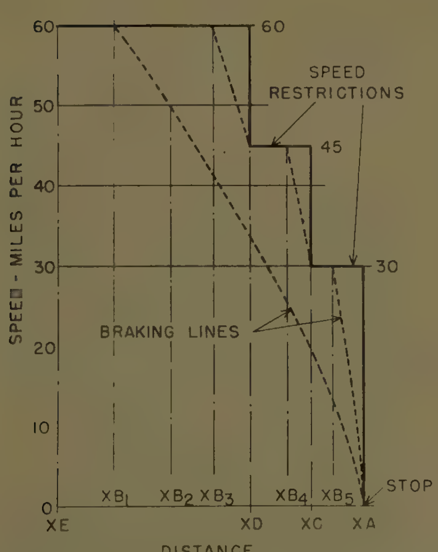

Fig. 2. Braking conditions affected by braking rates

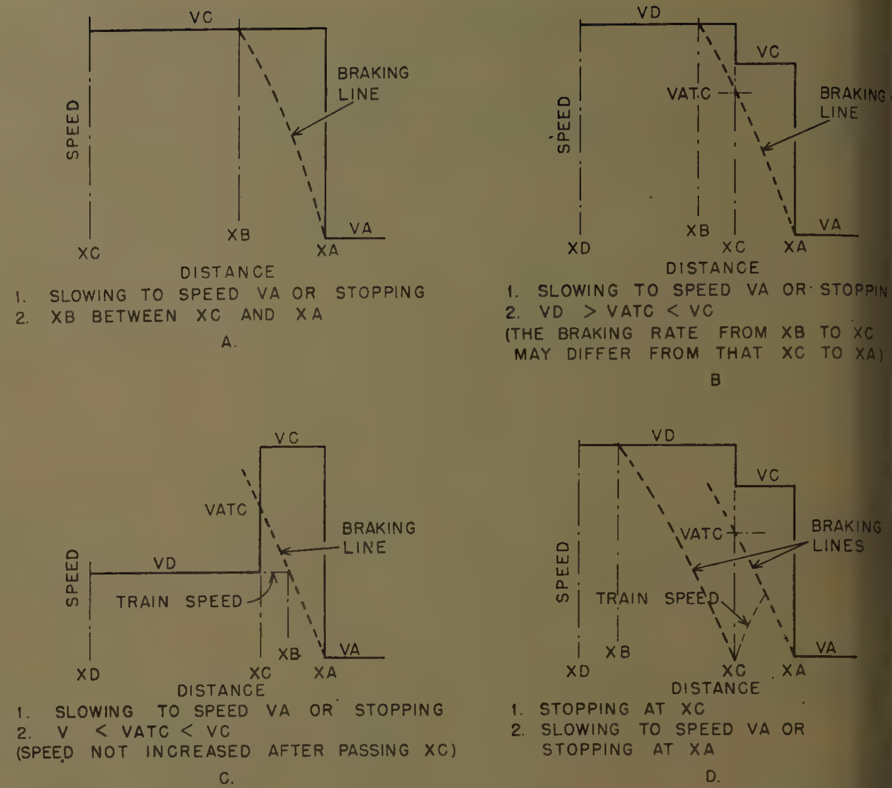

Fig. 3. Braking conditions affected by various combinations of speed restrictions and stop

where

$k_1 = 1.3$
$k_2 = 29$
$k_3 = 0.030$
$k_4 = 0.045$
$k_5 = 0.00200$
$k_6 = 0.00034$
$k_7 = 0.00050$

Two of the equations have been modified by using 0.00200 instead of 0.00240 as the coefficient K_5 for the term expressing the air resistance of the leading unit. This change was the result of comparing calculated running times of high-speed trains with the observed time of actual runs.

In the program the resistance or drag due to axle-driven air-conditioning apparatus is based on 25 horsepower per car at and above 30 miles per hour.

Program to Finalize Track Data

The Track Data Finalizing Program simplifies the preparation of track data. In the finalized (ready to use) deck of track data cards, before all slow-downs and station stops, the points where brakes are to be applied and the rate of braking deceleration must be specified. For runs in which speed restrictions or stops are frequent, such braking data are numerous. Furthermore, to calculate another run with a different maximum speed or with a different braking rate, the braking data must be changed accordingly. When done manually this entails not only recalcula[ting] the data for the braking points, b[ut] also repunching and replacing the braki[ng] cards in their proper places in the dec[k] of track data cards, or repunching th[e] entire deck.

With this new program, the manual[ly] prepared track data cards specify on[ly] the basic track data, i.e., grades, spee[d] restrictions, and stations; the finalizi[ng] program calculates the braking data a[c]curately and produces a second deck [of] track data cards with the braking card[s] in their proper places.

Prior to the finalizing process, the dec[k] of basic track data is reversed so that th[e] process becomes one of calculating speed[s] and distances during acceleration rath[er] than braking. The points where the ca[l]culated speeds reach the authorized speed[s] become the "braking points" in the fina[l]ized track data. Reasons for this pro[cedure] become evident from a study [of] Fig. 2.

In this case, approaching the statio[n] at XA, the speed must not exceed 60, 4[5] and 30 miles per hour when the trai[n] passes XE, XD, and XC respectivel[y]. For a train with a certain braking rate, [to] stop the train at XA, the brakes must [be] applied as the train passes XB_1, if at th[at] point the speed is 60 miles per hour. F[or] this braking rate the "braking line" X[B_1] to XA represents the locus of points [at] which, for the speed indicated, the brak[es]

st be applied to stop the train at XA. he train is limited to a maximum speed 0 miles per hour, for optimum braking, brakes should not be applied until the n passes XB_2. For a train with a ain higher braking rate, traveling at miles per hour initially, the brakes uld be applied at XB_3, released at XD, applied at XB_4, released at XC and re- lied at XB_5.

he braking rate is affected by the de. For the same speed reduction and ensity of brake application, the braking ance and the braking time on an ending grade will be less than on a cending grade because of the retarding ct of the ascending grade. Based on -service brake applications, for loco- tive-hauled passenger trains, the brak- rates used in the program are obtained use of the equation:

$$-(PBRC)(4+G) \qquad (6)$$

which

Braking rate (negative), miles per hour per second
Grade in per cent, positive for ascending grades, negative for descending grades
RC = Passenger train braking rate constant:
0.244 for reducing speed
0.220 for stopping

he passenger train braking rate con- nt is less for stopping, partly because coefficient of friction between wheels brake shoes increases materially as speed apprаches zero. Proper han- g of the train requires the pressure of ke shoes on wheels to be reduced just r to stopping avoid a "rough stop." o, to stop precisely at a certain loca- it is usually necessary to reduce speed run at a low speed for a short distance re the final brake application.

ests have indicated that the rate of king deceleration of freight trains ies widely. Therefore, regardless of grade, the freight train braking rate d in the program is 1/4 mile per hour second. This is probably not ac- ate but is conservative and in line with degree of accuracy required in calcula- s of performance of freight trains.

or other types of trains, any selected d value of braking rate may be read ually into the memory storage of the puter before starting the finalizing ulations.

raking distance is calculated by the ation:

$$(V_1^2 - V_2^2)/(-7{,}200B) \qquad (7)$$

hich

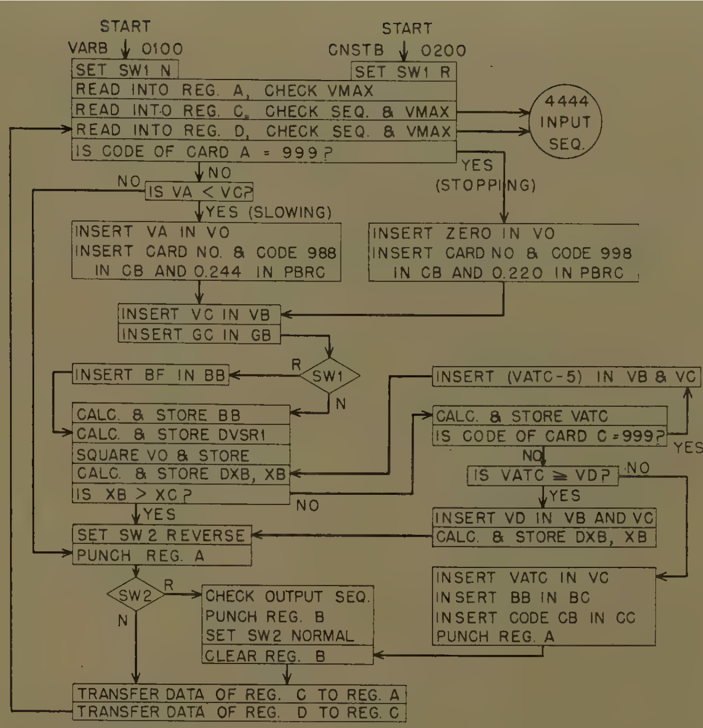

Fig. 4. Flow diagram, program to finalize track data

D = Braking distance, miles
V_1 = Speed at start of braking, miles per hour
V_2 = Speed at end of braking, miles per hour
B = Braking rate (negative), miles per hour per second

Various combinations or sequences of speed restrictions affect the calculations of braking lines as illustrated by Fig. 3, wherein:

XD, XC, and XA = Consecutive locations where speed restrictions change or where train is to stop
VD, VC, and VA = Speed restrictions which apply when the train passes locations XD, XC, and XA respectively
XB = Location where brakes should be applied, if the speed of the train at that point is sufficient to so warrant
$VATC$ = Speed characteristic of the braking line at XC

Fig. 4 shows the flow diagram of the Track Data Finalizing Program in which the following abbreviations or symbols are used:

BB = Braking rate, negative, miles per hour per second.
BF = Fixed braking rate, negative, normally −0.25 mile per hour per second
CNSTB = Program entry to finalize track data using braking rate BF
CODE = Train code
DVSR1 = (−7200)(BB)
DXB = Braking distance, miles
N = Outlet from switch set normal; R, reverse
PBRC = Passenger braking rate constant
REG. A = Storage location for track data for XA
SW2 = Switch No. 2
VARB = Program entry to finalize track data using passenger-train braking rates determined by grades
VATC = Speed at C during braking when $XB<XC$
VMAX = Maximum speed, normally 120 miles per hour, controls only if track data give authorized speeds greater than VMAX
VA, GA, BA, and CA are authorized speed, grade, braking rate, and code respectively of track location at distance XA. Symbols for XB, XC, and XD correspond

Conclusions

The advantages of using a digital computer, not only to calculate train performance but also to do some of the work of preparing the essential preliminary data, will be appreciated by those who are familiar with the complexities and the tediousness of the computations when done manually. The time-saving is particularly important. Like all such applications of the digital computer, by making engineering computations faster easier, and more dependable, these applications enable the engineer to obtain more answers and more accurate answers to the problems of management, research, and development.

References

1. A New Train Performance Calculator, S. V. Smith. *AIEE Transactions*, vol. 70, pt. I, 1951, pp. 657–60.

2. Train Performance and Locomotive Tonnage Ratings Calculated by Digital Computer, J. E. Hogan. *Ibid.*, pt. II (*Applications and Industry*), vol. 77, July 1958, pp. 119–26.

3. The Tractive Resistance of Electric Locomotives and Cars, W. J. Davis, Jr. *General Electric Review*, Schenectady, N. Y., Oct. 1926, pp. 18–24.

Discussion

D. R. MacLeod (The General Electric Company, Erie, Pa.): This paper by Mr. Hogan is a welcome sequel to his earlier work, reference 2 of the paper, which published for the first time a thoroughly tested IBM *650* program for calculating the speed-time-distance performance of trains. The two supplemental programs given in this paper will reduce the amount of time necessary for preparing the MALT and PROFILE data. The program for calculating the MALT is straightforward, and the only suggestion that can be made is that some computer time could be saved by using train resistance cards instead of making the calculation on the computer.

The second program has used the clever trick of reversing the regular profile deck and using the braking characteristic as if it were motoring to calculate the braking zone. In the original program published in 1958, it was necessary to average the grade in the braking zone and no change in braking rate was possible.

Fig. 3(B) of this paper has a note that the braking rate from XB to XC may differ from that from XC to XA. It is of course quite possible to have large changes in grade between XB and XA so that, with the braking rate constants that have been taken as standard, different braking rates will result.

In order to handle this for all possible changes of grade the computer would either have to average the grades and use a constant grade for the braking zone or, better still, it could calculate the speed at C and B that would be necessary when the motoring calculation was made. The averaged grade would be punched into the profile deck in the first case and the fictitious speeds at C and B would be punched into the profile deck as speed restrictions in the second case. It would be interesting to know if the author used either of these alternatives.

I. H. Cole (Canadian National Railways, Montreal, Quebec, Canada): The Canadian National Railways (CNR) are in the process of calculating the minimum running time versus power-to-weight ratio of their main line trains for the guidance of line operation staffs. It involves calculating, as a first step, train performances for about 200,000 train-miles and, obviously, it could not be done without a high-speed method of computing. The Pennsylvania Railroad Company made available to the CNR its excellent computer program for calculating train performance and, after trying out the method to confirm its accuracy, the CNR decided to reprogram it in order to effect a major reduction in the work of preparing track data for 25,000 miles of CNR main line.

Input Data

Track Data. First, raw track data comprising track elevations, curves, speed restrictions, and the corresponding mile-post locations are punched on three decks of punched cards. Next, a supplemental program resolves any minor inconsistencies in the mass-produced raw data and consolidates them on two decks of cards:

1. An Elevation Deck which contains information on track elevations and the equivalent feet of climb for curve resistance.
2. A Speed Deck which contains the speed limits dictated by track restrictions and curves. There are separate speed decks for passenger trains, freight trains, and rail-diesel cars.

Lastly, to complete the track data, there is a deck of Speed Orders for the run in question; it contains the stops, the passing points, and any temporary speed orders for the run.

The three decks of track data cards are read into the IBM *650* simultaneously from an on-line IBM *533* and two on-line IBM *407* units. Data for several miles of track are stored in the computer memory at all times and are renewed as the journey progresses. The decks serve for both directions of travel, merely by reversing them.

Train Data. The CNR Operation Department is not vitally interested in calculating the performances of a large variety of trains and the train data are prepared manually, much in the same way as they are with The Pennsylvania Railroad Company's original program.

Calculating Train Motion

The calculation of train motion with the CNR's program differs from The Pennsylvania Railroad Company's in the following respects:

1. A probe in front of the train senses a reduction in speed limit and automatically sets the "braking-line" for reducing speed. A train does not begin accelerating till its rear-end clears the prevailing speed limit.
2. The average train elevation is used in calculating the effective grade at each step of the computation; that is, train weight is assumed to be distributed over its length and the effect of the ruling grade is accurately calculated. A second advantage of dealing with the grade in this way, is that a longer time increment can be used for each step and, therefore, a faster computing speed, without introducing large errors.
3. The speed of calculating train performance with the CNR's program is not as fast as that obtained with The Pennsylvania Railroad Company's program, but the slower speed is acceptable in view of the reduction that has been effected in the work of preparing the track data.

Train Performance Outputs

The output of the CNR's program is in three parts: Summary List, Speed Graph, Detail List.

Summary List. A summary of the calculations is provided for every run; at each station stop or passing point the following items are listed: 1. Distance traveled; 2. Cumulative running time; 3. Cumulative locomotive output energy at rim of driving wheels; 4. Locomotive load factor between stops, i.e., fraction of available energy used; 5. Braking effort between stops; 6. The slowest speed reached below any arbitrarily chosen speed and its location (for locomotive tonnage ratings).

Speed Graph. The second output, which is optional, is a visual presentation of train speed versus distance traveled: train speed as well as the prevailing speed limit are plotted every quarter of a mile; also shown are the locations where the locomotive operated at full power and where brakes were applied.

Detail List. The third output, also optional, is a detail listing of the train performance calculations: the following items are listed every one quarter of a mile of the journey: 1. Distance traveled; 2. Running time; 3. Train speed; 4. Acceleration; 5. Effective grade; 6. Train resistance; 7. Locomotive tractive effort.

J. E. Hogan: The author expresses his sincere thanks to Mr. MacLeod and Mr. Cole for their interest and the discussions they have presented.

Previously, in the preparation of track data, to simplify the manual calculations, all data points within braking zones were eliminated. However, this had several disadvantages, one of which was the occasional elimination of a desired timing point. With the use of the supplemental program for finalizing the track data, all data points are retained. The speed of the slowing train at each intermediate point in a braking zone becomes a fictitious speed limit; for instance, in Fig. 3(B), VATC becomes the fictitious speed limit from XC to XA.

A welcome innovation is the method developed by the Canadian National Railways of using a probe in front of the train to sense reduction in speed limit or a station stop and to calculate the braking data while the simulated train is enroute. This eliminates the necessity for finalizing the track data before starting the train performance calculations.

Of great advantage in train performance calculations is the development by the CNR of a method of taking into account the length of the train. Calculations based on train weight concentrated in a point indicate that a train begins to lose appreciable speed at the instant the locomotive reaches the foot of a steep grade. Actually the grade will not have its full effect on reducing the train speed until the entire train is on the grade. The reverse effect takes place as the train passes over the summit. Usually, these two types of error cancel each other nicely in even the shortest train performance runs and sufficiently accurate values of total time are obtained. However, with certain fortunately rare combinations of grades, distances, and approach speeds, calculations based on concentrated train weight have indicated falsely that a heavy train would stall whereas with the distributed weight method, the calculations showed and actual runs proved that the train operating with momentum would be able to ascend the grade. Results of calculations based on distributed train weight closely approximate those of actual operation.

It would be interesting to know more of the procedures used by the CNR in their computer program.

Capacitance of Parallel Rectangular Cylinders

J. D. HORGAN
ASSOCIATE MEMBER AIEE

IE OBJECTIVES of this paper are 1) to provide curves displaying ac- tely determined values for the capaci- e per unit length of two parallel ıngular cylinders, and (2) to present ief explanation of the technique used btaining these curves in order to in- te its utility in the study of other luctor configurations. In addition to iding capacitance values, the curves useful in determining the magnetic ıeance associated with relay and con- or magnets of similar configuration. ood example of the latter is the inter- leakage permeance of the magnet in 1. The technique, a natural ex- ion of the method of subareas, as ounded by Higgins and Reitan,[1-3] was zed earlier by T. N. Feng in the work ribed in his unpublished thesis at the ersity of Wisconsin, Madison, Wis., 951. The depth of that investigation somewhat limited, however, for it carried on prior to the time that high- d computing equipment was generally lable. The present work obtains ıl results by taking full advantage of capabilities of the magnetic-drum -processing machine.

ıe motivation for the present investi- on arose out of a study of the perme- of the flux paths between the two s of the magnet of Fig. 1. While oximate methods for estimating this ıeance have been given previously,[4-6] order of accuracy of these estimates is ewhat uncertain. Fig. 1 illustrates technique for studying such a field, lving the use of imaginary magneti- insulating partitions to separate the . Such division enables each part of field to be considered as an entity. present investigation is concerned determining the permeance of that ion of the field which lies between the planes. Since the planes are perpendicular to the axis of the poles, the field configuration is identical with that between two rectangular cylinders of infinite extent.

Because most of the related works cited are reported in terms of electric capacitance, this term is also used here. The simple conversion of equation 1 permits the permeance of the related field to be determined:

$$P=(120\ \pi)^2\ (\mu_r/\epsilon_r)\ (C) \tag{1}$$

where C is the capacitance per unit length in farads per meter, P is the related permeance per unit length in webers per ampere-turn-meter, μ_r is the relative permeability of the medium in which the magnetic field is established, and ϵ_r is the dielectric constant of the medium in which the electric field is established.

The Analysis

Consider the following problem: Given two parallel rectangular cylinders of perfectly conducting material immersed in a homogeneous, isotropic, linear dielectric of permittivity ϵ, find the electric capacitance per unit length in the axial direction. Several methods of solution suggest themselves. Graphical, numerical, or analog field mapping might be utilized, but these are inefficient as they provide more detail than is required in the present problem. Direct measurement on an electroconducting analog can be used, but the accuracy of such a method is somewhat limited. The solution to the problem can be easily outlined using the Schwarz-Christoffel theorem concerning complex variable transformations. Actual results, however, are only obtained after long and involved numerical integration.

In view of the above, an extension of the method of subareas to the 2-dimensional case appears to provide the best approach. In this method, the conductors are divided into ribbonlike subareas and each of these is replaced with a line charge, as shown in Fig. 2. Three assumptions are made:

1. If the line charges are held at the same potential as the conductor which they represent, the charge on the conductor per unit length is equal to the total of the corresponding line charges per unit length.

2. For the purpose of calculating potential at the center of one subarea due to the charge on another subarea, the latter can be considered a concentrated line charge. Feng shows this to be a good approximation as long as the distance between the centers of the subareas exceeds the width of one subarea.

3. For the purpose of calculating potential at the center of a subarea due to its own charge, that charge is assumed to be uniformly distributed.

With these assumptions, the potential at the center of each subarea, V_i, can be expressed as a linear combination of all the charges:

$$V_i=\sum_{j=1}^{n} S_{ij}q_j \tag{2}$$

Because of symmetry, n need only be equal to the number of line charges representing one half of one conductor. If, in this system of equations, the constraint $V_i=Vo$ is imposed, then equation 2 represents n equations in n unknowns, the individual line charges per unit length. If this linear system be solved for the q_j's, then capacitance per unit length is easily determined from:

$$C=\sum_{j=1}^{n} q_j/Vo \tag{3}$$

Of course, before the linear system can be solved, the coefficients S_{ij} must be evaluated. These are calculated as logarithmic functions of certain distances. The potential at a radius R from a line charge q per unit length is

$$V=(q/2\pi\epsilon)\ (\ln_\epsilon\infty-\ln_\epsilon R) \tag{4}$$

The potential V_i in Fig. 2, due to the

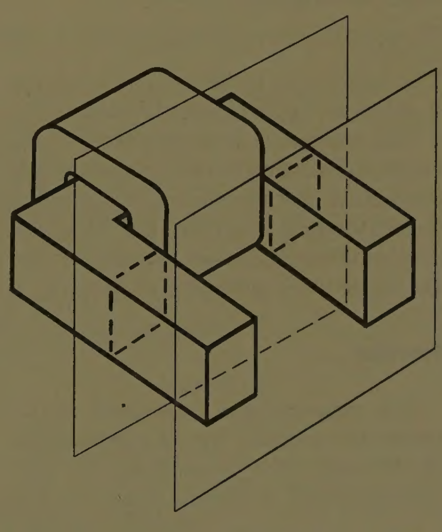

Fig. 1. Magnet with rectangular-cylindrical poles

59-111, recommended by the AIEE Basic ces Committee of the Communication and ronics Division and approved by the AIEE ıical Operations Department for presentation e AIEE Winter General Meeting, New York, , February 1–6, 1959, and re-presented for dis- on only at the AIEE Fall General Meeting, ıgo, Ill., October 11–16, 1959. Manuscript itted November 3, 1958; made available for ng October 2, 1959.

HORGAN is with Marquette University, Mil- ee, Wis.

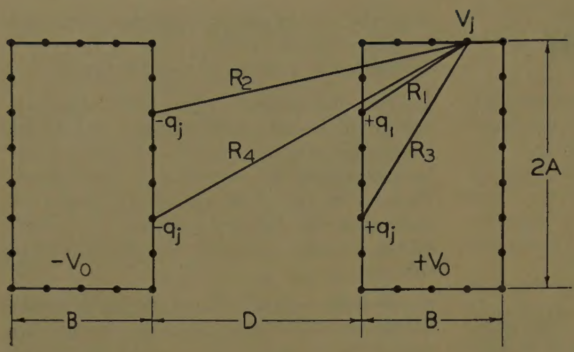

Fig. 2. Subareas for parallel rectangular cylinders

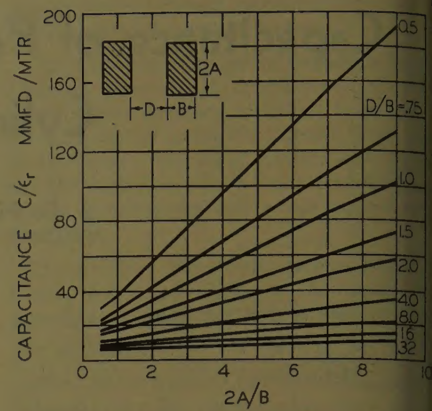

Fig. 3. Capacitance of parallel rectangular cylinders

Table I. Capacitance Per Unit Length for Parallel Square Conductors
Capacitance: C/ϵ_r in micromicrofarads per meter

D/B	Lower Limit (Inscribed Circle)	Results from T. N. Feng	Present Results	Upper Limit (Circumscribed Circle)
1	21.11	24.46	25.44	31.49
3	13.45	14.62	14.99	16.34
7	10.03	10.596	10.84	11.49
31	6.66	6.9310	7.027	7.29

Table II. Capacitance Per Unit Length as Dependent on Number of Subareas Representing Conductor

Number of Subareas	Difference Δn	Capacitance, Micromicrofarads per Meter	Difference	Difference, Per Cent	Per Cen Δn
28		26.39			
36	4	26.00	0.39	1.58	0.395
44	8	25.75	0.25	0.99	0.124
60	16	25.44	0.31	1.22	0.076
68	8	25.35	0.09	0.36	0.045

four line charges $\pm q_j$ symmetrically disposed, is

$$V_i = (q_j/2\pi\epsilon)\ [\ln_e(R_2R_4/R_1R_3)] \quad (5)$$

except for $i=j$. For the case of $i=j$, the assumed uniform charge distribution can easily be integrated to yield:

$$V_i = (q_j/2\pi\epsilon)\ [1+\ln_e 2+\ln_e(R_2R_4/R_3)] \quad (6)$$

The coefficients to be evaluated are the multipliers of q_j in equations 5 and 6.

The computer is programed to calculate the solution in three steps: (1) The coefficients S_{ij} are evaluated. (2) The linear system of equation 2 is solved. (3) The resulting charges are summed to yield the capacitance according to equation 3.

Results

The computer was programed to calculate the solution for 54 combinations of the ratio $2A/B$ representing the proportions of the individual conductor and D/B representing the spacing. This utilizes approximately 90 hours of computer time. Results are given in Fig. 3. Results in tabular form are available from the author on request. One check on the precision of the results is shown in Table I. For the square conductor ($2A/B=1$) the upper limit on the capacitance is given by that of the circumscribed circular cylinders, while the lower limit is given by the capacitance of the inscribed circular cylinder. These limits are given in the table, together with the results reported by Feng. He calculated only for the square conductors, and used only 16 line charges to represent one conductor. Nevertheless, this does provide a good independent check on the procedures and computer programing.

As in all numerical methods, the question of absolute precision is a difficult one. In the present problem, some idea can be obtained by solving the same problem with different numbers of line charges representing the conductor. Presumably, as this number approaches infinity, the result approaches the true value. Therefore, the difference between capacitance for increasing number of line charges is some indication of the precision. Table II shows the results of such calculations. In the actual calculations, the number of subareas per conductor was 30 for $2A/B=0.5$; 60 for $2A/B=1$, 5, and 9; 48 for $2A/B=7$; and 72 for $2A/B=3$. On this basis, Table II indicates the accuracy to be in the order of 1%.

Conclusions

An extension of the method of subareas has been used to obtain values for the capacitance per unit length associated with parallel rectangular cylinders with an accuracy in the order of 1%. These results are directly applicable for the determination of leakage flux permeance in magnets of similar configuration.

References

1. Calculation of the Electrical Capacitance of a Cube, D. K. Reitan, T. J. Higgins. *Journal of Applied Physics*, New York, N. Y., vol. 22, 1951, pp. 223–26.

2. Calculation of the Capacitance of a Circular Annulus by the Method of Subareas, T. J. Higgins, D. K. Reitan. *AIEE Transactions*, vol. 70, pt. I, 1951, pp. 926–33.

3. Accurate Determination of the Capacitance of a Thin Rectangular Plate, D. K. Reitan, T. J. Higgins. *Ibid.*, pt. I (*Communication and Electronics*), vol. 75, 1956 (Jan. 1957 section), pp. 761–66.

4. Electromagnetic Devices (book), H. C. Roters. John Wiley & Sons, Inc., New York, N. Y., 1941.

5. Switching Relay Design (book), R. L. Peek, Jr., H. N. Wagar. D. Van Nostrand Company, Inc., Princeton, N. J., 1955.

6. Estimating Leakage Factors for Permanent Magnets from Geometry of Magnetic Circuit, R. K. Tenzer. *Electrical Manufacturing*, New York, N. Y., vol. 59, no. 2, 1957, pp. 94–97.

Power Apparatus and Systems—April 1960

59-567	Dynamic Circuit Theory	Messerle	1
59-131	Synthesis of Induction Motor Designs on Digital Computer	Veinott	12
60-171	Electric Shock—II	Kouwenhoven, Knickerbocker, Milnor, Jude	19
	An Analysis of Solid Rotor Machines	Wood, Concordia	
60-21	Part III. Finite Length Effects		21
60-22	Part IV. An Approximate Nonlinear Analysis		26
59-1139	Analysis of Series Generator Series Motor Drive	Jones, Meyer	31
60-26	Bibliography of Relay Literature 1957–1958	Committee Report	39
60-89	Post-Irradiation of Magnet Wire Insulation	Kallander	42
60-5	Corona Suppression for H-V Rotating Machines	Manni, Schneider	49
60-1	Biblio. on Resistance and Gradient Measurements	Comm. Report	52
60-87	Thermal Life of Varnished Glass Cloth	Straka, Lindsay	58
60-58	Permalex, a New Insulation System	Beavers, Raab, Leslie	64
60-86	Aging of Wire Coating in Transformer Oil	Lipsey, Juneau	73
60-13	Gas-Filled Cavities in Solid-Type Cables	Klein	77
60-182	Pseudo-Final Voltage Distribution in Impulsed Coils	Abetti	87
60-81	Oil Preservation Systems	Chadwick, Ryder, Brierley	92
60-80	Dielectric Tests as Influenced by BIL Reductions	Meador, Dillow	99
60-55	Evaluating Power Systems for Refinery Process Units	Dickinson	110
60-243	Neutralizing Chokes for Telephone Lines	Ramsaur	124

Conference Paper Open for Discussion

The conference paper listed below has been accepted for AIEE Transactions and is now open for written discussion until June 27. Duplicate double-spaced typewritten copies for each discussion should be sent to Edward C. Day, Assistant Secretary for Technical Papers, American Institute of Electrical Engineers, 33 West 39th Street, New York 18, N. Y., on or before June 27.

Preprints may be purchased at 50¢ each to members; $1.00 each to nonmembers if accompanied by remittance or coupons. Please order by number and send remittance to:

AIEE Order Department
33 West 39th Street
New York 18, N. Y.

57-714 Adjustable-Frequency Drives with Rotating Machine Power Supply . . . . Bacheler, Helmick

AIEE PUBLICATIONS

	Member Prices	Nonmember Prices: Basic Prices*†	Nonmember Prices: Extra Posta for Foreig Subscriptio

Electrical Engineering

Official monthly publication containing articles of broad interest, technical papers, digests, and news sections: Institute Activities, Current Interest, New Products, Industrial Notes, and Trade Literature. Automatically sent to all members and enrolled students in consideration of payment of dues. (Members may not reduce the amount of their dues payment by reason of nonsubscription.) Additional subscriptions are available at the nonmember rates.

	Member Prices	Basic Prices*†	Extra Posta for Foreig Subscriptio
Electrical Engineering		annually $12*	$1.00
		Single copies $1.50*	

Bimonthly Publications

Containing all officially approved technical papers collated with discussion (if any) in three broad fields of subject matter as follows:

	Member Prices	Basic Prices*†	Extra Posta for Foreig Subscriptio
	annually	annually	
Communication and Electronics	$5.00	$8.00*	$0.75
Applications and Industry	$5.00	$8.00*	$0.75
Power Apparatus and Systems	$5.00	$8.00*	$0.75

Each member may subscribe to any one, two, or all three bimonthly publications at the rate of $5.00 each per year. A second subscription to any or all of the bimonthly publications may be obtained at the nonmember rate of $8.00 each per year.

	Member Prices	Basic Prices*†	Extra Posta for Foreig Subscriptio
Single copies may be obtained when available.	$1.50 each	$1.50* each	

AIEE Transactions

An annual volume in three parts containing all officially approved technical papers with discussions corresponding to six issues of the bimonthly publication of the same name bound in cloth with a stiff cover.

	Member Prices	Basic Prices*†	Extra Posta for Foreig Subscriptio
	annually	annually	
Part I Communication and Electronics	$4.00	$8.00*	$0.75
Part II Applications and Industry	$4.00	$8.00*	$0.75
Part III Power Apparatus and Systems	$4.00	$8.00*	$0.75
Annual subscription to all three parts (beginning with vol. 77 for 1958).	$10.00	$20.00*	$2.25
Annual subscription to any two parts.		$15.00*	$1.50

AIEE Standards

Listing of Standards, test codes, and reports with prices furnished on request.

Special Publications

Committee reports on special subjects, bibliographies, surveys, and papers and discussions of some specialized technical conferences, as announced in ELECTRICAL ENGINEERING.

---

*Discount 25% of basic nonmember prices to college and public libraries. Publishers and subscription agencies 15% of basic nonmember prices. For available discounts on Standards and special publications, obtain price lists from Order Department at Headquarters.

†Foreign prices payable i New York exchange

Send all orders to:

Order Department
American Institute of Electrical Engineers
33 West 39th Street, New York 18, N. Y.